

AD-A282 342

10

DTIC  
ELECTE  
JUL 27 1994  
S F

ANALYSIS OF A THREE-BEAM RADAR  
AS AN INSTRUMENT FOR DETERMINING  
OCEAN WAVE HEIGHTS AND VECTOR SLOPES

Christopher T. Evans

This document has been approved  
for public release and sale; its  
distribution is unlimited.

Radar Systems and Remote Sensing Laboratory  
Department of Electrical Engineering and Computer Science, University of Kansas  
2291 Irving Hill Road, Lawrence, Kansas 66045-2969  
TEL: 913/864-4835 \* FAX: 913/864-7789 \* OMNET: KANSAS.U.RSL

RSL Technical Report 8621-5

June 1994

94-22739



2020

Sponsored by:

Office of Naval Research  
Arlington VA 22217-5000

Grant N00014-89-J-3221

94 7 19 217

## Abstract

The Vector Slope Gauge (VSG) is a 35-GHz FM-CW scatterometer that has the unique capability of simultaneously (nearly) measuring the range and backscattered power to three points on the ocean surface. With three ranges and knowledge of the experimental geometry, the wave height at each footprint can be obtained. The three footprints form a plane surface which enable two orthogonal slope components to be obtained. Obtaining the slope of ocean waves is important because it is correlated with the backscattered power. By obtaining the vector slope, one does not have to make any assumptions about the linearity or long-crestedness of the ocean waves.

With a time series record of ocean wave heights and slopes, one can learn a great deal about the ocean surface. Spectral analysis of the recorded time series yields information about the wave height power spectral density, the mean wave direction vs. frequency, and the directional width spectrum. The results from the VSG are similar to those obtained from a pitch-and-roll buoy. In addition, since the slope distribution of ocean waves is nearly normal, the moments of a bivariate normal distribution can be used to fit an ellipse to the wave slopes. The orientation of the major axis of the ellipse indicates the direction of dominant wave travel, with 180° ambiguity. The ellipse also yields information about the statistics of the slope distribution. Due to the asymmetry of the waves, the center of the ellipse is shifted from the origin in the direction from which the dominant waves are traveling. Thus, the wave direction ambiguity can be resolved by fitting an ellipse to the directional histogram of the slope distribution using the least square method.

As with any instrument, the VSG has some inherent errors due to the method of measurement. These errors include phase shifts in the recorded time series due to measuring along a slant range, phase shifts due to non-simultaneous measurements,

and errors due to approximating the slope at a point with a plane. Slant-range measurements cause the measured time series of slopes to be greater than or equal to the actual slope at all times in any direction. The overestimate varies from 0° at the mean sea level to 2° at the crest and trough. The derivative approximation has little effect on either the wave height time series or the slope time series. Non-simultaneous measurements cause the magnitude of the slope to be overestimated in both directions at all times. The amount of overestimate is generally around 2°. This, although small, causes an error in the determination of the mean wave direction.

Accesion For	
NTIS	CRA&I <input checked="" type="checkbox"/>
DIC	TAB <input type="checkbox"/>
Unannounced <input type="checkbox"/>	
Justification .....	
By A 276568	
Distribution /	
Availability Codes	
Dist	Avail and/or Special
A-1	

## Table of Contents

Abstract	ii
Table of Contents	iii
Acknowledgments	v
1. Introduction	1
1.1 Background of Saxon experiment	1
1.2 Importance of studying ocean waves	2
1.3 Outline of thesis and summary of results	3
2. Theoretical Analysis of Errors	4
2.1 The Vector Slope Gauge	4
2.2 Coordinate Transformations	6
2.3 Measurement of Wave Height and Slope	9
2.4 Inherent errors in VSG measurements	10
2.5 Error in wave height time series due to slant-range measurement	13
2.6 Error in wave height time series due to non-simultaneous measurement	21
2.7 Error in slope time series due to slant range measurement	22
2.8 Error in slope time series due to first derivative approximation	26
2.9 Error in slope time series due to non-simultaneous measurement	32
3. Determination of Mean Wave Direction and the Effect of Errors	36
3.1 Two-Dimensional Slope Distribution and Best Fit Ellipse	36
3.2 Mean Wave Direction and Statistics of Slope Distribution	38
3.3 Resolving the directional ambiguity using a histogram of slopes	40
3.4 Effect of Inherent Measurement Errors on Determination of Direction	46
4. Determination of Ocean Spectra and Comparison with Pitch-and-Roll Buoy	53
4.1 Description of Pitch-and-Roll Buoy	53

<b>4.2 Directional Distribution of Ocean Waves and Longuet-Higgins Approach</b>	<b>54</b>
<b>4.3 Comparison of VSG and Pitch-and-Roll Buoy in Determining Ocean Spectra</b>	<b>56</b>
<b>4.4 Effect of Inherent Errors on VSG's Determination of Ocean Spectra</b>	<b>59</b>
<b>5. Conclusion</b>	<b>67</b>
<b>5.1 Recommendations for Further Study</b>	<b>70</b>
<b>References</b>	<b>72</b>
<b>Appendix A: MATLAB Programs</b>	<b>74</b>
<b>Appendix B: Ellipses Fit to SAXON Data</b>	<b>96</b>
<b>Appendix C: Wave Spectra of SAXON Data from VSG Measurements</b>	<b>130</b>

## 1. Introduction

### 1.1 Background of Saxon experiment

The Synthetic Aperture radar and X-band Ocean Nonlinearities (SAXON) experiment took place in November of 1990 on the Nordsee research platform. The tower was situated in about 30 meters of water just off the coast of Germany in the North Sea. The University of Kansas was one of several institutions involved in the experiment. The purpose of the experiment was to study microwave backscatter and SAR images of the ocean surface for high sea states [Plant & Alpers, 1991]. To that endeavor, The University of Kansas operated a 35-GHz scatterometer, as well as C- and X-band radars.

The 35-GHz scatterometer that KU operated is more commonly called the Vector Slope Gauge (VSG) in light of its unique capabilities (see section 2.1). The

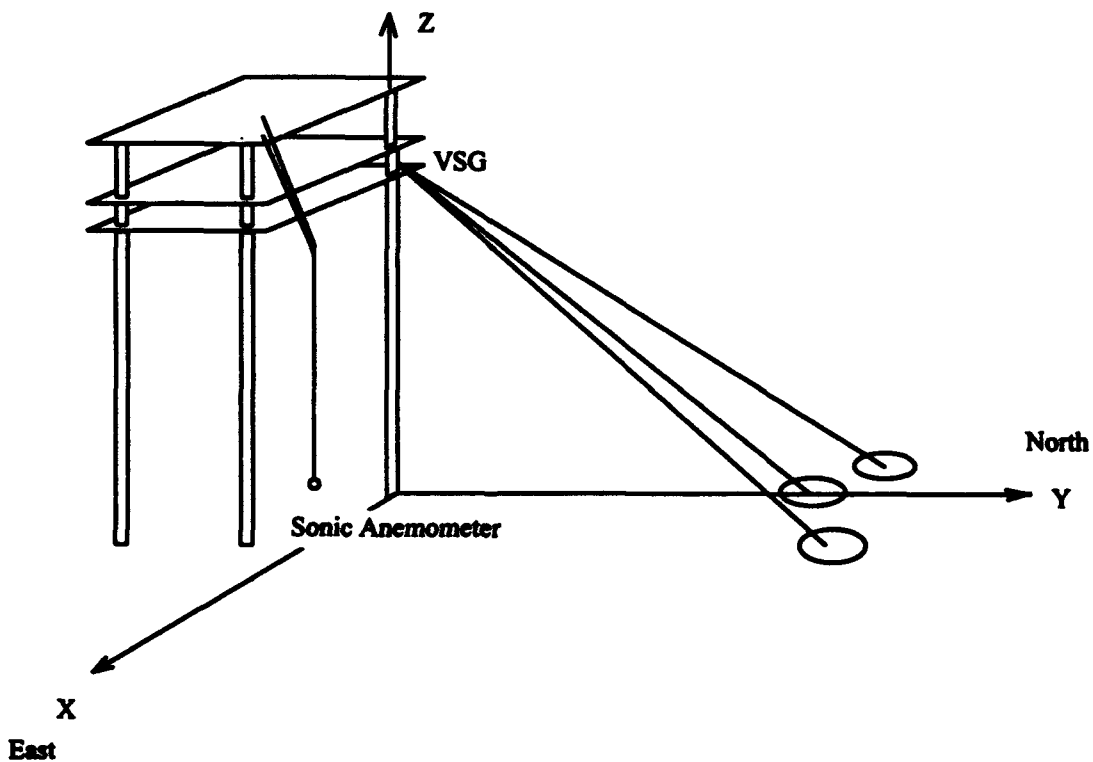


Figure 1.1. Diagram of Nordsee platform and location of VSG and 10-m anemometer.

VSG was located on the Northwest corner of the platform about 20 meters above the mean sea level (see Figure 1.1). The VSG was pointed in the general direction of oncoming waves at moderate angles of incidence. To avoid corruption of the data due to the location of the tower, we analyzed data collected only when waves were coming between 225° and 45° (0° is North), and when the wind was within the same region. The wind speed was obtained, when available, from a sonic anemometer 5 meters above the mean sea surface off the Northeast corner of the tower. When these data were unavailable the wind speed was obtained from a cup anemometer 47 meters above the mean sea level at the southwest corner of the platform. An algorithm was then used to estimate the wind speed at 5 meters.

Ocean measurements were also made with a Wavec pitch-and-roll buoy operated by the Federal Maritime and Hydrographic Agency of Hamburg, Germany. The buoy, located near the tower, recorded time series of heave and pitch and roll angles.

## **1.2 Importance of studying ocean waves**

In recent years, concern over the environment has increased dramatically with the revelation of the ozone "hole" and talk of the greenhouse effect. Since 70% of the earth's surface is covered by water, understanding the air-sea interface plays a major role in developing global climate models. To understand how wind affects ocean waves, it is important to understand how the energy in ocean waves is distributed with regard to frequency and direction (the directional spectrum). Knowledge of the directional spectrum of ocean waves is also important for determining the effect on shipping [Neumann & Pierson, 1963], on off-shore structures [Kuik et. al., 1988], coastal sediment transport, and wave diffraction and refraction from the shore [Trageser & Elwany, 1990].

The advantage of using satellite microwave remote-sensing instruments to measure ocean parameters is that they can be used in any type of weather. The backscattered power from the radar signal is affected by tilt and hydrodynamic modulation. Thus, to better understand how the radar signal is modulated by ocean waves, The University of Kansas operated several radars as part of the SAXON-FPN experiment.

### 1.3 Outline of thesis and summary of results

The objective of my thesis is to analyze the inherent errors involved with the VSG, and to show that they do not seriously detract from the VSG's capability of determining ocean wave heights and vector slopes. Errors occur with the VSG due to the radar's distance measurement along a slant range, approximation of the derivative at a point on the ocean surface by the slope of a plane, and nonsimultaneity of the three range measurements. These errors induce phase shifts in the measured time series of wave heights and slope. The effect on the slope time series is more significant due to the fact that individual range errors cannot be averaged.

The two-dimensional distribution of wave slopes measured by the VSG is nearly bivariate Gaussian. The moments of the slope distribution can be used to fit an ellipse to the wave slopes. The mean direction of wave travel is given by the orientation of the major axis of the ellipse, with  $180^\circ$  ambiguity. Due to the asymmetry of ocean waves, however, the center of the ellipse is shifted from the origin in the direction from which the waves are coming. Thus, by fitting an ellipse to a histogram of the wave slopes the directional ambiguity can be resolved.

Records of the wave-height time series and slope time series allow calculation of the directional spectrum of ocean waves. From the directional spectrum, the wave

height power spectral density, the mean wave direction spectrum, and the directional width spectrum can all be calculated. These same spectral properties are routinely calculated from pitch-and-roll buoy data. A WAVEC pitch-and-roll buoy was operated by the Federal Maritime and Hydrographic Agency of Hamburg, Germany during the SAXON-FPN experiment. The data from this buoy were analyzed by F. Zierner of GKSS, Geesthacht, Germany, and the results were made available to us for comparison. The spectral parameters determined from the VSG data compare favorably with those from the pitch-and-roll buoy.

## 2. Theoretical Analysis of Errors

### 2.1 The Vector Slope Gauge

The VSG is a 35-GHz FM-CW scatterometer that uses a single parabolic reflector with three switchable feeds to measure simultaneously the range to and the

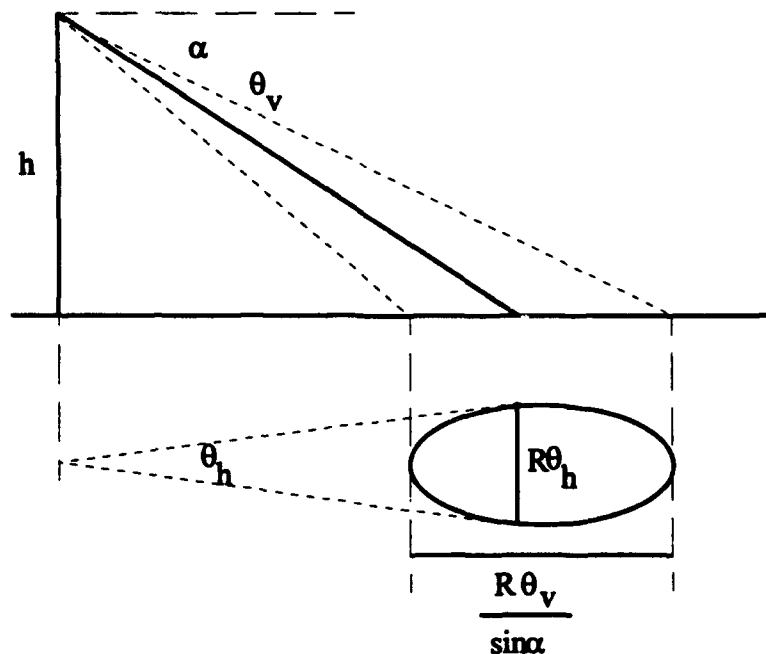


Figure 2.1.1. Area illuminated by a single radar beam.

backscattered power from three closely spaced points on the ocean surface. The three feeds are situated such that the radar footprints form a right angle on a surface perpendicular to the center beam. The 3-dB beamwidth of each beam is approximately  $2^\circ$ , and  $2.3^\circ$  separates the center of each beam from the vertex of the right triangle. The VSG was mounted roughly 20 meters above the mean sea level. Thus, at  $47^\circ$  the area of each footprint is approximately  $1.3 \text{ m}^2$ , and the center-to-center distance between footprints in each leg of the right triangle is roughly 1.8 m.

The beams of the VSG were switched at 30 Hz, and a measurement of the intermediate frequency (IF) and backscattered power was made at each sampling interval. Thus, data were recorded for each beam at 10 Hz. For an FM-CW radar, the difference between transmitted frequency and received frequency,  $f_b$ , is proportional to the range to the target, and is given by

$$f_b = \frac{4Brf_m}{c} \quad \text{Eq. 2.1.1}$$

where B is the bandwidth of the sweep signal, r is the range to the target,  $f_m$  is the modulation rate, and c is the speed of propagation. The VSG was swept over a 500 MHz bandwidth centered at 6 GHz. The modulation rate was chosen so that the mean IF frequency was 455 kHz.

With the range to three points on the ocean surface, and knowledge of the orientation of the radar, the height of the ocean surface within each footprint can be calculated. Since the three points define a plane, the slope of the plane can be determined with regard to any direction.

## 2.2 Coordinate Transformations

When working with data from the VSG, one needs frequently to transform between different coordinate systems. Figure 2.2.1 depicts the situation when the VSG is rotated from the earth coordinate system (non-primed axes) to the antenna coordinate system (double-primed axes). The VSG is first rotated an angle of  $\theta$  about

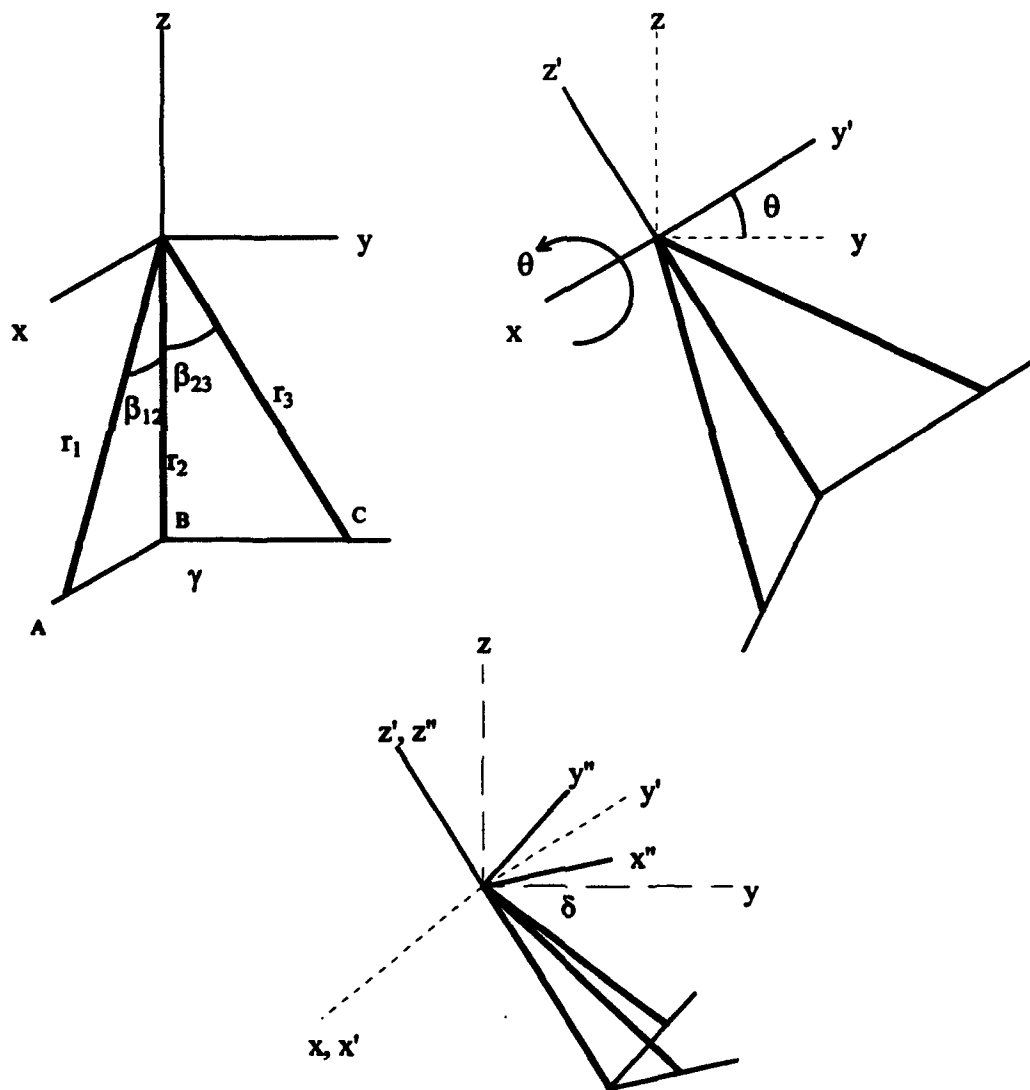


Figure 2.2.1 Transformation of radar coordinate system to earth coordinate system.

the x axis, and then an angle of  $\delta$  about the  $z'$  axis. To determine the coordinate transformation matrix that results from the rotation of  $\theta$ , see Figure 2.2.2. The

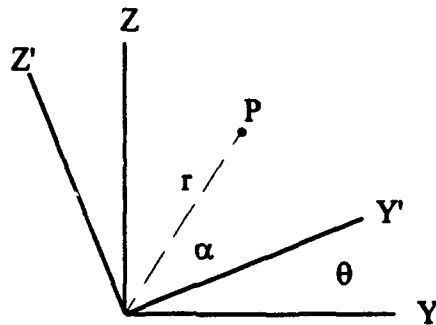


Figure 2.2.2 Rotation of  $\theta$  about the X axis.

coordinates of point P in the XYZ coordinate system are:

$$P_x = 0 \quad P_y = r \cos(\alpha) \quad P_z = r \sin(\alpha) \quad \text{Eq 2.2.1}$$

In the X'Y'Z' coordinate system, the coordinates of point P are:

$$\begin{aligned} P_x' &= P_x & P_y' &= r \cos(\alpha - \theta) & P_z' &= r \sin(\alpha - \theta) \\ P_y' &= r(\cos(\alpha)\cos(\theta) + \sin(\alpha)\sin(\theta)) & P_z' &= r(\sin(\alpha)\cos(\theta) - \sin(\theta)\cos(\alpha)) \\ P_y' &= P_y \cos(\theta) + P_z \sin(\theta) & P_z' &= P_z \cos(\theta) - P_y \sin(\theta) \end{aligned} \quad \text{Eq. 2.2.2}$$

Thus,

$$\begin{bmatrix} P_x' \\ P_y' \\ P_z' \end{bmatrix} = \begin{bmatrix} 1 & 0 & 0 \\ 0 & \cos(\theta) & \sin(\theta) \\ 0 & -\sin(\theta) & \cos(\theta) \end{bmatrix} \times \begin{bmatrix} P_x \\ P_y \\ P_z \end{bmatrix} \quad \text{Eq. 2.2.3}$$

To determine the coordinate transformation matrix that results from the rotation of  $\delta$ , see Figure 2.2.3. The coordinates of point P in the X'Y'Z' coordinate system are:

$$Px' = r \cos(\alpha) \quad Py' = r \sin(\alpha) \quad Pz' = 0 \quad \text{Eq. 2.2.4}$$

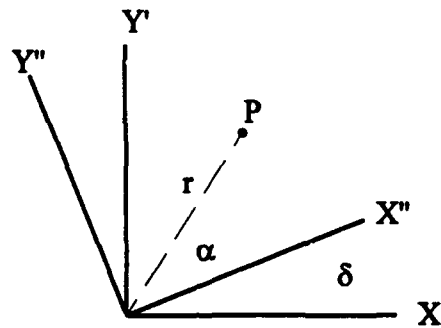


Figure 2.2.3 Rotation of  $\delta$  about the Z' axis.

In the X''Y''Z'' coordinate system, the coordinates of point P are:

$$\begin{aligned} Px'' &= r \cos(\alpha - \delta) & Py'' &= r \sin(\alpha - \delta) & Pz'' &= Pz' \\ Px' &= r(\cos(\alpha) \cos(\delta) + \sin(\alpha) \sin(\delta)) & Py' &= r(\sin(\alpha) \cos(\delta) - \sin(\delta) \cos(\alpha)) \\ Px' &= Px \cos(\delta) + Py \sin(\delta) & Py' &= Py \cos(\delta) - Px \sin(\delta) \end{aligned} \quad \text{Eq. 2.2.5}$$

Thus,

$$\begin{bmatrix} Px'' \\ Py'' \\ Pz'' \end{bmatrix} = \begin{bmatrix} \cos(\delta) & \sin(\delta) & 0 \\ -\sin(\delta) & \cos(\delta) & 0 \\ 0 & 0 & 1 \end{bmatrix} \times \begin{bmatrix} Px' \\ Py' \\ Pz' \end{bmatrix} \quad \text{Eq. 2.2.6}$$

Now, to transform from the earth coordinate system to the radar coordinate system, multiply the coordinate transformation matrix in Eq. 2.2.6 by the coordinate transformation matrix in Eq. 2.2.3.

$$\begin{bmatrix} P_x'' \\ P_y'' \\ P_z'' \end{bmatrix} = \begin{bmatrix} \cos(\delta) & \sin(\delta) & 0 \\ -\sin(\delta) & \cos(\delta) & 0 \\ 0 & 0 & 1 \end{bmatrix} \times \begin{bmatrix} 1 & 0 & 0 \\ 0 & \cos(\theta) & \sin(\theta) \\ 0 & -\sin(\theta) & \cos(\theta) \end{bmatrix} \times \begin{bmatrix} P_x \\ P_y \\ P_z \end{bmatrix}$$

$$\begin{bmatrix} P_x'' \\ P_y'' \\ P_z'' \end{bmatrix} = \begin{bmatrix} \cos(\delta) & \sin(\delta)\cos(\theta) & \sin(\delta)\sin(\theta) \\ -\sin(\delta) & \cos(\delta)\cos(\theta) & \cos(\delta)\sin(\theta) \\ 0 & -\sin(\theta) & \cos(\theta) \end{bmatrix} \times \begin{bmatrix} P_x \\ P_y \\ P_z \end{bmatrix} \quad \text{Eq. 2.2.7}$$

Conversely, if the coordinates are known with respect to the radar, then the matrix to transform them to the earth coordinate system is:

$$\begin{bmatrix} P_x \\ P_y \\ P_z \end{bmatrix} = \begin{bmatrix} \cos(\delta) & -\sin(\delta) & 0 \\ \sin(\delta)\cos(\theta) & \cos(\delta)\cos(\theta) & -\sin(\theta) \\ \sin(\delta)\sin(\theta) & \cos(\delta)\sin(\theta) & \cos(\theta) \end{bmatrix} \times \begin{bmatrix} P_x'' \\ P_y'' \\ P_z'' \end{bmatrix} \quad \text{Eq. 2.2.8}$$

### 2.3 Measurement of Wave Height and Slope

The vector slope gauge (VSG) measures the range to three separate points on the ocean surface through the use of its switched-beam antenna. Given the ranges, the location of each point in the antenna coordinate system is given by (see Figure 2.2.1):

$$\begin{aligned}
 \mathbf{A} &= (r_1 \sin(\beta_{12}) \cos(90 - \gamma), r_1 \sin(\beta_{12}) \sin(90 - \gamma), -r_1 \cos(\beta_{12})) \\
 \mathbf{B} &= (0, 0, -r_2) \\
 \mathbf{C} &= (0, r_3 \sin(\beta_{23}), -r_3 \cos(\beta_{23}))
 \end{aligned} \quad \text{Eq. 2.3.1}$$

To determine the wave heights with respect to the mean sea level, the coordinates in Eq. 2.3.1 are first transformed to the earth coordinate system using Eq. 2.2.8. Then, since the radar is located approximately 20 meters above the mean sea level, 20 meters is added to the z (earth) coordinate of each point.

Since the locations of three points on the ocean surface are known, two orthogonal slope components can be obtained. The normal to the plane containing the three points is given by (see Figure 2.2.1)

$$\vec{N} = \vec{BA} \times \vec{BC} \quad \text{Eq. 2.3.2}$$

The slope of the plane in the y-direction is  $\tan^{-1}(\frac{-N_y}{N_z})$  and the slope of the plane in the x-direction is  $\tan^{-1}(\frac{-N_x}{N_z})$ .

The Matlab program slopeab.m was written by Sam Haimov and Vahid Hesany to determine orthogonal components of the slope, given the range measurements. In slopeab.m, the coordinate transformation used is different than the one given in Eq. 2.2.7 or 2.2.8. The two coordinate transformation matrices give the same results, however, because the angles  $\theta$  and  $\phi$  in slopeab.m (corresponding to  $\theta$  and  $\delta$  in the derivation above) are positive when measured clockwise in program slopeab.m as opposed to counter-clockwise in the above derivation.

#### 2.4 Inherent errors in VSG measurements

In every instrument there are measurement errors due to noise, and potential errors due to calibration problems. With the VSG, there are also errors that occur

completely independent of noise and calibration problems. These errors are due simply to the way the measurements are made and some of them cannot, in general, be reduced purely by system design. (It may be possible, however, to reduce them by changing the experimental geometry.) The inherent errors are due to measuring along a slant range, approximating the slope at a point with a plane, and non-simultaneous measurements.

In the ideal situation and neglecting noise, the measured time series of a pure sinusoidal wave of one frequency, direction, and amplitude incident upon the radar measurement site would be an exact replica of the actual wave. Due to the inherent errors, however, phase shifts occur in the measured time series of wave heights (see Figure 2.4.1). The measured wave height time series depicted in Fig. 2.4.1 was calculated from the MATLAB program range.m and can be found in Appendix A. It

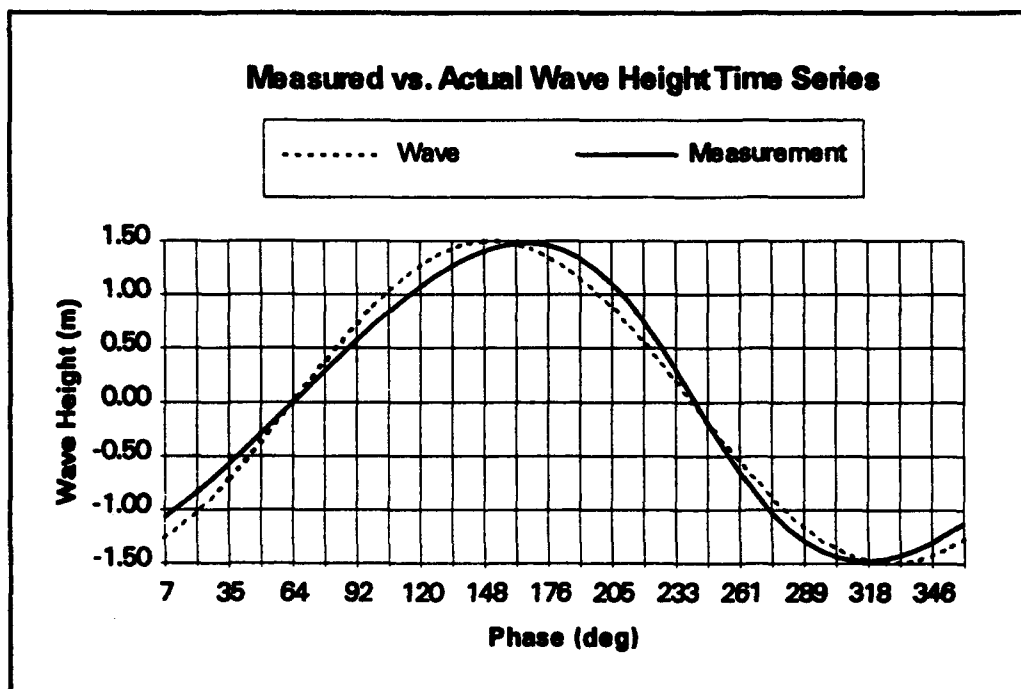


Figure 2.4.1. Example of phase error in 3-beam average wave height time series for a steep wave due to slant-range, non-simultaneous measurement. Incidence angle, 47°; Antenna height, 20 m; Wave frequency, 0.2 Hz,  $\delta = 0^\circ$ , Upwave look direction.

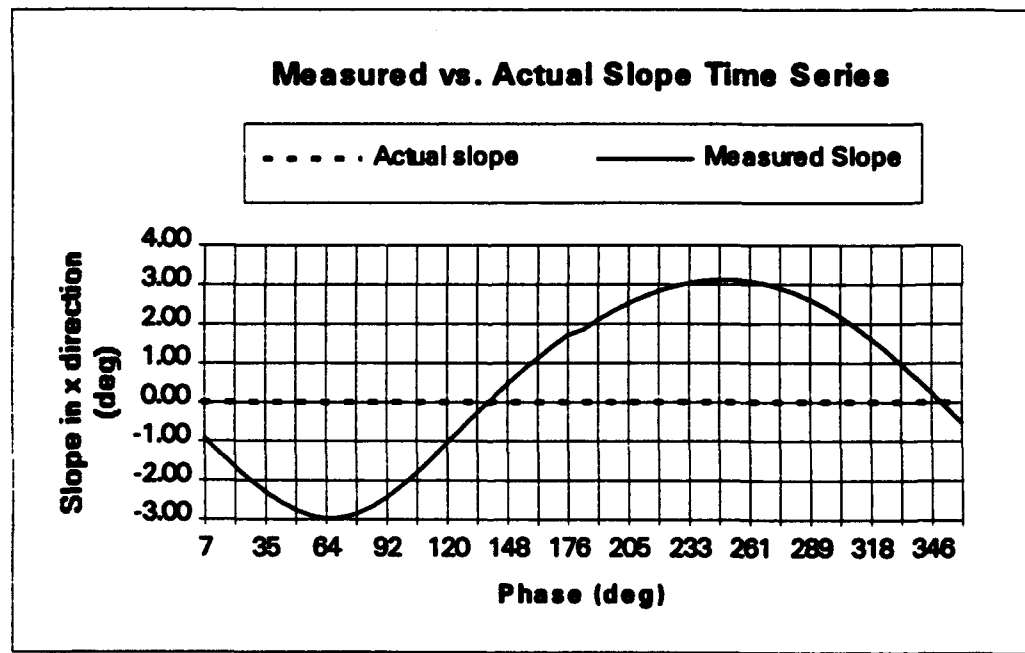
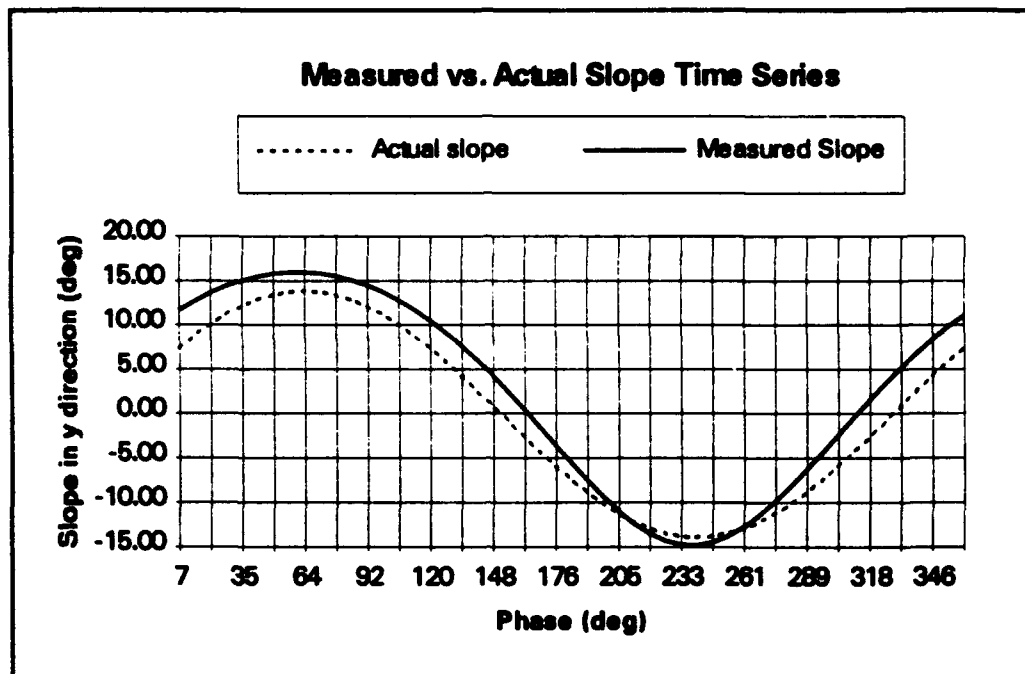


Figure 2.4.2. Example of total error in slope time series due to slant-range, non-simultaneous measurement, and the derivative approximation. Incidence angle,  $47^\circ$ ; Antenna height, 20 m; Wave frequency, 0.2 Hz; Wave height, 3 m;  $\delta = 0^\circ$ ; Upwave look direction.

takes into account measurement along the slant range as well as non-simultaneous measurements. The maximum phase shift occurs at the crest and the trough because at these points the measurement site is a maximum horizontal distance from the true location.

In the slope time series, the individual errors in each range measurement have a greater effect because they are not averaged. Measuring along the slant range induces a phase shift in the recorded time series; approximating the derivative causes the recorded time series to be modulated by a sinc function; and non-simultaneous measurements cause the estimated wave direction to be in error. The total effect of these errors is depicted in Figure 2.4.2. Since the oncoming wave is headed directly toward the radar, there is no slope in the cross (x) direction. Note that for this particular example, however, the measured slope in the x direction can be as much as  $\pm 3^\circ$ . As a result, the mean wave direction would be recorded as coming from

$$90^\circ - \tan^{-1}\left(\frac{15}{3}\right) \approx 11^\circ$$

an error of  $11^\circ$ . Now that the total error can be seen, it is worth looking at each source of error.

## 2.5 Error in wave height time series due to slant-range measurement

A radar measures the distance to a particular point along the radar beam. Thus, the VSG measures the distance to the points of intersection between each of the radar beams and the ocean surface. Since the ocean surface moves due to the waves, the points of measurement move along the radar beam rather than vertically. This causes a phase shift in the time series of ranges which affects the determination of ocean

wave heights and slope. To estimate the amount of error in the wave height time series and slope time series induced by the non-vertical displacement for waves of various frequencies and directions, it is necessary to simulate the ocean surface. Simplifying a great deal, the surface of the ocean can be described by:

$$z = A \cos(2\pi f t + k(\sin \phi)x + k(\cos \phi)y) \quad \text{Eq. 2.5.1}$$

where  $z$  is the wave height,  $A$  is the wave amplitude,  $f$  is the wave frequency,  $k$  is the wave number, and  $\phi$  is the angle (measured clockwise) between the  $+y$ -axis (RLD) and the direction from which the waves are coming. If we assume that the origin of the earth coordinate system is located where the radar signal originates with  $+z$  indicating an up direction, then the  $z$  coordinate of any point on the ocean surface is

$$z = A \cos(2\pi f t + k(\sin \phi)x + k(\cos \phi)y) - h \quad \text{Eq. 2.5.2}$$

where  $h$  is the height of the antenna above the mean ocean surface. Now, from Eq. 2.2.8 and Eq. 2.3.1, the locations of the points of measurement in the earth coordinate system are given by Eq. 2.5.3. The appropriate  $x$ ,  $y$ , and  $z$  values from Eq. 2.5.3 can

$$\begin{aligned} x_1 &= r_1 [\cos(\delta) \sin(\beta_{12}) \cos(\gamma - 90) + \sin(\delta) \sin(\beta_{12}) \sin(\gamma - 90)] \\ y_1 &= r_1 [\cos(\theta) \sin(\delta) \sin(\beta_{12}) \cos(\gamma - 90) - \cos(\delta) \cos(\theta) \sin(\beta_{12}) \sin(\gamma - 90) + \sin(\theta) \cos(\beta_{12})] \\ z_1 &= r_1 [\sin(\theta) \sin(\delta) \sin(\beta_{12}) \cos(\gamma - 90) - \cos(\delta) \sin(\theta) \sin(\beta_{12}) \sin(\gamma - 90) - \cos(\theta) \cos(\beta_{12})] \\ x_2 &= 0 \\ y_2 &= r_2 \sin(\theta) \\ z_2 &= r_2 \cos(\theta) \\ x_3 &= r_3 [\sin(\delta) \sin(\beta_{23})] \\ y_3 &= r_3 [\cos(\delta) \cos(\theta) \sin(\beta_{23}) + \sin(\theta) \cos(\beta_{23})] \\ z_3 &= r_3 [\cos(\delta) \sin(\theta) \sin(\beta_{23}) - \cos(\theta) \cos(\beta_{23})] \end{aligned} \quad \text{Eq. 2.5.3}$$

be substituted into Eq. 2.5.2, resulting in three equations and three unknowns. Newton's method is then used to solve for the three unknown ranges. Thus,

$$r_{n+1} = r_n - \frac{f(r_n)}{f'(r_n)} \quad \text{Eq. 2.5.4}$$

where  $r_n$  is the  $n^{\text{th}}$  value of the range.

In the simple case of waves of one frequency at moderate angles of incidence, one does not have to worry about local minima vs. global minima because each radar beam intercepts the ocean surface at only one point. However, if waves of multiple frequencies are added together, or if the angle of incidence is close to grazing angles, one needs to check to make sure that the range given as the solution to the problem is the actual range from which the radar signal came. The correct range should be the shortest range which is a solution to the nonlinear equation given above.

The program `srange.m` was written in MATLAB 3.5 to determine the  $x$ ,  $y$ , and  $z$  earth coordinates of the points of intersection and also the ranges to the points of intersection. It assumes that each set of three measurements is made simultaneously. To determine the phase error in wave height measurements associated with the non-vertical displacement of the point of measurement, one needs to determine the wave heights, assuming that the point of measurement is moving vertically. The MATLAB 3.5 program `vrange.m` was written to determine the  $x$ ,  $y$ , and  $z$  earth coordinates of the points of intersection and also the ranges to the points of intersection given the  $x$  and  $y$  coordinates obtained from `srange.m` and several other variables. The  $x$  and  $y$  coordinates are required so that the data from the two programs can be properly phase matched (see Figure 2.5.1). That is, the range time series and the wave height time series of the three points will be in phase exactly at the mean sea level.

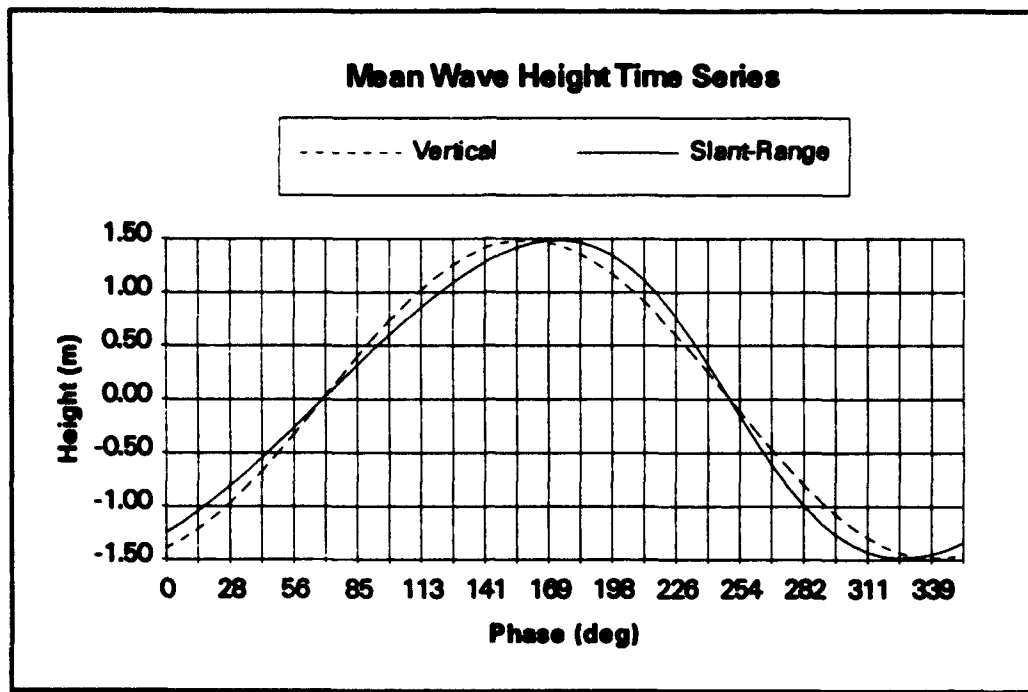


Figure 2.5.1 Mean time series of simulated wave height measurements illustrating the phase error due only to a non-vertically moving point of measurement. The solid line represents the average of each measurement made along the radar beam. The dashed line represents the average of three vertical beam measurements. Incidence angle,  $47^\circ$ ; Antenna height, 20 m; Wave frequency, 0.1953125 Hz,  $\delta = 0^\circ$ , Upwave look direction.

As previously noted, phase shifts in the time domain result in harmonics appearing in the frequency domain (see Figure 2.5.2). The particular example shown in Fig. 2.5.2 is for the same wave height time series depicted in Fig. 2.5.1. It is for a particularly steep wave; the wave height to wave length ratio in this case is near the theoretical limit of 1/7. As can be seen, even for such an extreme case the second harmonic is small, and higher order harmonics are even smaller.

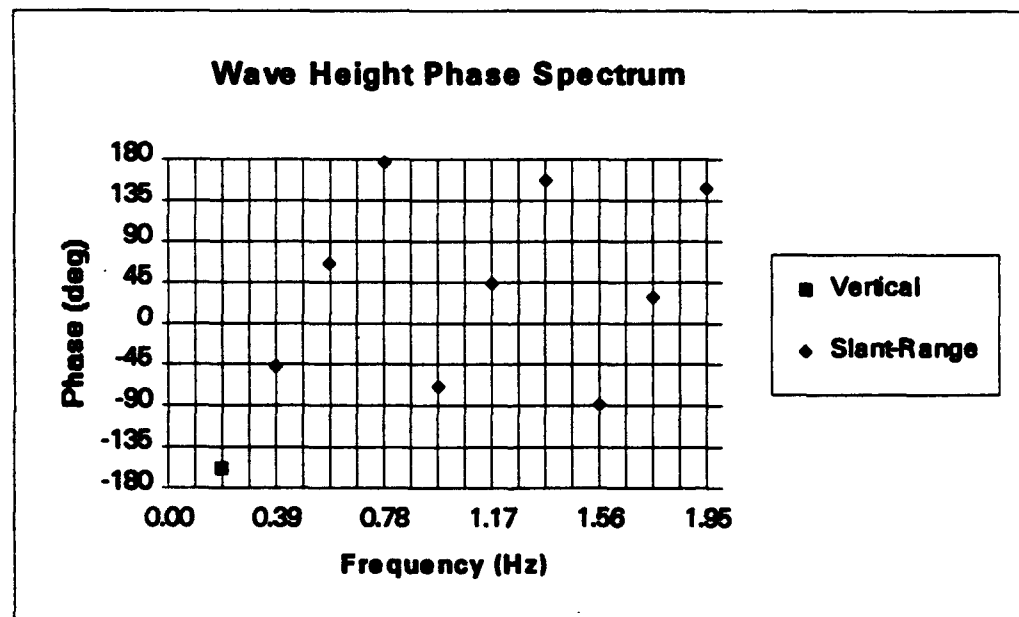
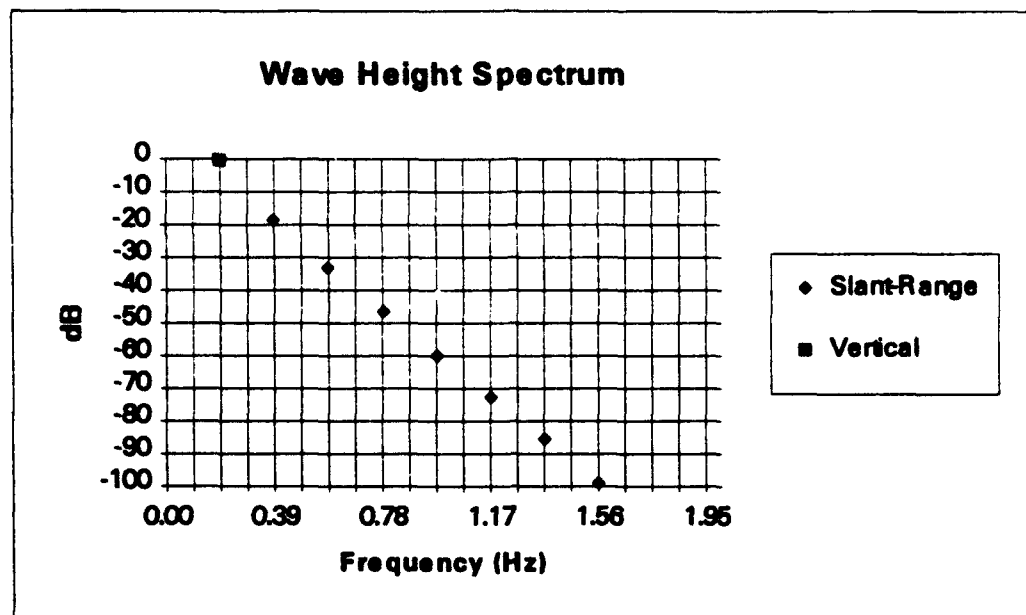


Figure 2.5.2. Harmonics occurring as a result of slant-range measurement. Incidence angle, 47°; Antenna height, 20 m; Wave frequency, 0.1953125 Hz; Wave height, 3 m;  $\delta = 0^\circ$ , Upwave look direction.

The maximum phase error for a single beam which occurs at the crest and trough can be determined from the amount of horizontal shift which occurs in the radar look direction as a result of slant-range measurement. According to Figure 2.5.3, the horizontal phase shift along the direction of wave propagation is  $A \tan(\theta)$ . The

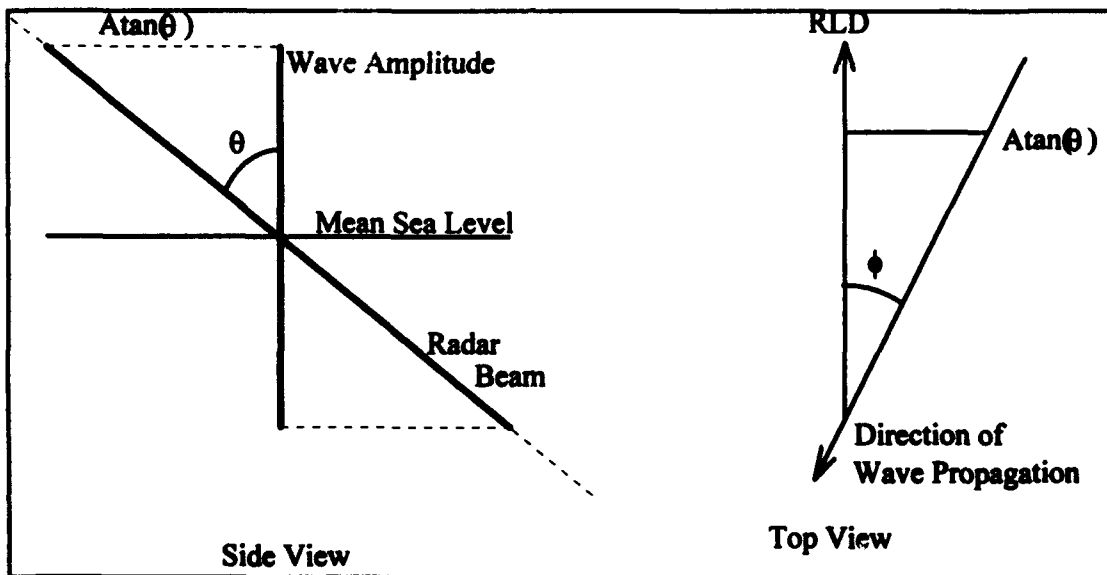


Figure 2.5.3. Geometry used to calculate maximum amount of phase error in a single beam occurring at the crest and trough due to slant-range measurement.

component of that phase shift lying in the radar look direction is simply  $A \tan(\theta) \cos(\phi)$ . Thus, the maximum amount of phase error for a single beam, in degrees, is

$$\frac{A \tan(\theta) \cos(\phi) 360^\circ}{\lambda} \quad \text{Eq. 2.5.5}$$

When the wave heights from the three beams are averaged together to form the mean wave height time series, the maximum phase error for the mean wave height

time series will be slightly different than this. It will generally be less than the error in a single beam unless the wave direction is perpendicular to the radar look direction.

The examples shown in Figures 2.5.1 and 2.5.2 are worst case scenarios for several reasons. The radar is looking directly at the oncoming waves so that the  $\cos(\phi + \zeta)$  term is 1. Both figures are also for steep waves; for the given  $\lambda$ ,  $A$  is near its maximum theoretical limit. From Eq. 2.2.5, one can see that for a wave of a given length and amplitude and for a given incidence angle, the phase error will be greater for a wave in the upwave or downwave look direction than for any other direction. For waves coming from other directions, the component of horizontal shift in the radar look direction is less than the horizontal shift in the direction of wave propagation. For a wave of a given frequency, amplitude, and direction, the phase error will be worse for a larger angle of incidence. As the incidence angle increases, there is more horizontal shift in the radar look direction.

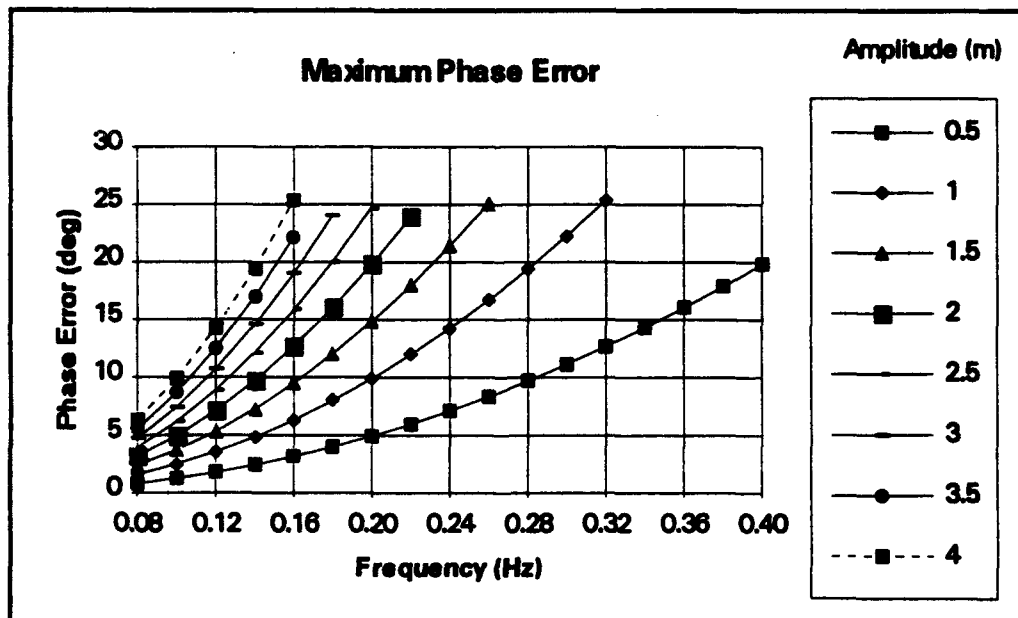


Figure 2.5.4. Maximum phase error in wave height time series due to slant-range measurement. Incidence angle,  $47^\circ$ ; Antenna height, 20 m;  $\delta = 0^\circ$ ; Upwave look direction.

Table 2.5.1 lists the maximum phase error for waves of various amplitudes and frequencies given that the angle of incidence is  $47^\circ$  and the direction of wave propagation is from  $0^\circ$ . The values are also plotted in Figure 2.5.4.

Table 2.5.1. Maximum phase error (deg) due to slant-range measurements for waves of various frequencies and amplitudes. Incidence angle,  $47^\circ$ ; Antenna height, 20 m;  $\delta = 0^\circ$ ; Upwave look direction.

Amplitude of Ocean Waves (meters)						
$\lambda$ (m)	f (Hz)	0.25	0.5	0.75	1	1.25
243.7	0.08	0.4	0.8	1.2	1.6	2.0
156.0	0.10	0.6	1.2	1.9	2.5	3.1
108.3	0.12	0.9	1.8	2.7	3.6	4.5
79.6	0.14	1.2	2.4	3.6	4.9	6.1
60.9	0.16	1.6	3.2	4.8	6.3	7.9
48.1	0.18	2.0	4.0	6.0	8.0	10.0
39.0	0.20	2.5	5.0	7.4	9.9	12.4
32.2	0.22	3.0	6.0	9.0	12.0	15.0
27.1	0.24	3.6	7.1	10.7	14.3	17.8
23.1	0.26	4.2	8.4	12.5	16.7	20.9
19.9	0.28	4.9	9.7	14.6	19.4	24.3
17.3	0.30	5.6	11.1	16.7	22.3	
15.2	0.32	6.3	12.7	19.0	25.3	
13.5	0.34	7.2	14.3	21.5		
12.0	0.36	8.0	16.0	24.1		
10.8	0.38	8.9	17.9	26.8		
9.7	0.40	9.9	19.8			

Amplitude of Ocean Waves (meters)					
$\lambda$ (m)	f (Hz)	1.75	2	2.25	2.5
243.7	0.08	2.8	3.2	3.6	4.0
156.0	0.10	4.3	5.0	5.6	6.2
108.3	0.12	6.2	7.1	8.0	8.9
79.6	0.14	8.5	9.7	10.9	12.1
60.9	0.16	11.1	12.7	14.3	15.8
48.1	0.18	14.0	16.0	18.0	20.0
39.0	0.20	17.3	19.8	22.3	24.8
32.2	0.22	21.0	24.0	27.0	

## 2.6 Error in wave height time series due to non-simultaneous measurement

The VSG records the range and backscattered power from the ocean surface every 33 ms. Thus, during the time between measurements the surface moves slightly. This movement shows up as an additional phase shift in the measurements from beams 2 and 3. For example, if the waves are coming directly at the radar, height measurements from beam 1 and 2 should be identical. Due to the finite switching time between feeds, however, the wave height measured by beam 2 will be greater than the wave height measured by beam 1 along the front face of the wave, while along the back face of the wave, the wave height measured by beam 2 will be less than that measured by beam 1.

By comparing Fig. 2.5.1 with Fig. 2.4.1, one can see that most of the error in the wave height time series is a result of measuring along a slant range. The error in the

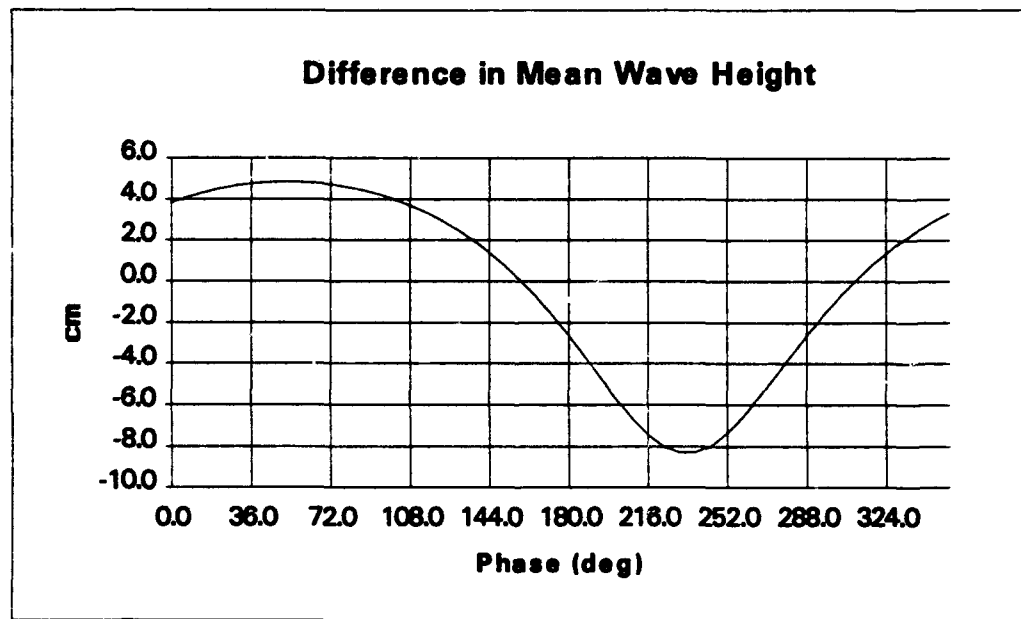


Figure 2.6.1. Difference between mean wave height time series measured simultaneously along a slant range and measured non-simultaneously along a slant range. The sampling interval of the non-simultaneous measurements is 33 ms. Incidence angle, 47°; Antenna height, 20 m; Wave frequency, 0.2 Hz; Wave height = 3 m;  $\delta = 0^\circ$ ; Upwave look direction.

mean wave height time series resulting from non-simultaneous measurement is not very significant because individual beam errors are averaged out. Figure 2.6.1 shows the difference in the mean wave height time series between measurements made simultaneously along a slant range and measurements made non-simultaneously along a slant range. Once again, this is for a steep wave. For a wave having less curvature, the difference will be even less. Since the errors in the mean wave height time series due to non-simultaneous measurements are so small, there is no point in investigating it any further.

## 2.7 Error in Slope Time Series due to Slant Range Measurement

Measuring along a slant range causes errors in the slope time series similar to those that occurred in the wave-height time series. Once again, there is a phase shift in the recorded time series (see Figure 2.7.1). In the slope time series, however, the maximum phase shift occurs when the measured slope is  $0^\circ$ . The slope is 0 when the measuring site is at the crest or trough of the wave; the point where maximum phase error occurred in the wave height time series. When the measuring site is at the mean sea level, the phase error in the slope time series is 0 just as it is in the wave height time series.

Another important observation from Fig. 2.7.1 is that the measured slope is always greater than or equal to the actual slope. The amount of difference can be seen in Fig. 2.7.2. During the time when the wave is above the mean sea level, the actual measurement site is closer to the radar than it would be if one were measuring vertically. The slope of the positive portion of a sinusoidal wave is a continuously decreasing function. Thus, since the actual measurement site is closer to the radar,

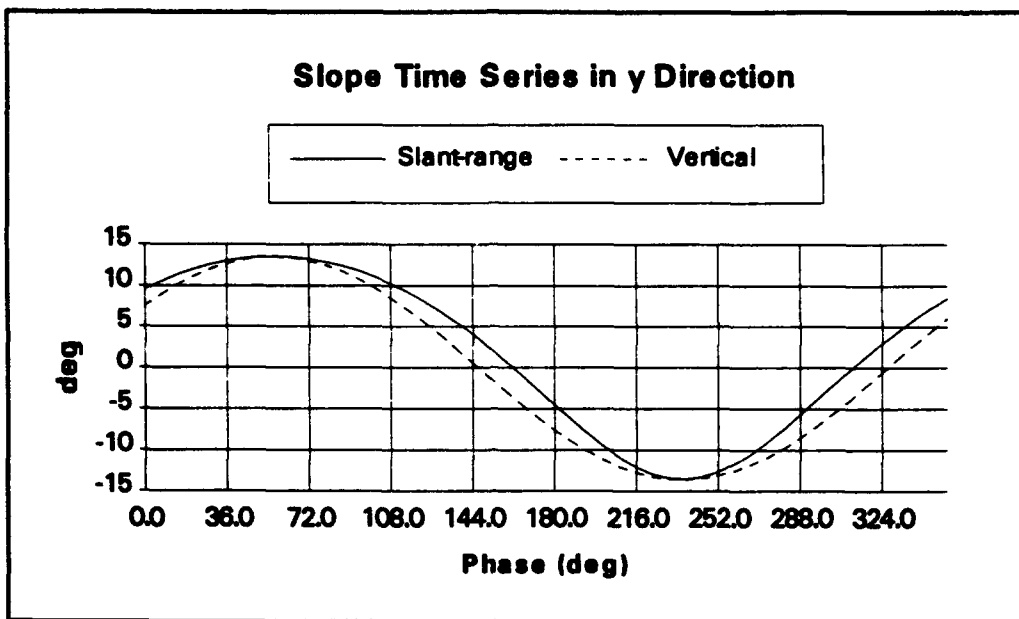


Figure 2.7.1. Error in slope time series due only to slant-range measurement. Both time series were obtained from simultaneous measurements, and slopes were calculated from the plane formed by the footprints. Incidence angle for slant range measurement,  $47^\circ$ ; Antenna height, 20 m; Wave frequency, 0.2 Hz; Wave height = 3 m;  $\delta = 0^\circ$ ; Upwave look direction.

the measured slope is greater than it should be. When the wave is below the mean sea level, the measurement site is farther from the radar than it would be if one were measuring vertically. The slope of the negative portion of a sinusoidal wave is a continuously increasing function. Thus, since the actual measurement site is farther from the radar, the measured slope is once again greater than it should be. It is also interesting to note from Fig. 2.7.2 that the difference in slope between slant range measurements and vertical measurements occurs at the 2<sup>nd</sup> harmonic of the frequency of the wave.

Equation 2.5.5 gives the amount of phase error in one height measurement for a sinusoidal wave of any length, amplitude, and direction. Obtaining a similar expression for the mean wave height time series or slope time series is not practical

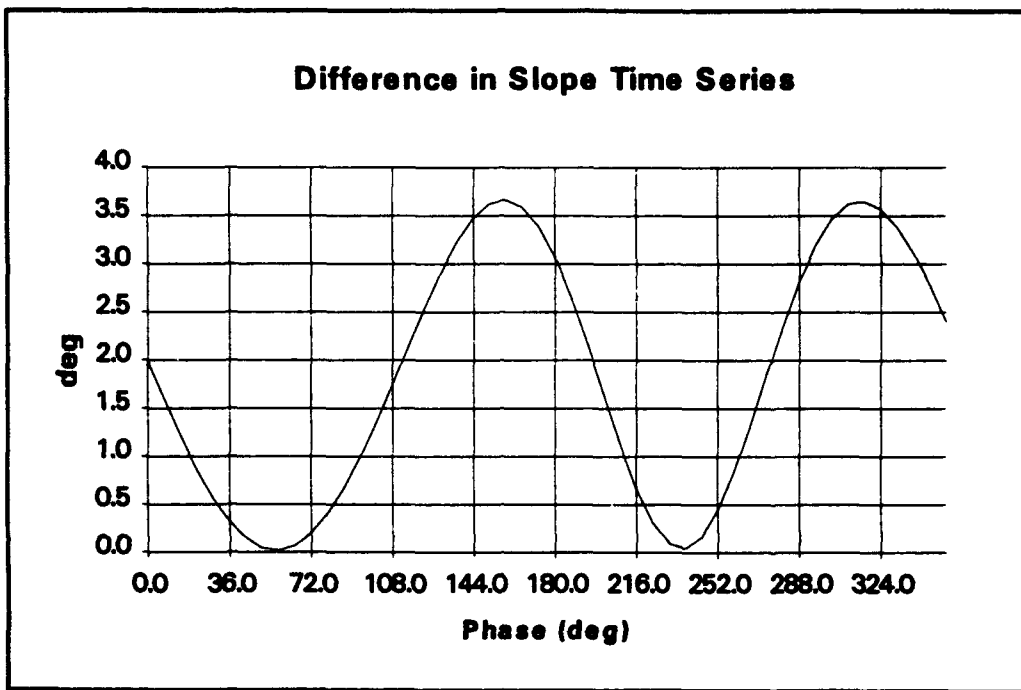


Figure 2.7.2. Difference in slope between slant range measurement and vertical measurement for the time series depicted in Fig. 2.7.1.

because of the interaction of the three beams with the ocean surface. However, Eq. 2.5.5 can be used qualitatively to estimate how much phase error will occur in the slope time series. One can see from the equation that larger incidence angles and steeper waves (higher  $A$  to  $\lambda$  ratios) will result in more phase error.

Both slope time series shown in Fig. 2.7.1 were calculated from the plane formed by the three radar footprints. The MATLAB 3.5 program, slopeab.m, determines the slope time series given the three time series of ranges, the incidence angle, and the angle of rotation about the  $z'$  axis. However, when all three beams are assumed to measure vertically, as in Fig. 2.7.1 and Fig. 2.7.2, the  $x$  and  $y$  coordinates of each point of measurement are fixed. (By setting the incidence angle to  $0^\circ$ , only beam 2 is truly vertical. The  $x$  and  $y$  coordinates of beams 1 and 3 will change, albeit very slightly.) Thus, the incidence angle would have to continuously change in order for the geometry to be correct. To avoid this problem, the program slopeab2.m was

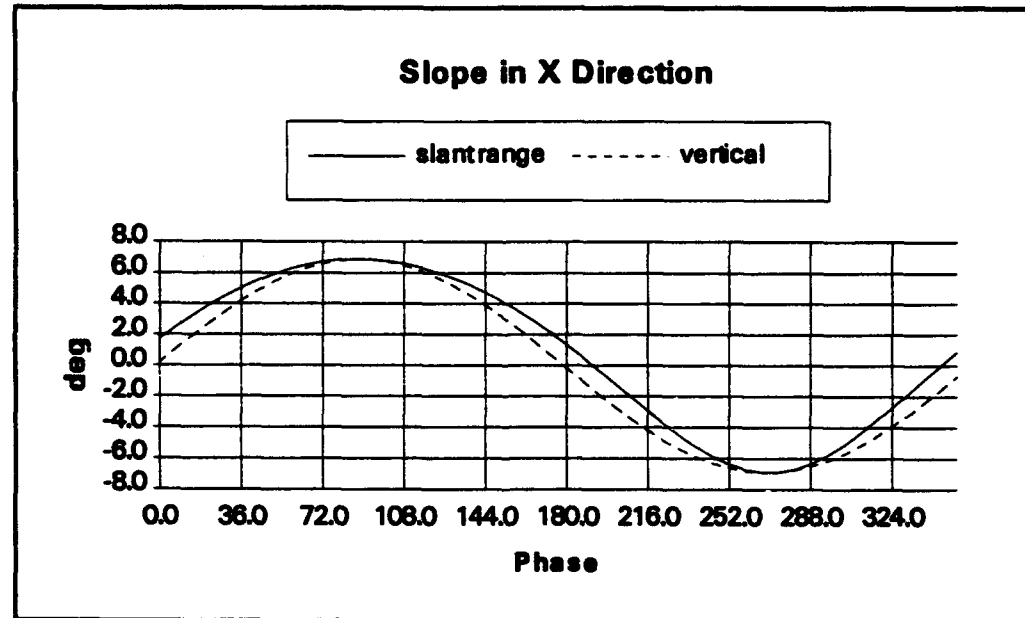
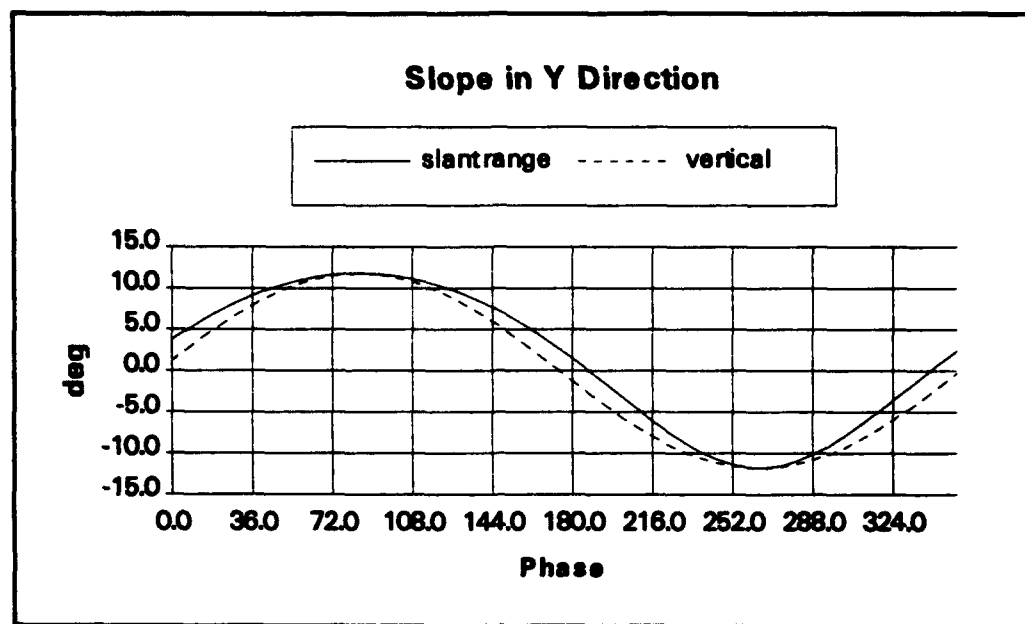


Figure 2.7.3. Error in slope time series due only to slant-range measurement. Both time series were obtained from simultaneous measurements. Incidence angle for slant range measurement,  $47^\circ$ ; Antenna height, 20 m; Wave frequency, 0.2 Hz, Wave height = 3 m,  $\delta = 0^\circ$ , Wave direction,  $30^\circ$ , RLD,  $0^\circ$ .

written and is given in Appendix A. Slopeab2.m calculates the slope time series given the x, y and z coordinates of the points of intersection.

In Fig. 2.7.1, only the slope in the y direction is shown. In that example, the waves were coming directly at the radar so there was no slope in the cross direction. In Fig. 2.7.3, the waves are coming from 30°, and all other characteristics of the waves are the same as in Fig. 2.7.1. As a result, there is slope in the x direction. As can be seen in the figure, the phase error in the x direction is similar to the error in the y direction. Thus, although the VSG accurately measures the slope (neglecting errors due to the derivative approximation and non-simultaneous measurements), the phase shift due to slant range measurements causes the measured slope to be greater than the actual slope at every point except at the mean sea level.

## 2.8 Error in Slope Time Series due to First Derivative Approximation

Error occurs in the slope time series whenever the plane used to calculate the slope is tangent to a point other than the one for which the slope is being estimated. The estimate of the slope in any given direction is [Hesany, 1994]

$$\hat{s}(r, t) = \frac{z(r + \frac{\Delta r}{2}, t) - z(r - \frac{\Delta r}{2}, t)}{\Delta r} \quad \text{Eq. 2.8.1}$$

assuming the plane is tangent to the midpoint of the radar footprints. The true wave height is given by

$$z(r, t) = A \cos(\omega t + kr) \quad \text{Eq. 2.8.2}$$

from which the slope is obtained as:

$$s(r,t) = -kA \sin(\omega t + kr) \quad \text{Eq. 2.8.3}$$

Substituting Eq. 2.8.2 into Eq. 2.8.1 results in:

$$\hat{s}(r, t) = s(r, t) \left[ \frac{\sin\left(\frac{k\Delta r}{2}\right)}{\frac{k\Delta r}{2}} \right] \quad \text{Eq. 2.8.4}$$

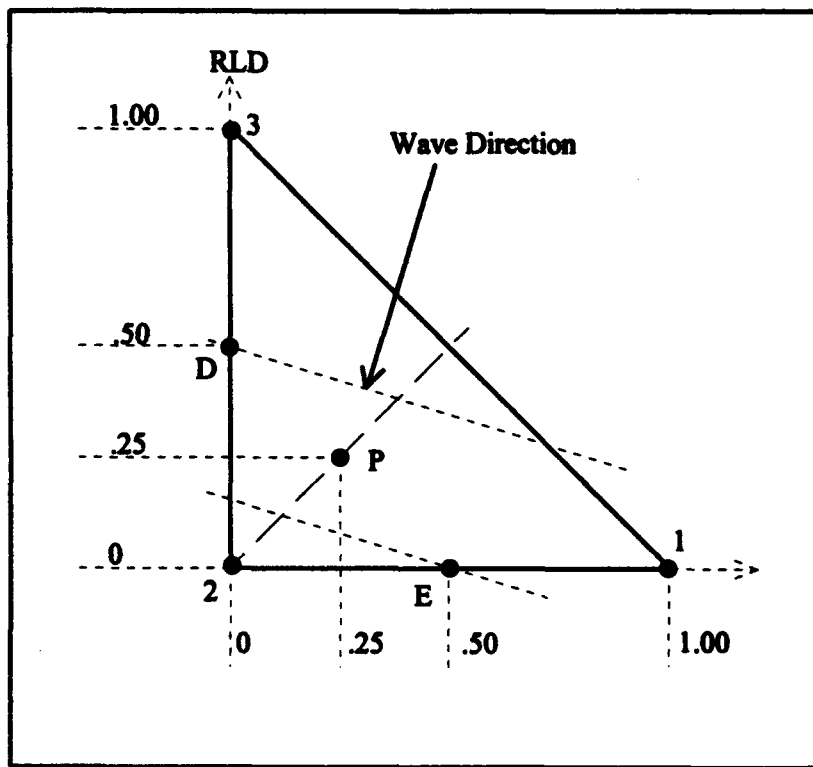


Figure 2.8.1. Location of point P which gives the minimum error in the derivative approximation.

Equation 2.8.1 assumes that we are estimating the slope at the midpoint of the three radar footprints. Actually, the point within the three radar footprints tangent to the plane is not stationary with respect to the three footprints. Of course, if it were stationary, there would be no error in the first order approximation of the derivative.

The location of the point where the slope is being estimated that gives the minimum amount of error in the first order approximation of the derivative depends upon the direction of oncoming waves with respect to the radar look direction. The approximation will have a minimum amount of error for slopes with respect to the RLD if the point lies along a line perpendicular to the wave direction and passing through point D (see Figure 2.8.1). Conversely, the approximation will have a minimum amount of error for slopes with respect to the cross direction if the point lies along a line perpendicular to the wave direction and passing through point E. The point of minimal error for both time series, then, lies along a line midway between and parallel to the lines passing through D and E. All such lines will pass through point P. However, if the radar is looking directly at the oncoming waves then, for the unidirectional waves being considered thus far, there is no slope in the cross direction. For such a case, point D will give the minimum error in the first order approximation.

If measurements are made with all three beams vertical,  $\Delta r$  in Eq. 2.8.4 is a constant. In such a case the error in the first order approximation depends only on the frequency of the waves and  $\Delta r$ . During the SAXON-FPN experiment, a common distance between the radar footprints at the mean sea level was 1.8 m. Figure 2.8.2 shows the relative error ( $[\hat{s}(r,t) - s(r,t)]/s(r,t)$ ) in the first order approximation of the derivative for waves of various frequencies.

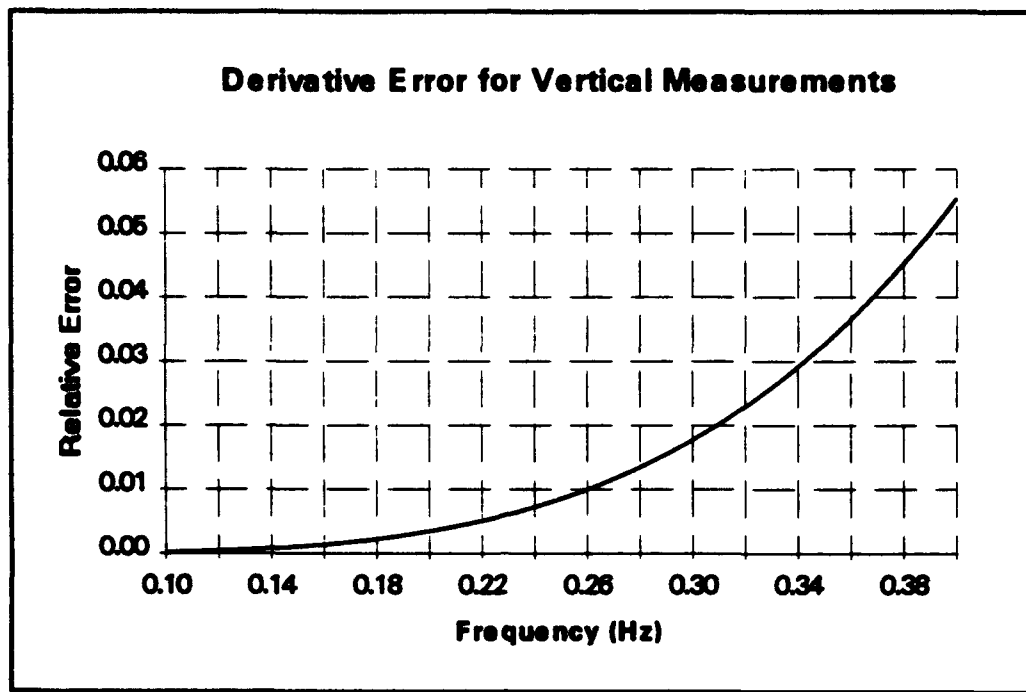


Figure 2.8.2. Relative error in the first order approximation of the derivative assuming all three beams are vertical.  $\Delta r = 1.8$  meters.

Although Fig 2.8.2 shows the error assuming all three beams are vertical, actual measurements were made along a slant range. Thus,  $\Delta r$  continuously changes and is a function of the phase of the ocean wave.

Figure 2.8.3 shows the derivative error for waves of various frequencies and heights assuming the measurements were made along a slant range. The higher frequency waves are steep—their corresponding heights are large relative to their length. The lower frequency waves, while not steep, are near the maximum height expected of waves near the Nordsee research platform.

As previously stated,  $\Delta r$  varies and is a function of the phase of the ocean wave. Figures 2.8.4a, b, and c illustrate the location and the amount of the error relative to the position along the wave. Figure 2.8.4a is the wave height time series for a steep 0.4 Hz wave when the radar is looking in the upwave direction. The time series from

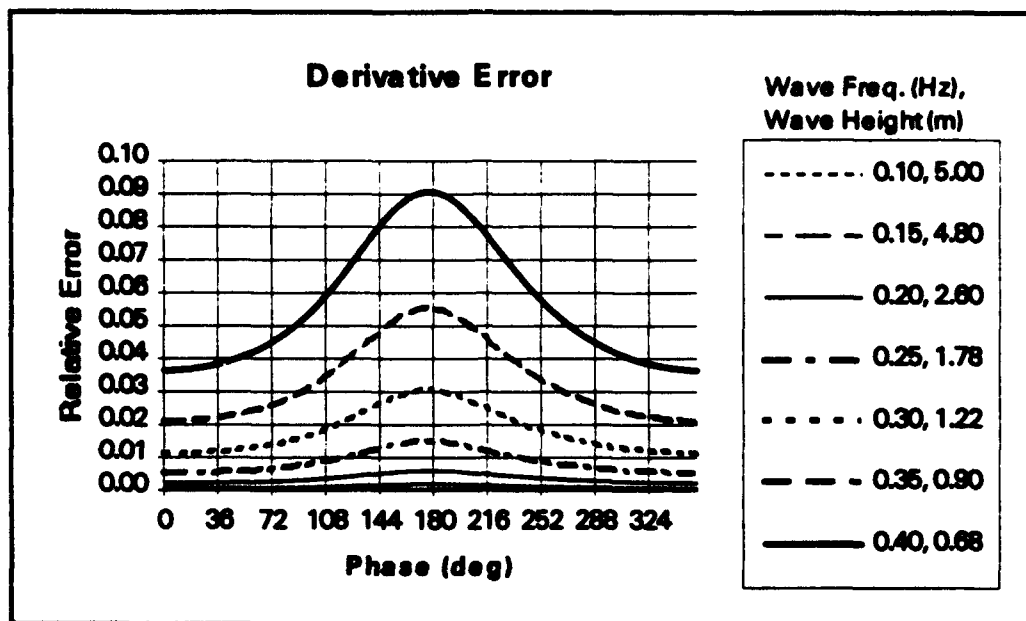


Figure 2.8.3. Error in the first of order approximation of the derivative. Measurements were made along a slant range. Incidence angle,  $47^\circ$ ; Antenna height, 20 m;  $\delta = 0^\circ$ , Wave direction,  $0^\circ$ , RLD,  $0^\circ$ .

beam 2 is not shown because it is identical to the time series from beam 1. Figure 2.8.4b shows the corresponding slope time series from the plane and from the point D in Fig. 2.8.1.

From Fig. 2.8.4, one can see that the largest error in the derivative approximation occurs near the trough of the wave. At this location  $\Delta r$  is the greatest because the footprints are a maximum distance from the radar. The smallest error occurs near the crest of the wave because at this location the footprints are a minimum distance from the radar.

From these results, one can see that the error due to the first order approximation is not very significant. Even for the steepest wave, the maximum error of 9% is less than  $2^\circ$ . Furthermore, the majority of energy-bearing waves during the SAXON-FPN

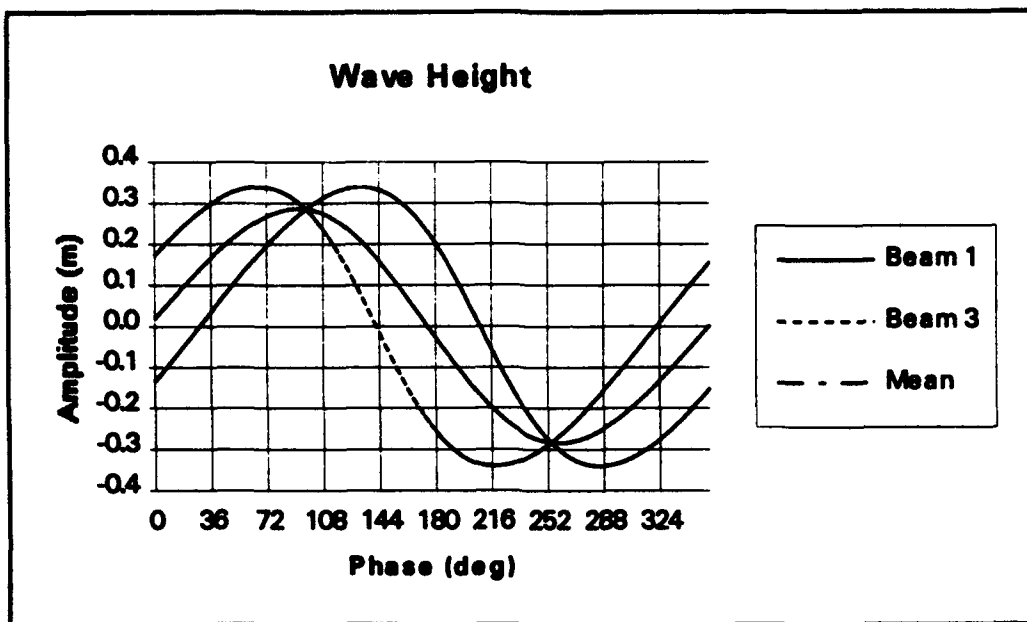


Figure 2.8.4. Wave height time series (a), corresponding slope time series (b), and relative error due to derivative approximation (c). Measurements were made along a slant range. Incidence angle,  $47^\circ$ ; Antenna height, 20 m;  $\delta = 0^\circ$ , Wave frequency, 0.4 Hz, Wave direction,  $0^\circ$ , RLD,  $0^\circ$ .

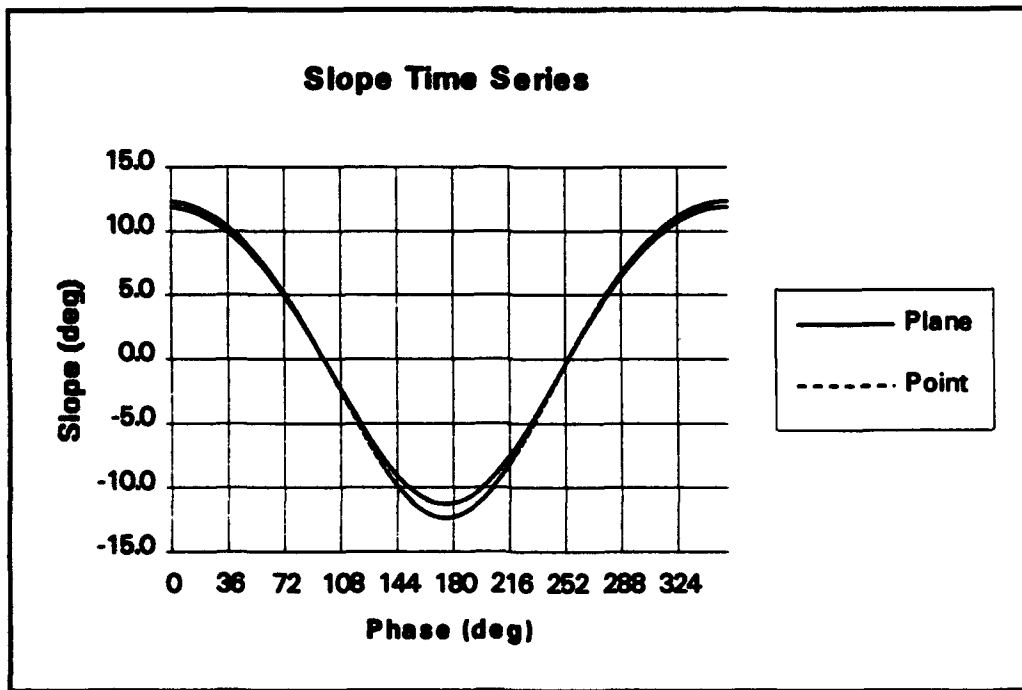


Figure 2.8.4b. Slope time series corresponding to the wave height time series in (a). This illustrates where along the wave the error is located.

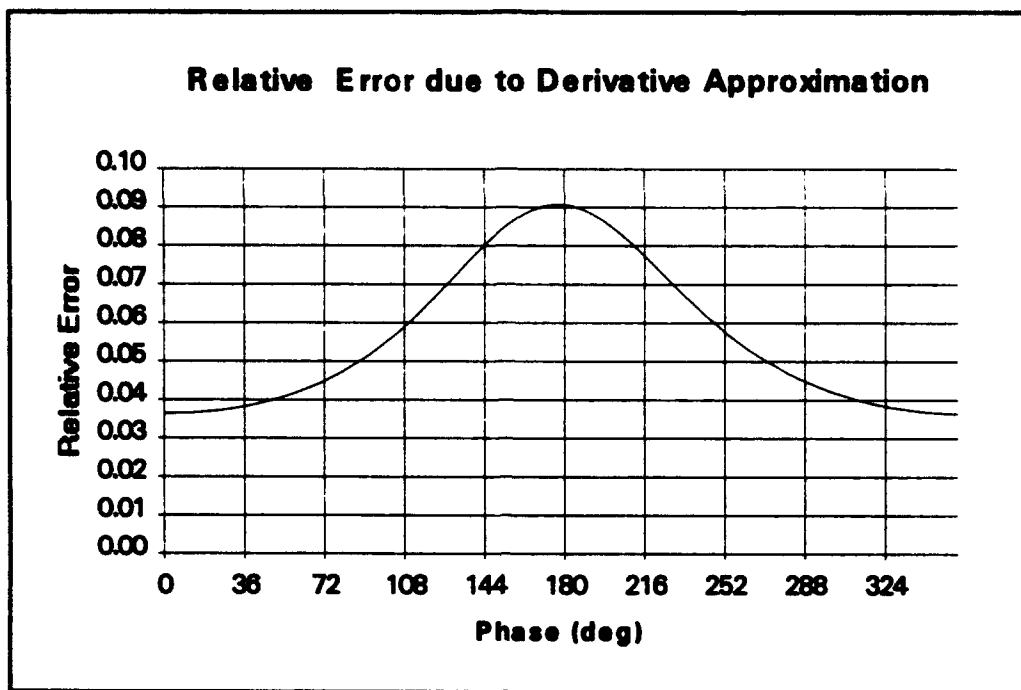


Figure 2.8.4c. Relative error in derivative approximation corresponding to the wave height time series in (a). This illustrates where along the wave the error is located.

experiment were between 0.1 Hz and 0.2 Hz. For waves in this frequency band, the derivative error is less than 1%.

## 2.9 Error in Slope Time Series due to Non-Simultaneous Measurements

Errors also occur in the slope measurements due to the fact that the range measurements are not simultaneous but instead are sampled 33 ms apart. Although 33 ms is a small amount of time compared to the period of waves which are measured (2.5 sec - 10 sec), enough movement in the ocean surface occurs during this time so that this problem cannot be neglected. The finite switching time between feeds causes a phase shift in the recorded time series of beams 2 and 3 (recall section 2.6).

Since the delay between the measurement at beam 3 and the measurement at beam 1 is 66 ms, the phase error of beam 3 will be twice as great as the error in beam 1 (see Figure 2.9.1).

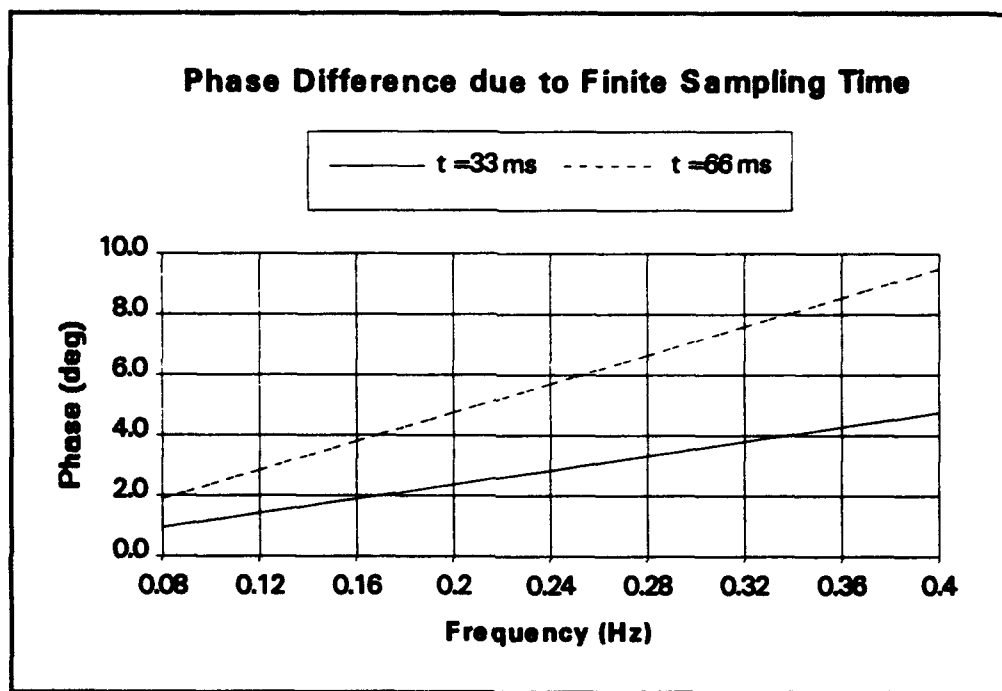


Figure 2.9.1. Phase difference in ocean wave due to a finite sampling time. This data assumes that the footprints are fixed with respect to one another.

The error due to non-simultaneous measurements depends upon the wave steepness. For long, low frequency waves, the height does not change as rapidly as it does for short, high frequency waves. However, the real importance here isn't the relative error but the absolute error. In section 2.6, it was noted that the finite sampling time did not have much of an effect on the mean wave height time series. From Figure 2.9.2, one can see that for these steep waves the error due to a finite sampling time is on the order of several centimeters. (Note that the errors shown are only for a sampling interval of 33 ms. Beam 3 will have twice as much error shown

because it is sampled 66 ms after beam 1.) This is not very significant for the calculation of the mean wave height time series, but it is significant for the calculation of the slope time series. The absolute error is greater for the low frequency waves because they have higher wave heights.

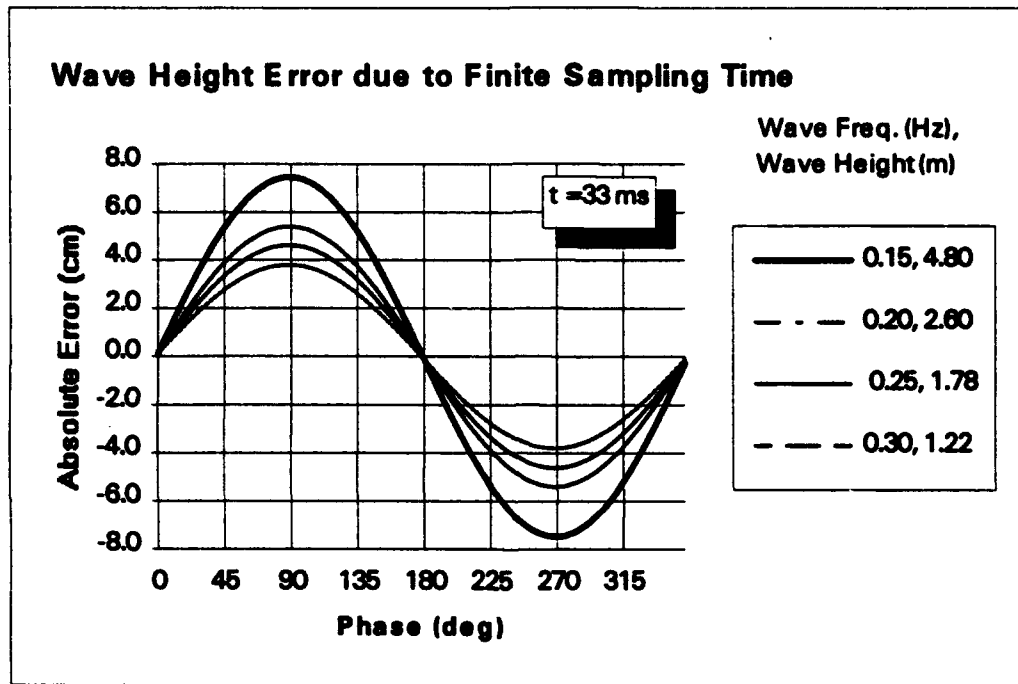


Figure 2.9.2. Absolute error in measured wave heights for waves of various frequencies and heights. The error is due to a finite sampling interval. Beams 1 and 2 are assumed to measure vertically.

If the footprints of beams 1 and 2 are assumed to be 1.8 m apart, then an overestimate of the wave height by beam 2 of 7 cm will result in a measured slope in the x direction of

$$\tan^{-1}\left(\frac{.07}{1.8}\right) \approx 2^\circ$$

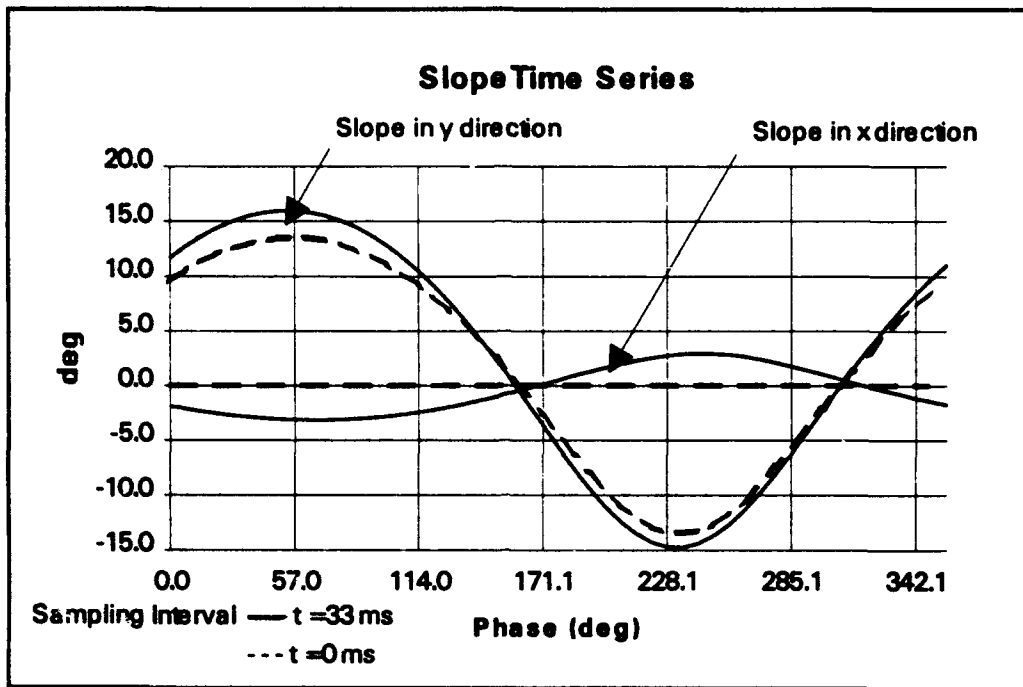


Figure 2.9.3. Slope time series calculated with a finite sampling interval between beam measurements vs. no sampling interval between beam measurements. All time series were calculated from the plane formed by the footprints along the slant range. Incidence angle,  $47^\circ$ ; Antenna height, 20 m;  $\delta = 0^\circ$ , Wave frequency, 0.2 Hz, Wave direction,  $0^\circ$ , RLD,  $0^\circ$ .

An over-estimate of the height by beam 3 will cause the plane to have an even greater slope in the x direction and also cause the plane to have a positive y slope. On the back face of the wave the opposite happens. The result of this is that the slope is over-estimated in both the y and x directions at all times. Evidence of this can be seen in Figure 2.9.3.

In Chapters 3 and 4, the effects of these errors on the VSG's capability to determine ocean parameters such as wave height PSD, the mean wave directional spectrum, and the directional width spectrum will be analyzed.

### 3. Determination of Mean Wave Direction and the Effect of Errors

#### 3.1 Two-Dimensional Slope Distribution and Best Fit Ellipse

The distribution of wave slopes measured during the SAXON experiment is nearly normal in both the radar look direction and the cross direction (see Figure 3.1.1). Thus, the distribution of slopes is approximately bivariate Gaussian.

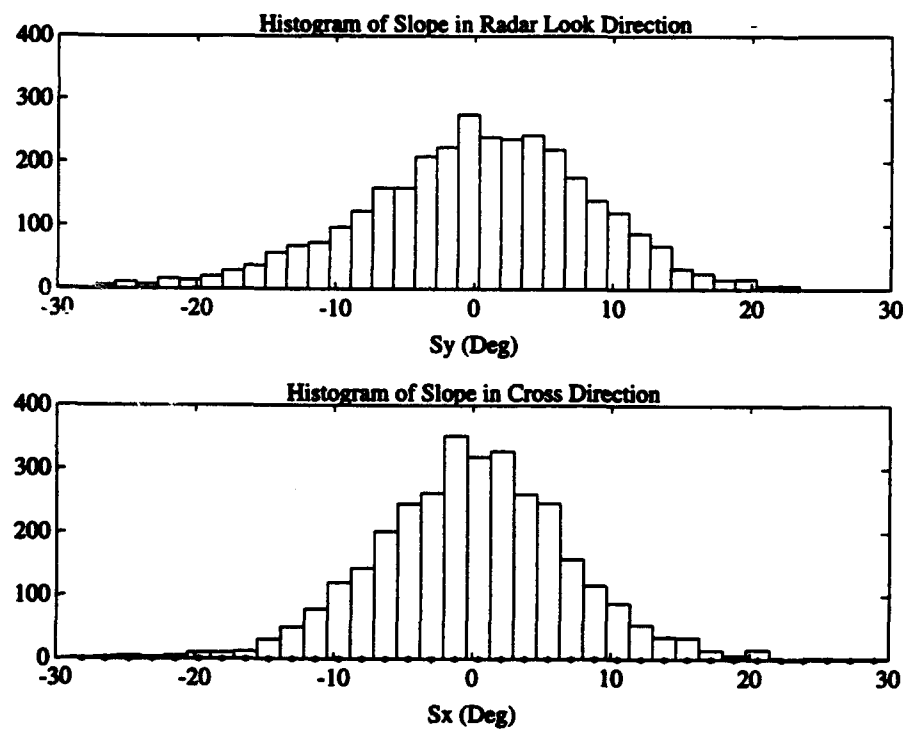


Fig. 3.1.1 Histogram of x and y slope components for data run 1749 on 11/19/90.

The pdf of a bivariate normal distribution is well known and is given by [Shanmugan and Breipohl]:

$$f(x, y) = \frac{1}{2\pi\sigma_x\sigma_y\sqrt{1-\rho^2}} \exp\left(\frac{-1}{2}g(x, y)\right) \quad \text{Eq. 3.1.1}$$

where

$$g(x, y) = \frac{1}{1-\rho^2} \left[ \left( \frac{x-\mu_x}{\sigma_x} \right)^2 - \frac{2\rho(x-\mu_x)(y-\mu_y)}{\sigma_x \sigma_y} + \left( \frac{y-\mu_y}{\sigma_y} \right)^2 \right] \quad \text{Eq. 3.1.2}$$

and  $\sigma$ ,  $\mu$ , and  $\rho$  represent the standard deviation, mean, and correlation coefficient respectively. Since  $\sigma_x$ ,  $\sigma_y$ , and  $\rho$  are known, Eq. 3.1.1 can be set to a constant and with some simple algebra gives the equation for the isoprobability lines as:

$$c(1-\rho^2) = \left( \frac{x-\mu_x}{\sigma_x} \right)^2 - \frac{2\rho(x-\mu_x)(y-\mu_y)}{\sigma_x \sigma_y} + \left( \frac{y-\mu_y}{\sigma_y} \right)^2 \quad \text{Eq. 3.1.3}$$

Comparing this with a standard equation for an ellipse,

$$A(x-\mu_x)^2 + 2B(x-\mu_x)(y-\mu_y) + C(y-\mu_y)^2 = D \quad \text{Eq. 3.1.4}$$

we see that the isoprobability contours form a family of ellipses. The coefficients in Eq. 3.1.4 are:

$$\begin{aligned} A &= \sigma_y^2 & B &= -\rho\sigma_x\sigma_y \\ C &= \sigma_x^2 & D &= c(1-\rho^2)\sigma_x^2\sigma_y^2 \end{aligned} \quad \text{Eq. 3.1.5}$$

The desired parameters of the ellipse--the length of the major axis (2a), the length of the minor axis (2b), and the ellipse orientation ( $\theta$ )--can be determined from the knowledge of these four coefficients [Batschelet, 1981]. The parameters of the ellipse are:

$$a = \sqrt{\frac{2D}{A+C-R}} \quad b = \sqrt{\frac{2D}{A+C+R}}$$

$$\theta = \tan^{-1}\left(\frac{2B}{A-C-R}\right) \quad \text{Eq. 3.1.6}$$

where  $R$  is given by  $\sqrt{(A-C)^2 + 4B^2}$ .

Since the moments of the slope distribution are readily obtainable, it is a simple procedure to fit an ellipse to the slope distribution. The MATLAB 3.5 program `ellipsef.m` in Appendix A was written to determine the parameters given in Eq. 3.1.6, and also calculates the parametric equations that are used to draw the ellipse.

### 3.2 Mean Wave Direction and Statistics of Slope Distribution

The geometry of the Gaussian-fit ellipse yields information about the ocean waves including their primary direction of travel and their degree of long-crestedness. Figure 3.2.1 is a two-dimensional slope distribution and its corresponding Gaussian-fit ellipse calculated from data recorded during the SAXON-FPN experiment. The variable  $y$  in Eq. 3.1.1 represents the radar look direction, while  $x$  represents the cross direction. When the constant  $c$  in Eq. 3.1.3 is set equal to one, approximately 40% of the volume under the bivariate normal distribution will lie above the ellipse. The particular distribution shown in Fig. 3.2.1 is from data taken between 1649-1739 UTC on Nov. 19, 1990.

The orientation of the major axis indicates the mean direction of wave travel during the time data were recorded. In the direction of mean wave travel, the variance of the wave slopes is greater than in the direction along the crest of the waves. Thus,

the data tends to spread farther from the origin in the direction of wave travel than in the cross direction.

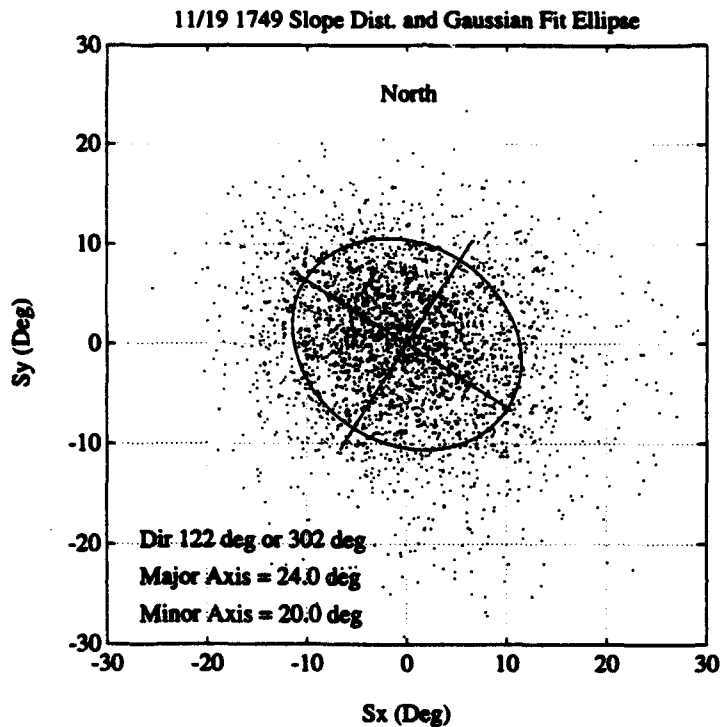


Fig. 3.2.1. Slope Distribution and Best Fit Ellipse for data run 1749 on 11/19/90. Wave direction =  $122^\circ$  or  $302^\circ$ , Major Axis =  $24.0^\circ$ , Minor Axis =  $20.0^\circ$ . The top of the diagram is North.

If the ocean waves are long-crested, then the variance of wave slopes will be much greater in the direction of wave travel than along the crest of the waves. How long crested the waves actually are can be determined by the ratio of the major axis length to the minor axis length. The larger the ratio, the more long-crested the waves are. From Fig. 3.2.1, we see that the length of the major axis is  $24.0^\circ$  and the length

of the minor axis is  $20.0^\circ$ . Clearly, the waves within the radar footprint during run 1749 were not long-crested.

In addition to giving the mean direction of wave travel, the Gaussian-fit ellipse enables statistics of the slope distribution to be easily obtained. When  $c$  in Eq. 3.1.3 is equal to one, the variance of the slope in the x-direction (East) is equal to the horizontal distance from the center of the ellipse to the farthest point in the x-direction on the ellipse. In a similar manner, the vertical component from the center of the ellipse to the farthest point in the y-direction on the ellipse is equal to the variance of the slope in the y-direction (North).

Although the orientation of the major axis gives the mean direction of wave travel, note that there is a  $180^\circ$  ambiguity in that direction. For example, in Fig. 3.2.1 we do not know if the waves are traveling toward  $122^\circ$  or if they are traveling toward  $302^\circ$ .

### **3.3 Resolving the Directional Ambiguity using a Histogram of Slopes**

The  $180^\circ$  directional ambiguity in Fig. 3.2.1 can be resolved by taking advantage of the asymmetry of ocean waves. Since the VSG recorded data at a constant rate of time, the VSG recorded more data from the back side of the waves than the front. By calculating the directional histogram of the two-dimensional slope time series, this asymmetry will show up as a shift in the centroid of the histogram. If an ellipse is fit to the histogram of the slope data, the origin of the ellipse will be shifted in the mean direction from which waves are traveling.

This procedure is illustrated with the data from Figure 3.2.1 and is shown in Figure 3.3.1. Due to the asymmetry of ocean waves, the center of the histogram has

shifted from the center. One can see from Fig. 3.3.1 that the mean direction from which the waves were traveling was  $301^\circ$ .

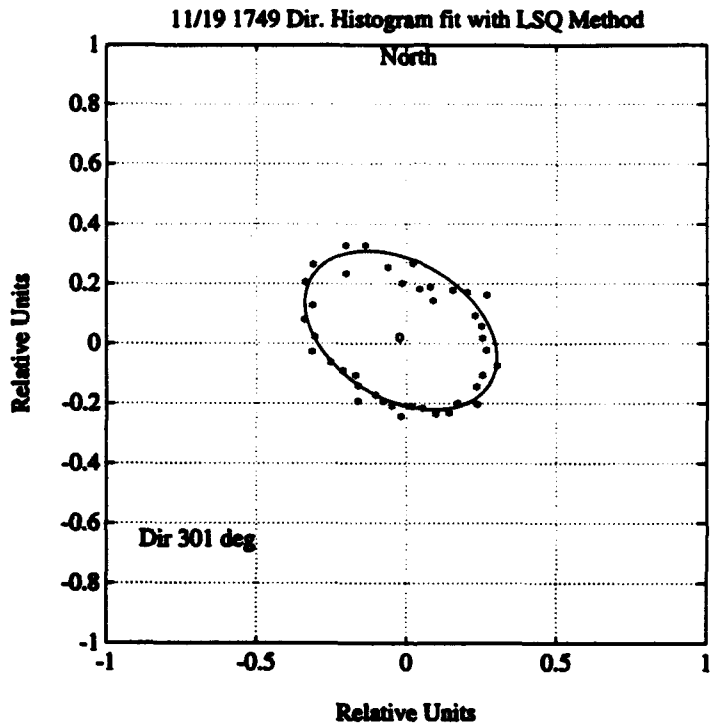


Fig. 3.3.1. Directional Histogram and Ellipse fit with Least Square Method for run 1749 on 11/19/90. The deviation of the ellipse center from the origin resolves the directional ambiguity.

The ellipse in Fig. 3.3.1 indicates that the mean direction of wave travel during the time data were recorded was  $301^\circ$ . This differs from the  $302^\circ$  suggested from Fig. 3.2.1 because the ellipse was fit with a different method. In Fig. 3.2.1, the data are nearly bivariate Gaussian. The moments of the two-dimensional slope distribution are used to fit an ellipse to the data. Clearly, the data in Fig. 3.3.1 are not bivariate

Gaussian. For this reason the method of least squares was used to fit an ellipse to the data in Fig. 3.3.1.

Given values of  $x$  and  $y$ , we want to minimize

$$F = \sum_{i=1}^M (Ax_i^2 + Bx_iy_i + Cy_i^2 + Dx_i + Ey_i - 1)^2 \quad \text{Eq. 3.3.1}$$

Taking the derivative of  $F$  with respect to each of the five constants,  $\lambda_j$ , and setting them equal to zero results in

$$\begin{aligned} \frac{\partial F}{\gamma_j} = & \\ 2 \sum_{i=1}^M & (Ax_i^2 + Bx_iy_i + Cy_i^2 + Dx_i + Ey_i - 1)(x_i^2) = 0 \\ 2 \sum_{i=1}^M & (Ax_i^2 + Bx_iy_i + Cy_i^2 + Dx_i + Ey_i - 1)(x_iy_i) = 0 \\ & \vdots \\ 2 \sum_{i=1}^M & (Ax_i^2 + Bx_iy_i + Cy_i^2 + Dx_i + Ey_i - 1)(y_i) = 0 \end{aligned} \quad \text{Eq. 3.3.2}$$

In matrix form this can be rewritten as

$$\begin{bmatrix} x_i^2 x_i^2 & x_i y_i x_i^2 & y_i^2 x_i^2 & x_i x_i^2 & y_i x_i^2 \\ x_i^2 x_i y_i & x_i y_i x_i y_i & y_i^2 x_i y_i & x_i x_i y_i & y_i x_i y_i \\ x_i^2 y_i^2 & x_i y_i y_i^2 & y_i^2 y_i^2 & x_i y_i^2 & y_i y_i^2 \\ x_i^2 x_i & x_i y_i x_i & y_i^2 x_i & x_i x_i & y_i x_i \\ x_i^2 y_i & x_i y_i y_i & y_i^2 y_i & x_i y_i & y_i y_i \end{bmatrix} \begin{bmatrix} A \\ B \\ C \\ D \\ E \end{bmatrix} = \begin{bmatrix} x_i^2 \\ x_i y_i \\ y_i^2 \\ x_i \\ y_i \end{bmatrix} \quad \text{Eq. 3.3.4}$$

Thus,

$$\begin{bmatrix} A \\ B \\ C \\ D \\ E \end{bmatrix} = \begin{bmatrix} x_i^2 x_i^2 & x_i y_i x_i^2 & y_i^2 x_i^2 & x_i x_i^2 & y_i x_i^2 \\ x_i^2 x_i y_i & x_i y_i x_i y_i & y_i^2 x_i y_i & x_i x_i y_i & y_i x_i y_i \\ x_i^2 y_i^2 & x_i y_i y_i^2 & y_i^2 y_i^2 & x_i y_i^2 & y_i y_i^2 \\ x_i^2 x_i & x_i y_i x_i & y_i^2 x_i & x_i x_i & y_i x_i \\ x_i^2 y_i & x_i y_i y_i & y_i^2 y_i & x_i y_i & y_i y_i \end{bmatrix}^{-1} \begin{bmatrix} x_i^2 \\ x_i y_i \\ y_i^2 \\ x_i \\ y_i \end{bmatrix} \quad \text{Eq. 3.3.5}$$

The MATLAB 3.5 program lsqfit.m was written to calculate the constants A, B, C, D, and E given a set of x and y values.

After determining the values of A, B, C, D, and E, the parameters of the ellipse had to be derived as a function of the constants. Since F was assigned to be -1, the equation of the ellipse is

$$Ax^2 + Bxy + Cy^2 + Dx + Ey - 1 = 0 \quad \text{Eq. 3.3.6}$$

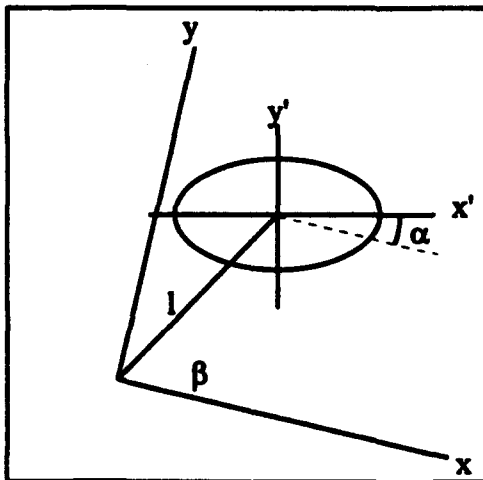


Figure 3.3.2. Geometry used to obtain ellipse parameters.

The first step is to write the equation of the ellipse in the x'-y' coordinate system. From Figure 3.3.2, we see that the x'-y' coordinate system is translated and rotated.

The transformation from the x-y coordinate system to the primed coordinate system is given by

$$\begin{aligned} x &= l \cos(\beta) + x' \cos(\alpha) - y' \sin(\alpha) \\ y &= l \sin(\beta) + x' \sin(\alpha) + y' \cos(\alpha) \end{aligned} \quad \text{Eq. 3.3.7}$$

Substituting the values of x and y into Eq. 3.3.6 gives:

$$\begin{aligned} &A(l^2 \cos^2(\beta) + 2lx' \cos(\alpha) \cos(\beta) - 2ly' \sin(\alpha) \cos(\beta) + x'^2 \cos^2(\alpha) \\ &\quad - 2x'y' \sin(\alpha) \cos(\alpha) + y'^2 \sin^2(\alpha)) \\ &+ B(l^2 \sin(\beta) \cos(\beta) + lx' \sin(\alpha) \cos(\beta) + ly' \cos(\alpha) \cos(\beta) + lx' \cos(\alpha) \sin(\beta) \\ &\quad + x'^2 \sin(\alpha) \cos(\alpha) + x'y' \cos^2(\alpha) - ly' \sin(\alpha) \sin(\beta) - x'y' \sin^2(\alpha) \\ &\quad - y'^2 \sin(\alpha) \cos(\alpha)) \\ &+ C(l^2 \sin^2(\beta) + 2lx' \sin(\alpha) \sin(\beta) + 2ly' \sin(\beta) \cos(\alpha) + x'^2 \sin^2(\alpha) \\ &\quad + 2x'y' \sin(\alpha) \cos(\alpha) + y'^2 \cos^2(\alpha)) \\ &+ D(l \cos(\beta) + x' \cos(\alpha) - y' \sin(\alpha)) \\ &+ E(l \sin(\beta) + x' \sin(\alpha) + y' \cos(\alpha)) - 1 = 0 \end{aligned} \quad \text{Eq. 3.3.8}$$

Now, to get the true ellipse equation we need to eliminate the  $x'y'$  terms. Doing so gives:

$$\begin{aligned} &-2Ax'y' \sin(\alpha) \cos(\alpha) + Bx'y' \cos^2(\alpha) - Bx'y' \sin^2(\alpha) \\ &+ 2Cx'y' \sin(\alpha) \cos(\alpha) = 0 \end{aligned} \quad \text{Eq. 3.3.9}$$

Simplifying, we get

$$\alpha = \frac{1}{2} \tan^{-1} \left( \frac{B}{A - C} \right) \quad \text{Eq. 3.3.10}$$

for the angle between the x-axis and the x'-axis. Now the equation of the ellipse in the primed coordinate system is

$$\begin{aligned}
 & (A \cos^2(\alpha) + B \sin(\alpha) \cos(\alpha) + C \sin^2(\alpha))x'^2 \\
 & + (A \sin^2(\alpha) - B \sin(\alpha) \cos(\alpha) + C \cos^2(\alpha))y'^2 \\
 & + (2Al \cos(\alpha) \cos(\beta) + Bl \sin(\alpha) \cos(\beta) + Bl \cos(\alpha) \sin(\beta) \\
 & \quad + 2Cl \sin(\alpha) \sin(\beta) + D \cos(\alpha) + E \sin(\alpha))x' \\
 & + (-2Al \sin(\alpha) \cos(\beta) + Bl \cos(\alpha) \cos(\beta) - Bl \sin(\alpha) \sin(\beta) \\
 & \quad + 2Cl \sin(\beta) \cos(\alpha) - D \sin(\alpha) + E \cos(\alpha))y' \\
 & + Al^2 \cos^2(\beta) + Bl^2 \sin(\beta) \cos(\beta) + Cl^2 \sin^2(\beta) \\
 & + Dl \cos(\beta) + El \sin(\beta) - 1 = 0
 \end{aligned} \tag{Eq. 3.3.11}$$

Since  $\alpha$ ,  $\beta$ ,  $l$ ,  $A$ ,  $B$ ,  $C$ ,  $D$ , and  $E$  are known, Eq. 3.3.11 can be written as

$$Gx'^2 + Hy'^2 + Ix' + Jy' + K = 0 \tag{Eq. 3.3.12}$$

Dividing through by GH and rearranging

$$\frac{x'^2}{H} + \frac{Ix'}{GH} + \frac{y'^2}{G} + \frac{Jy'}{GH} = \frac{-K}{GH} \tag{Eq. 3.3.13}$$

Now, if we complete the square and do some more rearranging we get

$$\frac{\left(x' + \frac{I}{2G}\right)^2}{\frac{-4KGH + HI^2 + GJ^2}{4G^2H}} + \frac{\left(y' + \frac{J}{2H}\right)^2}{\frac{-4KGH + HI^2 + GJ^2}{4GH^2}} = 1 \tag{Eq. 3.3.14}$$

Thus, we see that the parameters of interest are:

$$\text{Center of Ellipse } \left( \frac{-I}{2G}, \frac{-J}{2H} \right) \quad \text{Eq. 3.3.15}$$

$$\text{Length of Major Axis } 2 \sqrt{\frac{-4KGH + HI^2 + GJ^2}{4G^2H}} \quad \text{Eq. 3.3.16}$$

$$\text{Length of Minor Axis } 2 \sqrt{\frac{-4KGH + HI^2 + GJ^2}{4GH^2}} \quad \text{Eq. 3.3.17}$$

The MATLAB 3.5 program dirdist2.m in Appendix A uses these values to plot the least-square-fit ellipse to the histogram of slope data. If  $G^2H$  is larger than  $GH^2$ , then the length of the major axis will be given by Eq. 3.3.17 and the length of the minor axis will be given by Eq. 3.3.16.

### 3.4 Effect of Inherent Measurement Errors on Determination of Direction

In Chapter 2 the inherent errors involved with measurements made by the VSG were analyzed. Now, we would like to know what affect those errors have on determining the mean wave direction using the procedure described in sections 3.1 - 3.3.

Figure 3.4.1 shows a two-dimensional slope distribution for a simulated ocean surface. In this case and in the following examples the waves are coming from  $30^\circ$ , and have a frequency and amplitude of 0.2 Hz and 1.5 m respectively. This is an

ideal case in which the slope is measured at a single point. Ideally, we would like the VSG to give the same results, but due to the inherent errors there will be some differences. The histogram is not shown because with the simulated ocean surface there is no asymmetry to take advantage of.

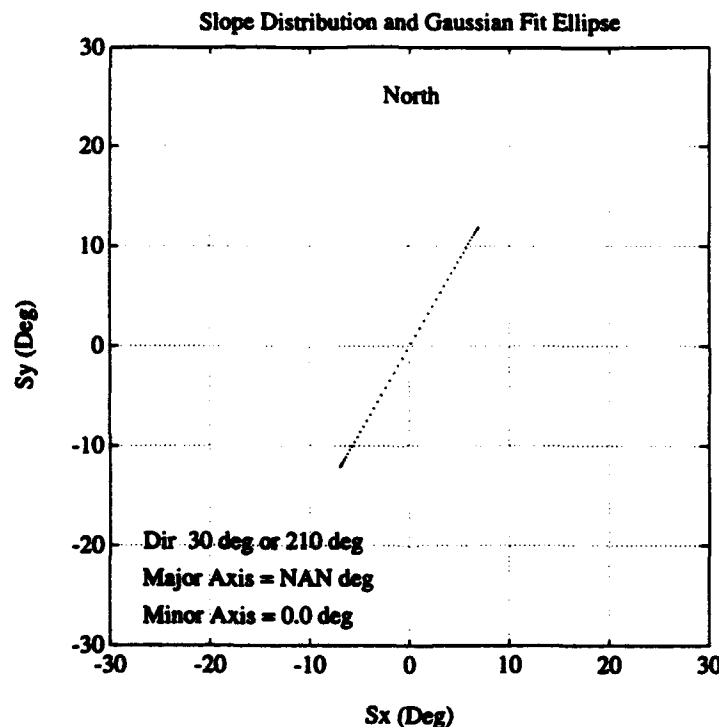


Figure 3.4.1. Slope distribution of simulated ocean surface. Slope was calculated analytically from a single point. Wave frequency, 0.2 Hz, Wave height = 3 m,  $\delta = 0^\circ$ , True wave direction,  $30^\circ$ ; RLD,  $0^\circ$ .

Figure 3.4.2 shows the slope distribution for the same ocean surface as in Fig. 3.4.1. The difference is that in this case the slope was calculated with three vertical beams making simultaneous measurements. Thus, it illustrates the error due to the first derivative approximation. We see from Fig. 3.4.2 that the derivative

approximation has the effect of widening ellipse (the ratio of the major axis length to minor axis length is reduced), albeit slightly. This occurs because the slope time series evaluated from the plane formed by the radar footprints is no longer a true sinusoid. Recall from section 2.8 that the derivative approximation has the effect of modulating the sinusoidal function by a sinc function.

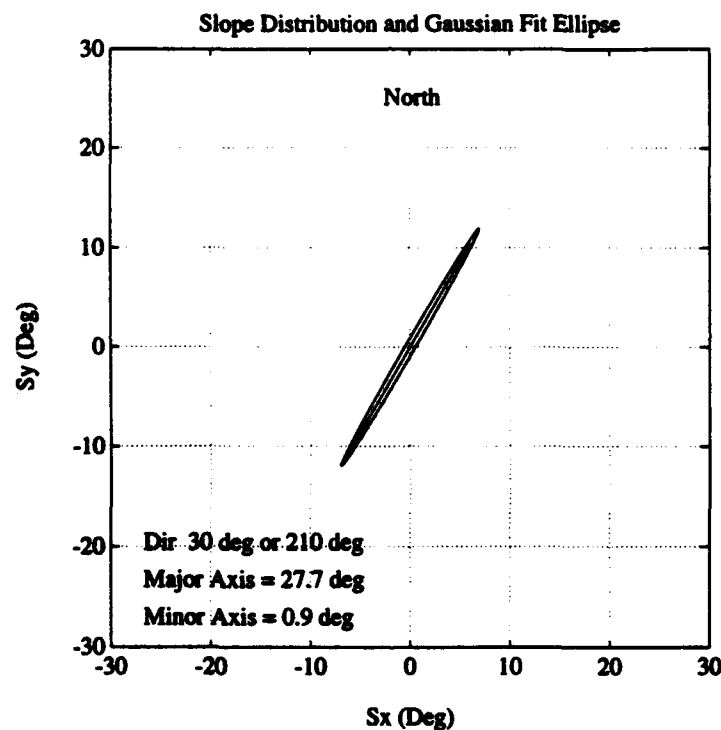


Figure 3.4.2. Slope distribution of simulated ocean surface. Slope was calculated from 3 vertical beams with simultaneous measurements. Wave frequency, 0.2 Hz, Wave height = 3 m,  $\delta = 0^\circ$ , True wave direction,  $30^\circ$ ; RLD,  $0^\circ$ .

Figure 3.4.3 shows what happens when measurements are made simultaneously along a slant range. Notice that the ratio of the major axis length to the minor axis

length is slightly less than in Fig. 3.4.2. This occurs because of the increased error in the derivative approximation when measuring along a slant range (recall section 2.8).

In Fig. 3.4.3, the orientation of the major axis indicates that the waves are coming from  $30^\circ$ --the correct determination. Thus, the error due to slant-range measurement and the derivative approximation has no appreciable affect on the determination of the mean direction of wave travel.

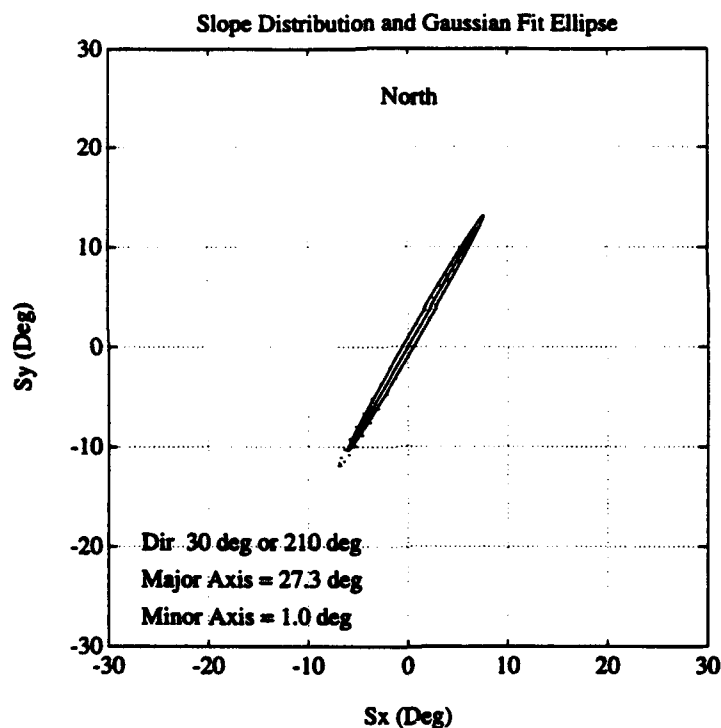


Figure 3.4.3. Slope distribution of simulated ocean surface. Slope was calculated along a slant range with simultaneous measurements. Incidence angle,  $47^\circ$ ; Antenna Height, 20 m; Wave frequency, 0.2 Hz; Wave height, 3 m;  $\delta = 0^\circ$ ; RLD,  $0^\circ$ ; True wave direction,  $30^\circ$ .

Even though slant-range measurement causes the VSG to over-estimate the slope in both directions at every point in time (see section 2.7), it has no noticeable effect

on the determination of the mean wave direction. The reason for this is that the ratio  $\frac{S_y}{S_x}$  remains approximately the same at all times. Thus, the mean direction of wave travel, which is determined by  $\tan^{-1}\left(\frac{S_y}{S_x}\right)$ , is not affected by slant range measurement.

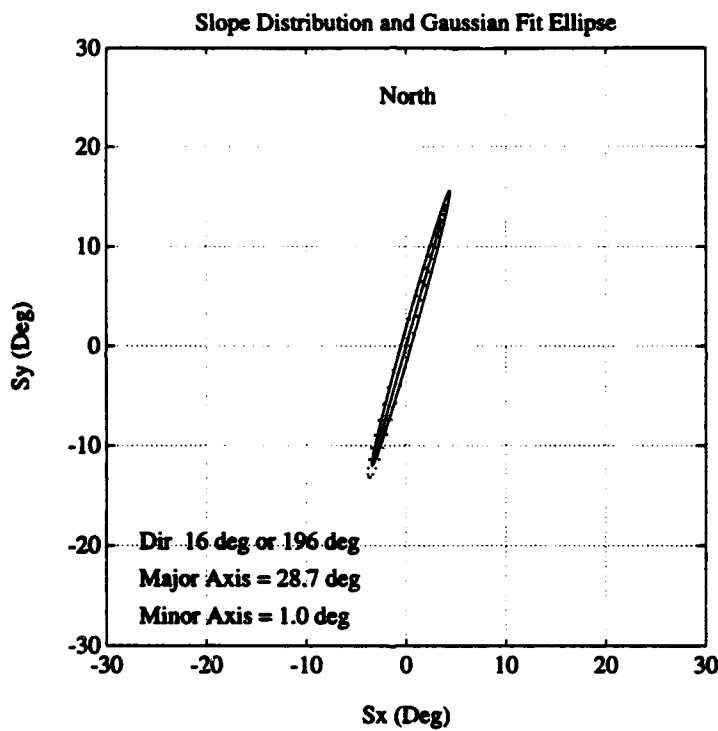


Figure 3.4.4. Slope distribution of simulated ocean surface. Slope was calculated along a slant range with non-simultaneous measurements. Incidence angle, 47°; Antenna Height, 20 m; Wave frequency, 0.2 Hz; Wave height, 3 m;  $\delta = 0^\circ$ ; RLD, 0°; True wave direction, 30°.

The most serious error, as far as determining mean wave direction is concerned, is due to a finite switching time between feeds. Figure 3.4.4 shows the results when all sources of error are taken into account. The slope is calculated from the plane

formed by the footprints whose locations are measured along a slant range, non-simultaneously. From Fig. 3.4.4 we see that the VSG would measure a linear, long-crested, sinusoidal wave train that is coming from  $30^\circ$  as coming from  $16^\circ$ . In this case, then, the finite time between measurements causes the VSG to estimate the mean wave direction  $14^\circ$  to the left of where the waves are actually coming from.

Figure 3.4.5 shows the results when the VSG measures the same ocean surface with 33 Hz switching. This shows that increasing the switching rate by a factor of 3.3 significantly improves the determination of the mean wave direction. If greater accuracy is required, Figure 3.4.6 shows the results if the feeds are switched every 3 ms. We see that at this rate the error is virtually nil.

In conclusion, then, the mean wave direction of ocean waves can be estimated, with  $180^\circ$  ambiguity, by the orientation of the major axis of an ellipse that is fit to the two-dimensional slope distribution. The directional ambiguity can be resolved by taking advantage of the asymmetry of ocean waves. When an ellipse is fit to the histogram of the slope distribution, the center of the ellipse is shifted in the direction from which waves are coming.

The derivative approximation causes the width of the ellipse to increase, and measuring along a slant range causes the ellipse to widen even further. Non-simultaneous measurement, however, has the most significant effect on the determination of the mean wave direction. It causes the VSG to miscalculate the mean wave direction by a significant amount-- $14^\circ$  when  $15^\circ$  separates the RLD and the wave direction.

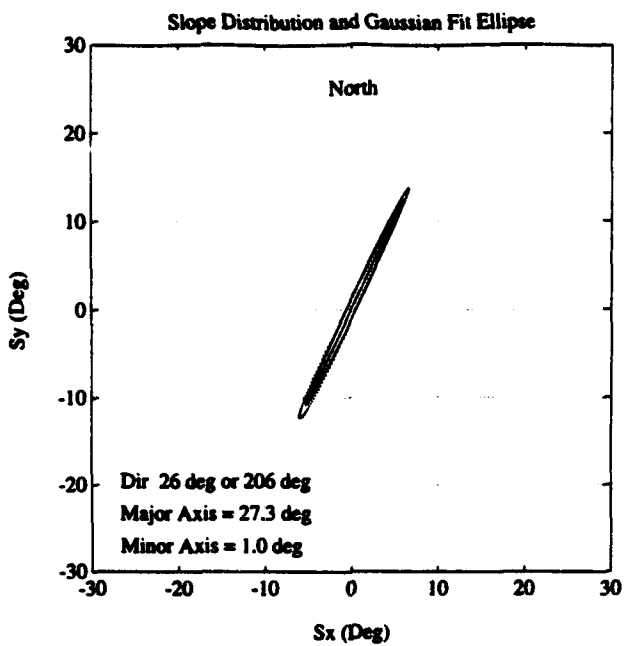


Figure 3.4.5. Slope distribution of simulated ocean surface. Slope was calculated along a slant range with 10 ms between each measurement. Incidence angle, 47°; Antenna Height, 20 m; Wave frequency, 0.2 Hz; Wave height, 3 m;  $\delta = 0^\circ$ ; RLD, 0°; True wave direction, 30°.

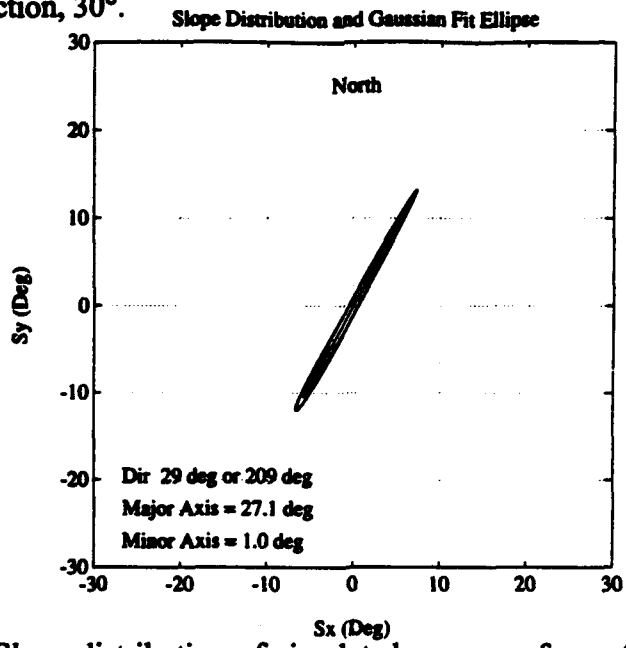


Figure 3.4.6. Slope distribution of simulated ocean surface. Slope was calculated along a slant range with 3 ms between each measurement. Incidence angle, 47°; Antenna Height, 20 m; Wave frequency, 0.2 Hz; Wave height, 3 m;  $\delta = 0^\circ$ ; RLD, 0°; True wave direction, 30°.

## 4. Determination of Ocean Spectra and Comparison with Pitch-and-Roll Buoy

### 4.1 Description of Pitch-and-Roll Buoy

During the SAXON-FPN experiment a WAVEC pitch-and-roll buoy was operated by the Federal Maritime and Hydrographic Agency of Hamburg, Germany [Plant and Alpers, 1991] (see Figure 4.1.1). Like the VSG, buoys have their own sources of error. The horizontal motion of the buoy must be accounted for [Kuik *et al.*, 1988]. The diameter of the buoy limits the length of ocean waves that can be accurately measured. In addition, mooring beneath the buoy may affect its capability to follow the water surface. In order to better understand the capability of directional wave measurement systems to accurately determine principal wave parameters, Allender and others [1989] studied the performance of a variety of such systems as part of the WADIC project.

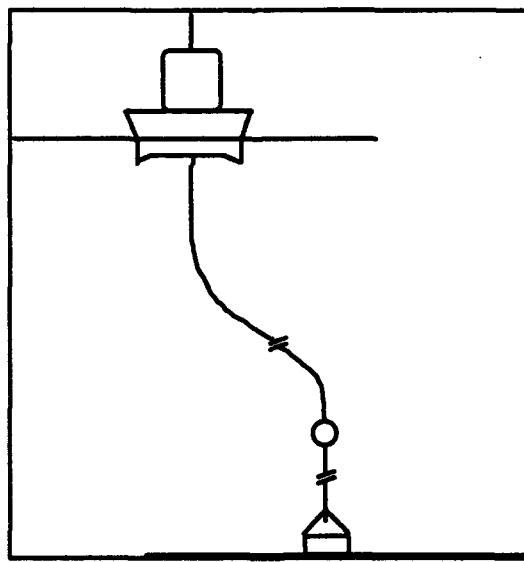


Figure 4.1.1. WAVEC buoy used during the SAXON-FPN experiment.

One such system studied during the WADIC project was the WAVEC buoy. The WAVEC buoy simultaneously determines three quantities--heave, pitch angle, and roll angle. Records of these time series are used to determine spectral parameters such as wave height spectrum, mean direction spectrum, and directional spread spectrum (see section 4.2). According to results from the WADIC project, the WAVEC buoy underestimates the wave height spectrum by 10% - 20% for high sea states and by 20% - 50% for low sea states for waves between 0.10 Hz and 0.25 Hz. These numbers are comparable with other buoy systems, and may be due to the buoy going through the wave when the wavelength approaches the diameter of the buoy. The mean wave direction at the spectral peak was generally within a few degrees of the best estimate data set (BEDS), and the wave spread estimate was not much different the BEDS either. However, there were a few problems with the WAVEC buoy capsizing in steep waves, and on one occasion it actually left its mooring. Thus, the length of the data record used to evaluate the accuracy of the buoy was not very long, and the results should be used accordingly.

#### **4.2 Directional Distribution of Ocean Waves and Longuet-Higgins Approach**

The pitch-and-roll buoy operated by the Federal Maritime and Hydrographic Agency recorded the vertical acceleration, the pitch-angle, and the roll-angle time series. With this information, the wave height spectrum, the mean-wave-direction spectrum, and the directional width spectrum can be calculated using the method developed by Longuet-Higgins et al., [1963]. The directional distribution of energy can be expanded in a Fourier series representation as:

$$D(\theta, \omega) = \frac{1}{2\pi} \left[ 1 + 2 \sum_{n=1}^{\infty} a_n(\omega) \cos(n\theta) + b_n(\omega) \sin(n\theta) \right] \quad \text{Eq. 4.2.1}$$

where

$$a_n(\omega) = \int_0^{2\pi} D(\theta, \omega) \cos(n\theta) d\theta$$

$$b_n(\omega) = \int_0^{2\pi} D(\theta, \omega) \sin(n\theta) d\theta \quad \text{Eq. 4.2.2}$$

The first four Fourier coefficients are related to the co- and cross-spectra of the time series of wave heights and slopes by [Kuik et al., 1988]:

$$a_1(\omega) = \frac{Q_{zz}}{\sqrt{C_{zz}(C_{xx} + C_{yy})}} \quad \text{Eq. 4.2.3}$$

$$b_1(\omega) = \frac{Q_{zy}}{\sqrt{C_{zz}(C_{xx} + C_{yy})}} \quad \text{Eq. 4.2.4}$$

$$a_2(\omega) = \frac{C_{xx} - C_{yy}}{C_{xx} + C_{yy}} \quad \text{Eq. 4.2.5}$$

$$b_2(\omega) = \frac{2C_{xy}}{C_{xx} + C_{yy}} \quad \text{Eq. 4.2.6}$$

where C represents co-spectra, Q represents quad-spectra, z represents the wave height, and x and y represent orthogonal slope components. It is also assumed that k, the wave number, is given by

$$k = \sqrt{\frac{C_{xx} + C_{yy}}{C_{zz}}} \quad \text{Eq. 4.2.7}$$

With this information, the spectra of interest are:

$$\text{wave height spectrum} \quad C_{zz}(f) \quad \text{Eq. 4.2.8}$$

$$\text{mean wave direction spectrum} \quad \tan^{-1}\left(\frac{b_1}{a_1}\right) = \tan^{-1}\left(\frac{Q_{xy}}{Q_{zx}}\right) \quad \text{Eq. 4.2.9}$$

$$\text{directional width spectrum} \quad \sqrt{2 - 2C_1(f)} \quad \text{Eq. 4.2.10}$$

where  $C_1(f) = \sqrt{a_1^2 + b_1^2}$ .

### 4.3 Comparison of VSG and Pitch-and-Roll Buoy in Determining Ocean Spectra

Since the VSG has the capability to record time series of wave heights and orthogonal slope components, the Longuet-Higgins procedure can also be used with the data from the VSG. The MATLAB 3.5 program whspec.m was written to determine the wave spectrum, the mean wave direction spectrum, and the directional width (about the mean) spectrum using the results from section 4.2.

The co- and cross-spectra from the VSG data were analyzed using 128 data points padded with zeros so that a 256 point FFT was used. The data were filtered using 5 point decimation, and each window of data overlapped the previous window by 32 points.

Figure 4.3.1 shows the wave height spectrum calculated by the VSG and that calculated by the pitch-and-roll buoy. The data were taken between 1700 - 1730 UTC on November 19, 1990. Figure 4.3.2 shows the mean wave direction spectrum

calculated by the two instruments, and Figure 4.3.3 shows the angular spread about the mean as a function of frequency. The angular spread is approximately equal to the rms angular deviation from the mean wave direction [Longuet-Higgins, et al, 1963]. Further examples of spectral parameters calculated by the VSG are compiled in Appendix C.

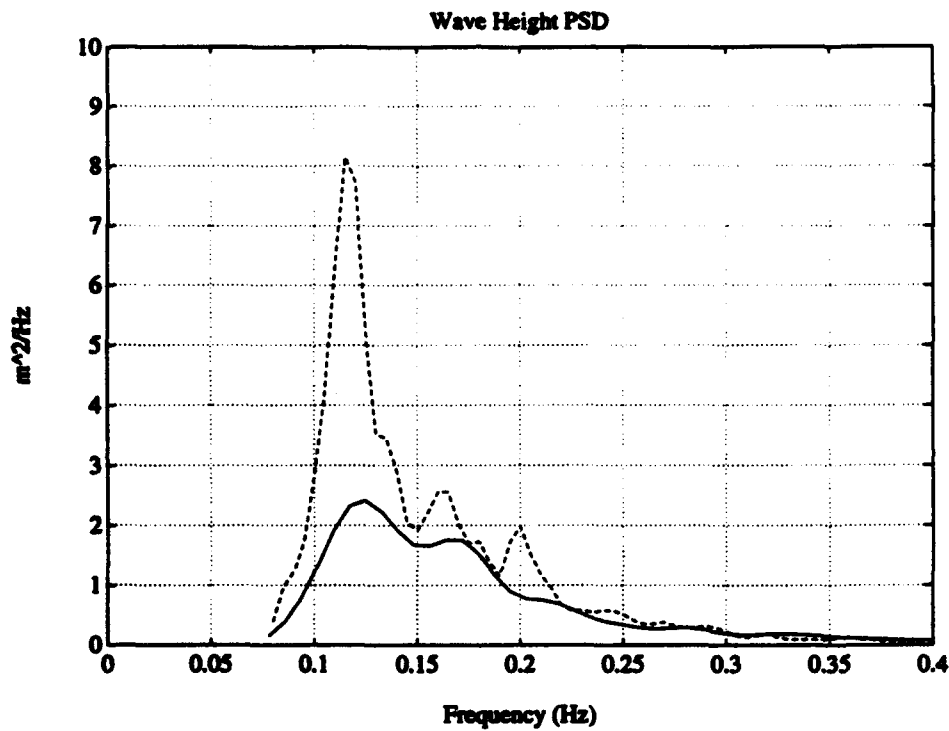


Figure 4.3.1. One-sided wave height power spectral density calculated from data taken during 1700-1730 UTC on Nov. 19, 1990. The solid line was calculated from VSG data and the dashed line represents data obtained from the WAVEC buoy.

The one-sided wave height PSD and the mean wave direction spectrum calculated by the two instruments compare favorably as can be seen in the figures. The angular spread, however, is generally 20° - 40° greater for the VSG at all frequencies--most likely due to noise and due somewhat to the error induced from slant-range measurement (see section 4.4).

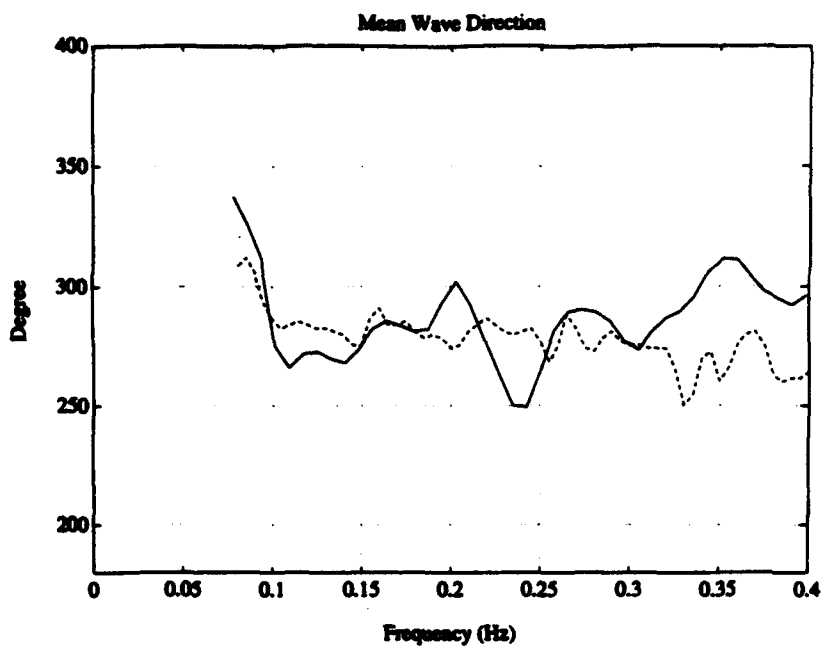


Figure 4.3.2. Mean wave direction spectrum calculated from data taken during 1700-1730 UTC on Nov. 19, 1990. The solid line was calculated from VSG data and the dashed line represents data obtained from the WAVEC buoy.

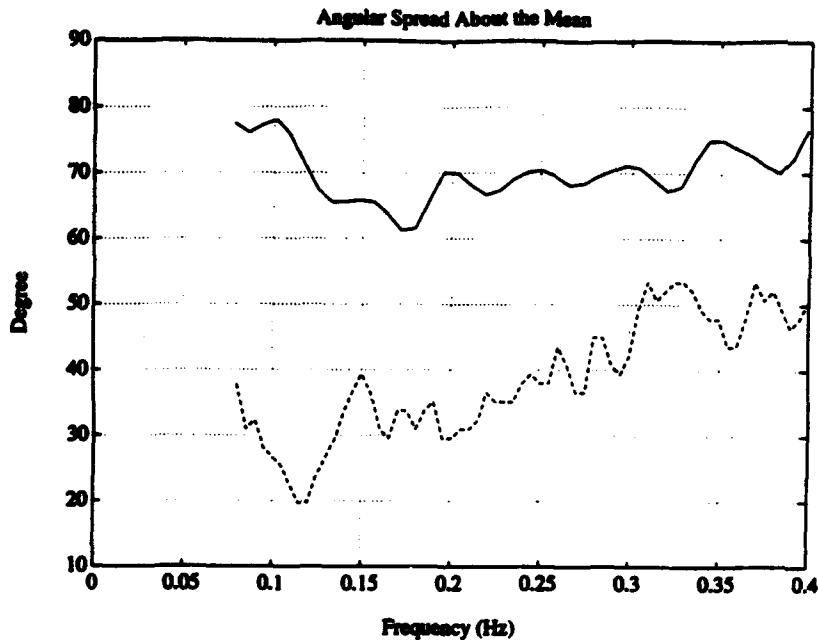


Figure 4.3.3. Directional width spectrum calculated from data taken during 1700-1730 UTC on Nov. 19, 1990. The solid line was calculated from VSG data and the dashed line represents data obtained from the WAVEC buoy.

#### 4.4 Effect of Inherent Errors on VSG's Determination of Ocean Spectra

The wave height PSD, the mean wave direction spectrum, and the directional width spectrum for an ideal measurement system are shown in Figures 4.4.1-3 respectively. The time series of wave heights and slopes were determined analytically at a single point. The waves have an amplitude of 1.5 m, a frequency of .1953125 Hz, (the frequency was chosen so that 10 periods is exactly 512 points with 10 Hz sampling) and are coming from 30°. The MATLAB program whspec2.m uses the Longuet-Higgins method given the time series of wave heights and slopes to calculate the spectra of interest. A 512 point FFT was used with no padding, no overlapping of data, no decimation, and no windowing.

The cross-spectral components,  $q_{12}$  and  $q_{23}$  (equivalent to  $Q_{zy}$  and  $Q_{zx}$ , respectively, in Eq. 4.2.9) were set to 1 and 0, respectively whenever either component's magnitude was less than  $10^{-8}$ . This has the effect of setting the mean wave direction to 0° and the angular spread to 0° when data are not present or exists in small quantities. Figures 4.4.1-3 show the results for an ideal deterministic noise-free ocean surface when measured from a single point.

In Figures 4.4.4-6, the wave spectra are shown for the same simulated ocean surface. In these figures, however, the measurements were made with three beams--each one measuring vertically. Thus, these figures illustrate the effect of the derivative approximation on the determination of such spectra. The only noticeable effect is that the angular spread is now 2° at the fundamental frequency.

In Figures 4.4.7-9, the spectra are calculated for the same ocean surface. In these figures, though, the measurements are made along a slant range. The radar in this simulation is mounted at 20 m and the angle of incidence is 47°. These figures, then, illustrate the error due to slant-range measurements. Notice the harmonic that appears

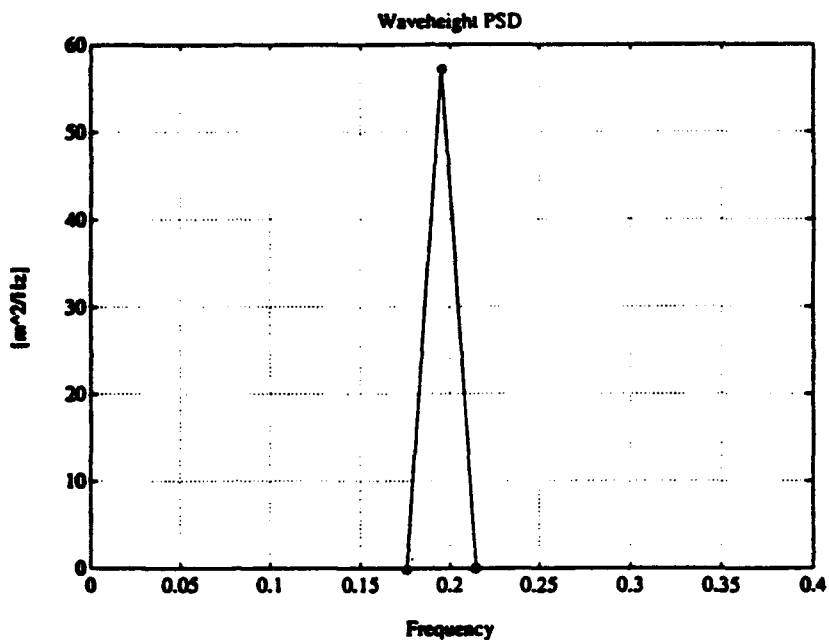


Figure 4.4.1. One-sided wave height PSD calculated from simulated ocean surface data. Wave Amplitude, 1.5 m; Wave Frequency, 0.1953125 Hz; Wave direction, 30°.

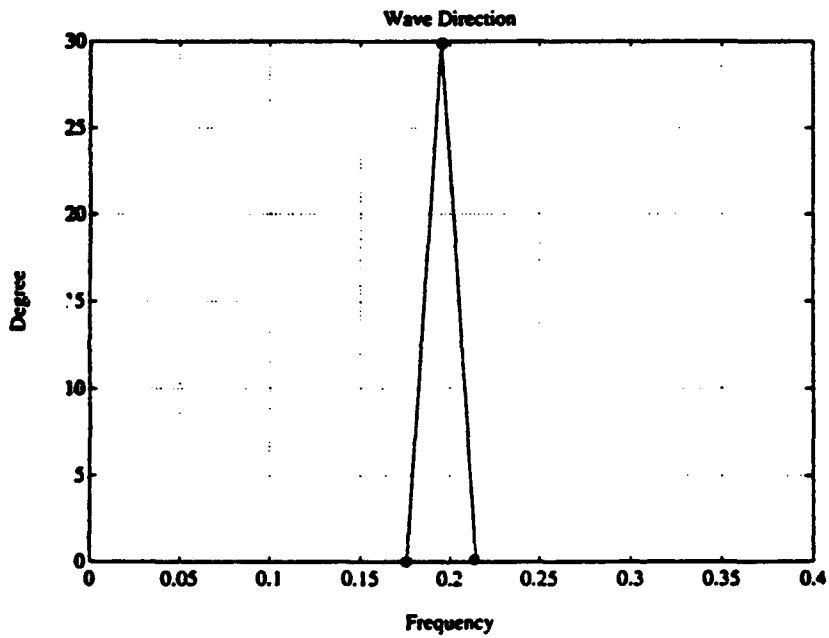


Figure 4.4.2. Mean wave direction spectrum calculated from simulated ocean surface data. Wave Amplitude, 1.5 m; Wave Frequency, 0.1953125 Hz; Wave direction, 30°.

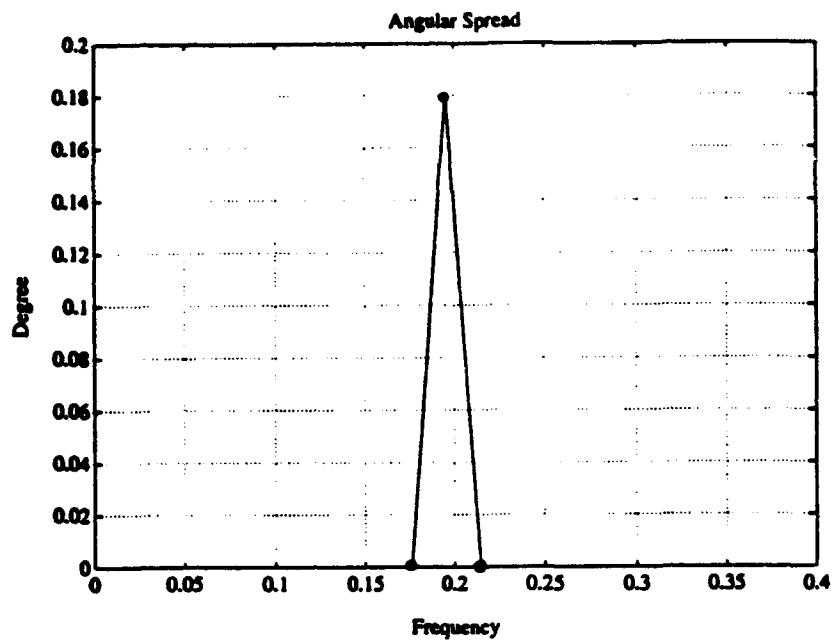


Figure 4.4.3. Directional width spectrum calculated from simulated ocean surface data. Wave Amplitude, 1.5 m; Wave Frequency, .1953125 Hz; Wave direction, 30°.

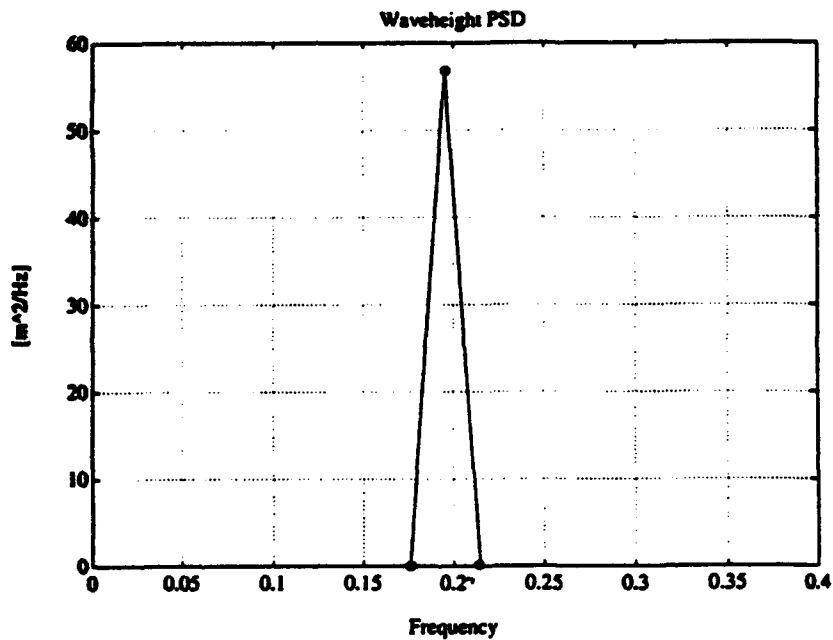


Figure 4.4.4. One-sided wave height PSD calculated from simulated ocean surface data. Wave Amplitude, 1.5 m; Wave Frequency, .1953125 Hz; Wave direction, 30°. Measurements were taken simultaneously along three vertical beams.

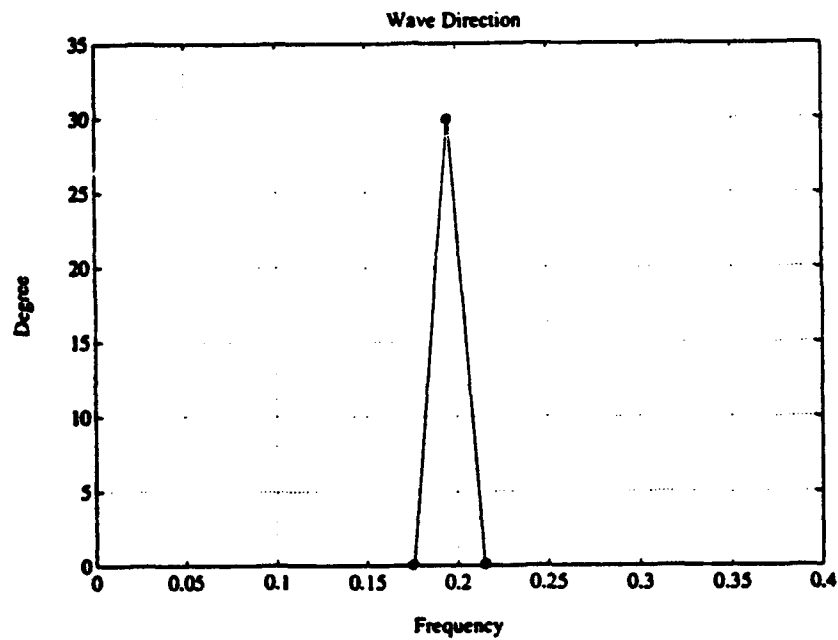


Figure 4.4.5. Mean wave direction spectrum calculated from simulated ocean surface data. Wave Amplitude, 1.5 m; Wave Frequency, .1953125 Hz; Wave direction, 30°. Measurements were taken simultaneously along three vertical beams.

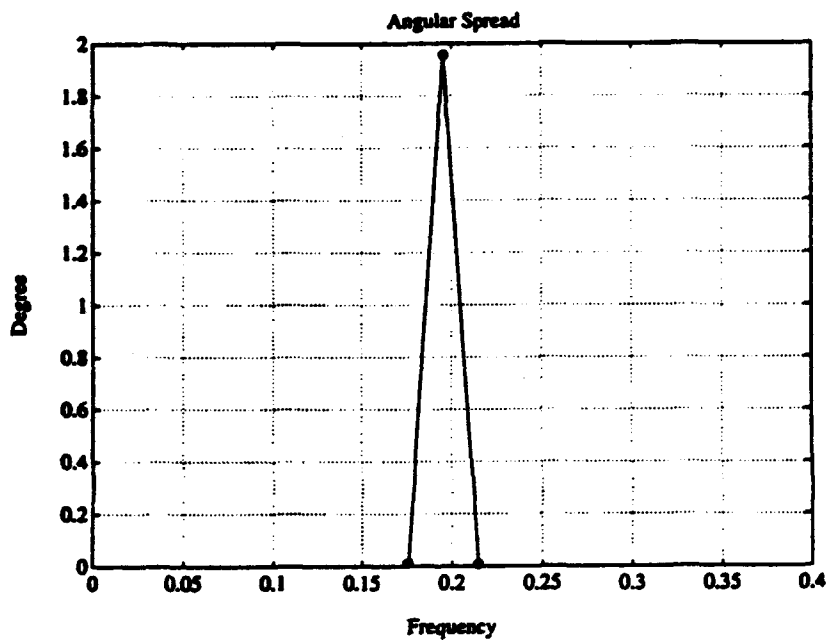


Figure 4.4.6. Directional width spectrum calculated from simulated ocean surface data. Wave Amplitude, 1.5 m; Wave Frequency, .1953125 Hz; Wave direction, 30°. Measurements were taken simultaneously along three vertical beams.

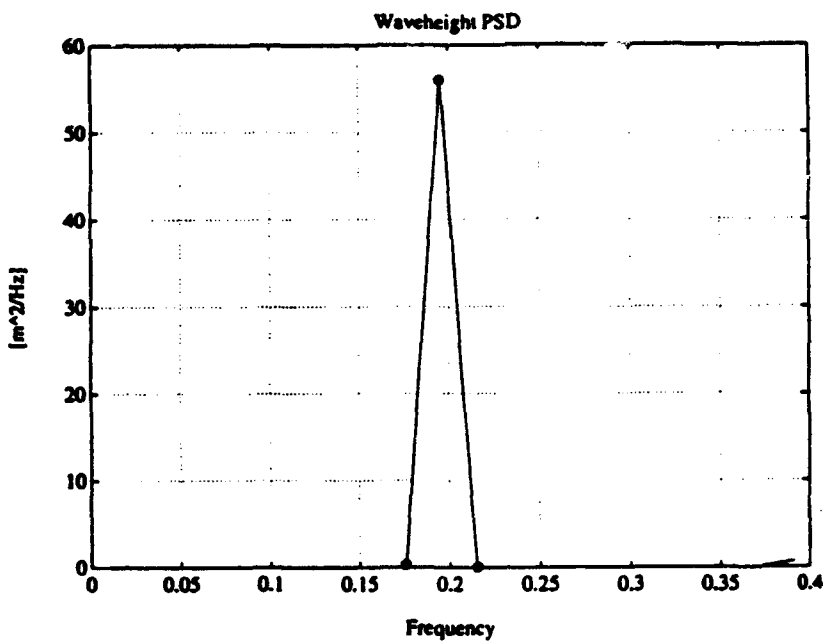


Figure 4.4.7. One-sided PSD calculated from simulated ocean surface data. Wave Amplitude, 1.5 m; Wave Frequency, .1953125 Hz; Wave direction, 30°, Incidence angle, 47°; Antenna height, 20 m. Measurements were made simultaneously along a slant range.

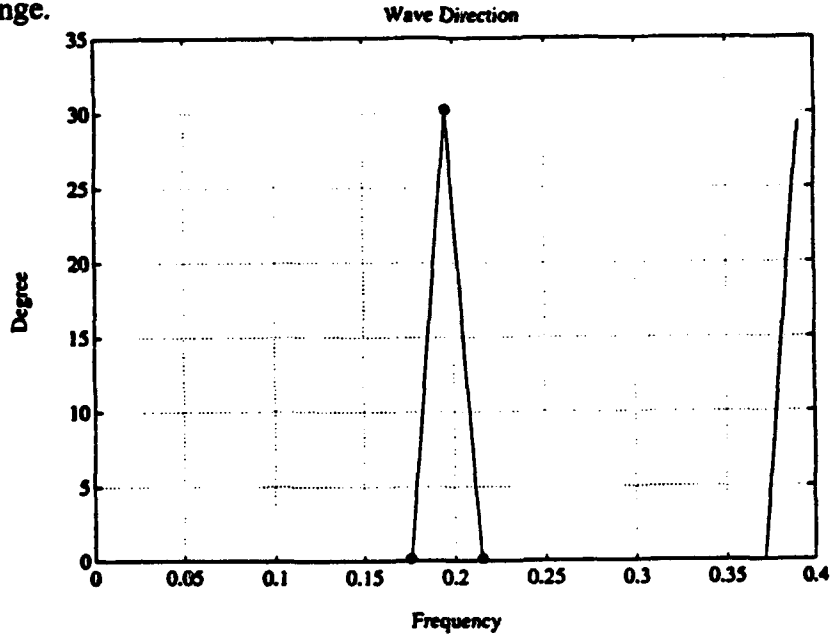


Figure 4.4.8. Mean wave direction spectrum calculated from simulated ocean surface data. Wave Amplitude, 1.5 m; Wave Frequency, .1953125 Hz; Wave direction, 30°, Incidence angle, 47°; Antenna height, 20 m. Measurements were made simultaneously along a slant range.

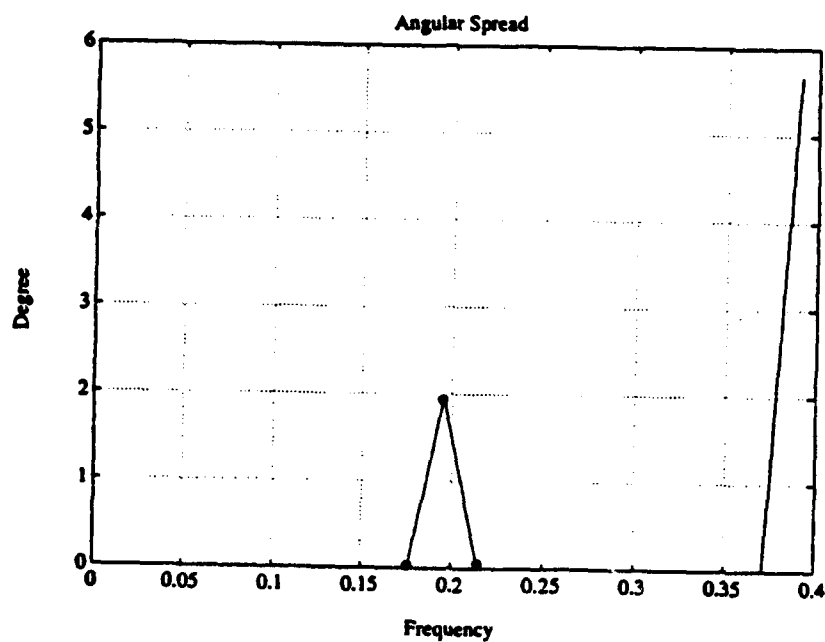


Figure 4.4.9. Directional width spectrum calculated from simulated ocean surface data. Wave Amplitude, 1.5 m; Wave Frequency, .1953125 Hz; Wave direction, 30°, Incidence angle, 47°; Antenna height, 20 m. Measurements were made simultaneously along a slant range.

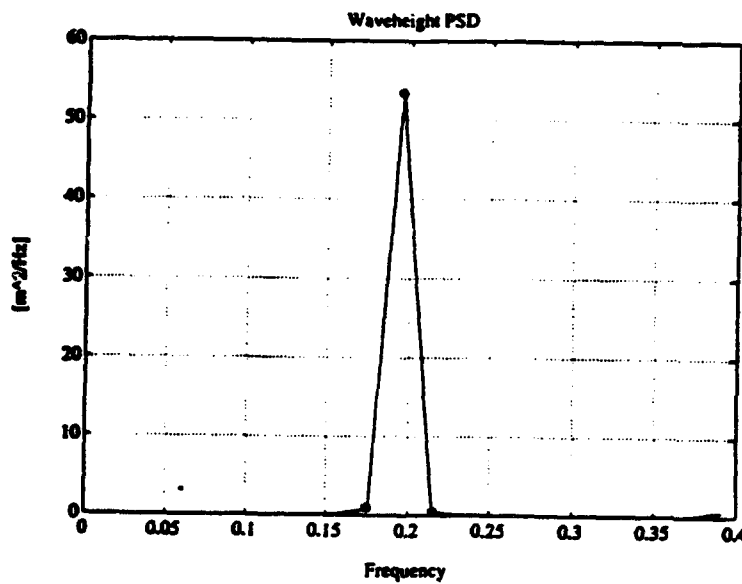


Figure 4.4.10. One-sided PSD calculated from simulated ocean surface data. Wave Amplitude, 1.5 m; Wave Frequency, .1953125 Hz; Wave direction, 30°, Incidence angle, 47°; Antenna height, 20 m. Measurements were made non-simultaneously along a slant range.

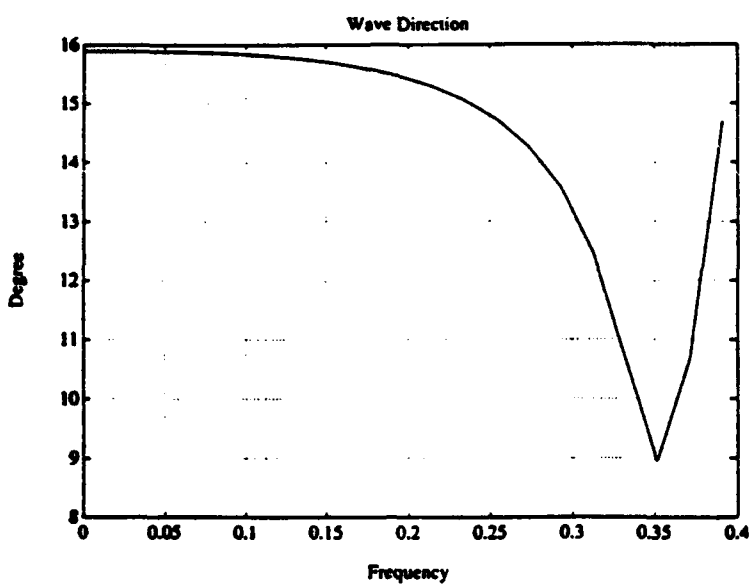


Figure 4.4.11. Mean wave direction spectrum calculated from simulated ocean surface data. Wave Amplitude, 1.5 m; Wave Frequency, .1953125 Hz; Wave direction, 30°, Incidence angle, 47°; Antenna height, 20 m. Measurements were made non-simultaneously along a slant range.

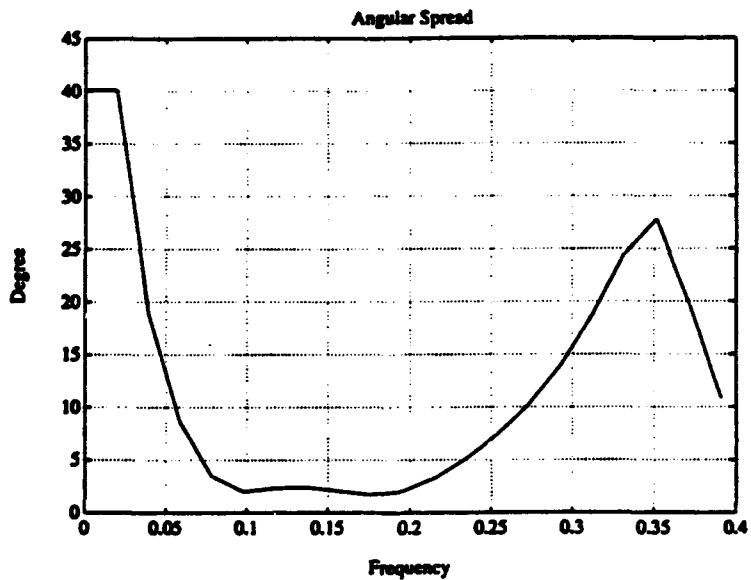


Figure 4.4.12. Directional width spectrum calculated from simulated ocean surface data. Wave Amplitude, 1.5 m; Wave Frequency, .1953125 Hz; Wave direction, 30°, Incidence angle, 47°; Antenna height, 20 m. Measurements were made non-simultaneously along a slant range.

in the wave height PSD. Just as slant-range measurement had no appreciable effect on the determination of mean wave direction with the ellipse fit, it also has no effect using the Longuet-Higgins approach. The angular spread, however, is affected by slant range measurements. Figure 4.4.9 shows that the angular spread at the second harmonic is  $\approx 5.5^\circ$ . This suggests that in a continuous spectrum, there could be a significant increase in the angular spread due to harmonics.

Figures 4.4.10-12 show the ocean spectra taking into account all inherent errors. Measurements were made non-simultaneously along a slant range. The wave height PSD is still determined accurately, but the mean wave direction spectrum has dramatically changed. Similar to the ellipse fit, the mean wave direction is now approximately  $16^\circ$  for most frequencies. Thus, we have further evidence of the detrimental effects due to non-simultaneous measurements.

It is not clearly understood why spectral components appear at all frequencies in the mean wave direction spectrum and the angular width spectrum. Although 512 data points are used in the FFT, this does not constitute a full 10 periods of data. Since there are 99 ms between samples at the same point, 512 samples takes 50.688 sec. However, 10 periods of data at .1953125 Hz takes 51.2 sec. However, the fact that we do not have a full 10 periods of data does not completely account for the additional spectral components.

## 5. Conclusion

We have seen that, like any system, the VSG has inherent errors associated with its method of measurement. The errors inherent to the VSG include phase shifts in time series of wave heights and slopes due to measuring along a slant range, modulation of the slope time series due to the first order approximation of the derivative, and miscalculation of the mean direction of wave travel due to finite switching time between the feeds.

Measuring along a slant range induces phase shifts because the measurement site has some horizontal motion. The maximum amount of phase error in the wave height and slope time series occurs at the crest and trough of the wave while. The maximum amount of error depends upon the wave steepness, the angle of incidence, and the wave direction. It is worse for steep waves, large angles of incidence, and for upwave or downwave look direction. Slant-range measurements cause the slope time series to be overestimated at every point in time in both directions.

The slant-range measurements cause harmonics to appear in the frequency domain. Even for relatively steep waves the second harmonic is small ( $\approx 20$  dB), and higher harmonics are even smaller.

Approximating the slope at point by a plane causes the slope time series to be modulated by a sinc function. The relative error depends upon the wave number,  $k$ , and the distance between the radar footprints. Slant-range measurements cause the distance between the footprints to be modulated. The error is a maximum near the trough of a wave when the distance between the footprints is a maximum. For the steepest waves the error is about 9%, but for most of the energy-laden waves the error is less than 2%. The derivative approximation causes the VSG to underestimate the magnitude of the slope time series at every point.

The finite time between beam measurements seems to have the most serious effect on the slope time series. Due to the finite time between measurements, there is phase error in the second and third measurements. In the wave height time series this does not have much effect because the three measurements are averaged. However, the slope time series depends on an accurate measurement of each position. Therefore, any error in single measurement has serious effects.

The distribution of ocean waves measured during the SAXON experiment is nearly bivariate Gaussian. This enabled us to fit an ellipse to the two-dimensional slope distribution. The orientation of the major axis indicates the mean direction of wave travel with  $180^\circ$  ambiguity. In addition, statistics of the slope distribution are easily obtained from the ellipse fit to the distribution.

Slant-range measurements cause the ellipse width to increase slightly, but have no effect on the determination of the mean wave direction. The derivative approximation also causes the width of the ellipse to increase slightly. This source of error also has no affect on the determination of the mean wave direction. Non-simultaneous measurements, however, cause the mean wave direction to be miscalculated. For the particular example in section 3.4, the VSG would have measured the waves as coming from  $16^\circ$  when then they were actually coming from  $30^\circ$ .

The directional ambiguity can be resolved by taking advantage of the asymmetry of ocean waves. Since the back side of ocean waves is longer than the front, and since the VSG records data at a constant rate of time, more data is recorded along the back side of the waves. Therefore, a histogram of the slope distribution will aid in resolving the directional ambiguity. By fitting an ellipse to the histogram of slopes

using the method of least squares, the center of the ellipse will indicate the mean direction from which waves were traveling.

The Longuet-Higgins method for determining ocean spectra has been used for a number of years with pitch-and-roll buoy data. Since the same parameters are available from the VSG, the Longuet-Higgins approach can be used with the VSG data. This enabled a comparison to be made between the VSG and a pitch-and-roll buoy.

The wave height spectrum and the mean wave direction spectrum compare favorably between the two instruments. However, the angular spread about the mean is generally  $20^\circ$  -  $40^\circ$  greater at all frequencies for the VSG than for the pitch-and-roll buoy. There may be several explanations for this. Higher frequency waves have a shorter wavelength, and thus are more susceptible to changes in the wind direction. In addition, since the waves are shorter fewer measurements are along each wave which results in more noise. As the wavelength approaches the size of the buoy, the buoy may no longer follow the surface very closely.

The derivative approximation causes the angular spread to increase slightly--from roughly  $0^\circ$  to  $2^\circ$ . Measuring along a slant range causes a harmonic to appear in the spectral parameters. The angular spread at the first harmonic is approximately  $5.5^\circ$ . Due to non-simultaneous measurements, the mean wave direction was roughly  $16^\circ$  instead of the correct direction of  $30^\circ$ . The angular spread at the fundamental frequency remained about  $2^\circ$ .

### 5.1 Recommendations for Further Study

It would seem that the most important item that could be done to improve the VSG's performance would be to decrease the time between measurements from each feed. This should improve the accuracy of the determination of the mean wave direction.

Although slant-range measurements do not seem to affect the calculation of the mean wave direction, they do cause the slope time series to be overestimated at every point in both directions. This may be important when analyzing the modulation of the radar signal due to tilt modulation. The only solution (and its only partial) is to operate the radar at small angles of incidence.

It seems that the first order approximation of the derivative does a good job at estimating the slope at a point within the plane formed by the radar footprints. It has little effect on the wave height time series or the slope time series.

All the analysis in this paper has been done with a deterministic ocean surface. The next step would be to do the same analysis with a random ocean surface and noise added to the system. This would give more realistic examples of the inherent errors involved with measuring wave ~~heights~~ and vector slopes with the VSG.

It would be nice to have an analytical description of the error in the slope time series due to non-simultaneous measurements. However, it is an extremely complicated process. A finite time between switching causes the measurements of from beam 1 and beam 2 to have some phase error. The amount of phase error depends only on the frequency of the wave and the time between sampling (see Fig. 2.9.1). Once the phase error has been determined, the error in the height measurement (which will be a function of time) can be determined. This requires that the height at each footprint be known assuming that the heights were measured

simultaneously. The difference in height at each point can be used to determine the equation of the plane (which will be a function of time), and hence the error in the slope time series in any direction. Since all three points are required to determine the slope time series, it is not enough to determine the error in the wave number at each point. At this point only empirical evidence is available to illustrate the error due to non-simultaneous measurements.

## REFERENCES

Allender, J., T. Audunson, S. F. Barstow, S. Bjerken, H. E. Krogstad, P. Steinbakke, L. Vardal, L. E. Borgman, and C. Graham, "The WADIC Project: A Comprehensive field evaluation of directional wave instrumentation," *Ocean Engng.*, vol. 16, no 5/6, 1989, pp. 505-536.

Batschelet, E., *Circular Statistics in Biology*, London: Academic Press, 1981, pp 246-274.

Evans, C., S. Haimov, and R. K. Moore, "Calculation of Ocean Environmental Parameters from a Ka-Band Scatterometer using the Longuet-Higgins Approach," to be presented at IGARSS '94, 8-12 Aug., 1994, Pasadena, CA.

Evans, C., S. Haimov, R. K. Moore, and V. Hesany, "Determination of Ocean Environmental Parameters from a Ka-Band Scatterometer," *Proc. of Oceans '93*, vol. 2, 18-21 October 1993, Victoria, Canada, pp. 1-4.

Gross, M. G., *Oceanography: A View of the Earth*, Englewood Cliffs, NJ: Prentice Hall, 1982, pp. 211-235.

Hesany, V., R. K. Moore, and S. P. Gogineni, "A Vector Slope Gauge and Scatterometer for Ocean Measurements," *Proceedings of URSI Microwave Signatures '92 Conference*, July 1-3, 1992, Igls, Austria 1D/25-1D/30.

Hesany, V., *A radar vector slope gauge for ocean measurements*, Ph.D. Thesis in Department of Electrical Engineering and Computer Science, The University of Kansas, May 1994, pp 70-73.

Kuik, A. J., G. PH. Van Vledder, and L. H. Holthuijsen, "A Method for the Routine Analysis of Pitch-and-Roll Buoy Wave Data," *J. of Physical Oceanography*, vol. 18, July, 1988, pp. 1020-1034.

Longuet-Higgins, M.S., D. E. Cartwright, and N. D. Smith, "Observations of the Directional Spectrum of Sea Waves Using the Motions of a Floating Buoy," *Proceedings of Ocean Wave Spectra Conference*, Easton, Maryland, 1-4 May 1961, pp. 111-136, Englewood Cliffs, NJ: Prentice Hall, 1963.

Neumann, G., and W. J. Peirson, Jr., "Known and Unknown Properties of the Frequency Spectrum of a Wind-Generated Sea," *Proceedings of Ocean Wave Spectra Conference*, Easton, Maryland, 1-4 May 1961, pp. 9-25, Englewood Cliffs, NJ: Prentice Hall, 1963.

Plant, W. J., and W. Alpers, "The SAXON-FPN Experiment," *IGARSS '91 Digest*, IEEE 91CH2971-0, Espoo, Finland, 3-6 June, 1991, pp. 1983-1986.

Shanmugan, K. S., and A. M. Breipohl, *"Random Signals: Detection, Estimation, and Data Analysis,"* John Wiley & Sons, Inc., New York, 1988, p. 46.

Steele, K. E., C. Teng, and D. W. C. Wang, "Wave Direction Measurements using Pitch-Roll Buoys," *Ocean Engng.*, vol. 19, no. 4, 1992, pp. 349-375.

## Appendix A

```
function [ran, x, y, z] = range(theta,delta,beta12,beta23,gamma,r,phi,f,A)
% [ran, x, y, z] = range(theta,delta,beta12,beta23,gamma,r,phi,f,A)
% determines the range to the ocean surface along the three beams taking
% into account all possible angles. This program solves the nonlinear
% equation that arises from finding the point of intersection of the
% radar beam with the ocean surface.
%
% theta - the angle the radar was rotated about the x-axis (angle of inc.)
% delta - the angle the radar was rotated about the z' axis
% beta12 - the angle between beams 1 and 2
% beta23 - the angle between beams 2 and 3
% gamma - the angle between beams 1 and 3
% r - initial guess of length of beam 1, 2, and 3 in meters
% [1, 2, 3]
% phi - the angle between the RDL and the direction from which the waves
% are coming
%
% Since there may be multiple solutions to the nonlinear equation, it is best
% to guess the most accurate length of r, while making sure that the guess is
% shorter than the resulting solution.
%
% Chris Evans, RSL, The University of Kansas, May 26, 1994
%
theta = theta*pi/180; % theta and delta are measured positive from CCW
delta = delta*pi/180;
beta12 = beta12*pi/180;
beta23 = beta23*pi/180;
gamma = gamma*pi/180;
phi = phi*pi/180;

h = 20; % height of radar (meters) above mean sea surface
%A = 5.0; % amplitude of ocean wave in meters

R11 = cos(delta)*sin(beta12)*cos(gamma-pi/2) + sin(delta)*sin(beta12)*sin(gamma-pi/2);
R21 = sin(delta)*cos(theta)*sin(beta12)*cos(gamma-pi/2) -
cos(delta)*cos(theta)*sin(beta12)*sin(gamma-pi/2) + sin(theta)*cos(beta12);
R31 = sin(delta)*sin(theta)*sin(beta12)*cos(gamma-pi/2) -
cos(delta)*sin(theta)*sin(beta12)*sin(gamma-pi/2) - cos(theta)*cos(beta12);
```

```

R12 = 0;
R22 = sin(theta);
R32 = -cos(theta);
R13 = -sin(delta)*sin(beta23);
R23 = cos(delta)*cos(theta)*sin(beta23) + sin(theta)*cos(beta23);
R33 = cos(delta)*sin(theta)*sin(beta23) - cos(theta)*cos(beta23);

k = ((2*pi*f)^2)/9.8; %spatial frequency of waves (2*pi/lambda)

r1(1) = 0; r1(2) = r(1);
r2(1) = 0; r2(2) = r(2);
r3(1) = 0; r3(2) = r(3);

for t = 1:10/f+1, % t is in tenths of seconds; 10/f gives 1 period
i = 2;
while (abs(r1(i)-r1(i-1)) > 1e-13) | (abs(r3(i)-r3(i-1)) > 1e-13), % error must be less
than this #
x1(i) = r1(i)*R11; x2(i) = 0; x3(i) = r3(i)*R13;
y1(i) = r1(i)*R21; y2(i) = r2(i)*R22; y3(i) = r3(i)*R23;
z1(i) = r1(i)*R31; z2(i) = r2(i)*R32; z3(i) = r3(i)*R33;
zeta1(i) = 2*pi*f*33*3*t/1000 + k*sin(phi)*x1(i) + k*cos(phi)*y1(i);
zeta2(i) = 2*pi*f*33*(3*t+1)/1000 + k*sin(phi)*x2(i) + k*cos(phi)*y2(i);
zeta3(i) = 2*pi*f*33*(3*t+2)/1000 + k*sin(phi)*x3(i) + k*cos(phi)*y3(i);
sea1(i) = A*cos(zeta1(i)) - h;
sea2(i) = A*cos(zeta2(i)) - h;
sea3(i) = A*cos(zeta3(i)) - h;
F1(i) = z1(i) - sea1(i); F2(i) = z2(i) - sea2(i); F3(i) = z3(i) - sea3(i);
Fder1(i) = R31 + A*sin(zeta1(i))*(k*sin(phi)*R11 + k*cos(phi)*R21);
Fder2(i) = R32 + A*sin(zeta2(i))*(k*sin(phi)*R12 + k*cos(phi)*R22);
Fder3(i) = R33 + A*sin(zeta3(i))*(k*sin(phi)*R13 + k*cos(phi)*R23);
r1(i+1) = r1(i) - F1(i)/Fder1(i);
r2(i+1) = r2(i) - F2(i)/Fder2(i);
r3(i+1) = r3(i) - F3(i)/Fder3(i);
i = i+1;
end
ran(t,:) = [r1(i), r2(i), r3(i)];
x(t,:) = [x1(i-1), x2(i-1), x3(i-1)];
y(t,:) = [y1(i-1), y2(i-1), y3(i-1)];
z(t,:) = [z1(i-1), z2(i-1), z3(i-1)];
end

```

```

function [ran, x, y, z] = strange(theta,delta,beta12,beta23,gamma,r,phi,f,A)
% [ran, x, y, z] = strange(theta,delta,beta12,beta23,gamma,r,phi,f,A) determines the
% range to the ocean surface along the three beams taking into account all
% possible angles. This program solves the nonlinear equation that arises
% from finding the point of intersection of the radar beam with the ocean
% surface.

%
% theta - the angle the radar was rotated about the x-axis (angle of inc.)
% delta - the angle the radar was rotated about the z' axis
% beta12 - the angle between beams 1 and 2
% beta23 - the angle between beams 2 and 3
% gamma - the angle between beams 1 and 3
% r - initial guess of length of beam 1, 2, and 3 in meters
% [1, 2, 3]
% phi - the angle between the RDL and the direction from which the waves
% are coming
%
% Since there may be multiple solutions to the nonlinear equation, it is best
% to guess the most accurate length of r, while making sure that the guess is
% shorter than the resulting solution.
%
% Chris Evans, RSL, The University of Kansas, March 1, 1994
%

theta = theta*pi/180; % theta and delta are measured positive from CCW
delta = delta*pi/180;
beta12 = beta12*pi/180;
beta23 = beta23*pi/180;
gamma = gamma*pi/180;
phi = phi*pi/180;

h = 20; % height of radar (meters) above mean sea surface
%A = 5.0; % amplitude of ocean wave in meters

R11 = cos(delta)*sin(beta12)*cos(gamma-pi/2) + sin(delta)*sin(beta12)*sin(gamma-pi/2);
R21 = sin(delta)*cos(theta)*sin(beta12)*cos(gamma-pi/2) -
cos(delta)*cos(theta)*sin(beta12)*sin(gamma-pi/2) + sin(theta)*cos(beta12);
R31 = sin(delta)*sin(theta)*sin(beta12)*cos(gamma-pi/2) -
cos(delta)*sin(theta)*sin(beta12)*sin(gamma-pi/2) - cos(theta)*cos(beta12);
R12 = 0;
R22 = sin(theta);

```

```

R32 = -cos(theta);
R13 = -sin(delta)*sin(beta23);
R23 = cos(delta)*cos(theta)*sin(beta23) + sin(theta)*cos(beta23);
R33 = cos(delta)*sin(theta)*sin(beta23) - cos(theta)*cos(beta23);

k = ((2*pi*f)^2)/9.8; %spatial frequency of waves (2*pi/lambda)

r1(1) = 0; r1(2) = r(1);
r2(1) = 0; r2(2) = r(2);
r3(1) = 0; r3(2) = r(3);

for t = 1:10/f, % t is in tenths of seconds; 40/f gives 4 periods
    i = 2;
    while (abs(r1(i)-r1(i-1)) > 1e-13) | (abs(r3(i)-r3(i-1)) > 1e-13), % error must be less
    than this #
        x1(i) = r1(i)*R11; x2(i) = 0; x3(i) = r3(i)*R13;
        y1(i) = r1(i)*R21; y2(i) = r2(i)*R22; y3(i) = r3(i)*R23;
        z1(i) = r1(i)*R31; z2(i) = r2(i)*R32; z3(i) = r3(i)*R33;
        zeta1(i) = 2*pi*f*t/10+ k*sin(phi)*x1(i) + k*cos(phi)*y1(i);
        zeta2(i) = 2*pi*f*t/10+ k*sin(phi)*x2(i) + k*cos(phi)*y2(i);
        zeta3(i) = 2*pi*f*t/10+ k*sin(phi)*x3(i) + k*cos(phi)*y3(i);
        seal(i) = A*cos(zeta1(i)) - h;
        sea2(i) = A*cos(zeta2(i)) - h;
        sea3(i) = A*cos(zeta3(i)) - h;
        F1(i) = z1(i) - seal(i); F2(i) = z2(i) - sea2(i); F3(i) = z3(i) - sea3(i);
        Fder1(i) = R31 + A*sin(zeta1(i))*(k*sin(phi)*R11 + k*cos(phi)*R21);
        Fder2(i) = R32 + A*sin(zeta2(i))*(k*sin(phi)*R12 + k*cos(phi)*R22);
        Fder3(i) = R33 + A*sin(zeta3(i))*(k*sin(phi)*R13 + k*cos(phi)*R23);
        r1(i+1) = r1(i) - F1(i)/Fder1(i);
        r2(i+1) = r2(i) - F2(i)/Fder2(i);
        r3(i+1) = r3(i) - F3(i)/Fder3(i);
        i = i+1;
    end
    ran(t,:) = [r1(i), r2(i), r3(i)];
    x(t,:) = [x1(i-1), x2(i-1), x3(i-1)];
    y(t,:) = [y1(i-1), y2(i-1), y3(i-1)];
    z(t,:) = [z1(i-1), z2(i-1), z3(i-1)];
end

```

```

function [ran, x, y, z] = vrangle(x, y, f, A, phi)
% [ran, x, y, z] = vrangle(x, y, f, A, phi) determines the
% range to the ocean surface assuming the three points of intersection are
% moving vertically and assuming the measurements are made simultaneously.
%
% x : time series of x coordinates from range.m [x1, x2, x3]
% y : time series of y coordinates from range.m [y1, y2, y3]
% f : frequency of ocean waves used in range.m
% A : amplitude of ocean wave in meters used in range.m
% phi : direction from which ocean waves are coming in deg. (from range.m)
%
% ran : time series of ranges [r1, r2, r3]
% x : time series of x coordinates in earth system [x1, x2, x3]
% y : time series of y coordinates in earth system [y1, y2, y3]
% z : time series of z coordinates in earth system [z1, z2, z3]
%
% Chris Evans, RSL, The University of Kansas, March 28, 1994
%

phi = phi*pi/180;

h = 20; % height of radar (meters) above mean sea surface
k = ((2*pi*f)^2)/9.8; %spatial frequency of waves (2*pi/lambda)
[r,c] = size(x);
x1 = mean(x(:,1)); x2 = mean(x(:,2)); x3 = mean(x(:,3));
y1 = mean(y(:,1)); y2 = mean(y(:,2)); y3 = mean(y(:,3));

t = 1:r;
t = t';

z1 = A*cos(2*pi*f*t/10 + k*sin(phi)*x1 + k*cos(phi)*y1) - h;
z2 = A*cos(2*pi*f*t/10 + k*sin(phi)*x2 + k*cos(phi)*y2) - h;
z3 = A*cos(2*pi*f*t/10 + k*sin(phi)*x3 + k*cos(phi)*y3) - h;

ran1 = sqrt(x1^2 + y1^2 + z1.^2);
ran2 = sqrt(x2^2 + y2^2 + z2.^2);
ran3 = sqrt(x3^2 + y3^2 + z3.^2);

x = [x1*ones(r,1), x2*ones(r,1), x3*ones(r,1)];
y = [y1*ones(r,1), y2*ones(r,1), y3*ones(r,1)];
z = [z1, z2, z3];
ran = [ran1, ran2, ran3];

```

```
function [Sy,Sx] = slopeab2(x,y,z)
% [Sy,Sx] = slopeab2(x,y,z)
%
% Slopeab2 determines the slope time series from the plane given the x, y,
% and z, coordinates of the points of intersection of the radar beams
% with the ocean surface.
%
% x - x coordinate of the point of intersection. (n x 3)
% y - y coordinate of the point of intersection. (n x 3)
% z - z coordinate of the point of intersection. (n x 3)
%
% Sy - time series of slope in y (RLD) direction (degrees)
% Sx - time series of slope in x (cross) direction (degrees)
%
% Chris Evans, RSL, The University of Kansas, March 28, 1994
%
```

% B & C are vectors in the plane, and N is the normal to the plane

```
B = [(x(:,1) - x(:,2)), (y(:,1) - y(:,2)), (z(:,1) - z(:,2))];
C = [(x(:,3) - x(:,2)), (y(:,3) - y(:,2)), (z(:,3) - z(:,2))];
```

% Normal components are found from the cross product of B and C.

```
Nx = B(:,2).*C(:,3) - C(:,2).*B(:,3);
Ny = B(:,3).*C(:,1) - C(:,3).*B(:,1);
Nz = B(:,1).*C(:,2) - C(:,1).*B(:,2);
```

% The slope of the plane is the negative inverse of the slope of the line.

```
Sy = 180/pi*atan(-Ny./Nz);
Sx = 180/pi*atan(-Nx./Nz);
```

```

function [Sy,Sx] = slopepoi(ran,theta,delta,beta12,beta23,gamma,A,phi,f)
%
% [Sy,Sx] = slopepoi(ran,theta,delta,beta12,beta23,gamma,A,phi,f)
% calculates the slope at the point for which the slope is being
% approximated with slopeab.m.
%
% ran    : n x 3 time series of ranges
% theta  : radar angle of incidence in degrees
% delta   : angle of CCW rotation about the z' axis
% beta12 : angle between beams 1 and 2
% beta23 : angle between beams 2 and 3
% gamma  : angle between the planes formed by beams 1 & 2 and 2 & 3 in degrees
% A      : amplitude of ocean waves in meters (1/2 waveheight)
% phi    : direction from which the waves are traveling
% f      : frequency of ocean wave in Hz
%
% Sy    : Slope in y direction in degrees
% Sx    : Slope in x direction in degrees
%
% Chris Evans, RSL, The University of Kansas, March 10, 1994
%

theta = theta*pi/180;
delta = delta*pi/180;
gamma = gamma*pi/180;
beta12 = beta12*pi/180;
beta23 = beta23*pi/180;

[r,c] = size(ran);

% coordinates in the antenna system
x1a = ran(:,1)*sin(beta12)*cos(pi/2-gamma);
y1a = ran(:,1)*sin(beta12)*sin(pi/2-gamma);
z1a = -ran(:,1)*cos(beta12);
x2a = zeros(r,1);
y2a = zeros(r,1);
z2a = -ran(:,2);
x3a = zeros(r,1);
y3a = ran(:,3)*sin(beta23);
z3a = -ran(:,3)*cos(beta23);

% rot transforms from the antenna to the earth coordinate system

```

```

rot = [cos(delta), -sin(delta), 0;
       cos(theta)*sin(delta), cos(delta)*cos(theta), -sin(theta);
       sin(theta)*sin(delta), cos(delta)*sin(theta), cos(theta)];
```

```

for t = 1:r,
Ant = [x1a(t), x2a(t), x3a(t);
        y1a(t), y2a(t), y3a(t);
        z1a(t), z2a(t), z3a(t)];
```

```

E = rot*Ant;
x1e(t) = E(1,1); x2e(t) = E(1,2); x3e(t) = E(1,3);
y1e(t) = E(2,1); y2e(t) = E(2,2); y3e(t) = E(2,3);
z1e(t) = E(3,1); z2e(t) = E(3,2); z3e(t) = E(3,3);
```

```

% coordinates are now in the earth system
```

```

A1 = (y1e(t)-y2e(t))*(z3e(t)-z2e(t)) - (y3e(t)-y2e(t))*(z1e(t)-z2e(t));
B1 = (x3e(t)-x2e(t))*(z1e(t)-z2e(t)) - (x1e(t)-x2e(t))*(z3e(t)-z2e(t));
C1 = (x1e(t)-x2e(t))*(y3e(t)-y2e(t)) - (x3e(t)-x2e(t))*(y1e(t)-y2e(t));
A2 = x3e(t)-x2e(t);
B2 = y3e(t)-y2e(t);
C2 = z3e(t)-z2e(t);
A3 = x1e(t)-x2e(t);
B3 = y1e(t)-y2e(t);
C3 = z1e(t)-z2e(t);
```

```

R = [A1, B1, C1; A2, B2, C2; A3, B3, C3];
```

```

D1 = A1*x2e(t) + B1*y2e(t) + C1*z2e(t);
D2 = 0.5*(x3e(t)^2 + y3e(t)^2 + z3e(t)^2 - x2e(t)^2 - y2e(t)^2 - z2e(t)^2);
D3 = 0.5*(x1e(t)^2 + y1e(t)^2 + z1e(t)^2 - x2e(t)^2 - y2e(t)^2 - z2e(t)^2);
```

```

S = [D1; D2; D3];
```

```

Q = inv(R)*S;
Px = Q(1);
Py = Q(2);
```

```

k = (2*pi*f)^2/9.8;
Sy(t) =
atan(A*k*cos(phi)*cos(2*pi*f*t/10+k*sin(phi)*Px+k*cos(phi)*Py))*180/pi;
```

```
Sx(t) =  
atan(A*k*sin(phi)*cos(2*pi*f*t/10+k*sin(phi)*Px+k*cos(phi)*Py))*180/pi;  
end  
Sy = Sy'; Sx = Sx';
```

```

function [a,b,theta,Ro,beta,freq,ang,X,Y,xr,yr] = ellipsef(x,y,dir,binwidth)
% ELLIPSEF. Ellipse fit.
% [a,b,theta,Ro,beta,freq,ang,X,Y,xr,yr] = ellipsef(x,y,dir,binwidth)
%
% x      - x-data vector
% y      - y-data vector
% dir    - y axis orientation with respect to North in degree (East is 90)
% binwidth - bin width for x-y phase histogram (in degree)
%
% a      - length of major axis
% b      - length of minor axis
% theta  - major axis orientation in radians:
%          theta(1) - standard trig. presentation (with respect to x axis)
%          theta(2) - with respect to North
% Ro     - distance from ellipse center to the origin
% beta   - location angle of ellipse center
% freq   - frequency counts of the phase histogram
% ang    - bin angles of the phase histogram
% X      - x-coordinates of the ellipse for Earth map orientation
% Y      - y-coordinates of the ellipse for Earth map orientation
% xr    - rotated x-data vector
% yr    - rotated y-data vector (yr axis points North)

```

```
% Samuel Haimov, 3/23/93, RSL, The University of Kansas
```

```
if nargin < 4 binwidth = 18; end
if nargin < 3 dir = 0; end
```

```
% Rotate the coordinates relative to the RLD and North
r = (360-dir)*pi/180;
xr = x*cos(r) - y*sin(r);
yr = x*sin(r) + y*cos(r);
```

```
% Find directional histogram
binnum = fix(360/binwidth);
angp = angle(xr+j*yr);
[freq,ang] = hist(angp,binnum);
```

```
% Ellipse fit (Bivar. Normal Distrb.); A(xr-mx)^2+2B(xr-mx)(yr-my)+C(yr-my)^2=D
cv=cov([xr(:) yr(:)]);
mx=mean(xr); my=mean(yr); % center of the ellipse
```

```

beta = 0; Ro = 0;
if abs(mx)>1e-6 | abs(my)>1e-6
    beta=atan2(my,mx);      % ellipse center in polar
    Ro=sqrt(mx^2+my^2);      % coordinates
end
vx=cv(1,1); vy=cv(2,2);
A=vy; B=-cv(2,1); C=vx;    % ellipse eq. polinomial coeffs.
D=2*(vx*vy-B^2);          % free coeff. in the ellipse polinom.
R=sqrt((A-C)^2+4*B^2);
a=sqrt(2*D/(A+C-R));      % major axis
b=sqrt(2*D/(A+C+R));      % minor axis
theta(1)=atan(2*B/(A-C-R)); % ellipse orientation
                            % also theta=0.5*atan(2*B/(A-C));

% Calculate ellipse parametric equations
phi=0:pi/128:2*pi;
X=mx+a*cos(theta(1)).*cos(phi)-b*sin(theta(1)).*sin(phi);
Y=my+a*sin(theta(1)).*cos(phi)+b*cos(theta(1)).*sin(phi);

% Modify theta with respect to North

if theta(1) >= -pi & theta(1) < pi/2 theta(2) = -theta(1) + pi/2; end
if theta(1) >= pi/2 & theta(1) <= pi theta(2) = -theta(1) + 2.5*pi; end

```

```

function [a,b,theta,Ro,beta,freq,ang,X,Y,xr,yr] = ellipseh(x,y,dir,binwidth)
% ELLIPSEH. Ellipse fit of the x-y data histogram.
% [a,b,theta,Ro,beta,freq,ang,X,Y,xr,yr] = ellipseh(x,y,dir,binwidth)
%
% x - x-data vector (e.g., slope in x-direction)
% y - y-data vector (e.g., slope in y-direction)
% dir - y axis orientation with respect to North in degree (e.g., RLD)
% binwidth - bin width for x-y phase histogram (in degree)
%
% a - length of major axis
% b - length of minor axis
% theta - major axis orientation with respect to North (radians)
% theta(1) - standard trig. presentation (with respect to x axis)
% theta(2) - with respect to North
% Ro - distance from ellipse center to the origin
% beta - location angle of ellipse center
% freq - frequency counts of the phase histogram
% ang - bin angles of the phase histogram
% X - x-coordinates of the ellipse for Earth map orientation
% Y - y-coordinates of the ellipse for Earth map orientation
% xr - rotated x-component of the histogram
% yr - rotated y-component of the histogram (yr axis points North)

```

```
% Samuel Haimov, 3/23/93, RSL, The University of Kansas
```

```
% Rotate the coordinates relative to the RLD and North
```

```
r = (360-dir)*pi/180;
xr = x*cos(r) - y*sin(r);
yr = x*sin(r) + y*cos(r);
```

```
% Find directional histogram
```

```
binnum = fix(360/binwidth);
angp = angle(xr+j*yr);
[freq,ang] = hist(angp,binnum);
xr = freq.*cos(ang);
yr = freq.*sin(ang);
```

```
% Ellipse fit (Bivar. Normal Distrb.); A(xr-mx)^2+2B(xr-mx)(yr-my)+C(yr-my)^2=D
```

```
cv=cov([xr(:) yr(:)]);
mx=mean(xr); my=mean(yr); % center of the ellipse
beta = 0; Ro = 0;
```

```

if abs(mx)>1e-6 | abs(my)>1e-6
    beta=atan2(my,mx);      % ellipse center in polar
    Ro=sqrt(mx^2+my^2);      % coordinates
end
vx=cv(1,1); vy=cv(2,2);
A=vy; B=-cv(2,1); C=vx;      % ellipse eq. polinomial coeffs.
D=2*(vx*vy-B^2);           % free coeff. in the ellipse polinom.
R=sqrt((A-C)^2+4*B^2);
a=sqrt(2*D/(A+C-R));        % major axis
b=sqrt(2*D/(A+C+R));        % minor axis
theta(1)=atan(2*B/(A-C-R)); % ellipse orientation
% also theta=0.5*atan(2*B/(A-C));

% Calculate ellipse parametric equations
phi=0:pi/128:2*pi;
X=mx+a*cos(theta(1)).*cos(phi)-b*sin(theta(1)).*sin(phi);
Y=my+a*sin(theta(1)).*cos(phi)+b*cos(theta(1)).*sin(phi);

% Modify theta with respect to North
if theta(1) >= -pi & theta(1) < pi/2 theta(2) = -theta(1) + pi/2; end
if theta(1) >= pi/2 & theta(1) <= pi theta(2) = -theta(1) + 2*pi+pi/2; end

```

```

function [a,b,theta,Ro,beta,X,Y]=slopdist(date, fname, ndec, inc, rld, bwidth, po, go)
% SLOPDIST: Plots the data points and the best fit ellipse for the slope dist.
%
% [a,b,theta,Ro,beta,X,Y] = slopdist(date, fname, ndec, inc, rld, bwidth, po, go)
%
% date - day of the month for a particular run i.e. 19
% fname - file name of a particular run i.e. 1047
% ndec - number of points of decimation. Default is no decimation.
% inc - radar incidence angle
% rld - radar look direction
% bwidth - bin width of phase histogram in degrees (9 is default)
% po - print option: 'n' - nothing (default) 'm'-create meta file
% 's' create ps file 'b' create meta & ps files 'q'- create ps & print
% 'p' create meta & ps files & print 'd' dump ps file to network printer
% go - graphics option: 'op' - portrait, half page (default)
% 'ol' - landscape, 'ot' - portrait, full page
% 2a - length of major axis in degrees
% 2b - length of minor axis in degrees
% theta - most likely direction of wave propagaton in degrees
% Ro - distance from origin to center of ellipse
% beta - location angle of ellipse center
% X - x coordinates of best fit ellipse
% Y - y coordinates of best fit ellipse

% Chris Evans, 4/13/93, RSL, The University of Kansas

if nargin == 5 bwidth = 9; po = 'n'; end
if nargin == 6 po = 'n'; end
if nargin == 7 go = 'op'; end

rng = loadsax(fname,'r',ndec); % loads the range data
s = slopeab(rng,inc); % calculates the x and y slope components
s = s - ones(length(s),1)*mean(s);
s = -s; % positive slope is back face of the wave

% Ellipse fit for the slope distribution

[a,b,theta,Ro,beta,freq,ang,X,Y,xr,yr] = ellipself(s(:,1),s(:,2),rld,bwidth);

% Graphics

xr = xr*180/pi; yr = yr*180/pi; % Convert to degrees

```

```

X = X*180/pi; Y = Y*180/pi;
a = a*180/pi; b = b*180/pi;

r = min(X):max(X); % x-coordinate
s = tan(theta(1))*r+Ro; % eqn of line for major axis

u = min(Y):max(Y); % y-coordinate
t = (u-Ro)/tan(pi/2+theta(1)); % eqn of line for minor axis

axis('normal');
axis('square'), axis([-30 30 -30 30]);
plot(X,Y,xr,yr,'x',s,'-t,u,'-'); grid;
%title(['11/' num2str(date) ' ' num2str(fname) ' Slope Dist. and Best Fit Ellipse']);
%ylabel('Sy (Deg)');
%xlabel('Sx (Deg)');

text(.25,.25,['Dir ' sprintf('%3.0f,180/pi*theta(2)) ' deg'],'sc');
text(.25,.20,['Major Axis = ' sprintf('%2.1f ,2*a) ' deg'],'sc');
text(.25,.15,['Minor Axis = ' sprintf('%2.1f ,2*b) ' deg'],'sc');
text(.50,.85,'North','sc')

if po == 'n'
    pause
else
    printps([num2str(fname) 'dir'],go,po);
end

```

```

function [A,B,C,D,E,F] = lsqfit(x,y)
% LSQFIT: finds the least square fit for a 2nd order, 2-D polynomial.
% i.e. Ax^2 + Bxy + Cy^2 + Dx + Ey + F = 0
%
% function [A,B,C,D,E,F] = lsqfit2(x,y)
%
% x - x vector of real data values
% y - y vector of real data values
%
% A,B,C,D,E,F - coefficients of the best-fit polynomial
%
% Written 5/12/93 by Chris Evans, RSL, University of Kansas

x = x(:); y = y(:);

v = [x.^2 x.*y y.^2 x y];
V = v' * v;

a = inv(V);
b = sum(v)';
c = a*b;

A = c(1,1); B = c(2,1); C = c(3,1); D = c(4,1); E = c(5,1); F = -1;

```

```

function [maj,min,alpha] = dirdist2(fname,date,inc,rld,ndec,bwidth)
% DIRDIST2: plots the least square fit for the dir. hist. of the slope data
%
% function [major,minor,alpha] = dirdist2(fname,date,inc,rld,ndec,bwidth)
%
% fname - filename of particular run i.e. 1047
% date - date of run i.e. 19
% inc - radar angle of incidence
% rld - radar look direction
% ndec - number of decimation points (default is 10)
% bwidth - width of bin in deg for phase histogram (9 is default)
%
% maj - length of major axis
% min - length of minor axis
% alpha - most likely direction of wave prop. in deg (rel. to North)
%
% Written 4/20/93 by Chris Evans, RSL, University of Kansas
%

rng = loadsax(fname,'r',ndec);
s = slopeab(rng,inc);
s = s-ones(length(s),1)*mean(s);
s = -s; % positive slope is back face of wave

% Rotate the coordinates relative to the RLD and North
r = (360-rld)*pi/180;
xr = s(:,1)*cos(r)-s(:,2)*sin(r);
yr = s(:,1)*sin(r)+s(:,2)*cos(r);

% Find the directional histogram
binnum = fix(360/bwidth);
angp = angle(xr+j*yr);
[freq,ang] = hist(angp,binnum);
xr = freq.*cos(ang);
yr = freq.*sin(ang);

mx = mean(xr);
my = mean(yr);
l = sqrt(mx^2 + my^2); % Distance from origin to center of ellipse
beta = atan2(my,mx); % Angle between x-axis and ray to center of ellipse

[A,B,C,D,E,F] = lsqfit(xr,yr);

```

```
alpha = 0.5*atan(B/(A-C)); % angle between major axis and pos. x axis
```

```
ca = cos(alpha); sa = sin(alpha); cb = cos(beta); sb = sin(beta);
```

```
% Constants needed to calculate ellipse parameters
```

```
G = A*ca^2 + B*sa*ca + C*sa^2;
```

```
H = A*sa^2 - B*sa*ca + C*ca^2;
```

```
I = 2*A*I*ca*cb+B*I*sin(alpha+beta)+2*C*I*sa*sb+D*ca+E*sa;
```

```
J = -2*A*I*sa*cb+B*I*cos(alpha+beta)+2*C*I*sa*ca-D*sa+E*ca;
```

```
K = A*I^2*(ca^2)+B*I^2*sb*cb+C*I^2*(sb^2)+D*I*cb+E*I*sb+F;
```

```
h = -I/(2*G); k = -J/(2*H); % center coord. of ellipse
```

```
numer = -4*K*G*H + H*I^2 + G*J^2;
```

```
a = sqrt(numer/(4*(G^2)*H)); % 1/2 of major axis
```

```
b = sqrt(numer/(4*G*H^2)); % 1/2 of minor axis
```

```
theta = 0:pi/180:2*pi;
```

```
% Ellipse parametric equations
```

```
x = I*cb+(h+a*cos(theta))*ca-(k+b*sin(theta))*sa;
```

```
y = I*sb+(h+a*cos(theta))*sa+(k+b*sin(theta))*ca;
```

```
% Determine the "true" major axis
```

```
if a>b maj = 2*a; min = 2*b; alpha = (pi/2-alpha)*180/pi;
elseif alpha>0 alpha = (pi-alpha)*180/pi; maj = 2*b; min = 2*a;
else alpha = -alpha*180/pi; maj = 2*b; min = 2*a;
end
```

```
% Normalize area to 1
```

```
norm = sqrt(pi*maj*min);
```

```
x = x/norm; y = y/norm; maj = maj/norm; min = min/norm;
```

```
xr = xr/norm; yr = yr/norm; h = h/norm; k = k/norm;
```

```
if h < 0 alpha = alpha + 180; end
```

```
% Graphics
```

```
axis('square'), axis([-1 1 -1 1]);
plot(xr,yr,'*',h,k,'o',x,y);grid;
%title(['11/' num2str(date) '' num2str(fname) ' Dir. Histogram fit with LSQ
Method']);
%ylabel('Relative Units');
%xlabel('Relative Units');
text(.5,.9,'North','sc');
text(.25,.25,['Dir ' sprintf('%3.0f',alpha) ' deg'],'sc');
text(.25,.20,['Major axis = ' sprintf('%3.2f',maj)],'sc');
text(.25,.15,['Minor axis = ' sprintf('%3.2f',min)],'sc');
```

```

function whspec(name,inc,rld,ndec,m,nooverlap)
% WHSPEC(name,inc,ndec,rld,m,nooverlap) calculates the waveheight spectrum
% the directional spectrum, and the angular spread about the mean
% direction using the Longuet-Higgins approach. It plots the results
% along with the results from F. Ziemer of Geekstacht, Germany who
% used a pitch-and-roll buoy.
%
% name   : 4 digit name of file run. i.e. for 19111047 enter 1047
% inc    : radar incidence angle
% rld    : radar look direction in deg (North is 0, East is 90, etc.)
% ndec   : number of decimation points
% m      : 3-valued row vector where
%           m(1) is the length of the Kth segment of data
%           m(2) is the number of FFT points used (use a power of 2)
%           m(3) is the sampling interval in sec (0.1*ndec)
% nooverlap : m(1) - point sections should overlap nooverlap points
%
% For more information about periodogram analysis, see Discrete-Time
% Signal Processing by Oppenheim and Schafer, pgs 730-742.
%
% Chris Evans, RSL, The University of Kansas, June 16, 1994
%
clf; hold off;

rld = rld*pi/180;
[wh, rng] = loadsax(name,'wr',ndec);
wh = (wh(:,1) + wh(:,2) + wh(:,3))./3;
[s] = slopeab(rng,inc);
s = s - ones(length(s),1)*mean(s);
Sx = s(:,1); Sy = s(:,2);
sx = Sy*sin(rld)+Sx*cos(rld);    % transforms slopes to North and East
sy = Sy*cos(rld)-Sx*sin(rld);

[P] = spec(wh,sx,m,nooverlap);
a = P(:,1); b = P(:,2); q13 = P(:,3);

[Q] = spec(wh,sy,m,nooverlap);
c11 = Q(:,1); c = Q(:,2); q12 = Q(:,3);

[R] = spec(sx,sy,m,nooverlap);
c33 = R(:,1); c22 = R(:,2); c23 = R(:,3);
clear a; clear b; clear c;

```

```

A = q12 ./sqrt(c11 .*(c22 + c33)); % Equations are from Ziemer
B = q13 ./sqrt(c11 .*(c22 + c33));

mwd = (180/pi)*atan2(q12,q13); % Mean wave direction
angsp = (180/pi)*sqrt(2-2*sqrt(A.^2 + B.^2)); % Angular Spread

mwd = -mwd + 90; % Coordinate Transformation
a = find(mwd<0);
mwd(a) = mwd(a) + 360;

% This loop keeps adjacent points near
% each other. i.e. 350 deg, 10 deg.
%for i = 2:m(1) + 1; % would be plotted as 350, 370.
% if (mwd(i) - mwd(i-1)) > 235, mwd(i) = mwd(i) - 360; end
% if (mwd(i) - mwd(i-1)) < -235, mwd(i) = mwd(i) + 360; end
%end

[n,m] = size(c11);
if rem(n,2) == 0
    f = (10/ndec)*(-n:2:n-2)/(2*n);
    select = [2:n/2 n/2+2:n];
else
    f = (10/ndec)*(0:n-1)/(2*(n-1));
    select = 2:n-1;
end

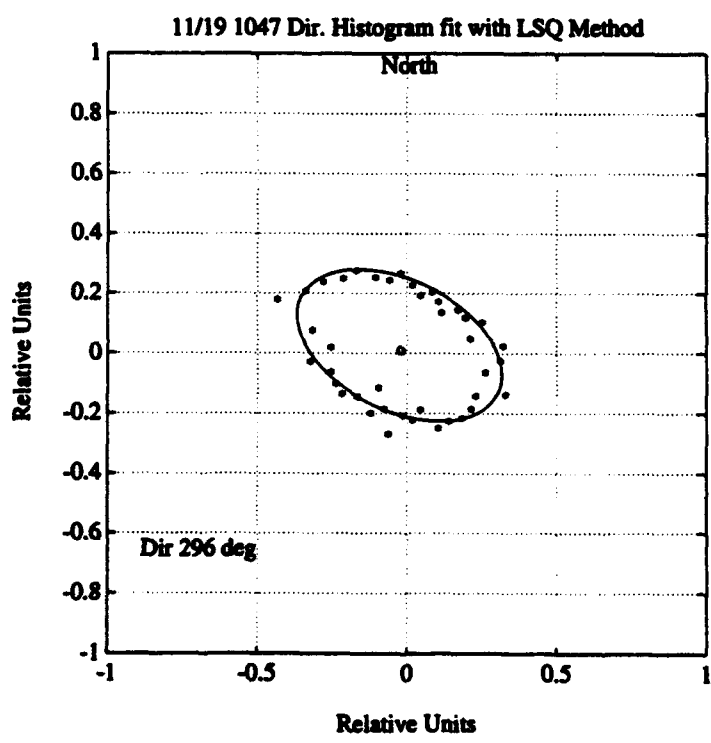
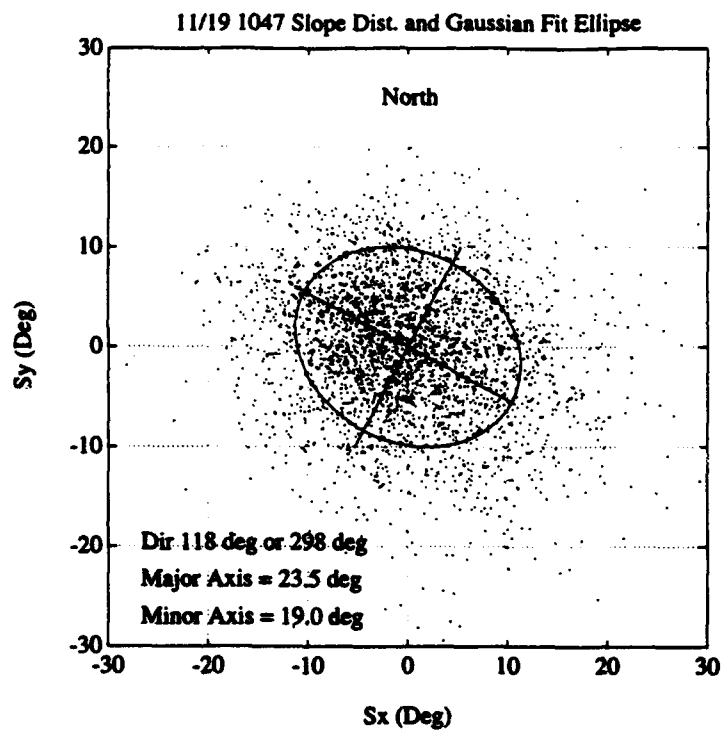
df = 0.5*abs(f(2)-f(1));
zoom(1) = find(f > 0-df & f < 0+df);
zoom(2) = find(f > 0.4-df & f < 0.4+df);
select = zoom(1):zoom(2);

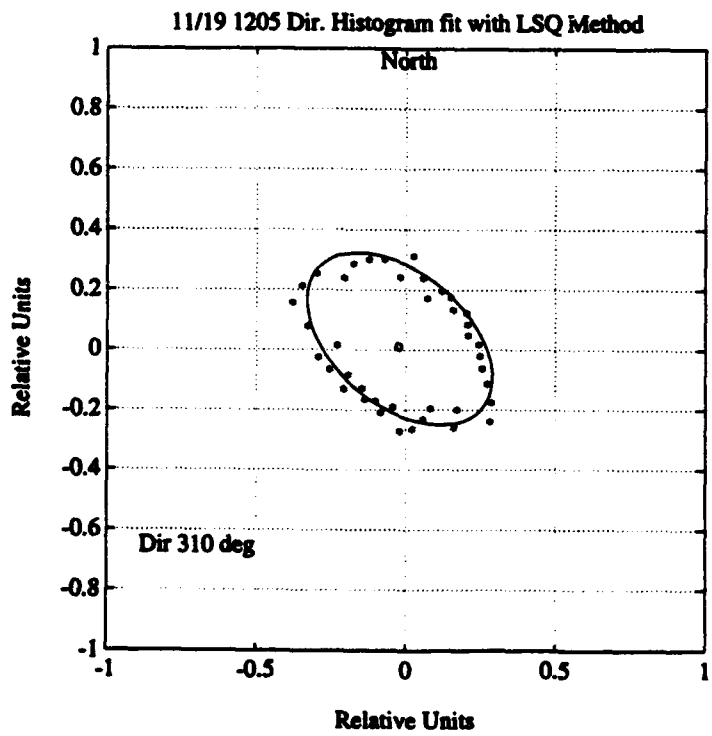
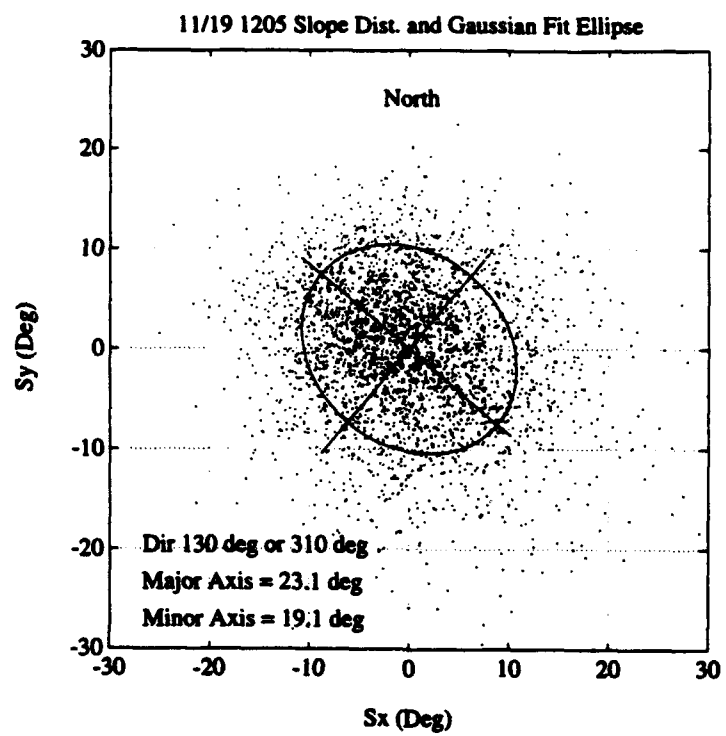
plot(f(select),c11(select)),grid
title([num2str(name) ' Waveheight PSD']);
xlabel('Frequency');
ylabel('['m^2/Hz]');
%printps([num2str(name) 'a'],'op','b');
pause
plot(f(select),mwd(select)),grid
title([num2str(name) ' Wave Direction']);
xlabel('Frequency');
ylabel('Degree');

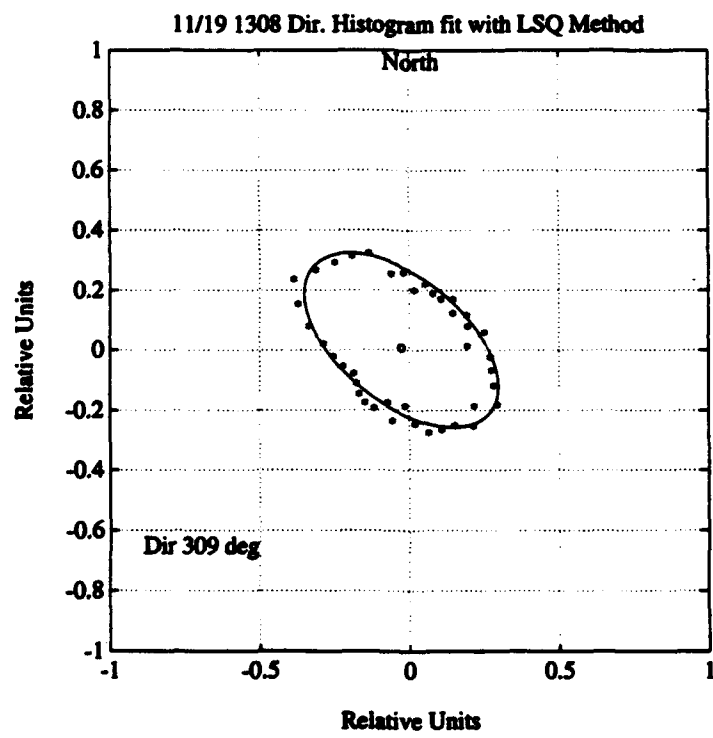
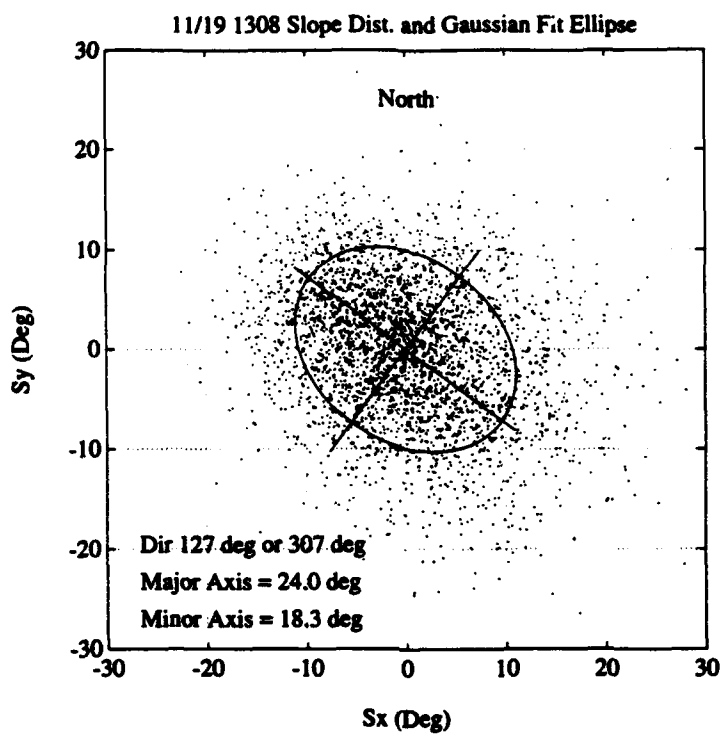
```

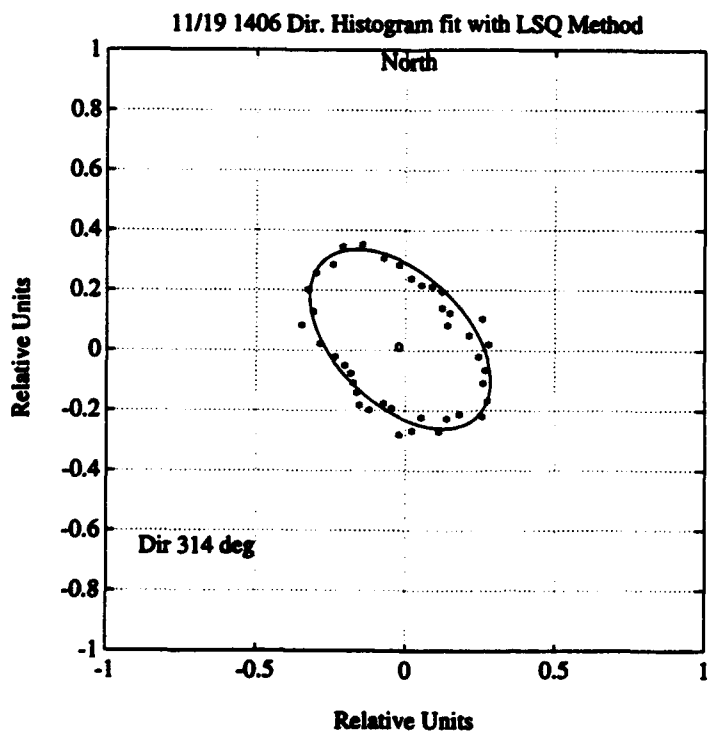
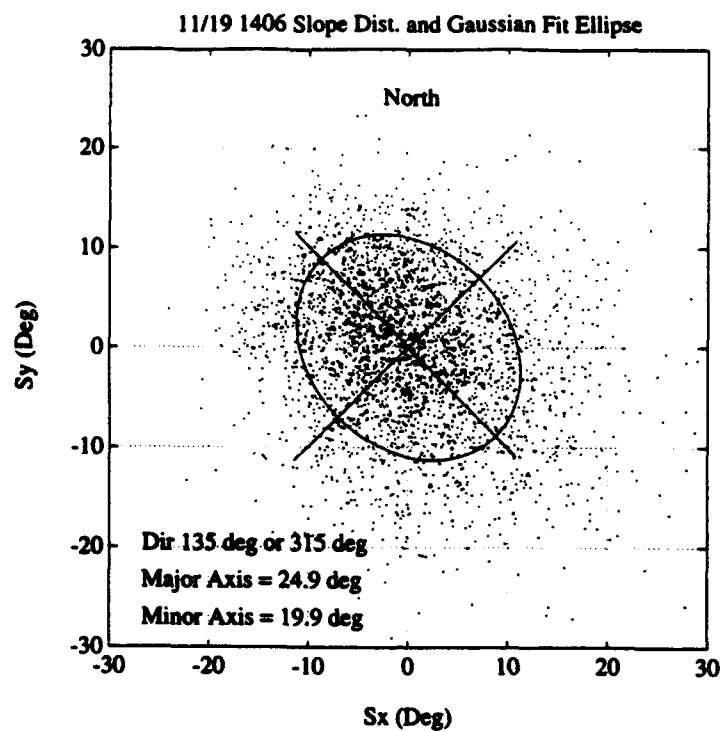
```
%printps([num2str(name) 'a'],'op','b');
pause
plot(f(select),angsp(select)),grid
title([num2str(name) ' Angular Spread']);
xlabel('Frequency');
ylabel('Degree');
%printps([num2str(name) 'b'],'op','b');
```

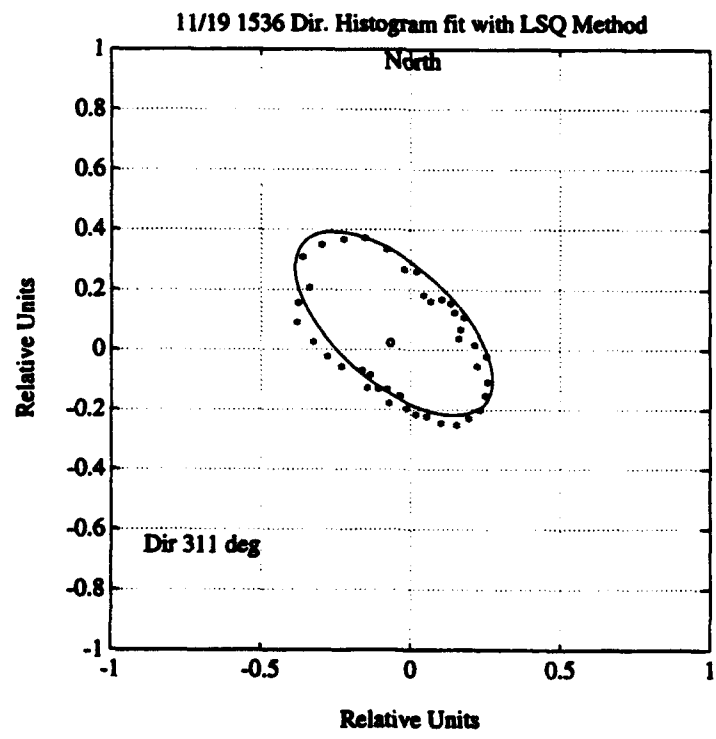
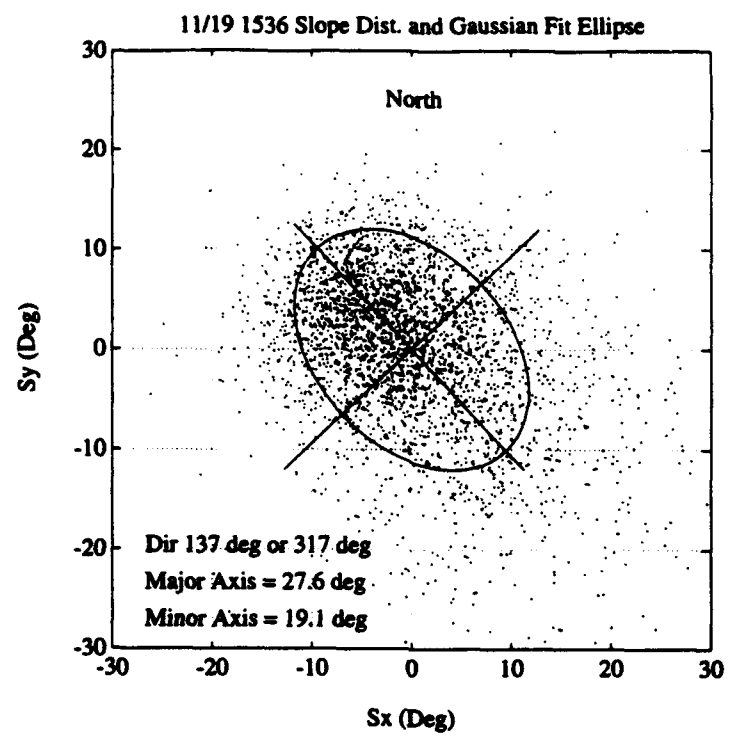
## Appendix B

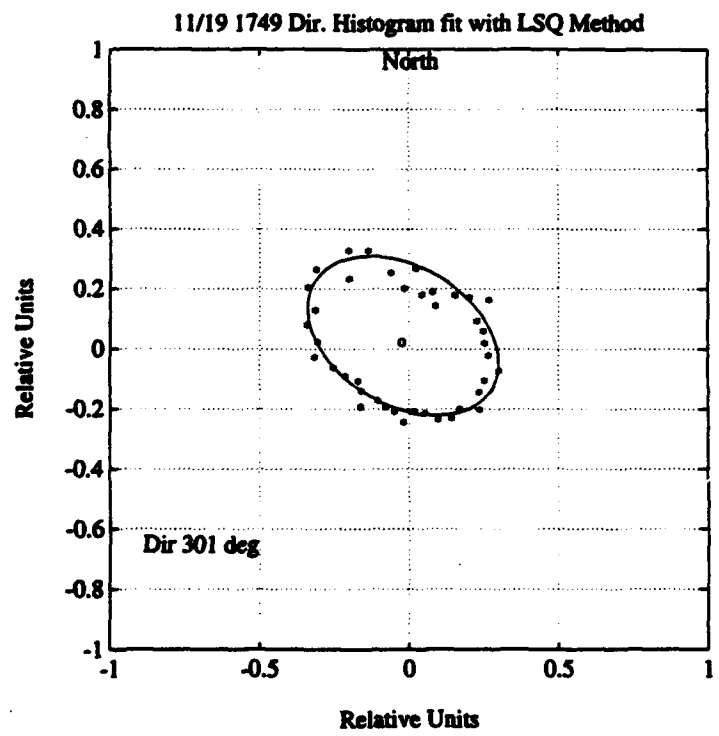
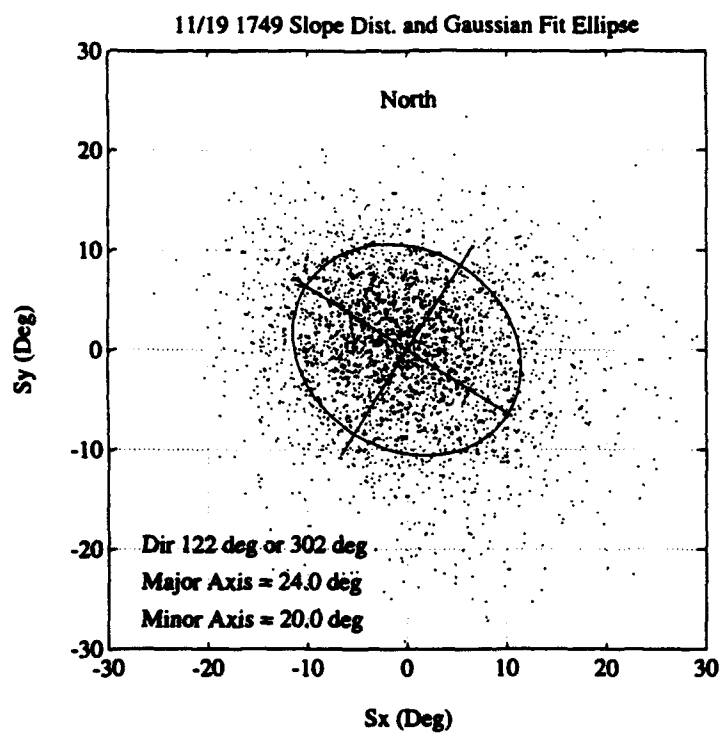


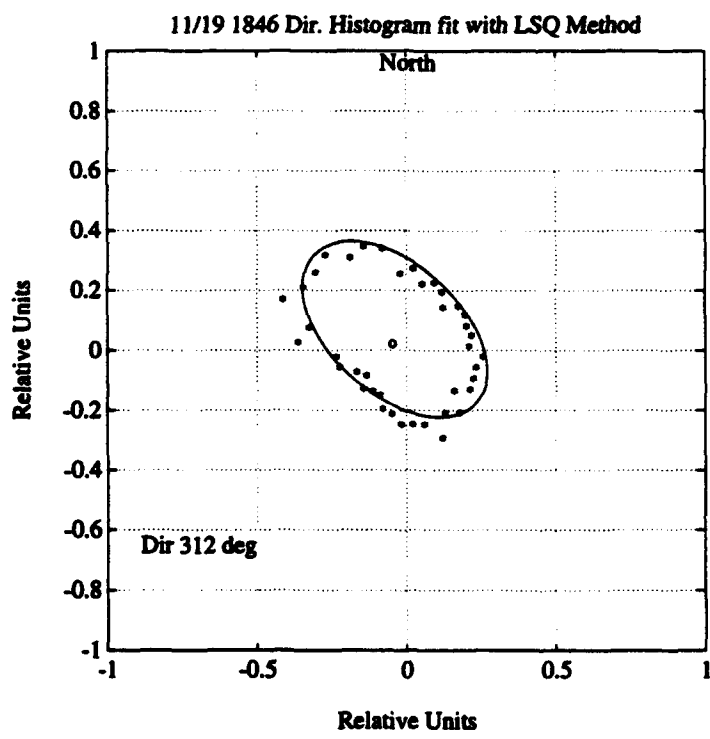
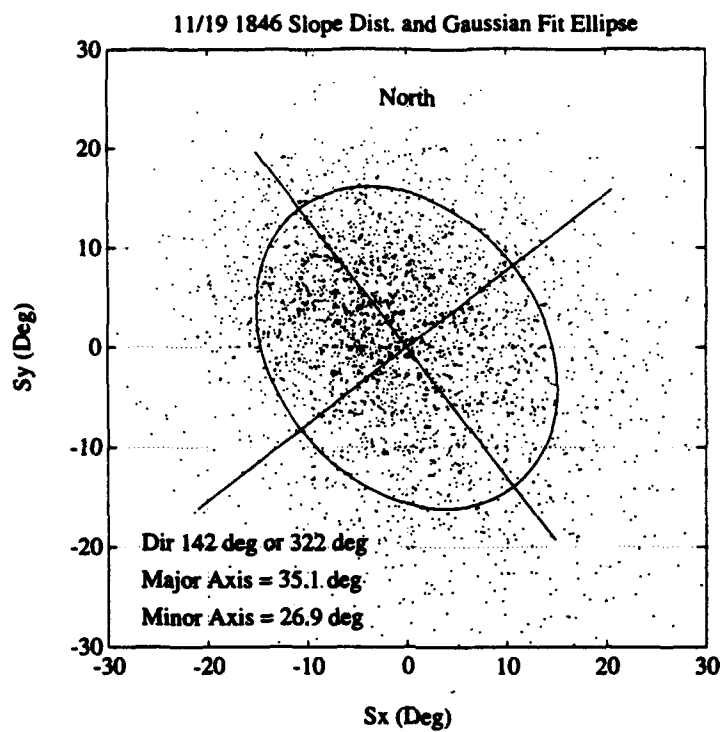


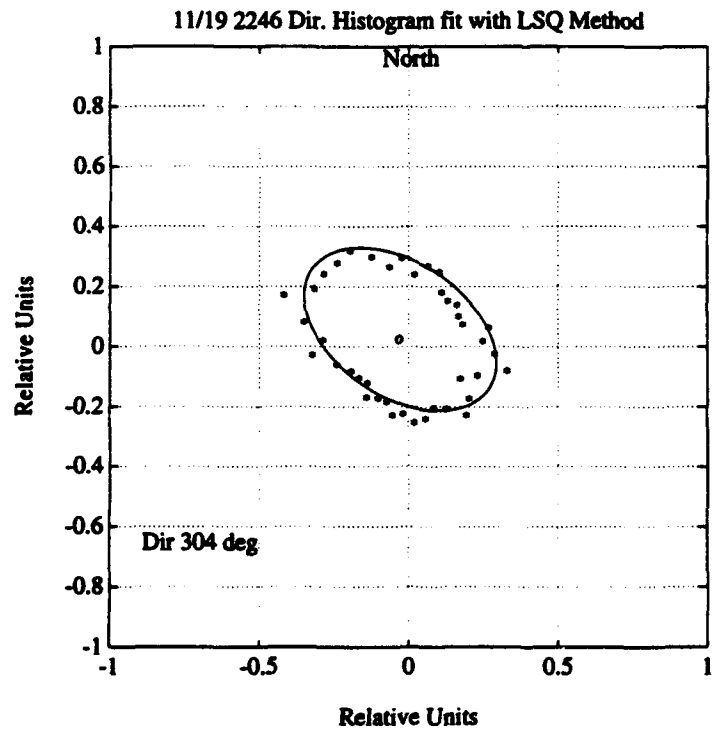
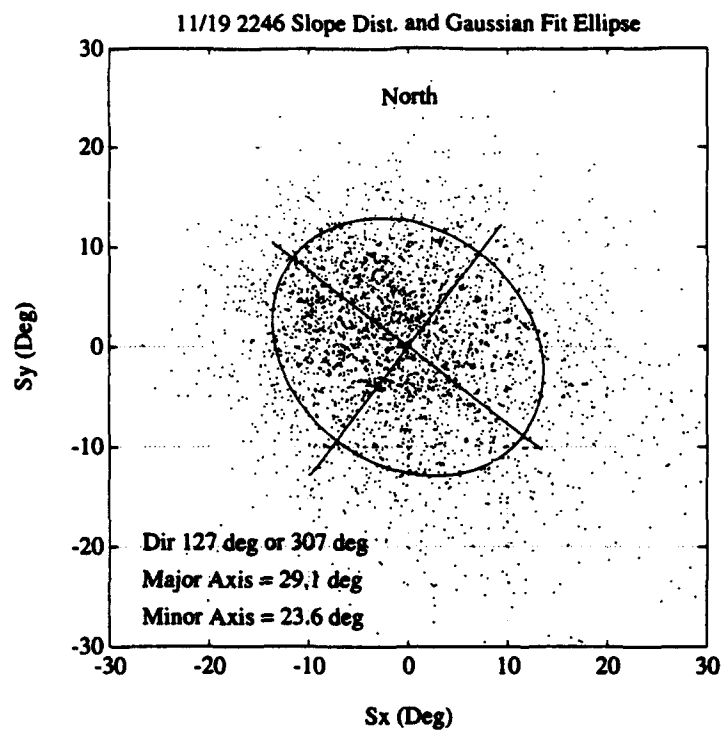


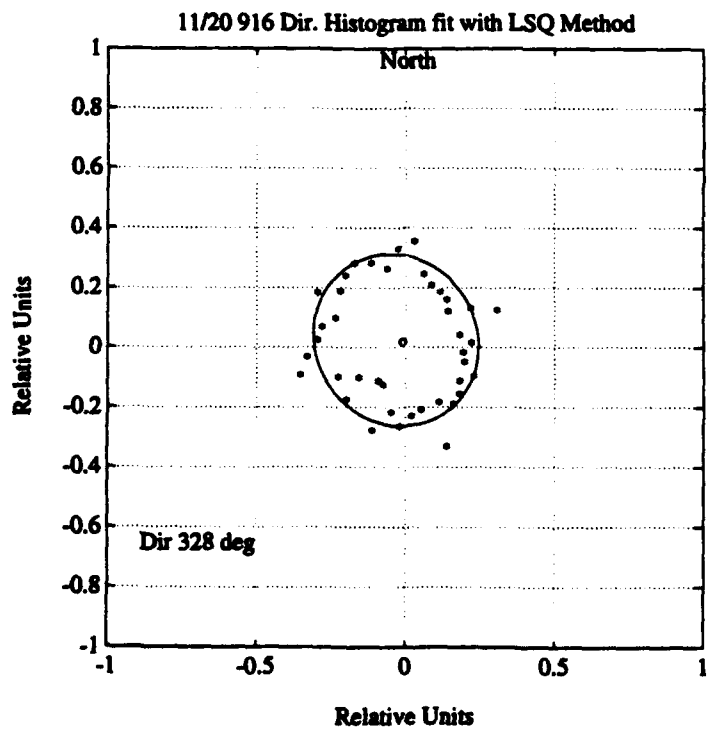
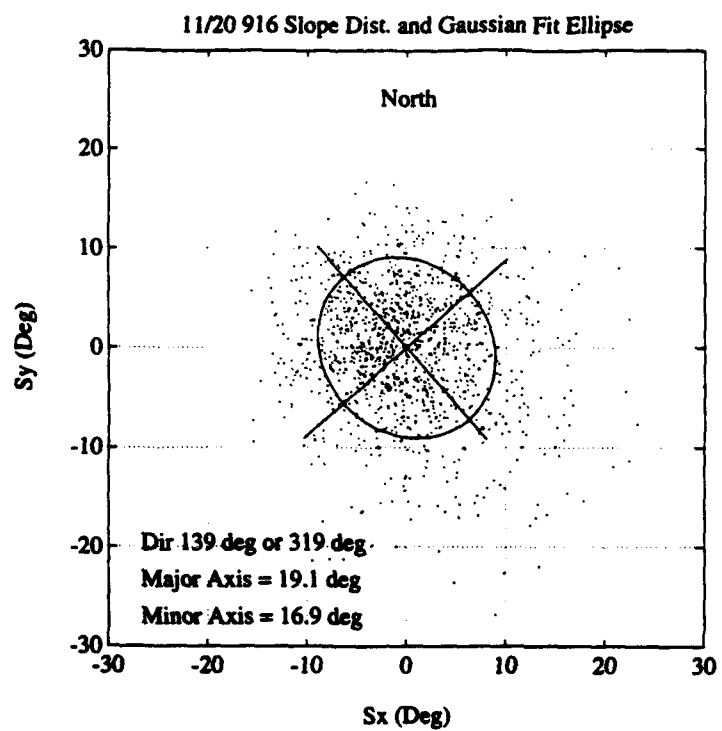


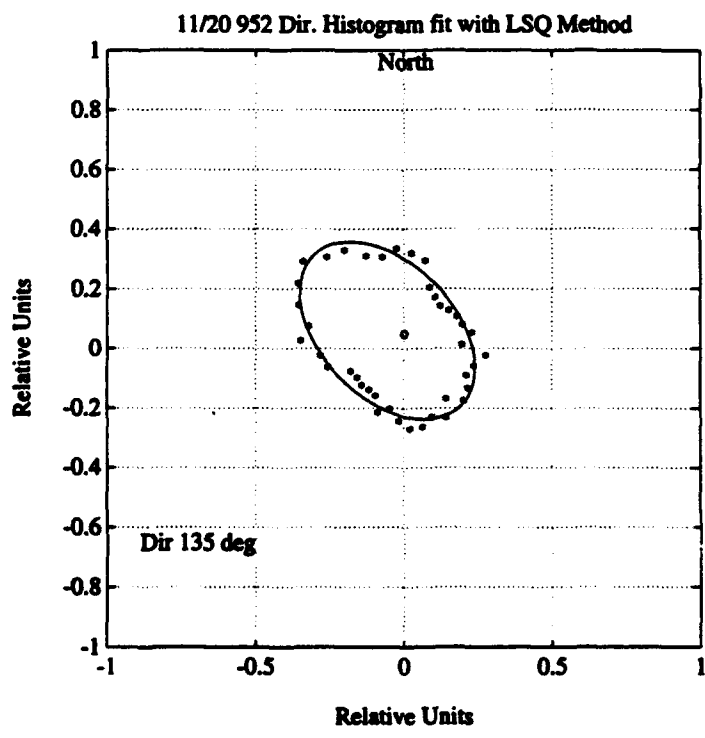
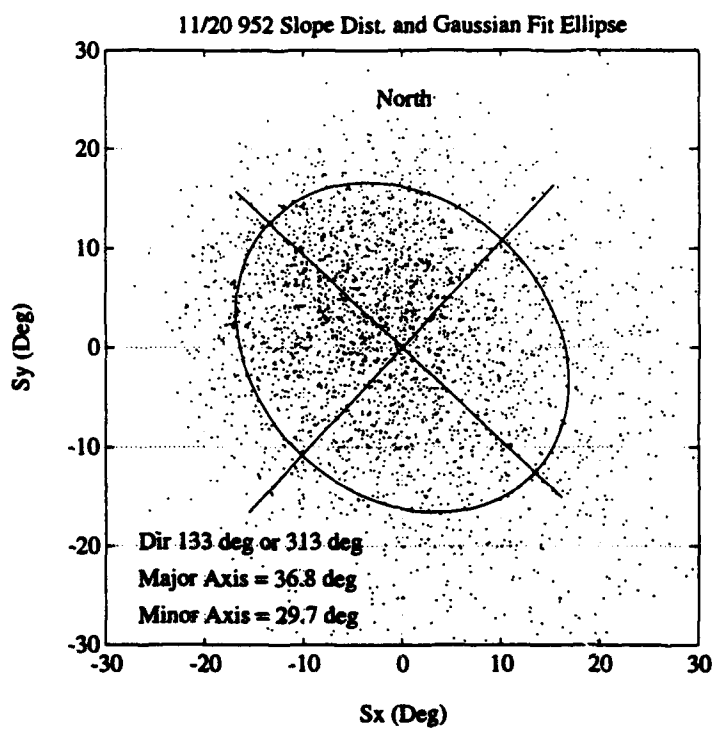


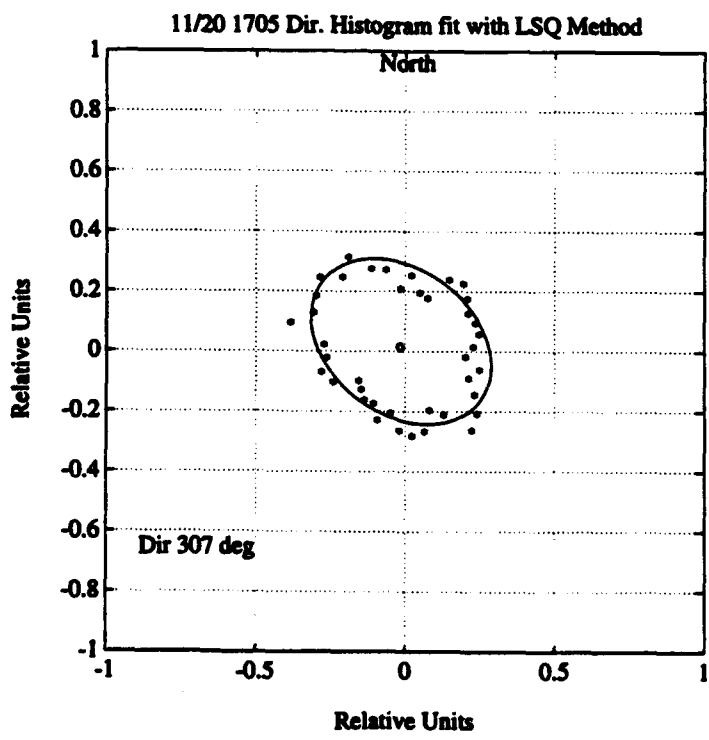
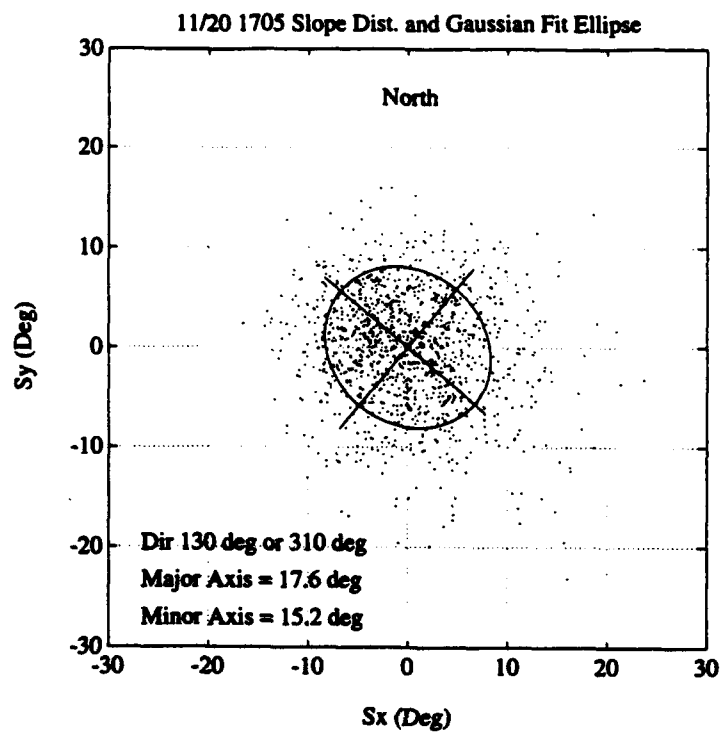


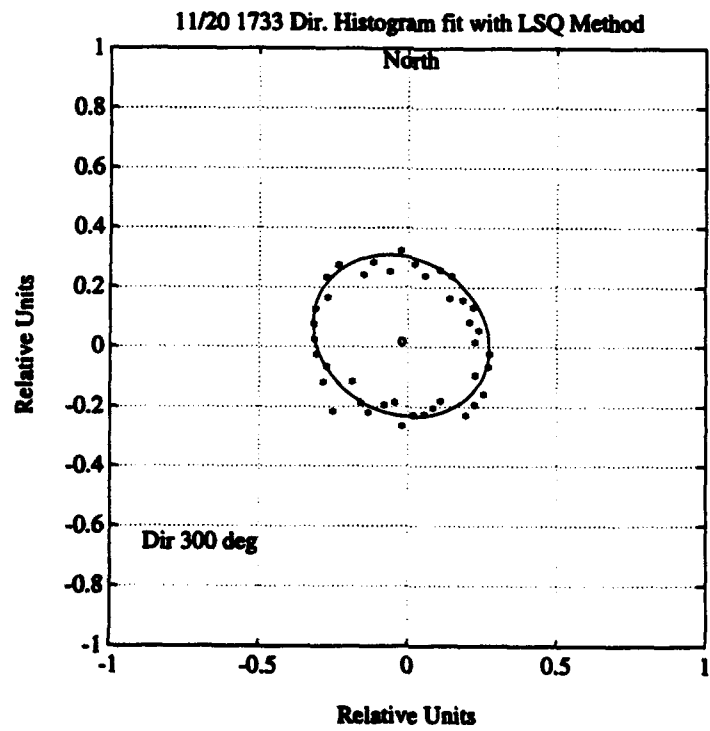
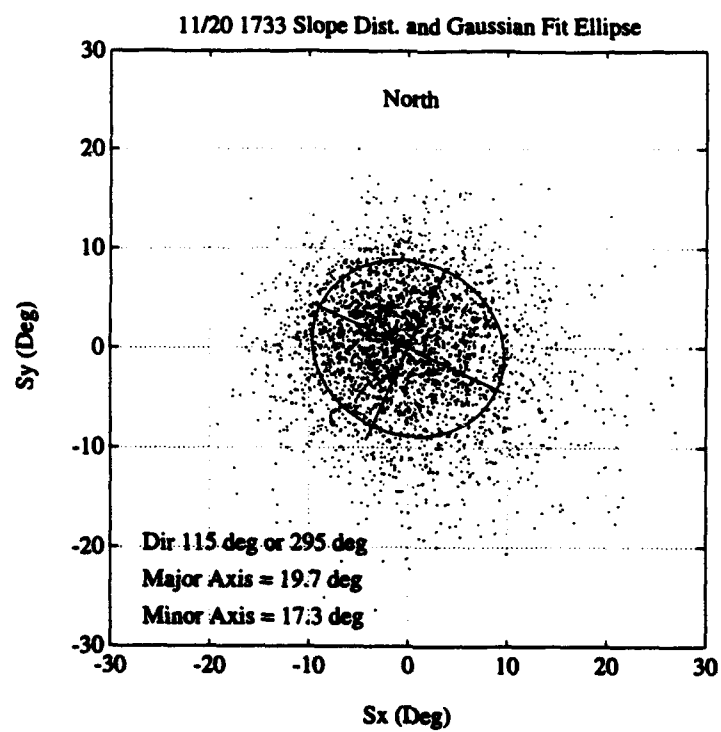


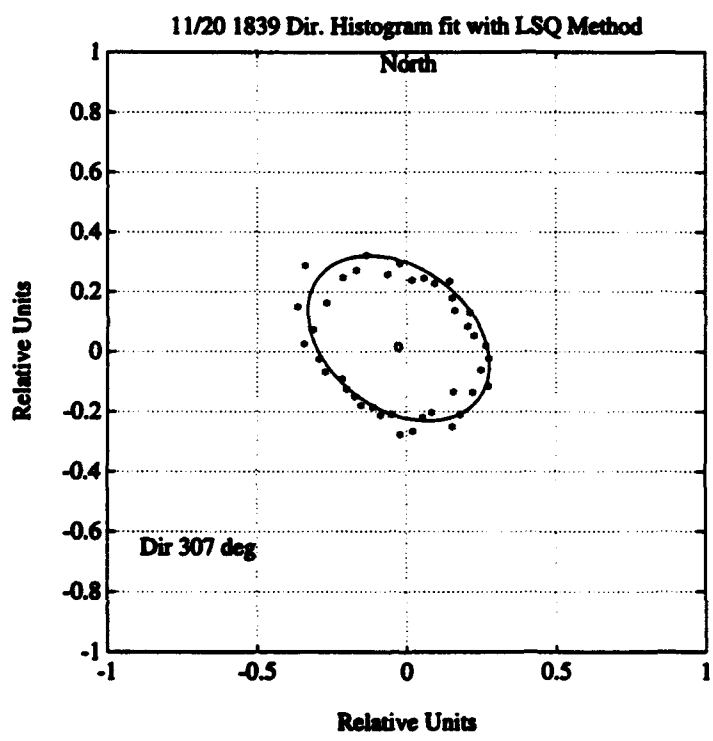
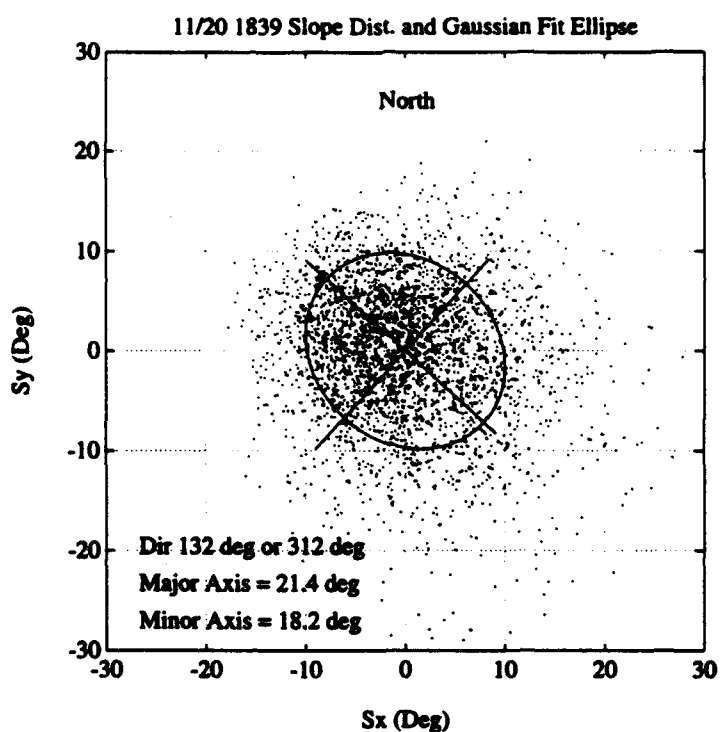


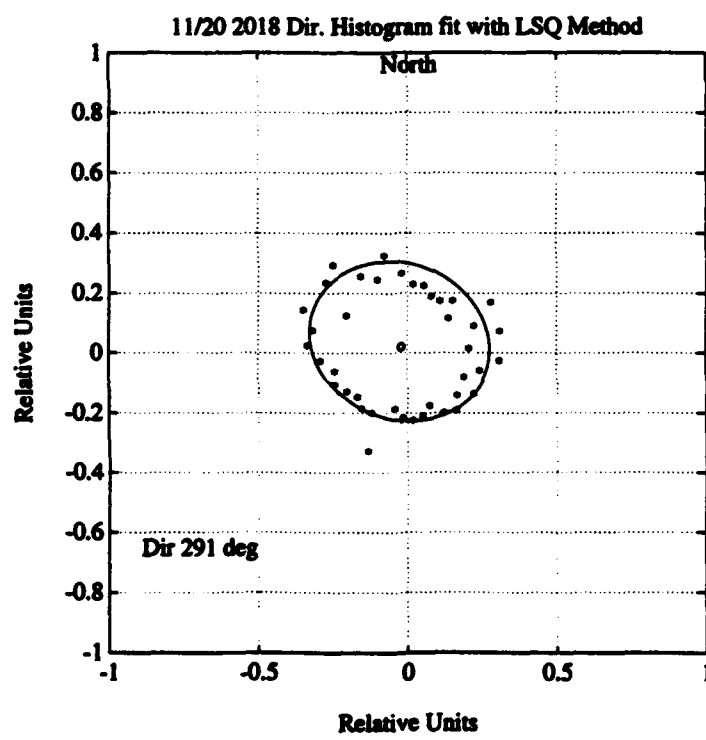
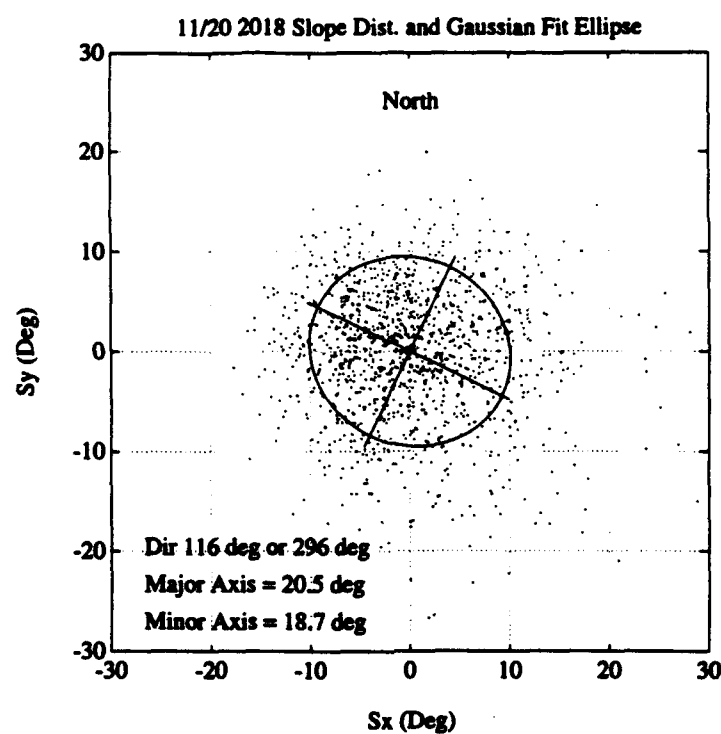


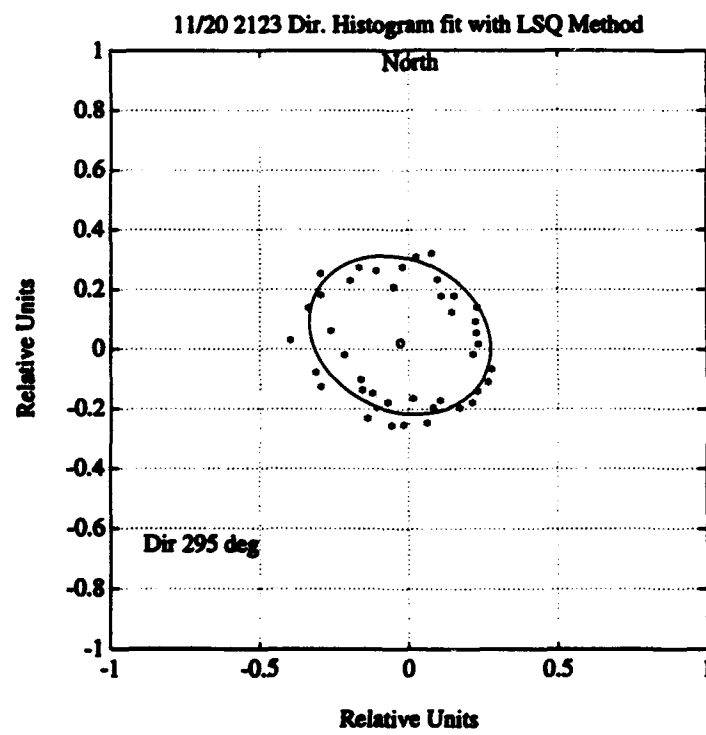
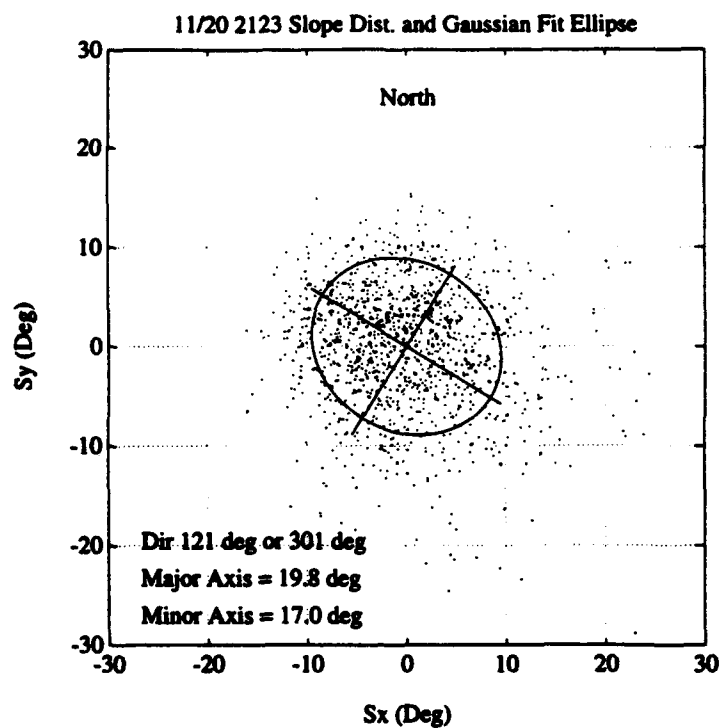


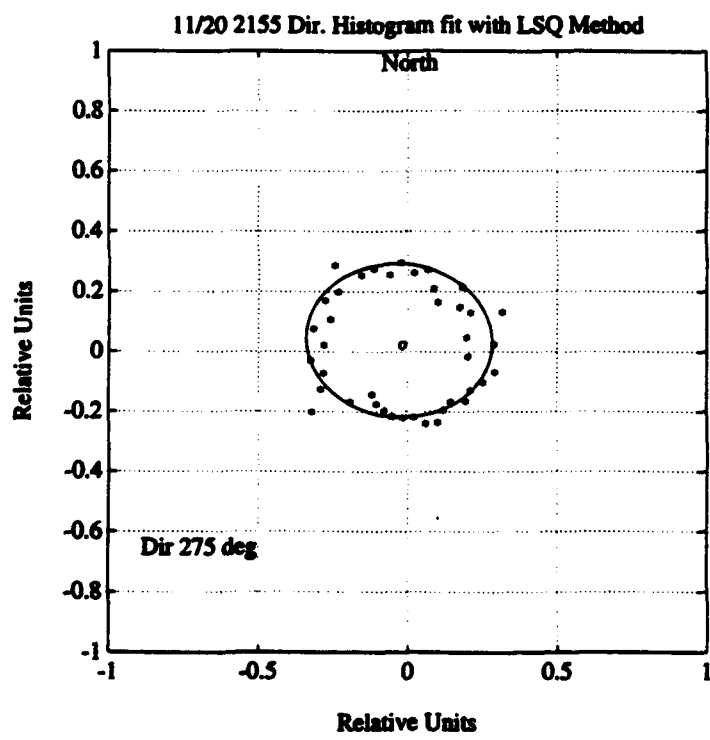
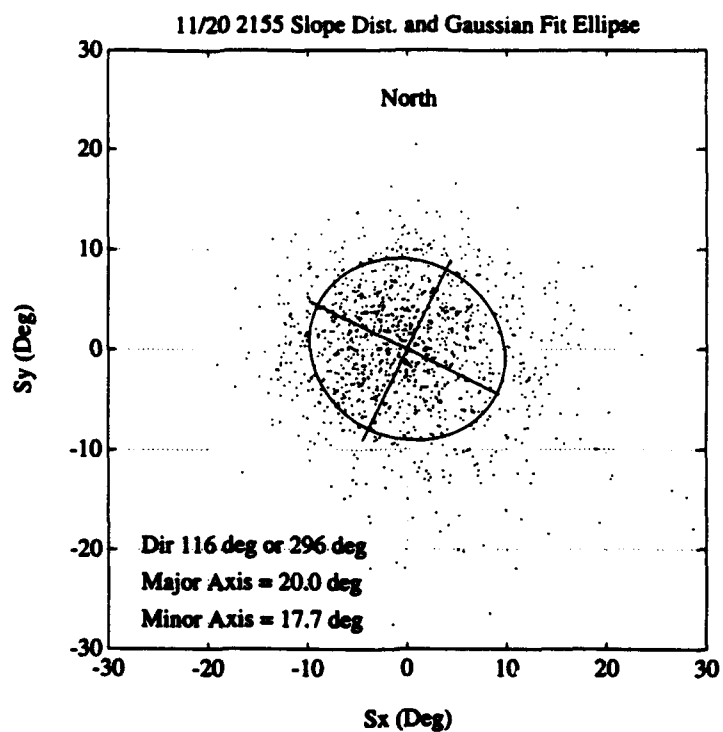


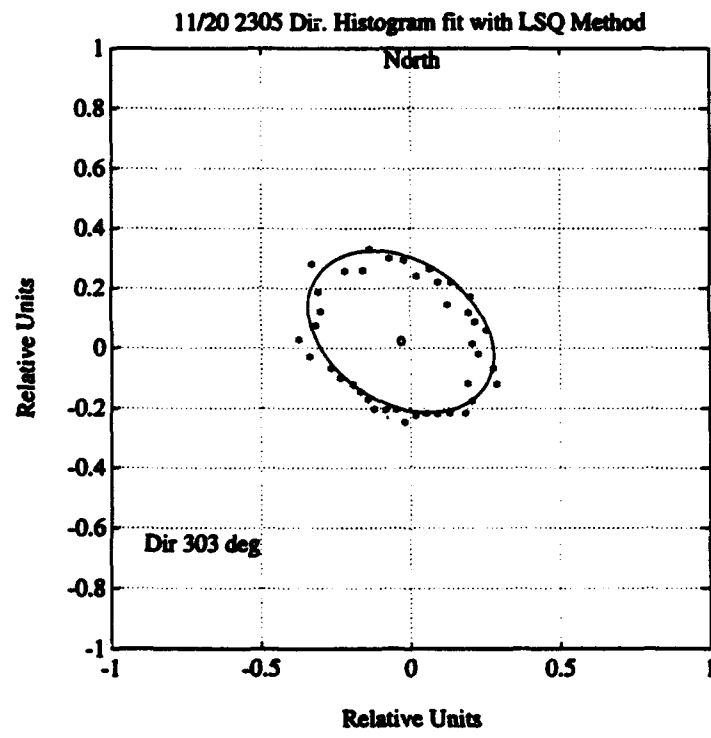
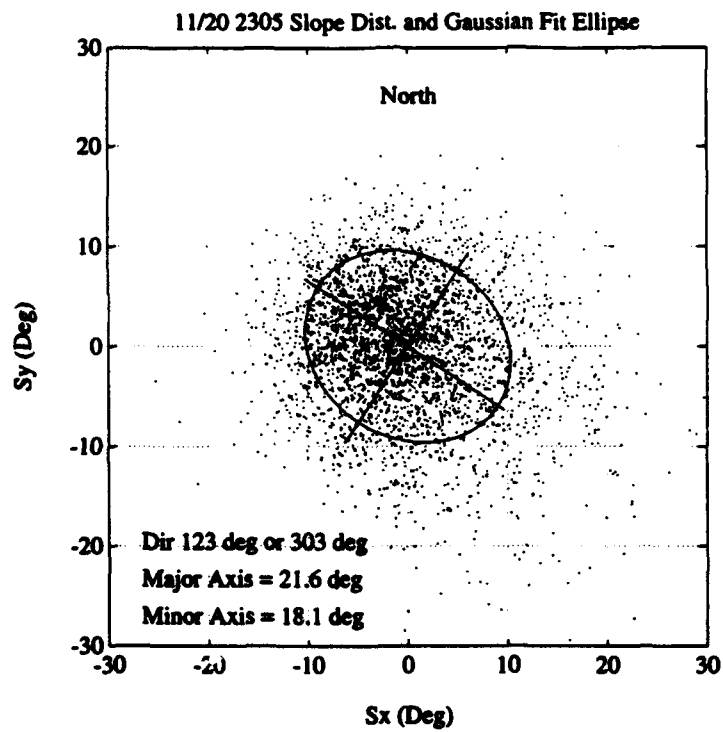


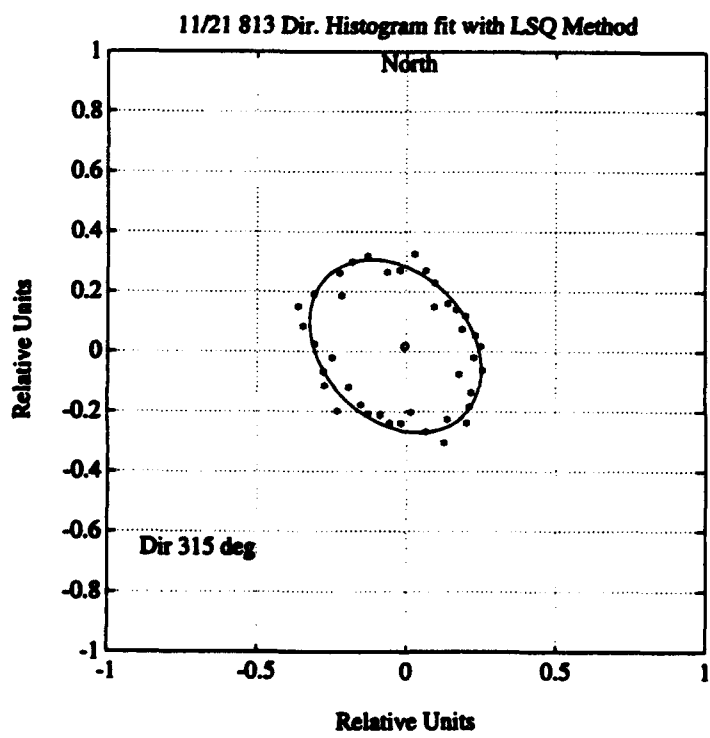
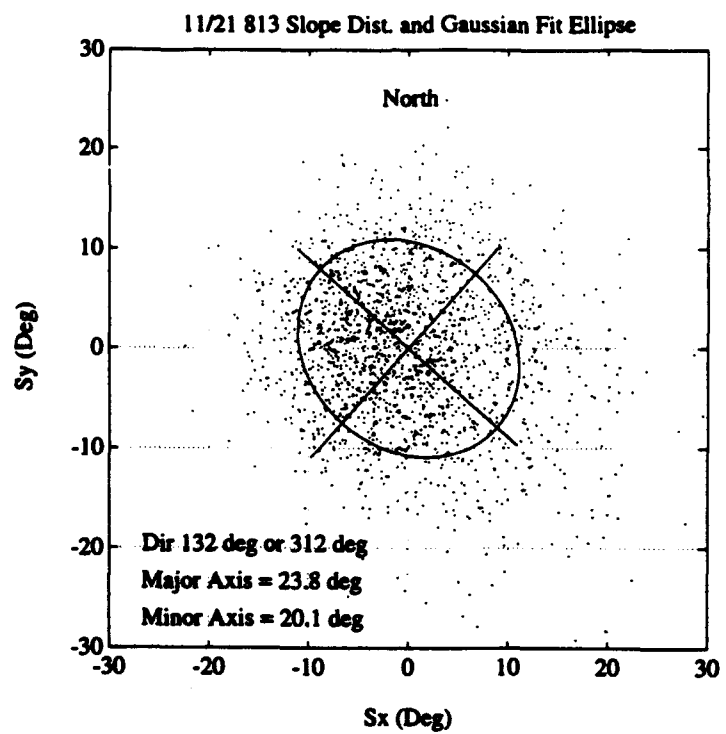


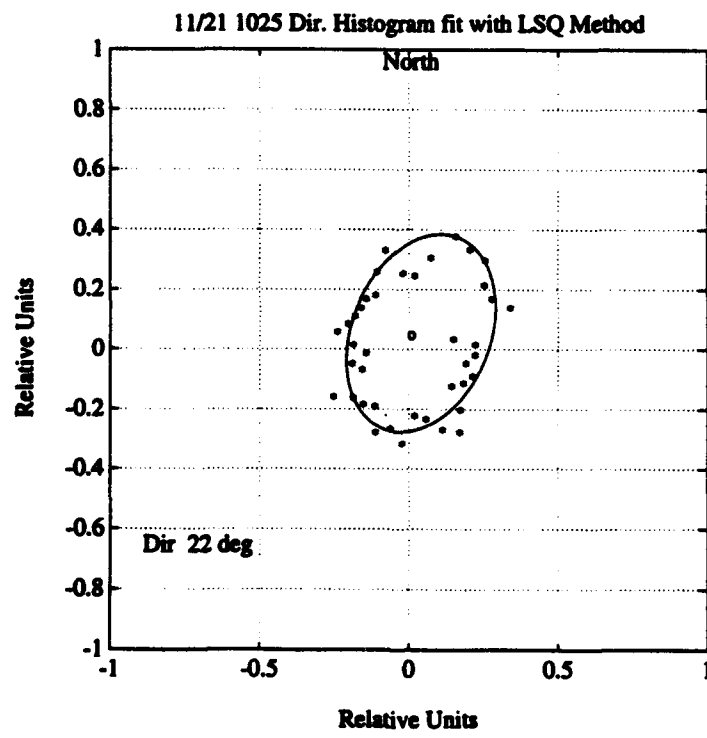
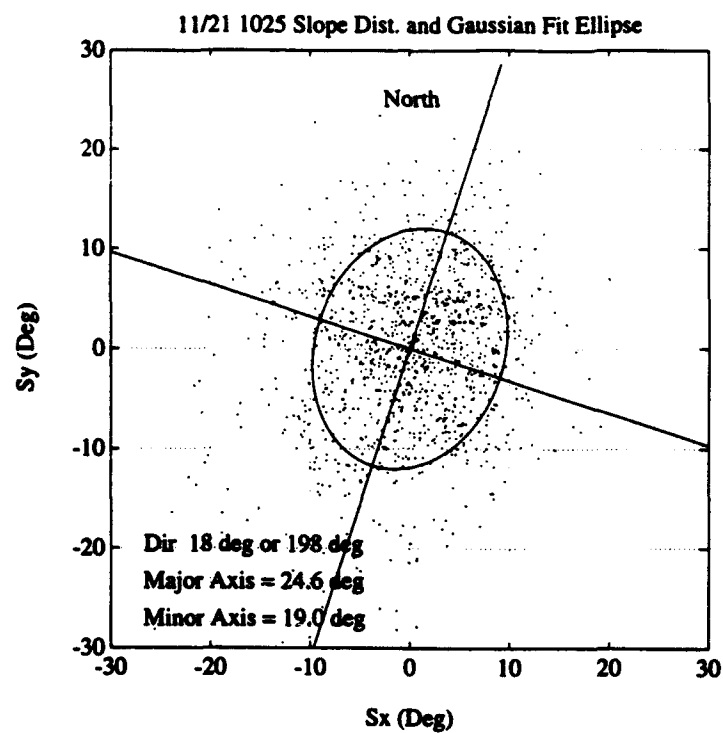


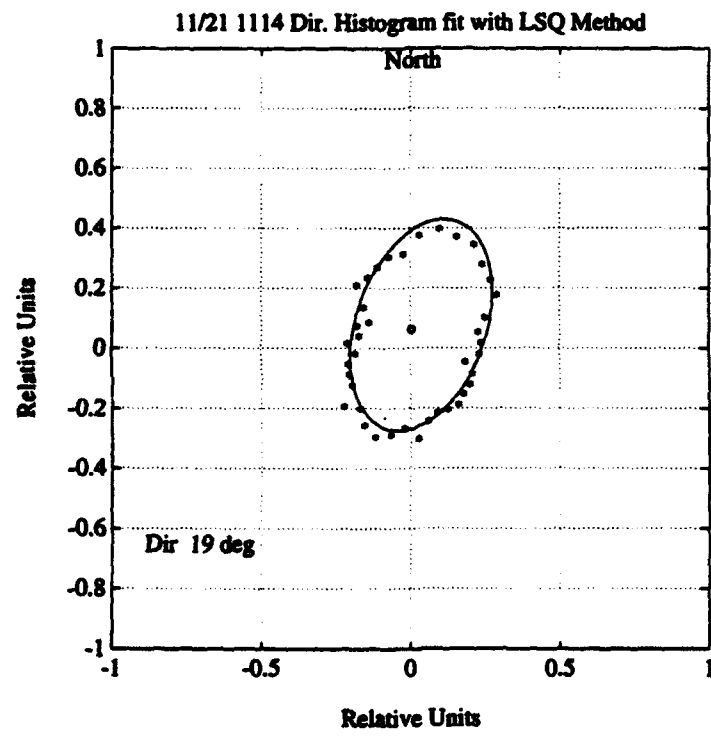
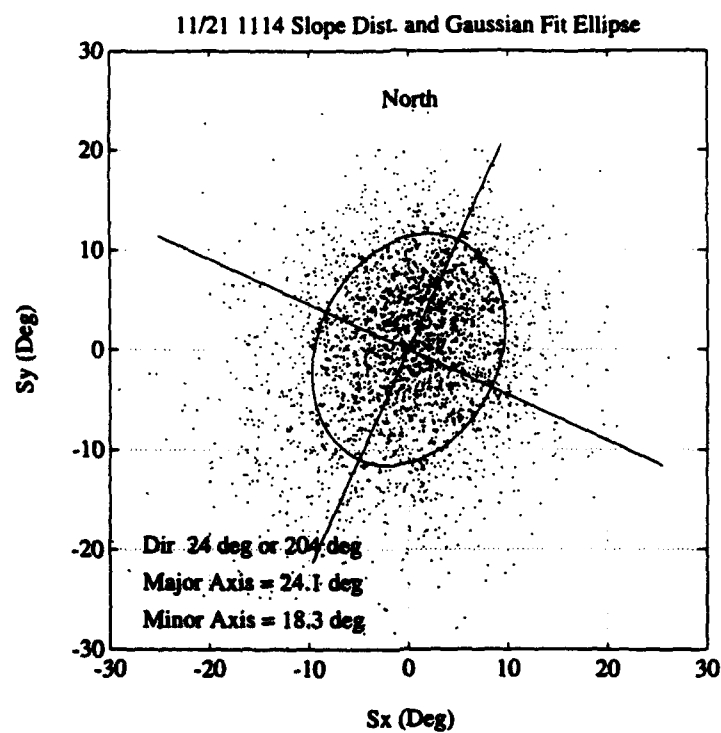


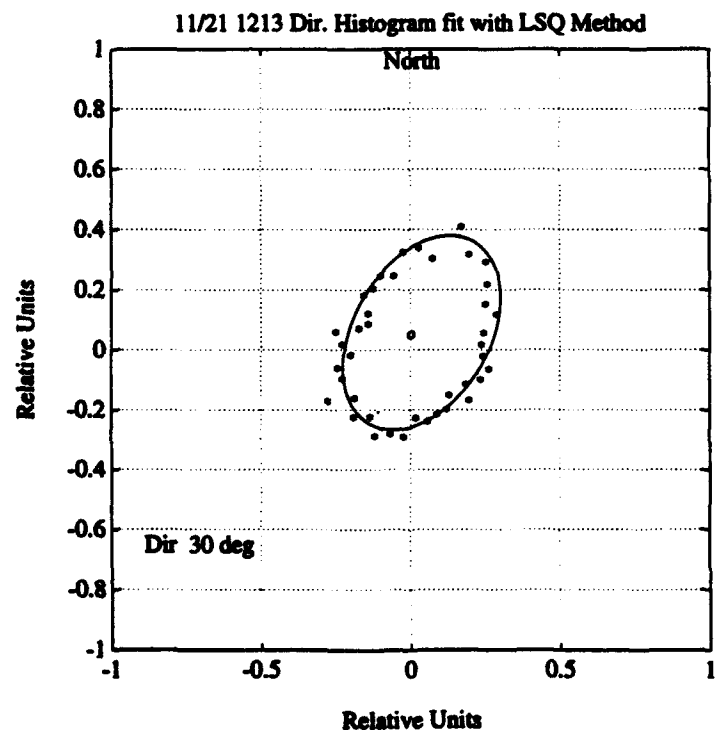
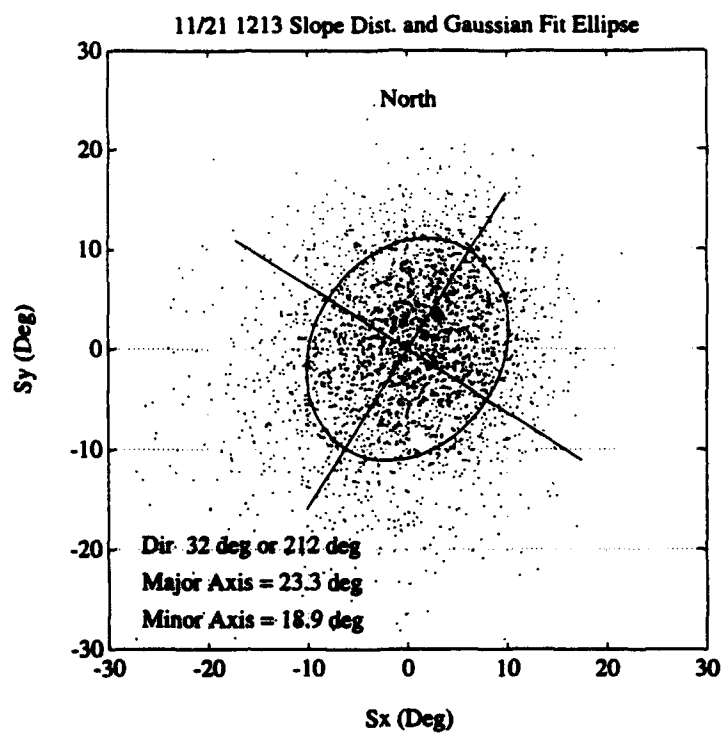


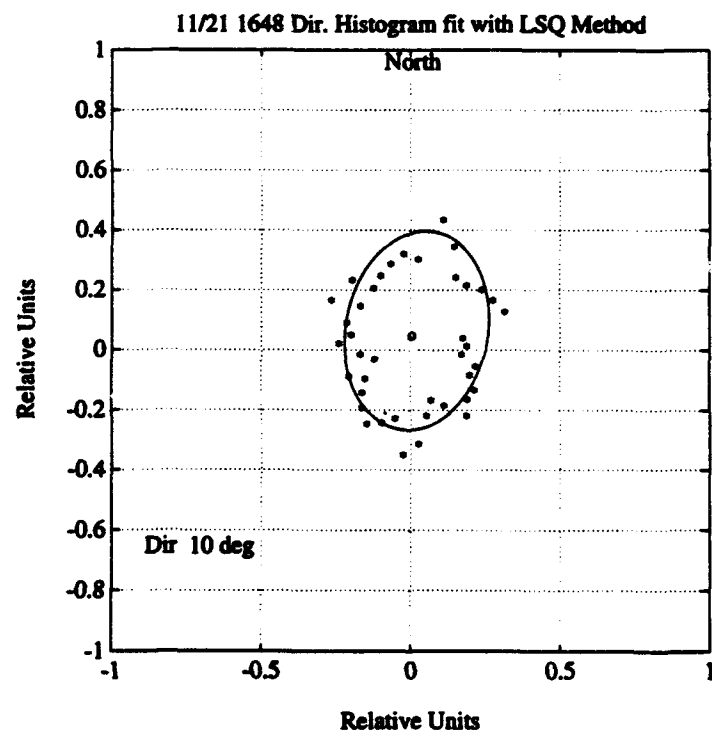
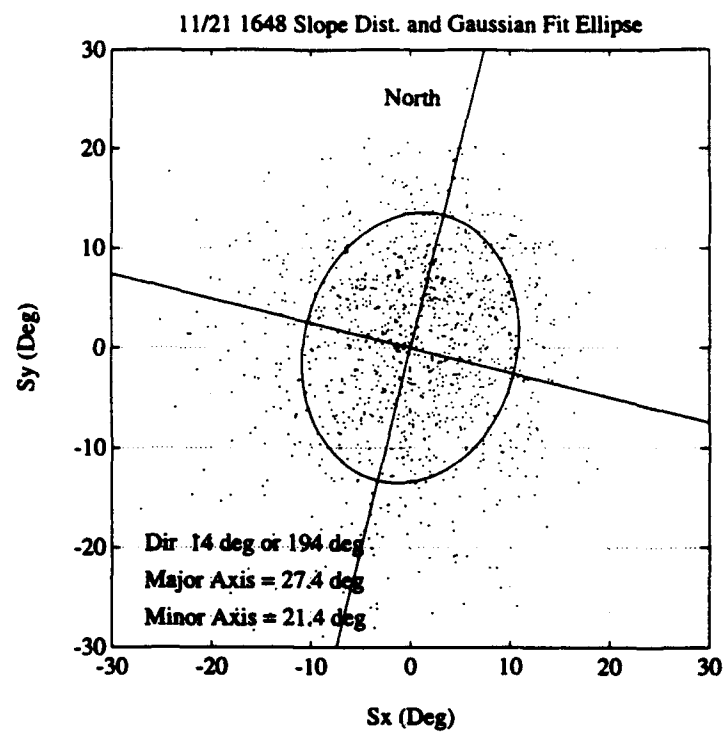


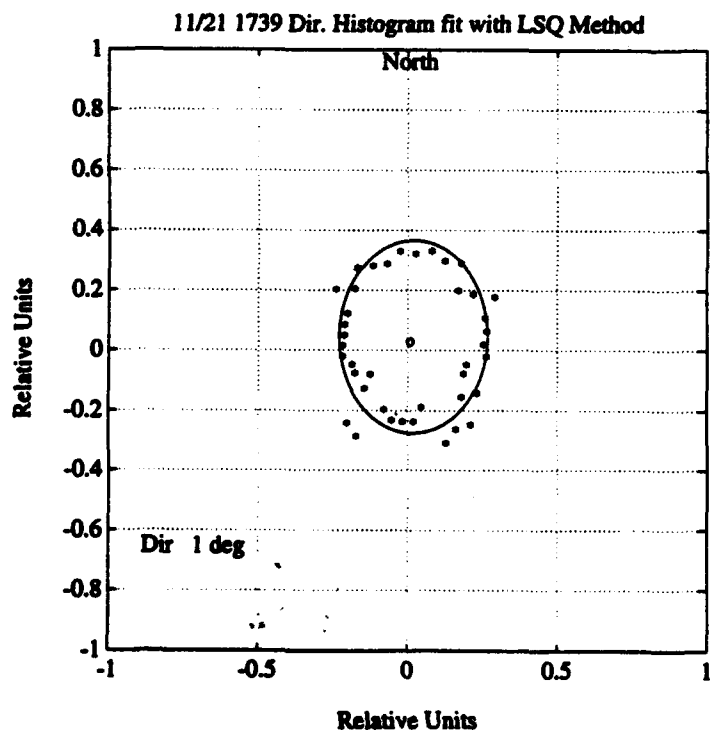
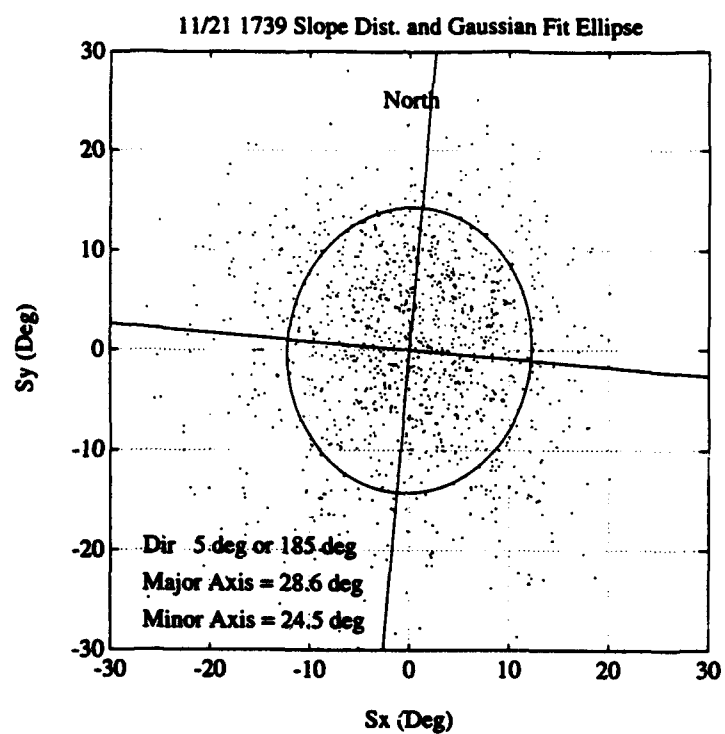


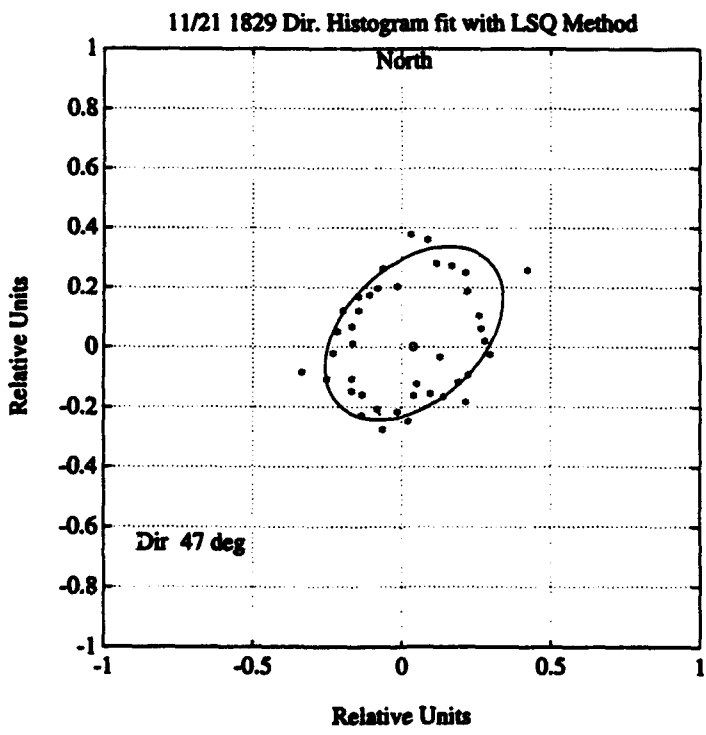
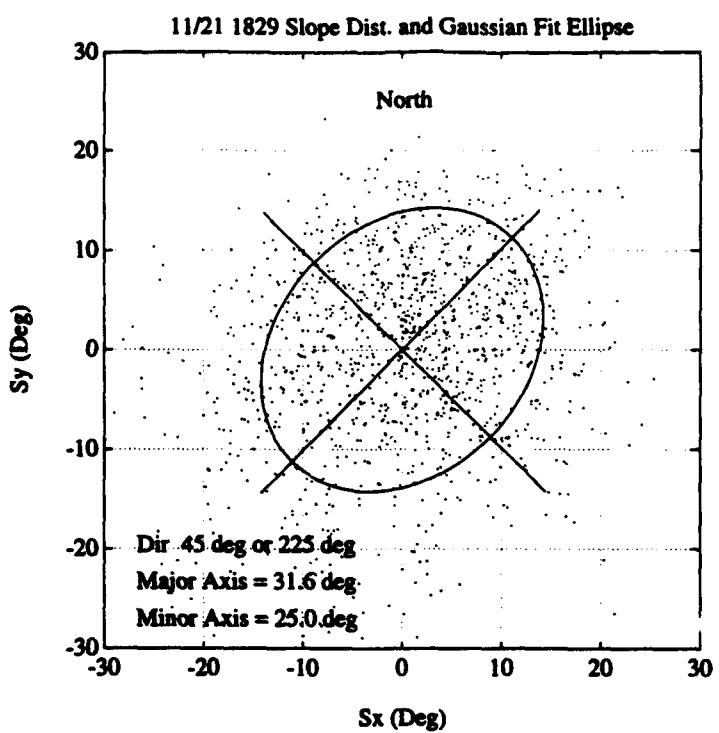


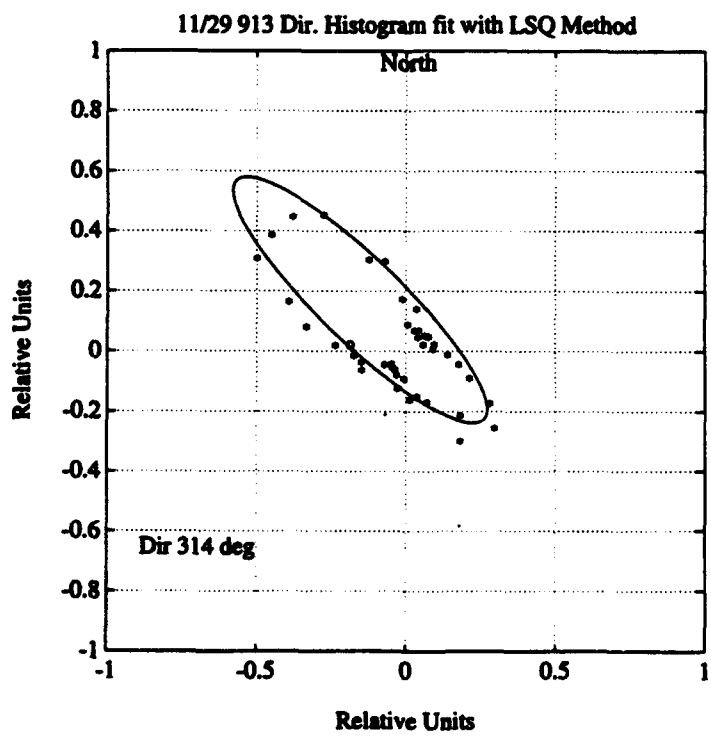
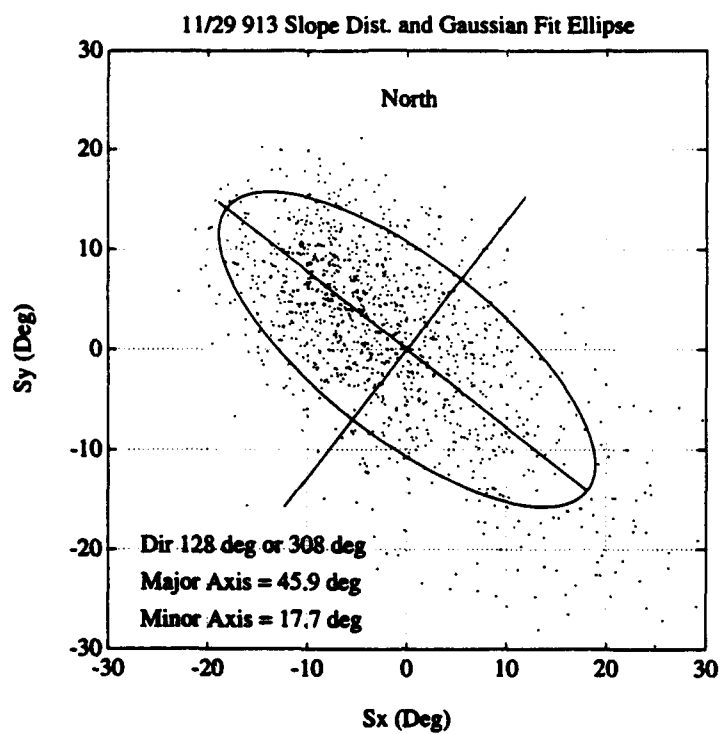


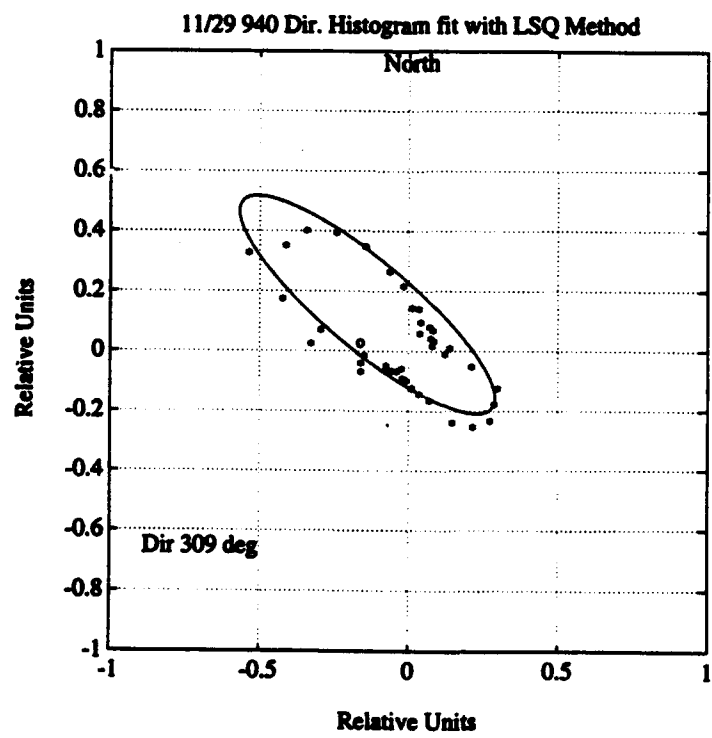
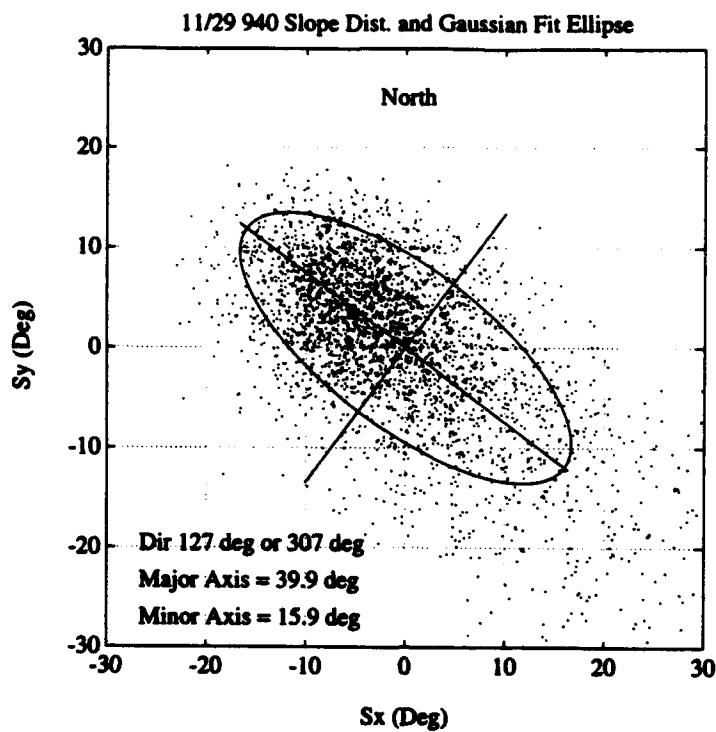


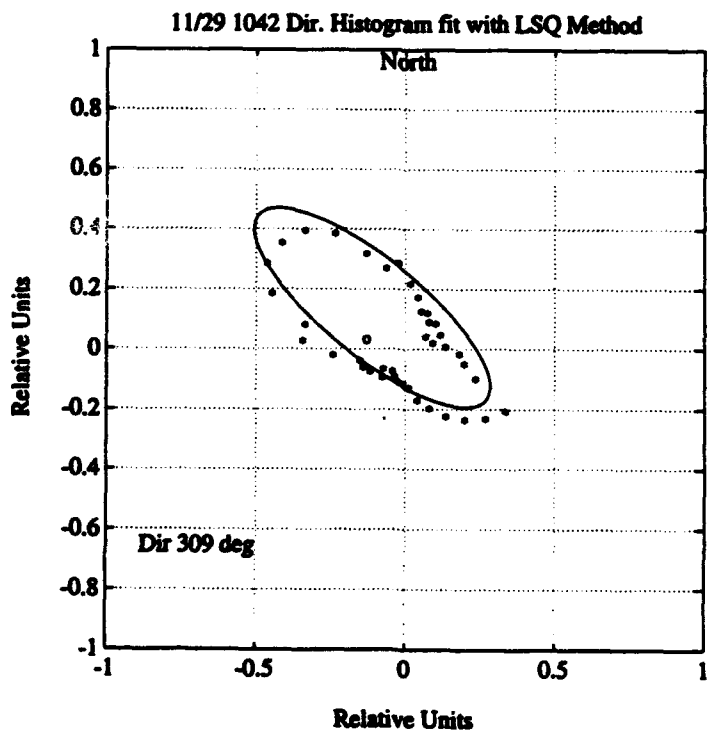
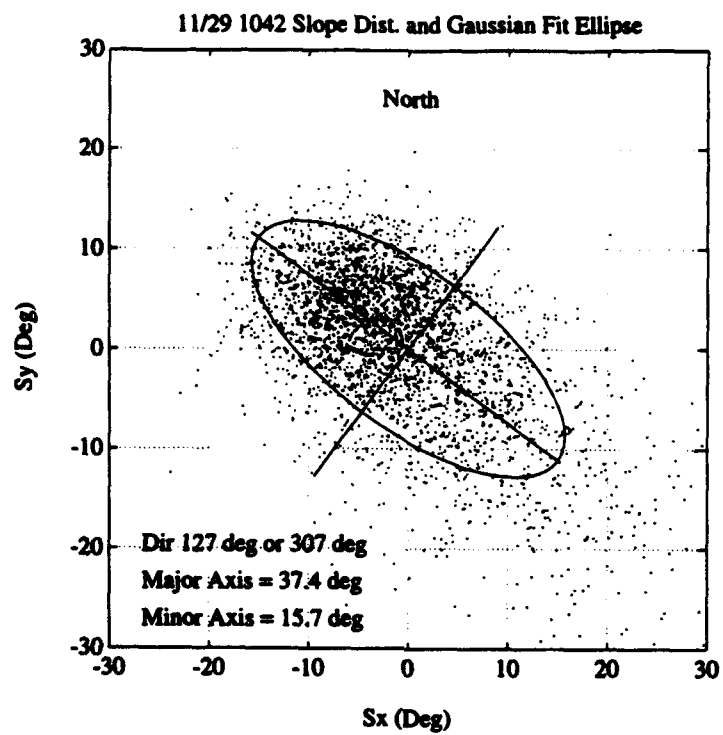


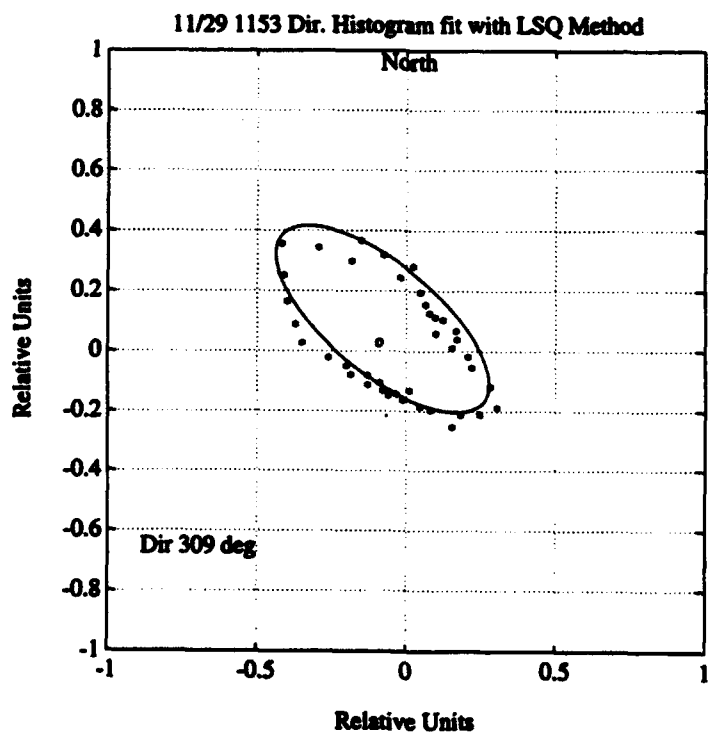
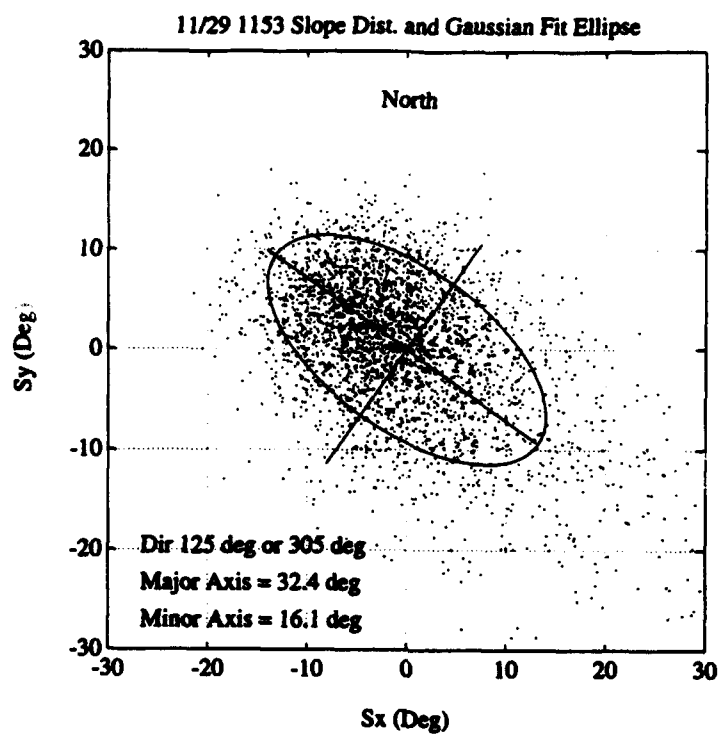


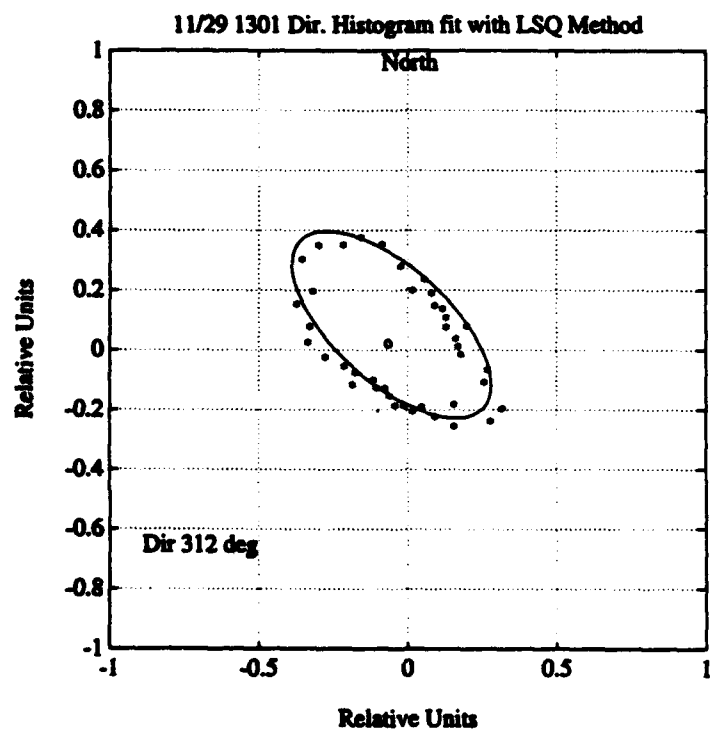
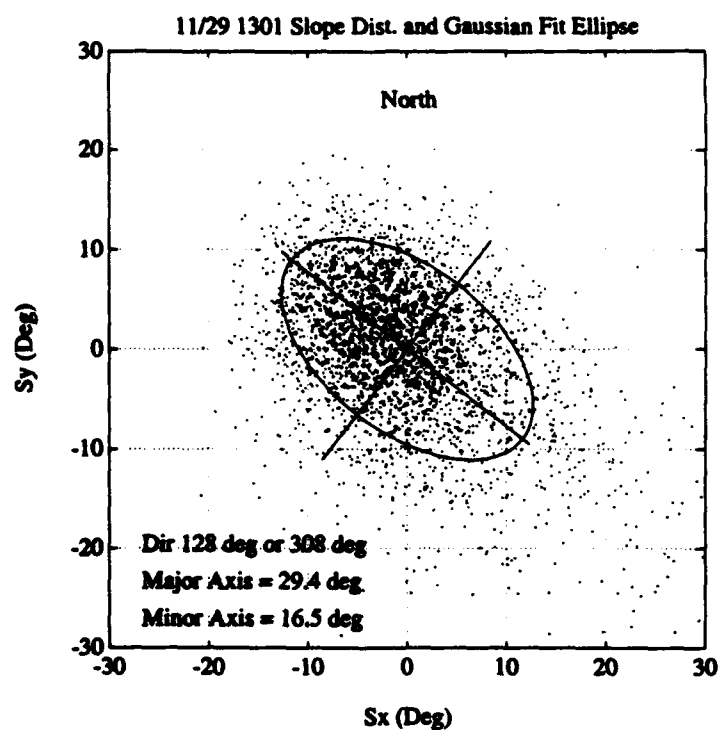


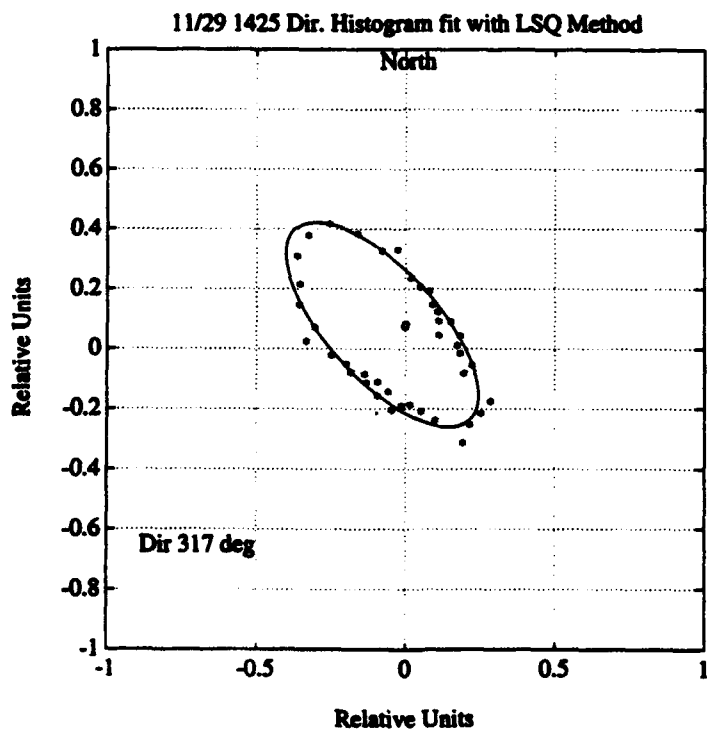
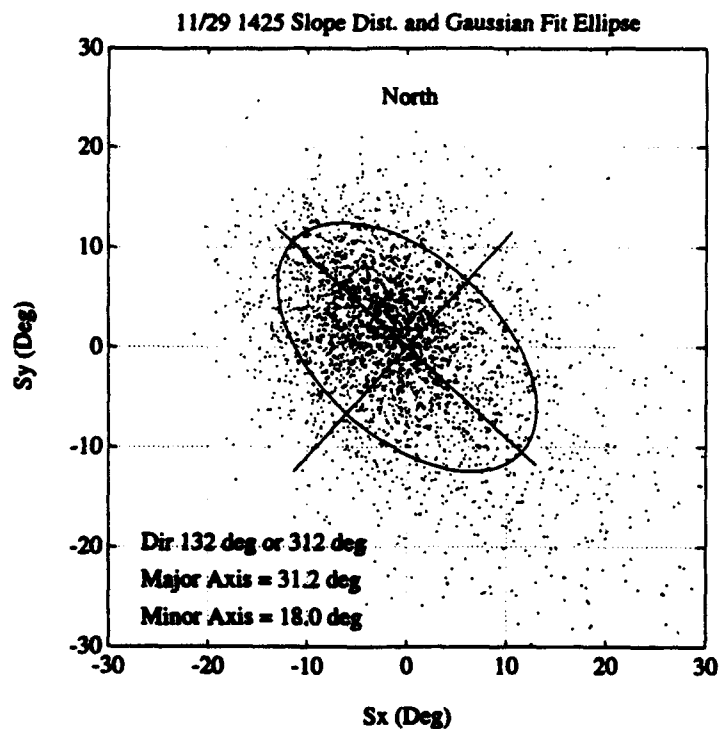


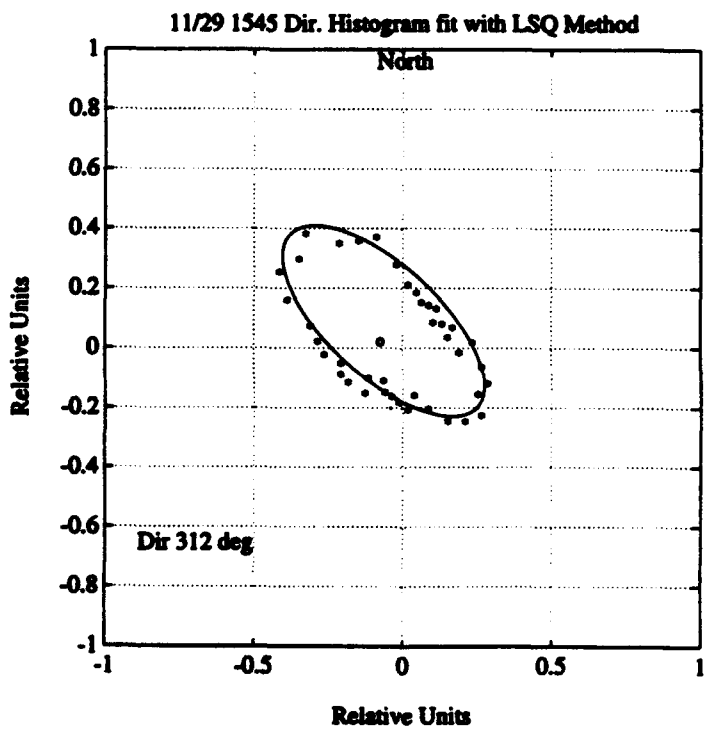
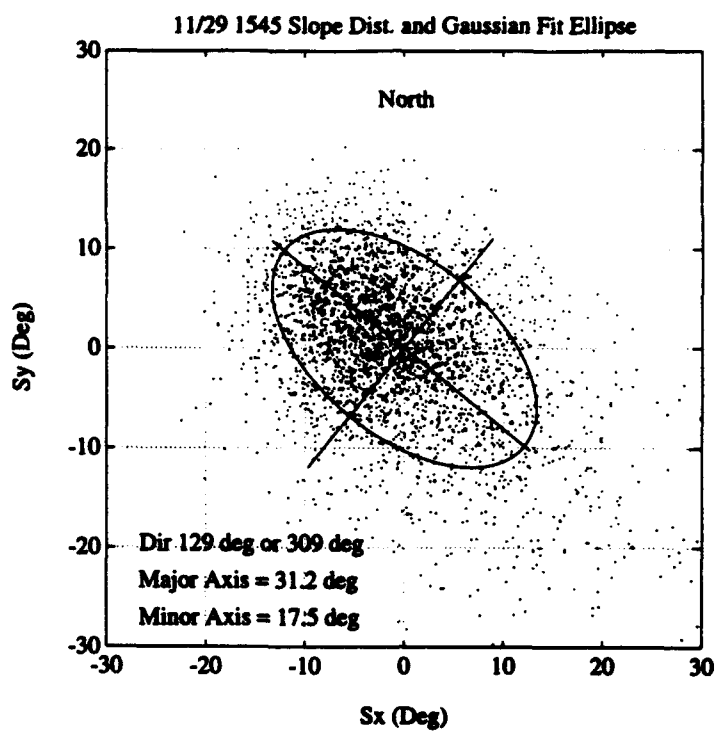


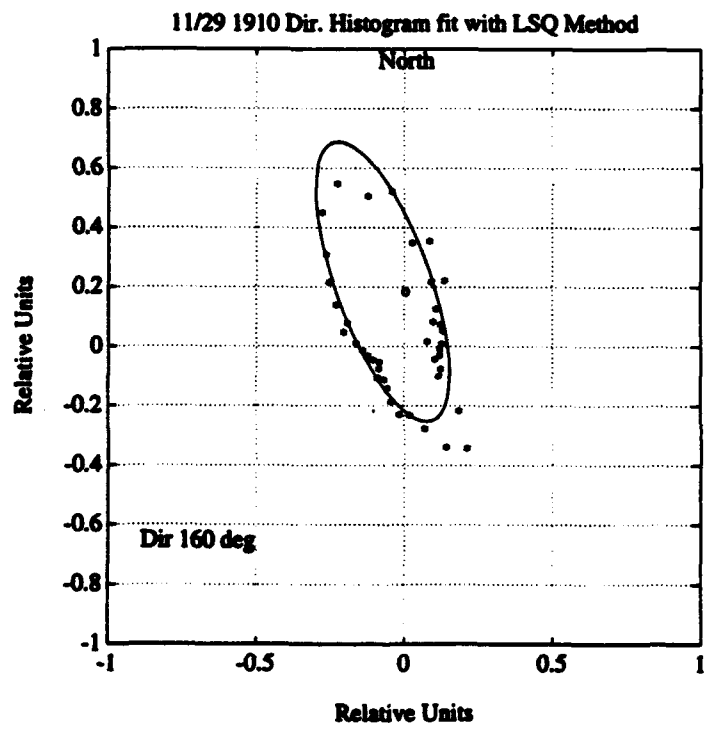
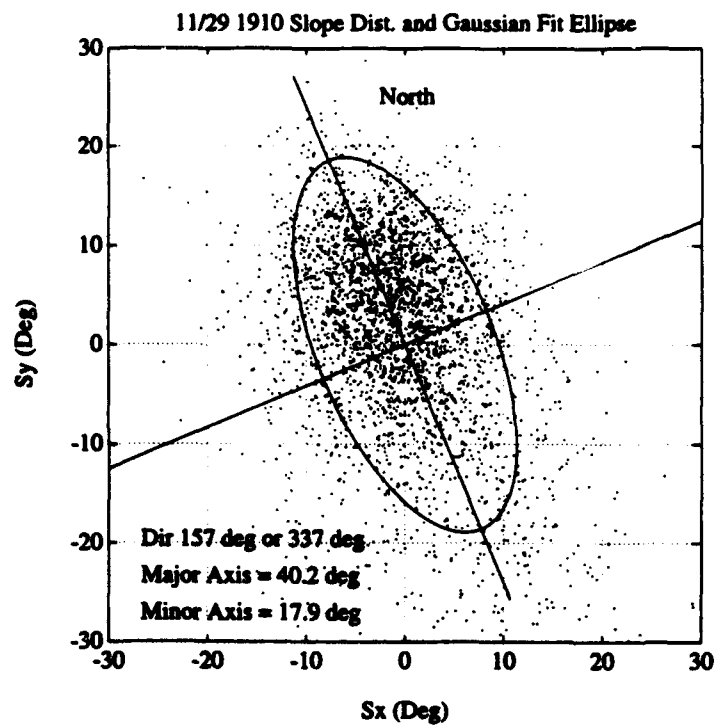


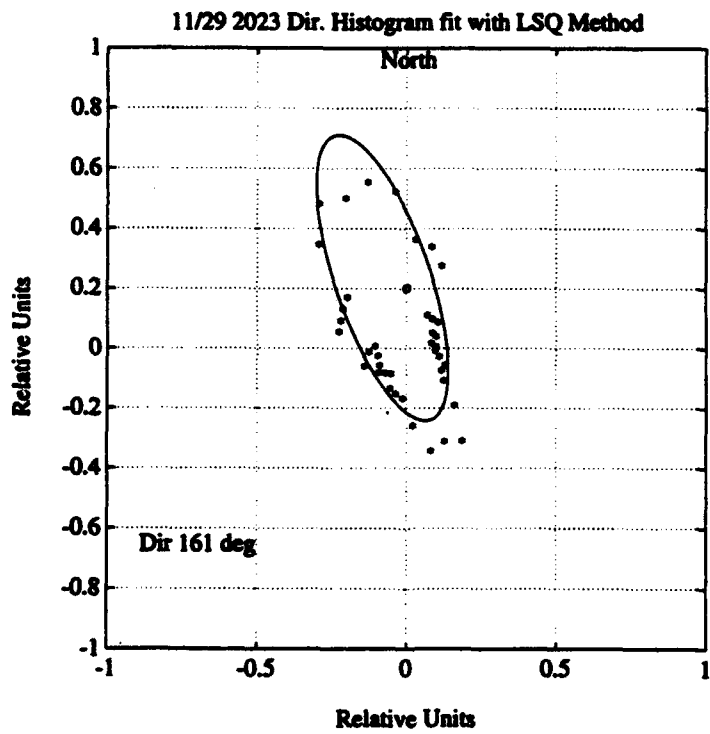
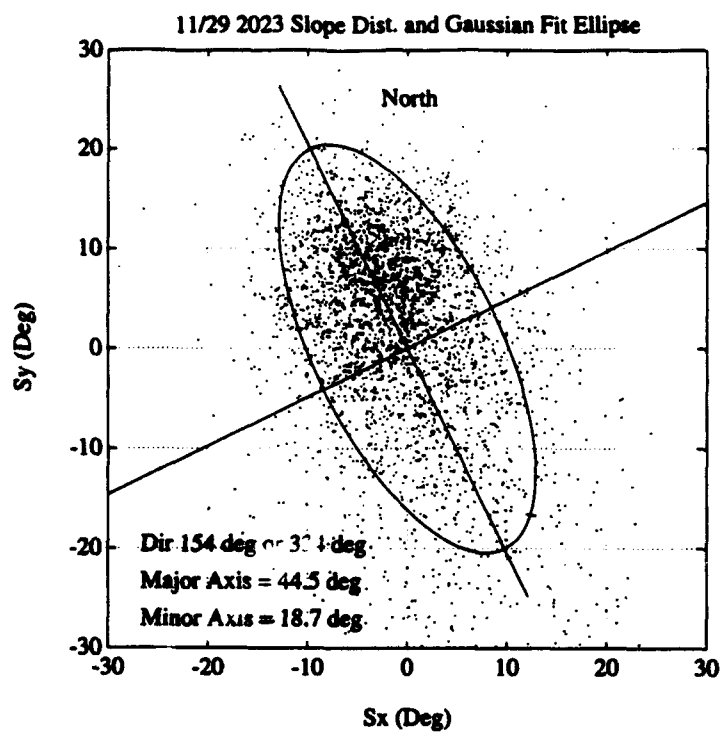


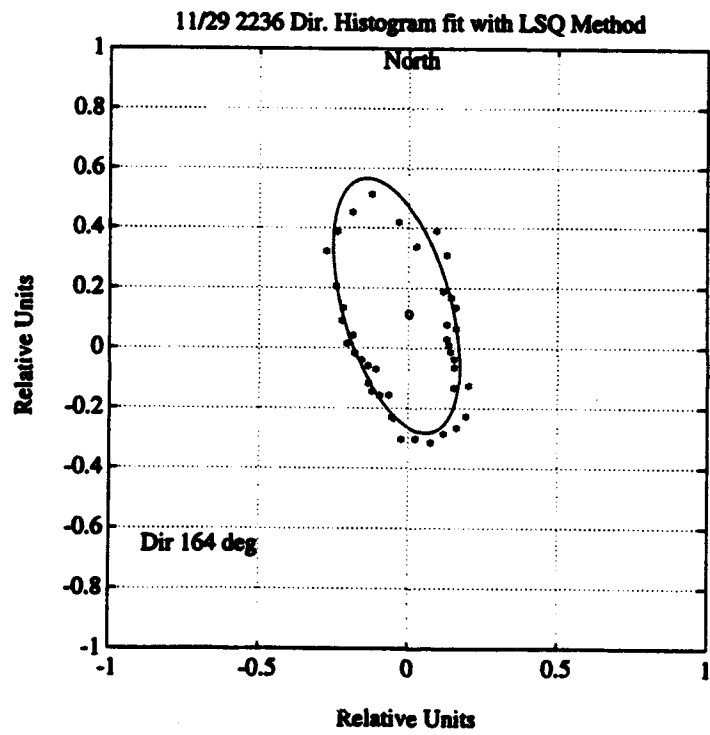
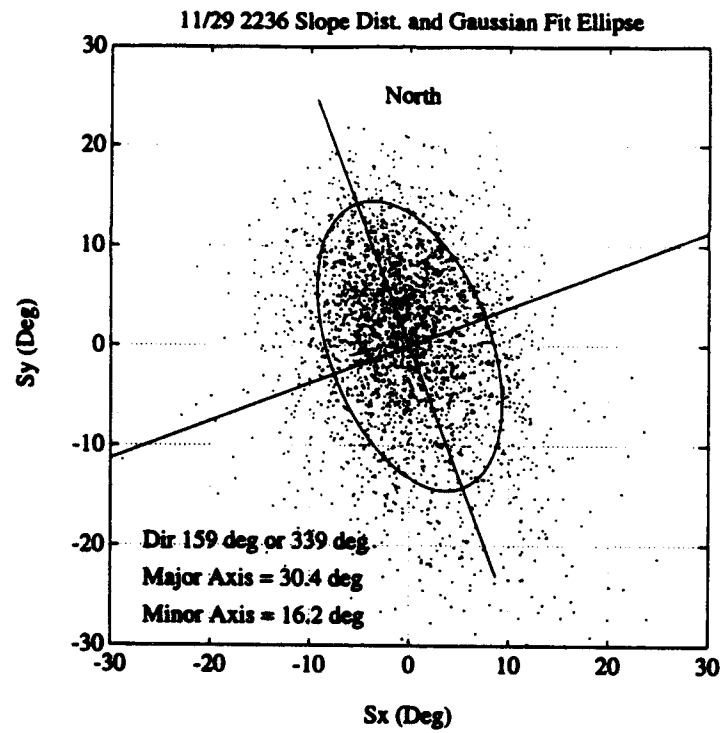




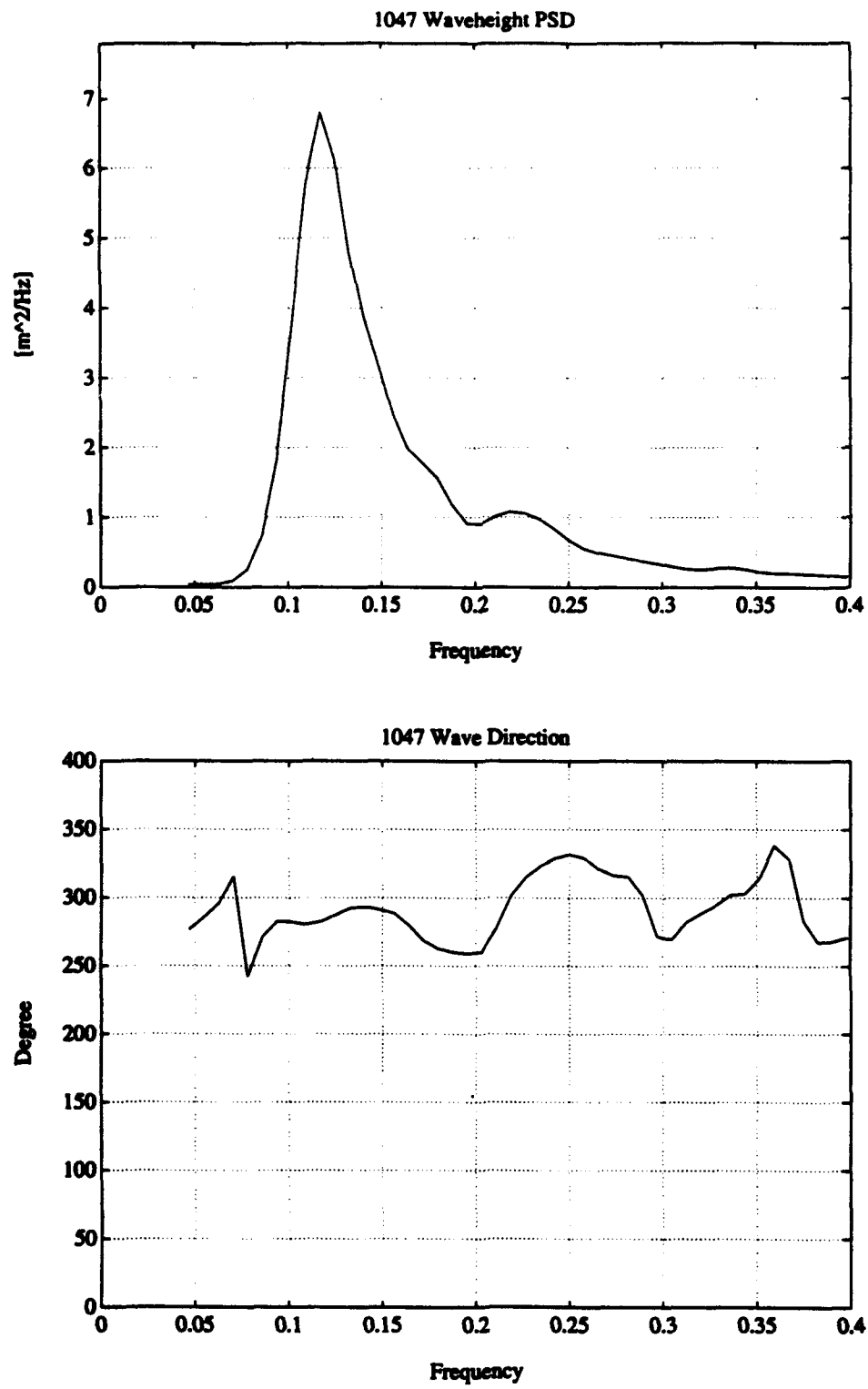


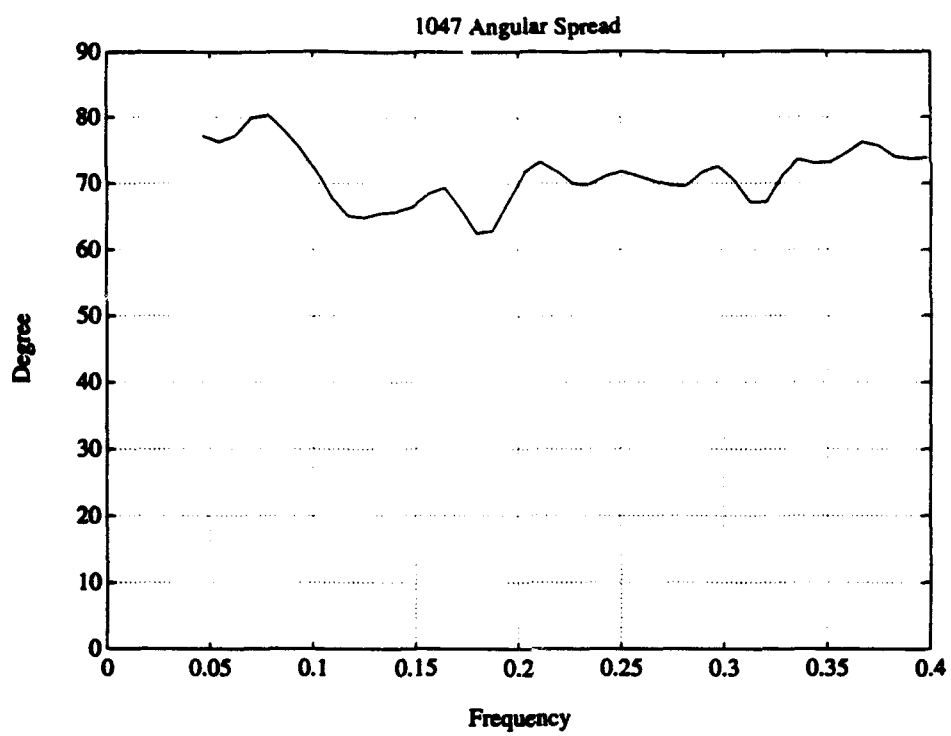




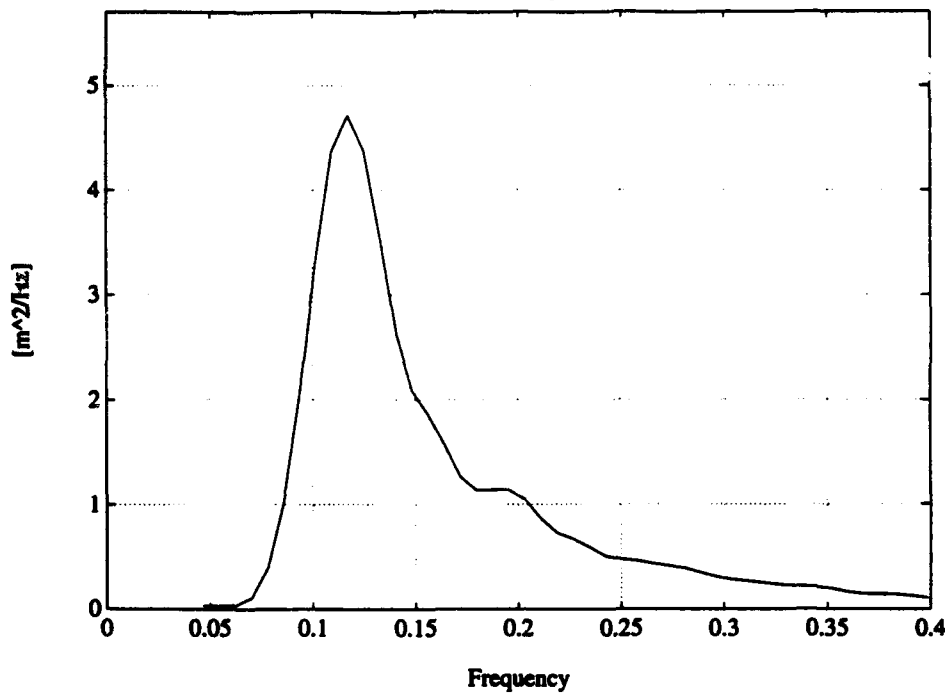


## Appendix C

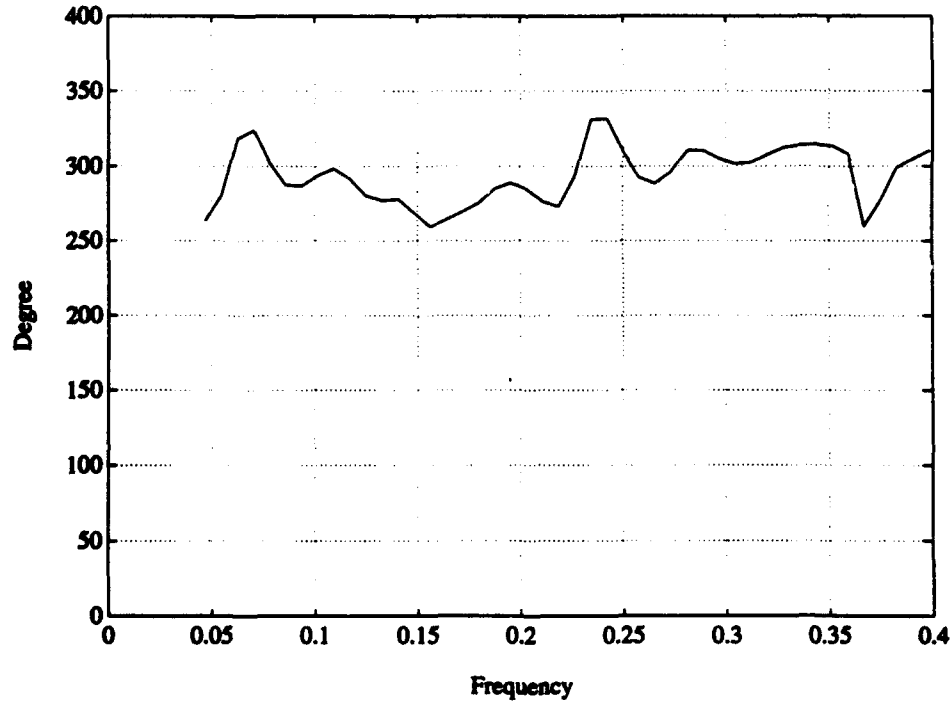


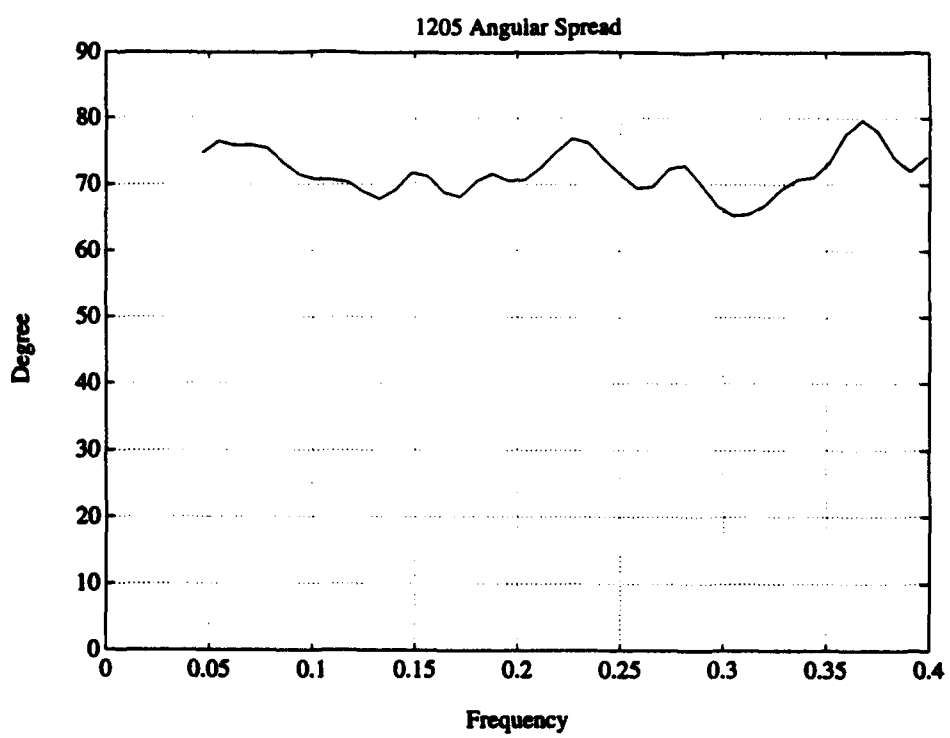


1205 Waveheight PSD

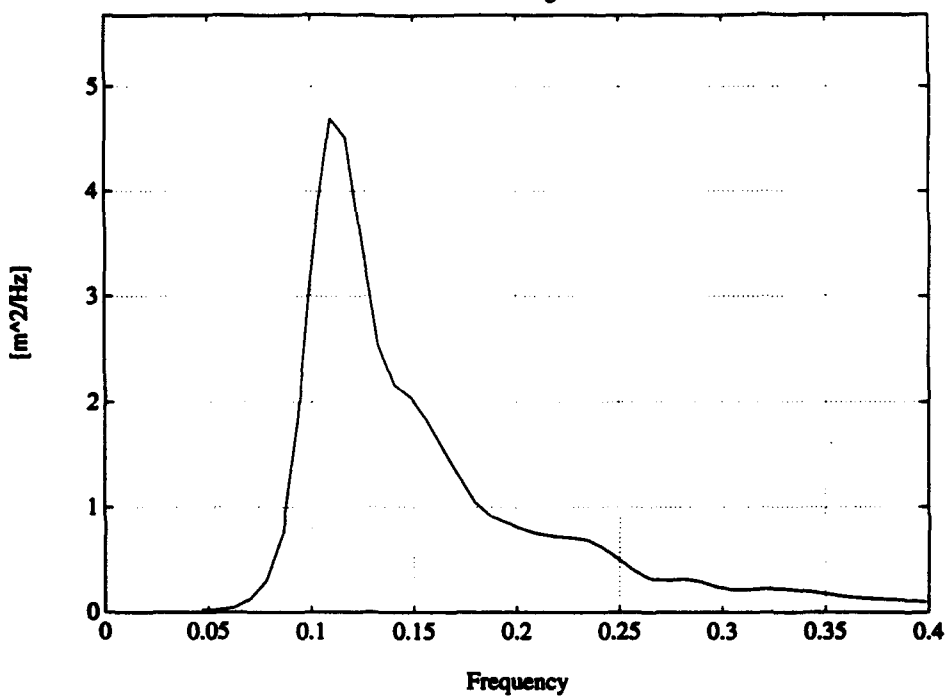


1205 Wave Direction

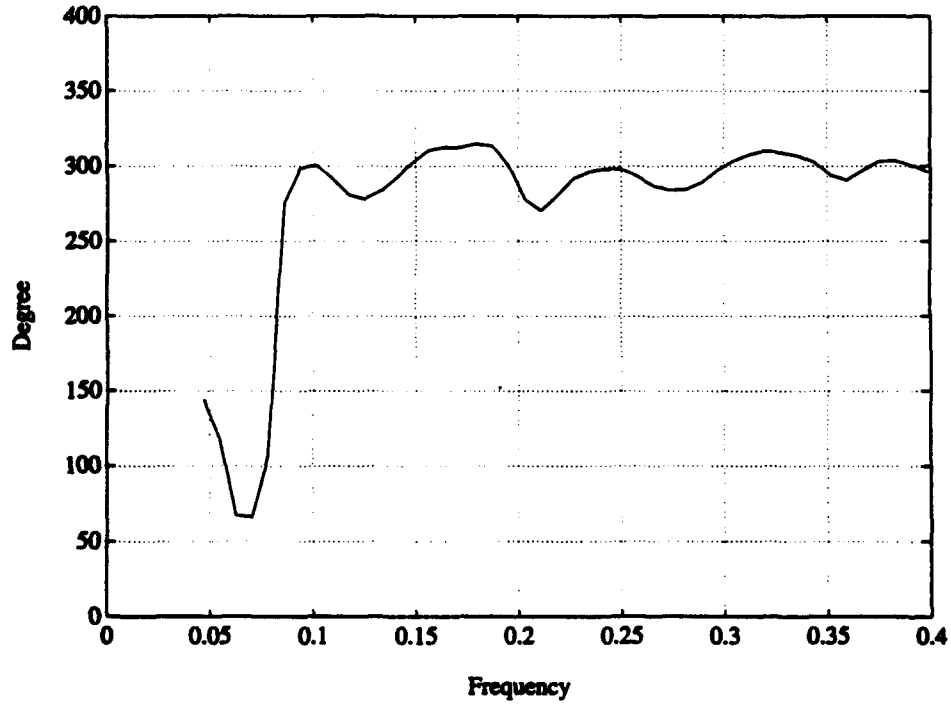


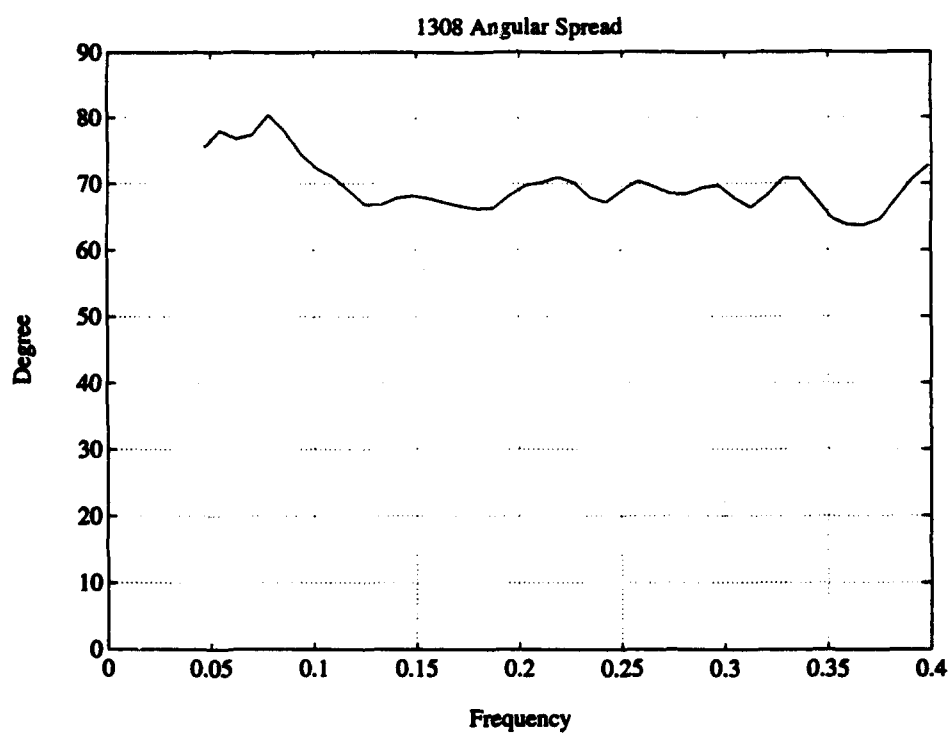


1308 Waveheight PSD

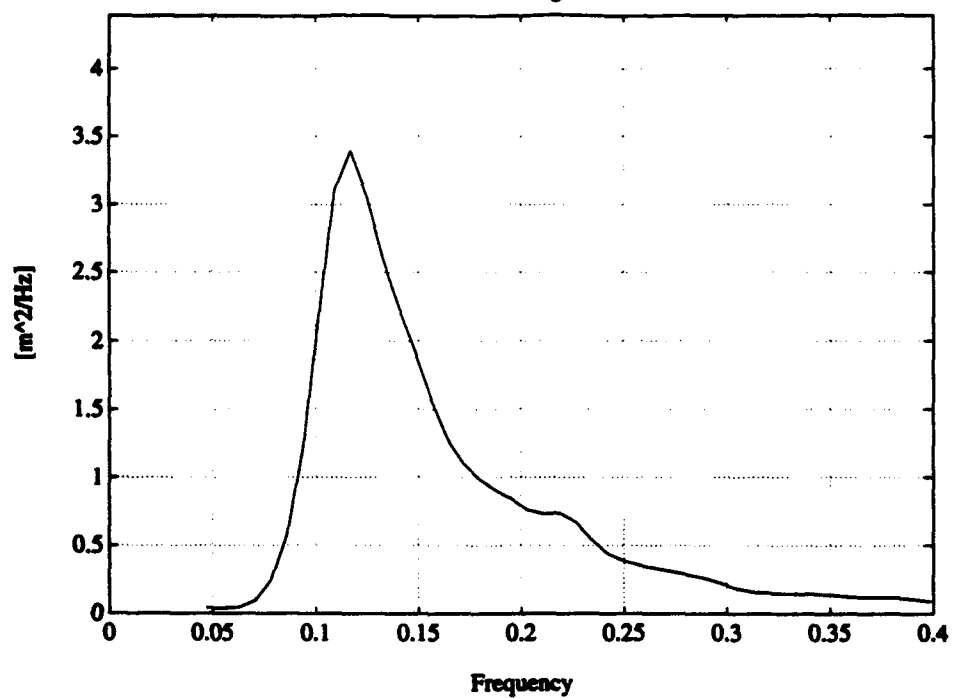


1308 Wave Direction

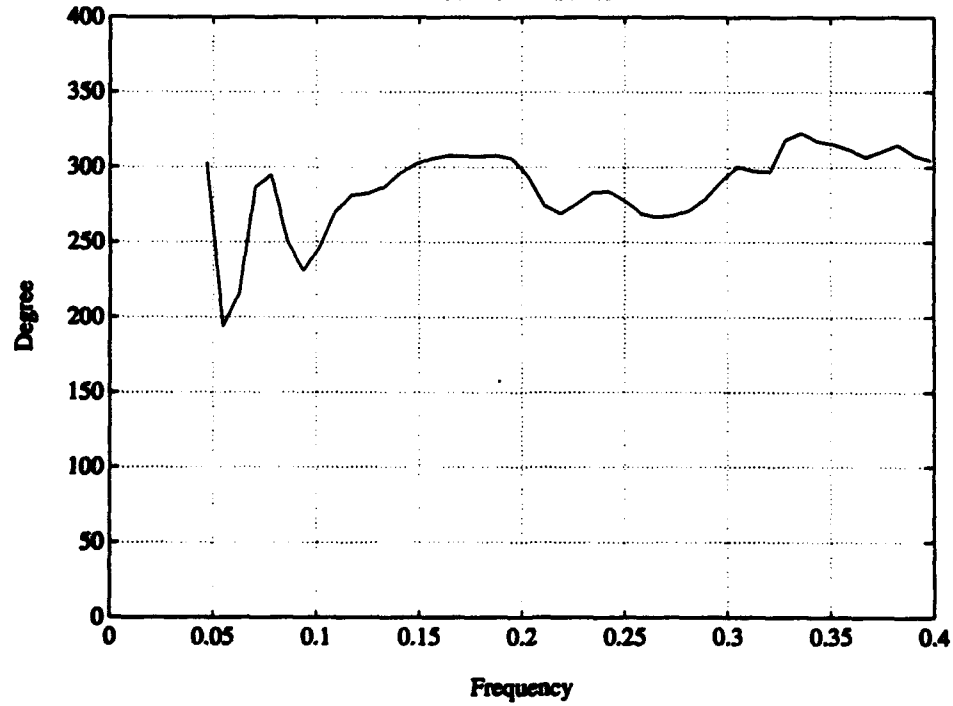


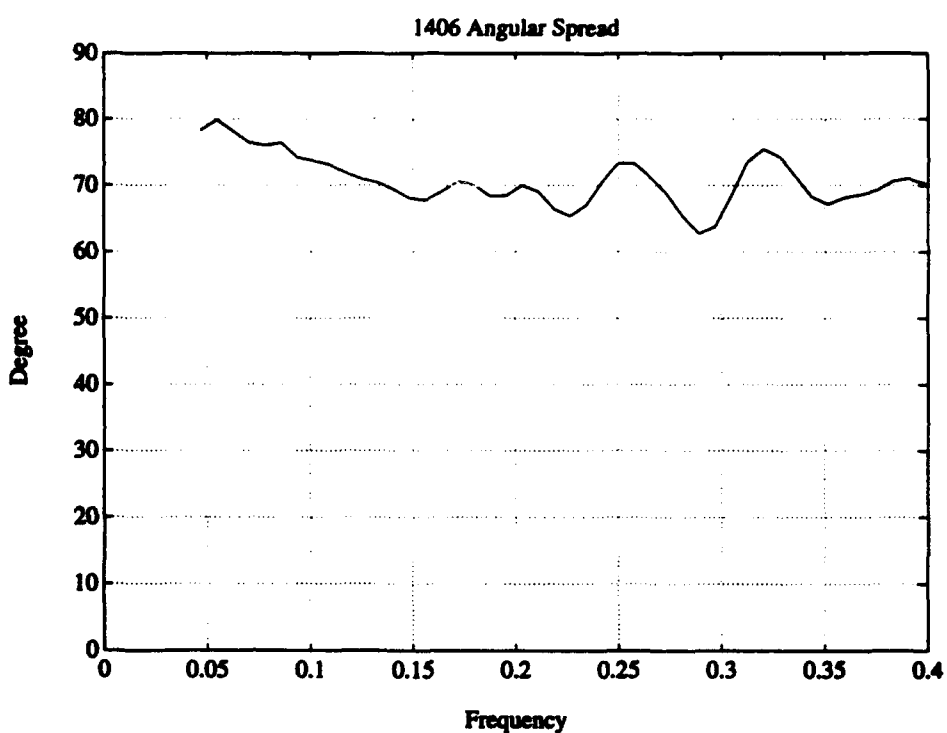


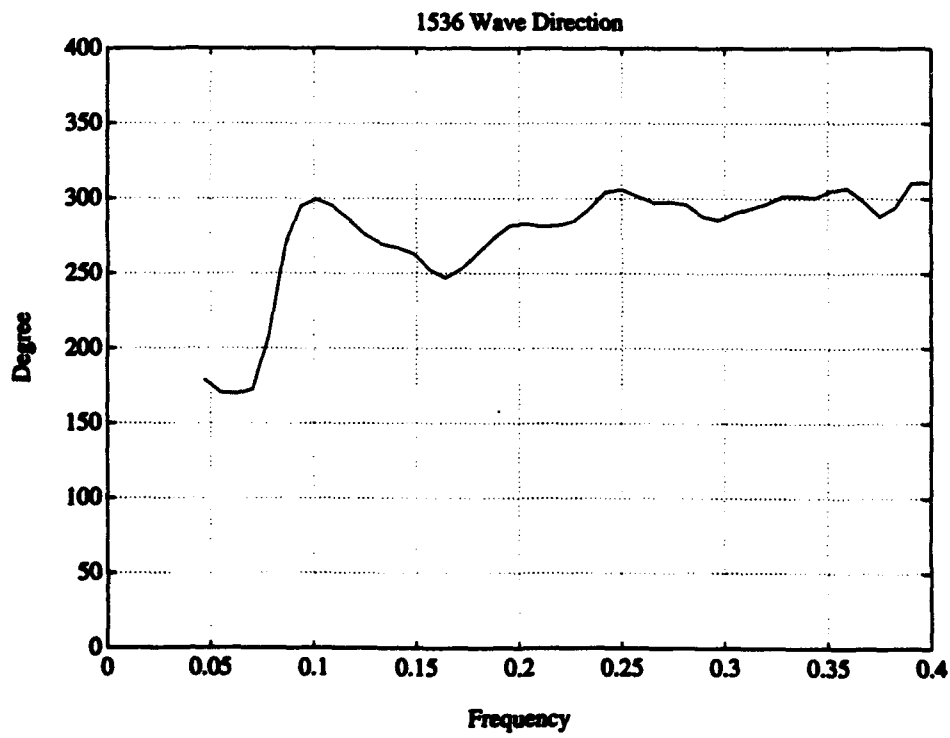
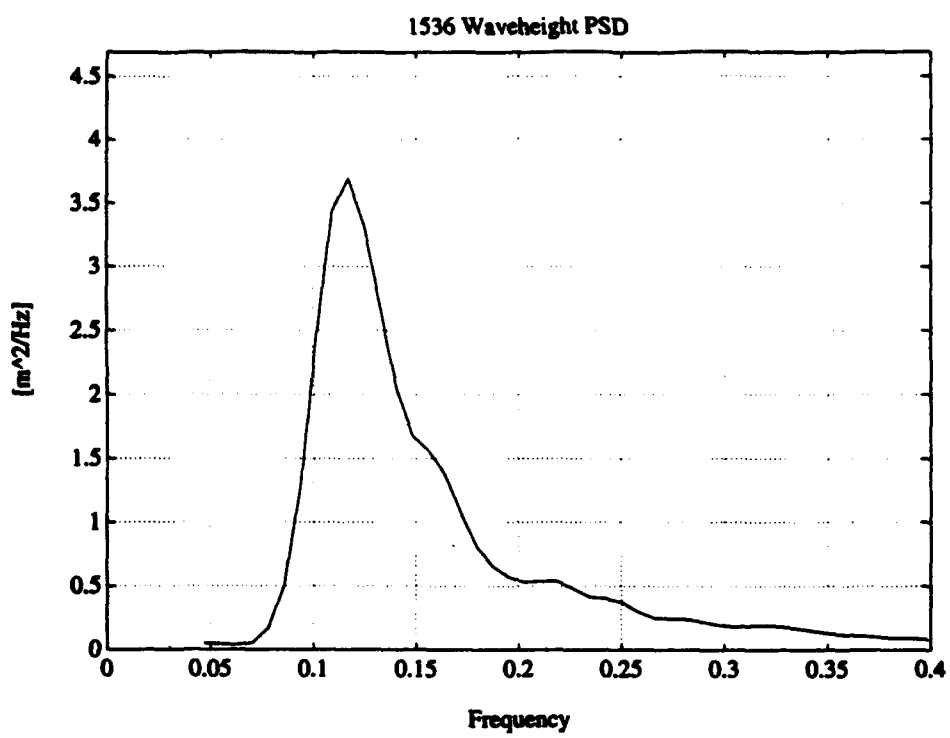
1406 Waveheight PSD

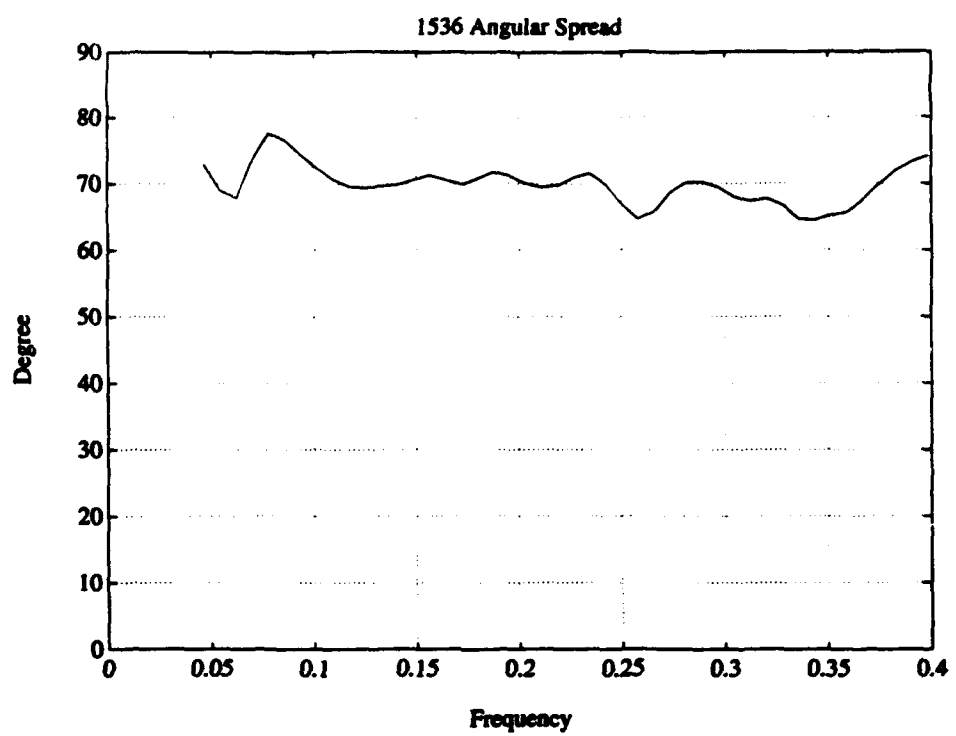


1406 Wave Direction

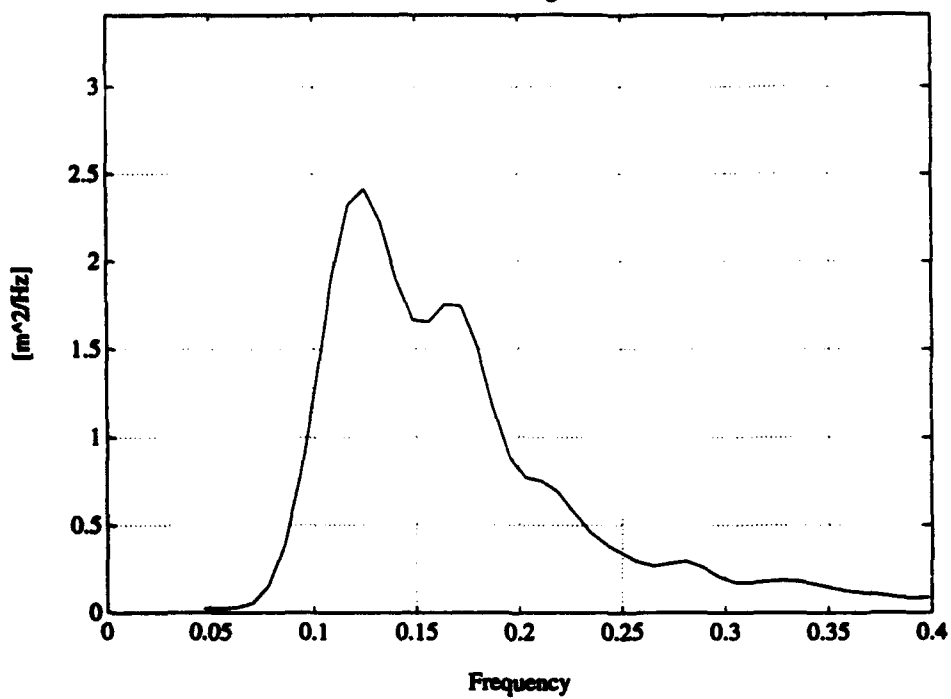




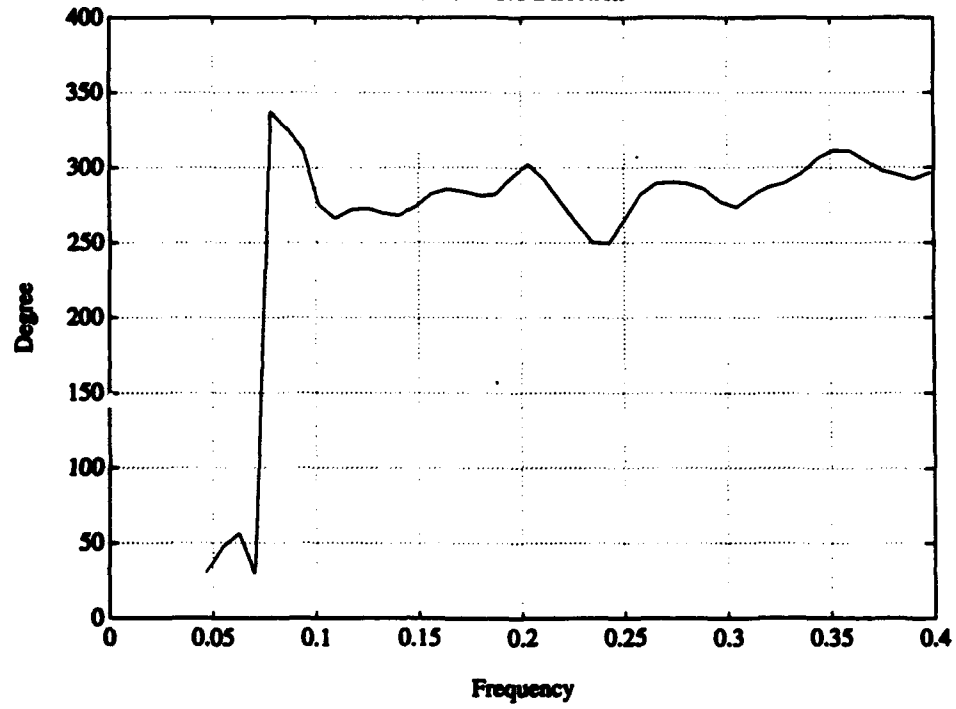


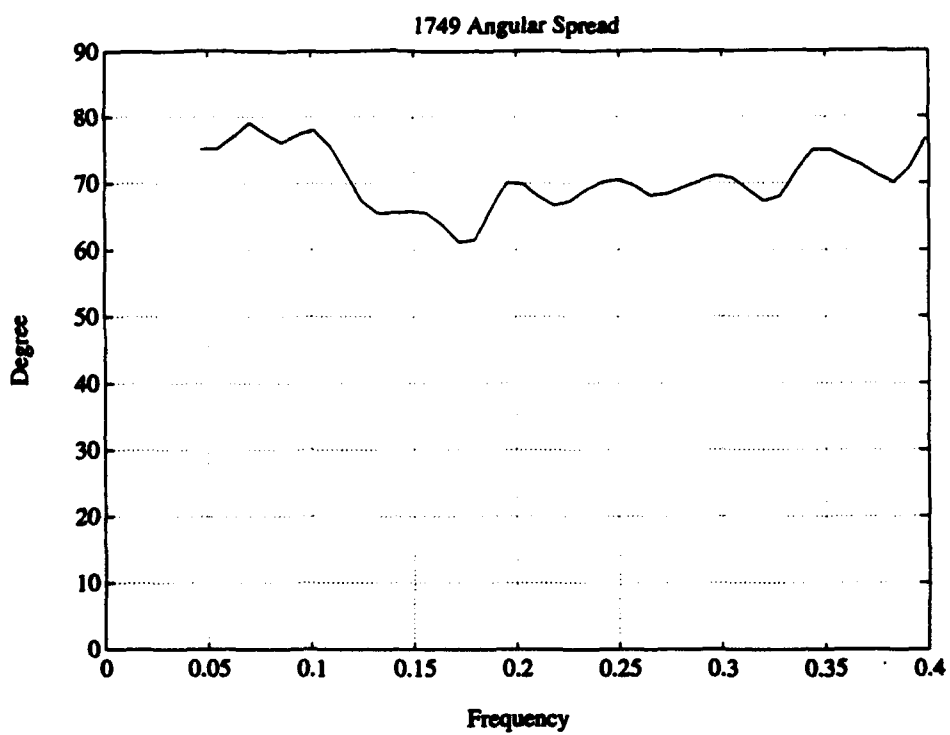


1749 Waveheight PSD

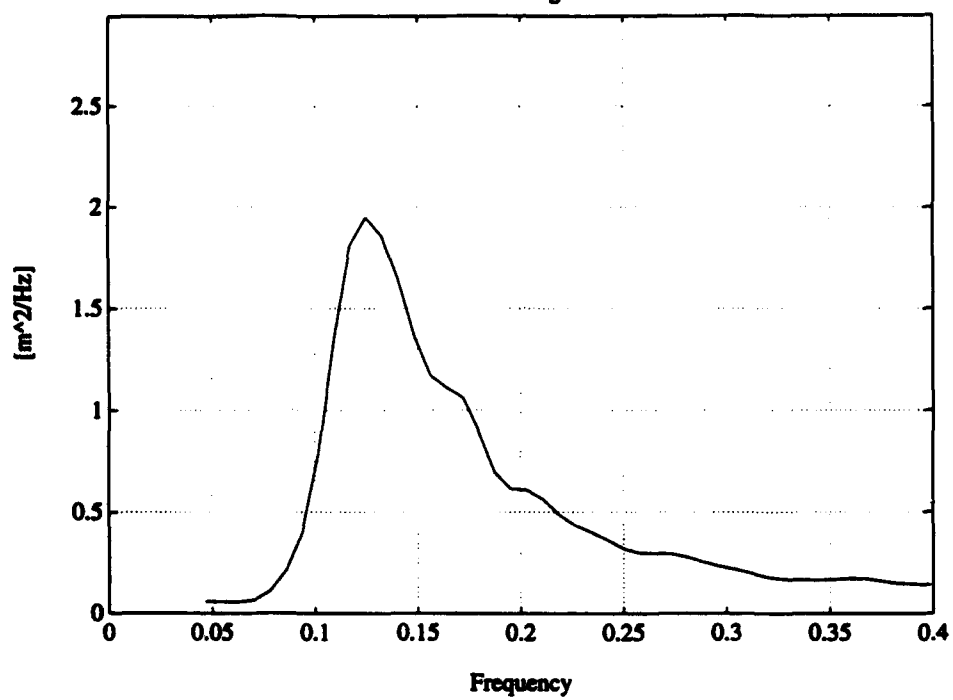


1749 Wave Direction

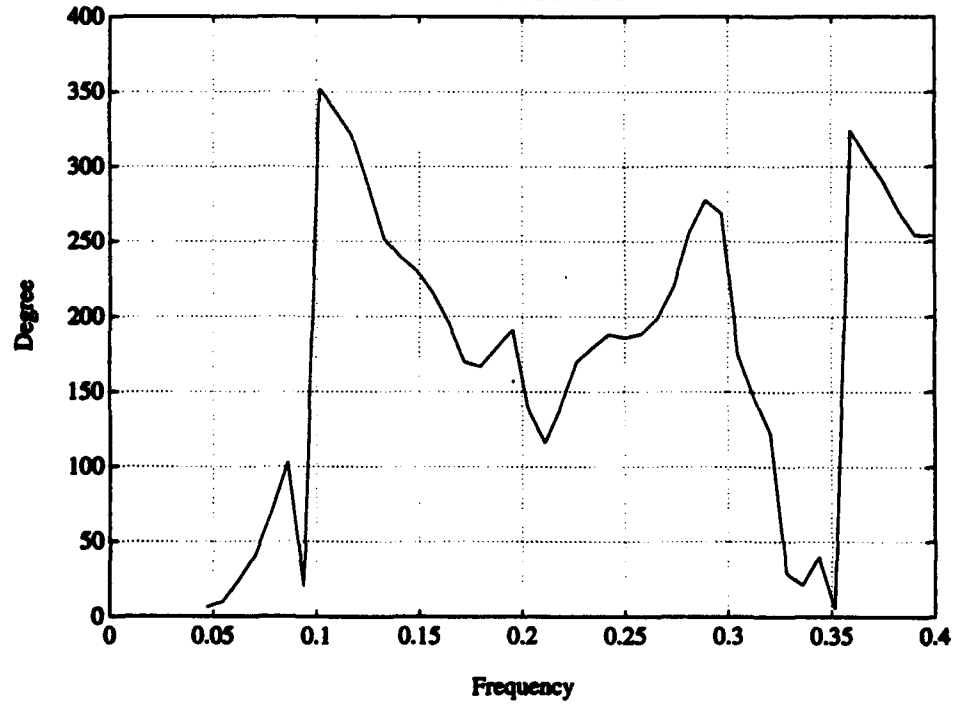


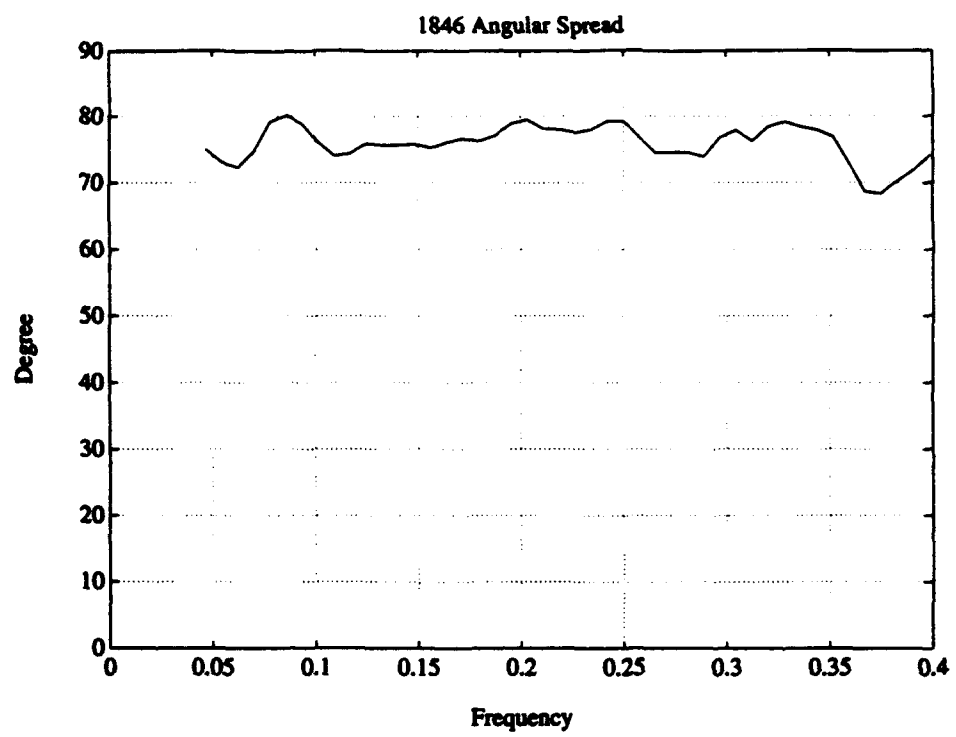


1846 Waveheight PSD

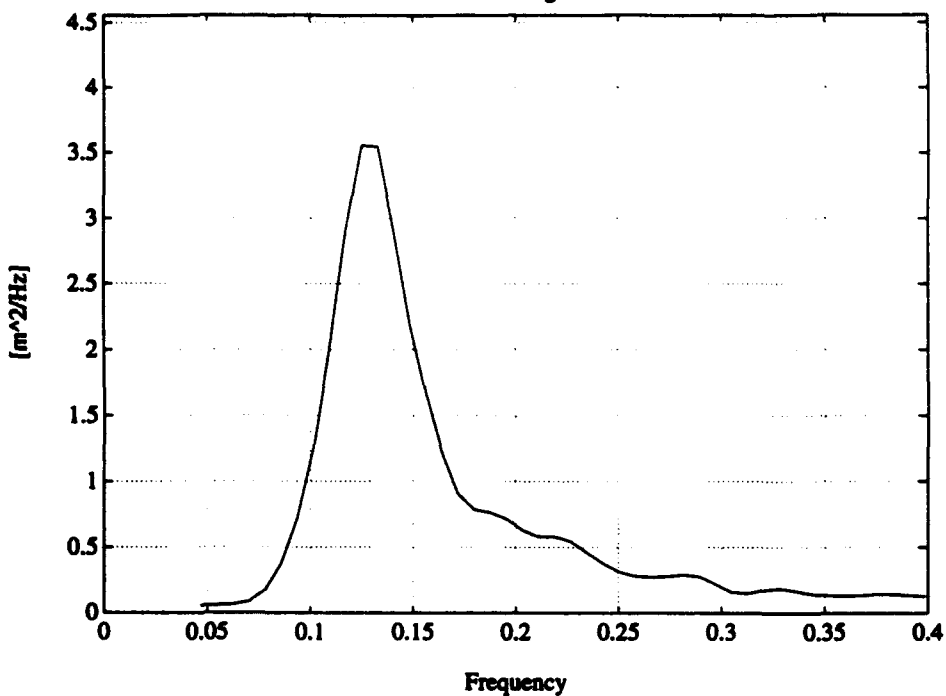


1846 Wave Direction

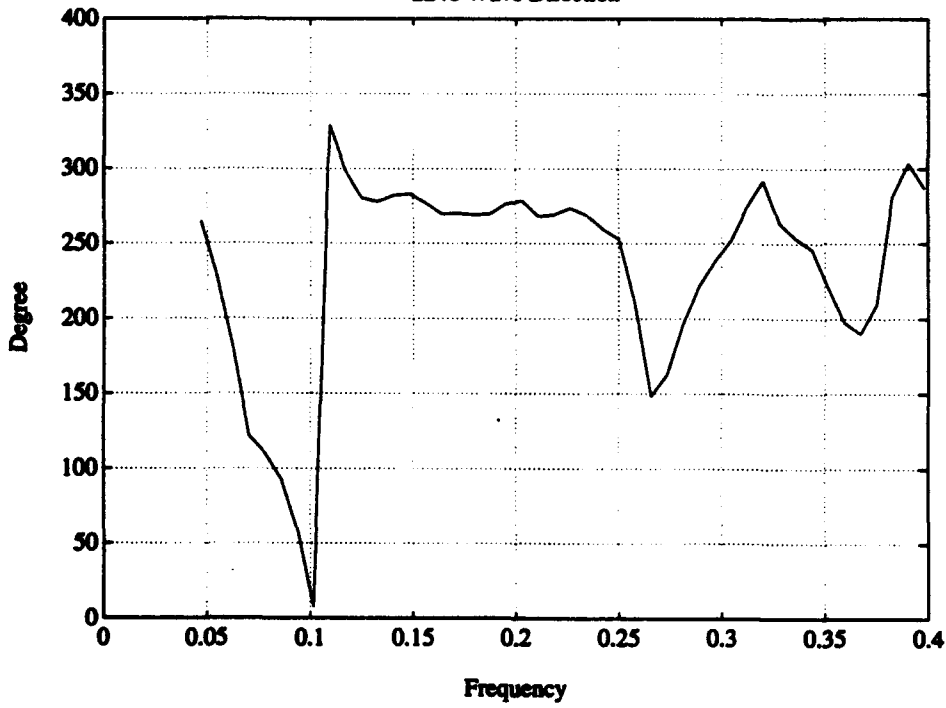


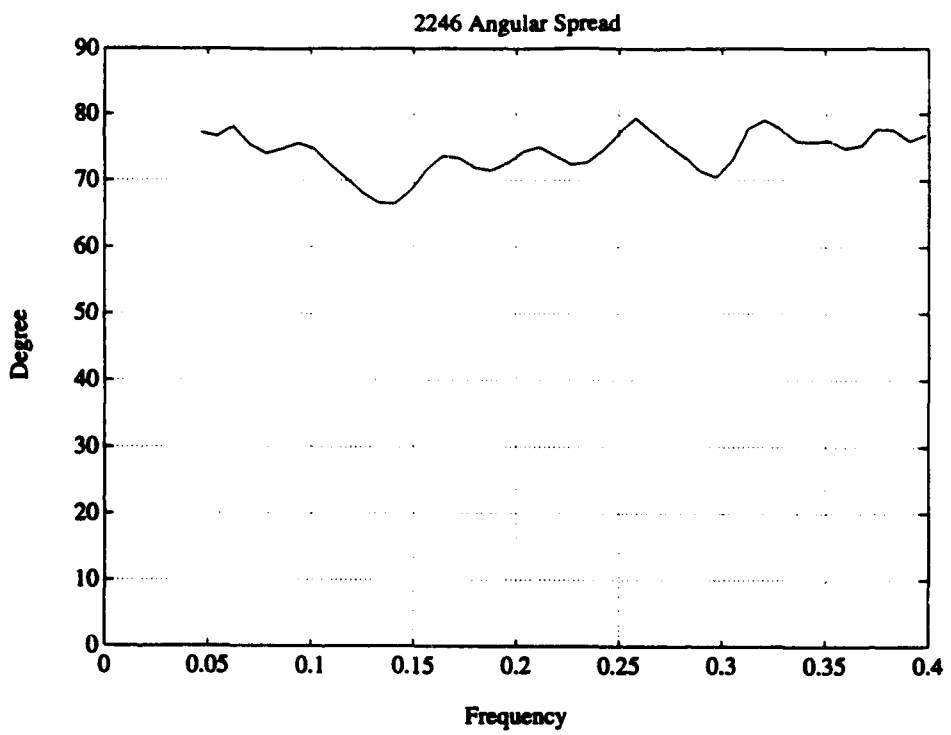


2246 Waveheight PSD

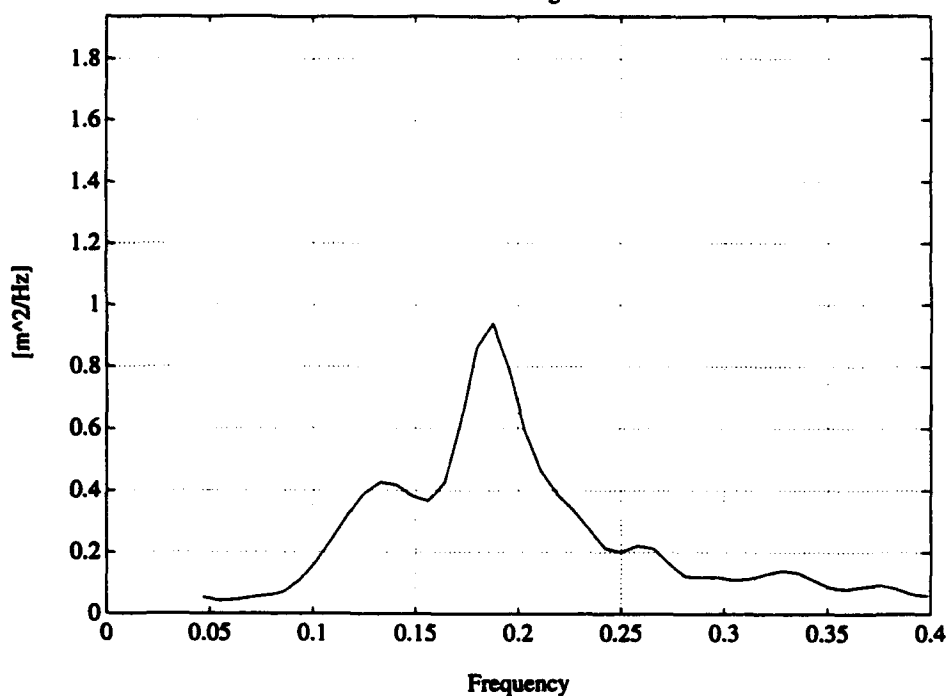


2246 Wave Direction

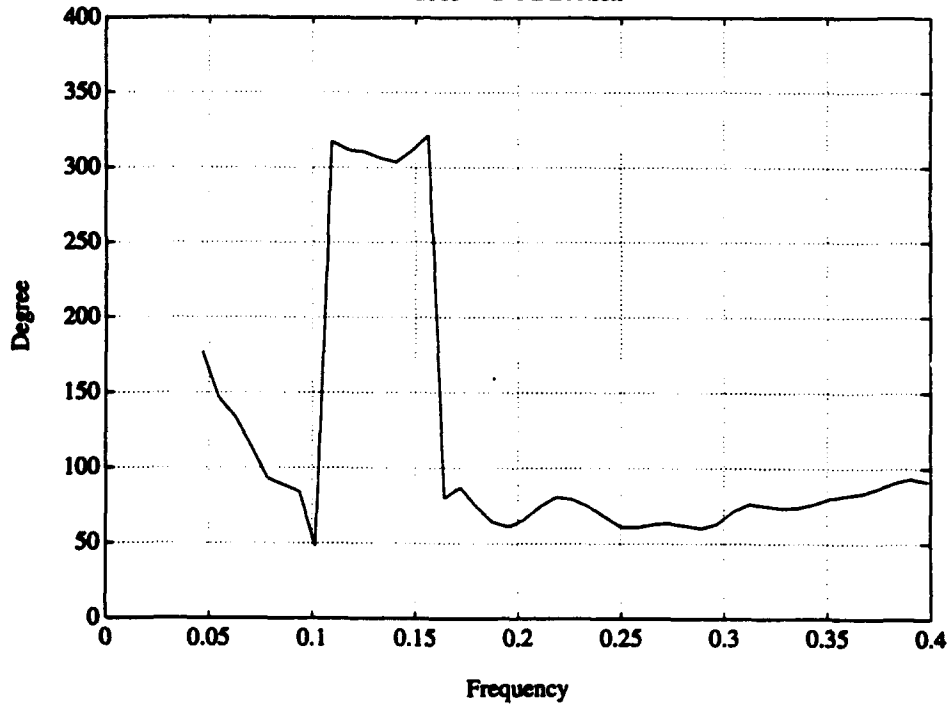


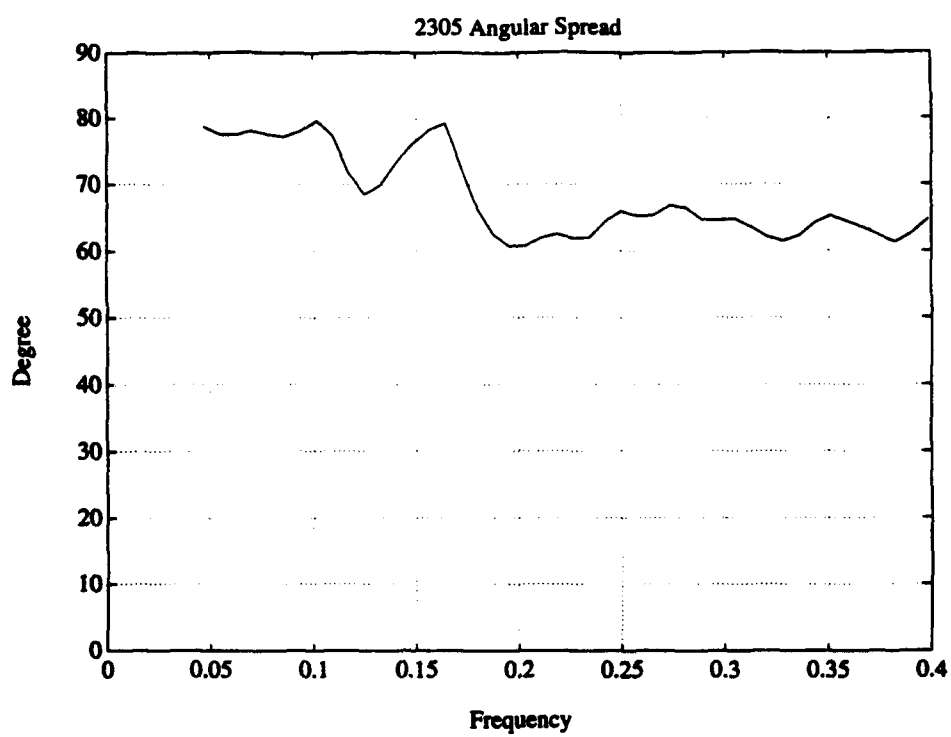


2305 Waveheight PSD

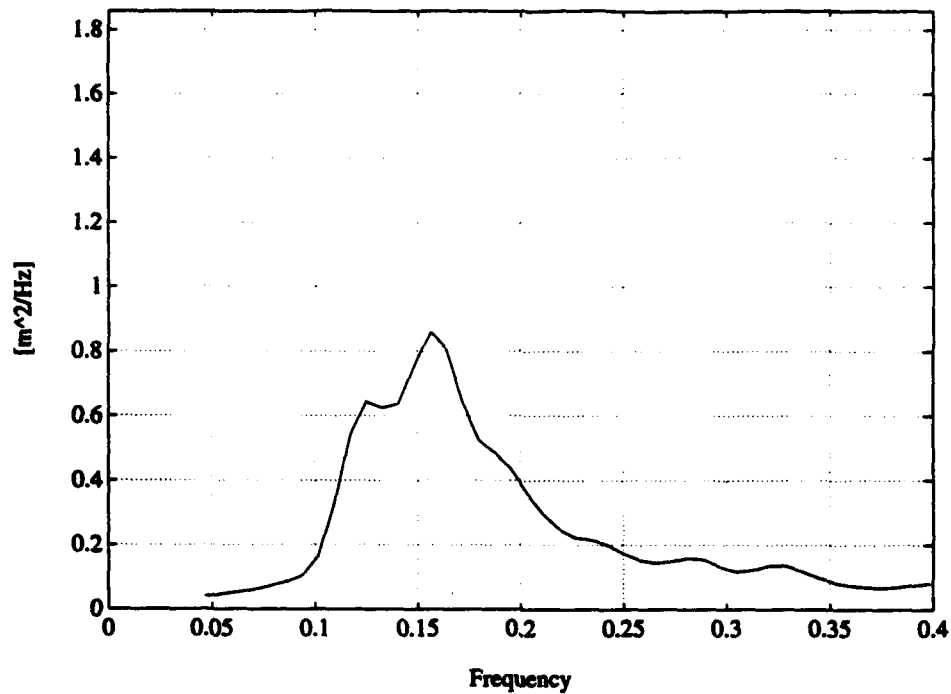


2305 Wave Direction

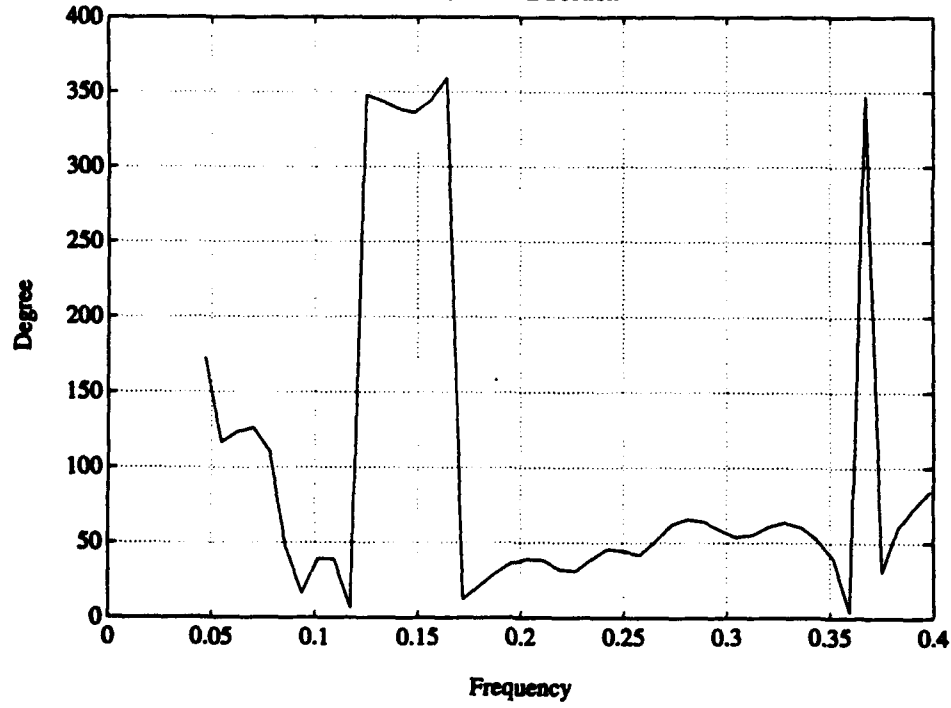


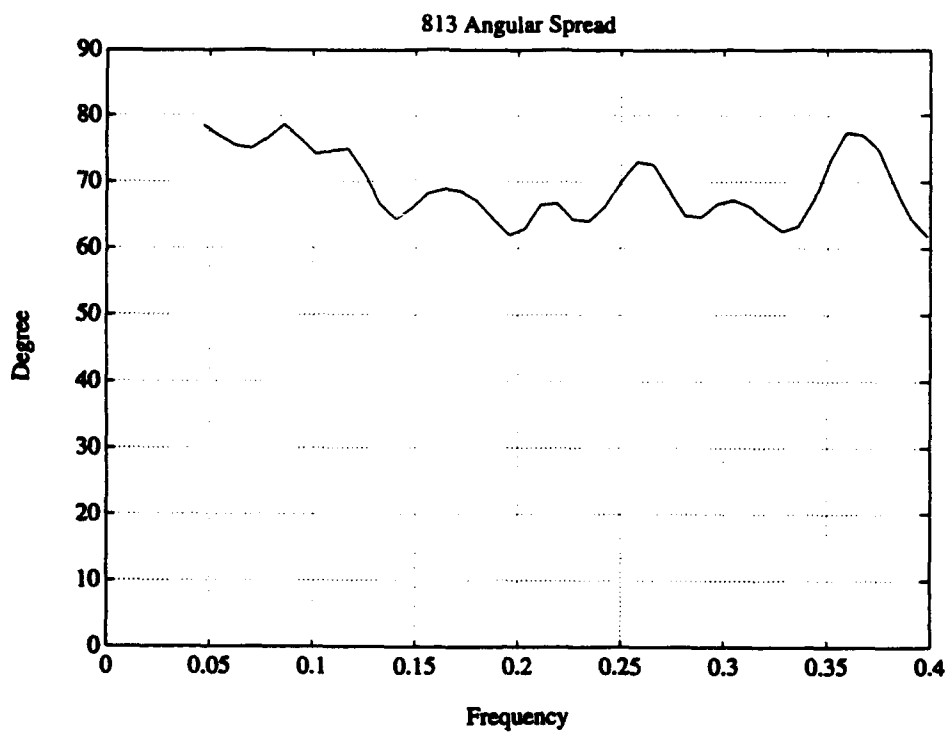


813 Waveheight PSD

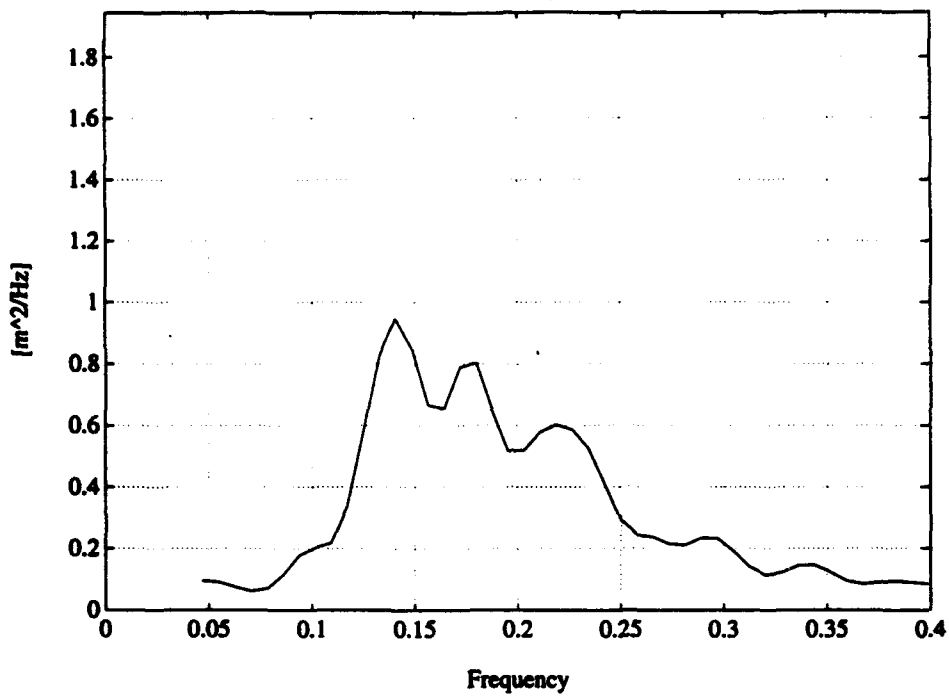


813 Wave Direction

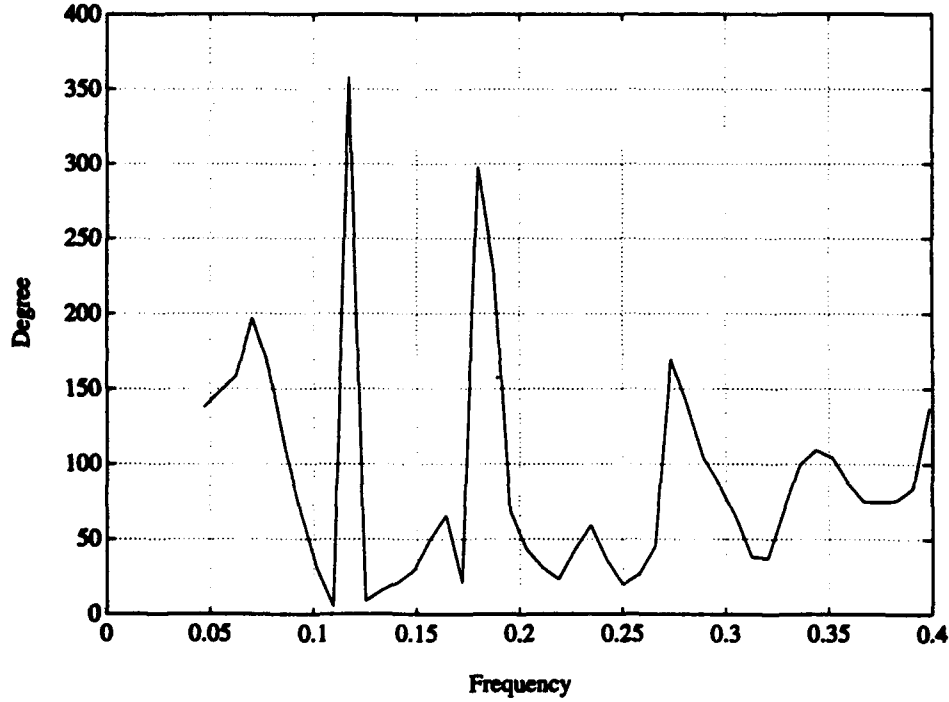


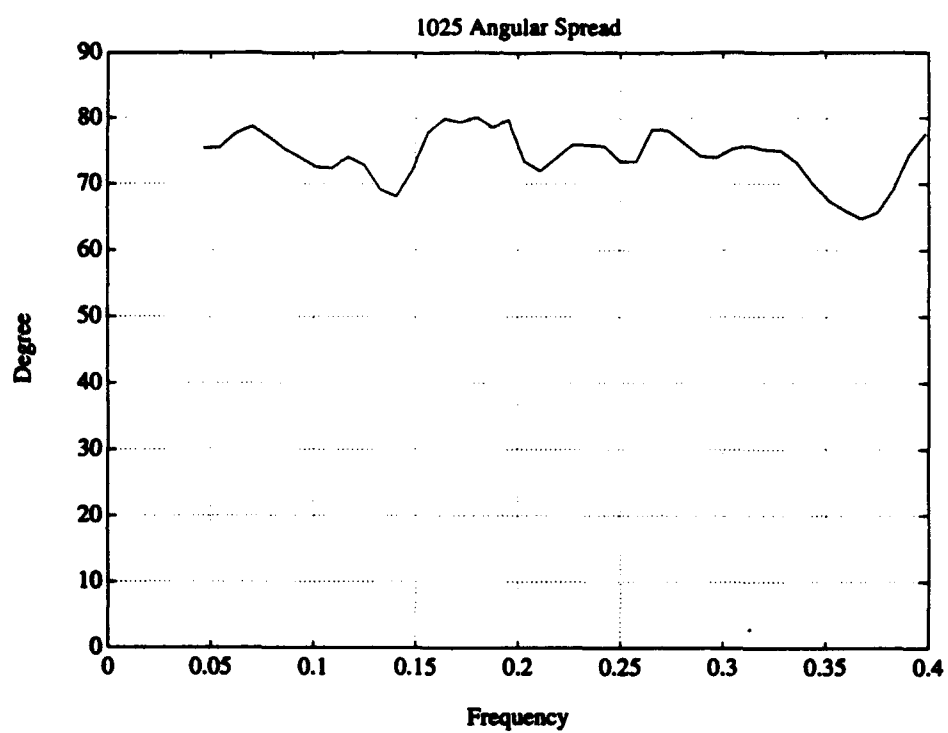


1025 Waveheight PSD

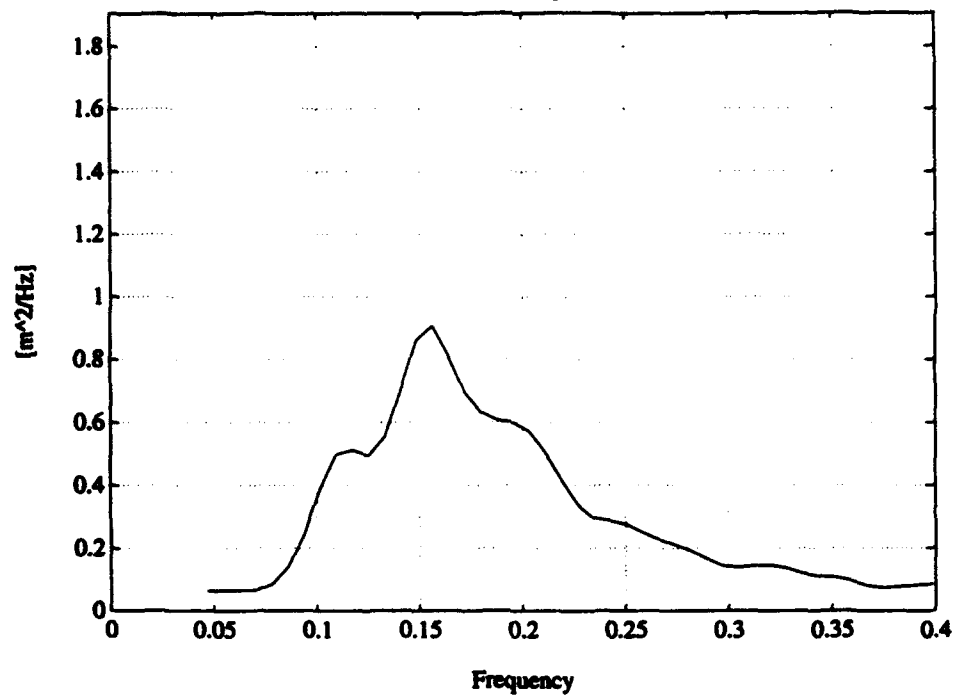


1025 Wave Direction

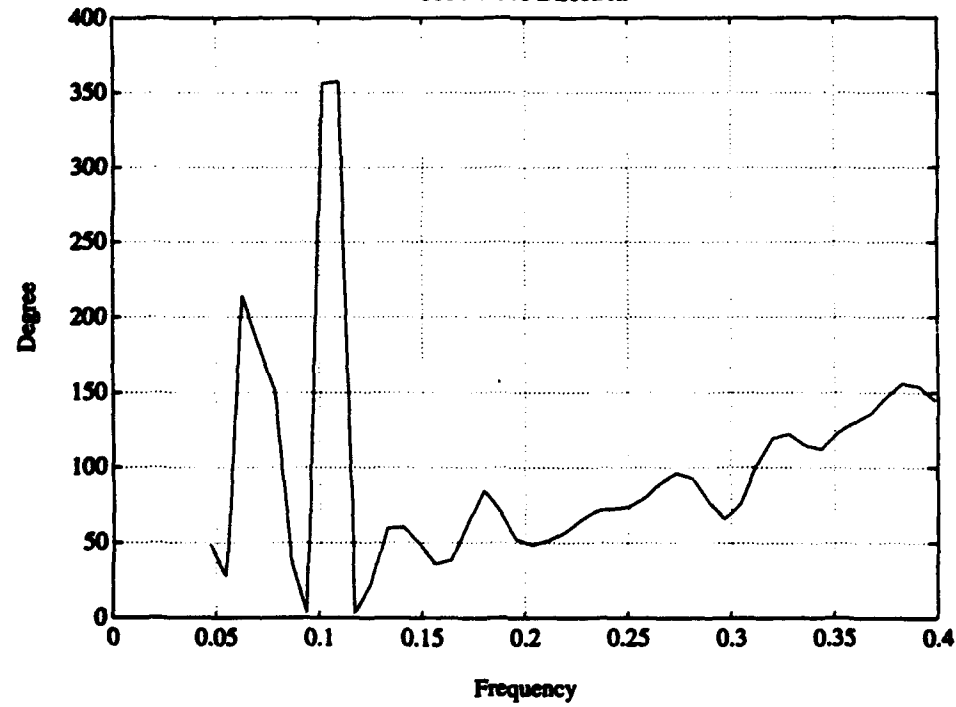


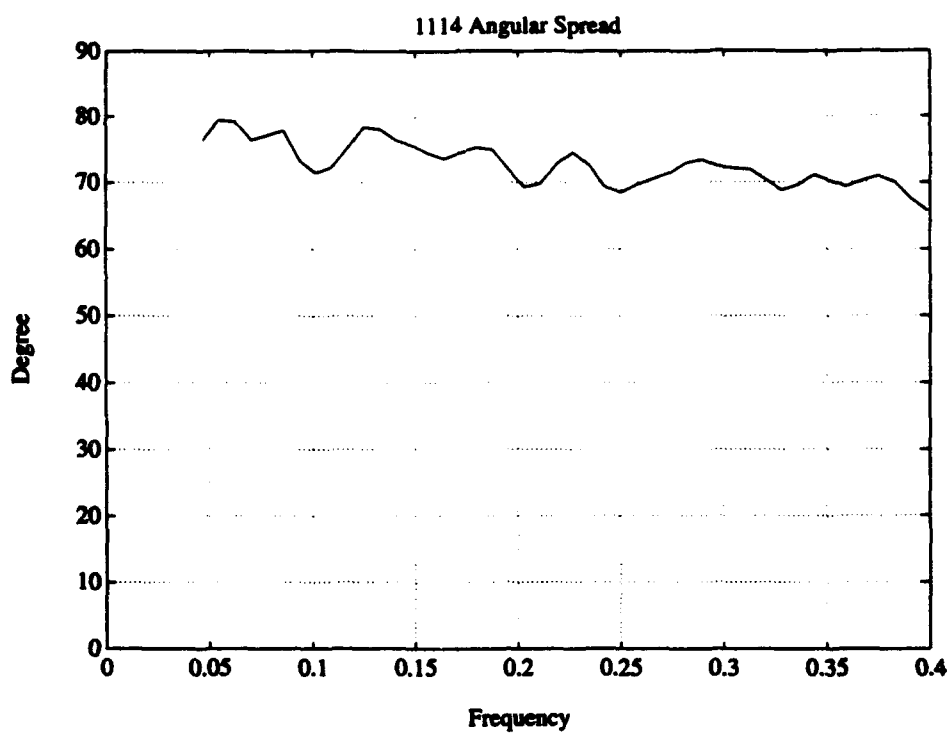


1114 Waveheight PSD

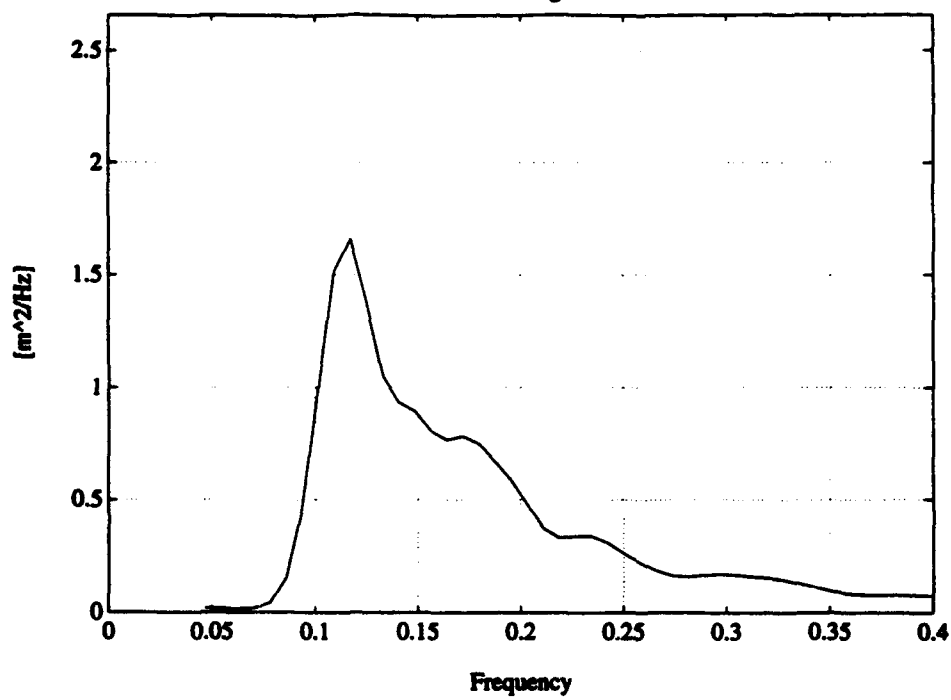


1114 Wave Direction

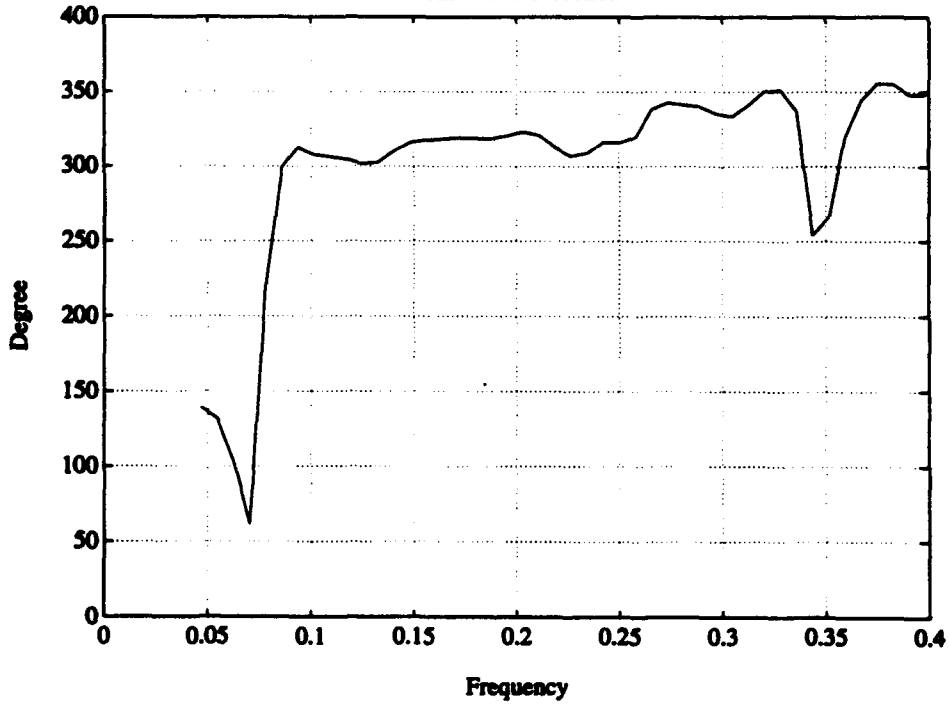


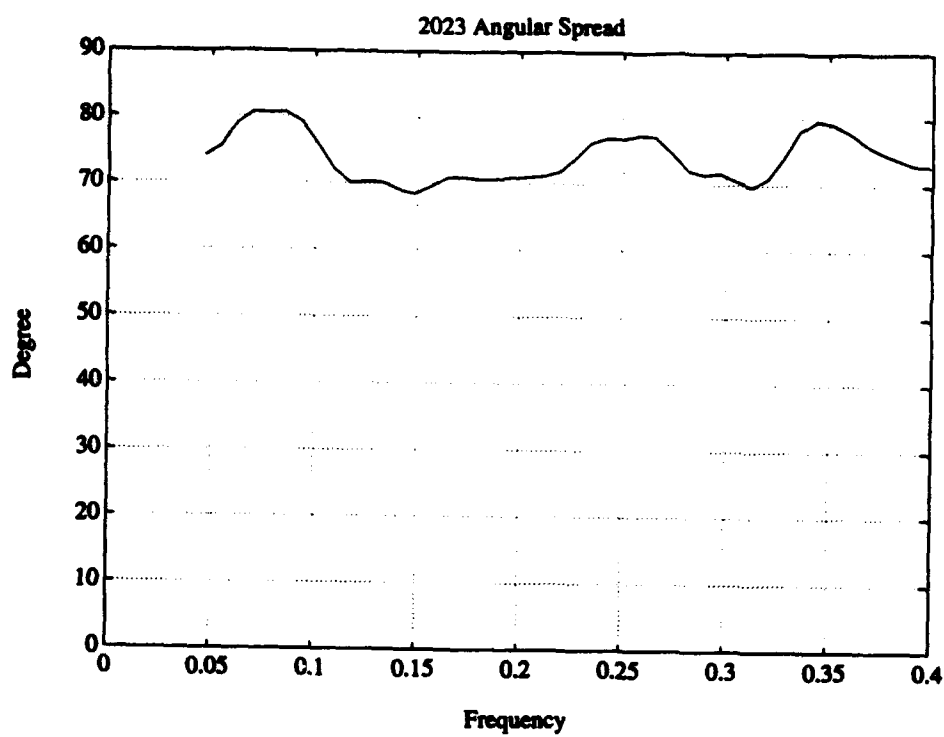


2023 Waveheight PSD

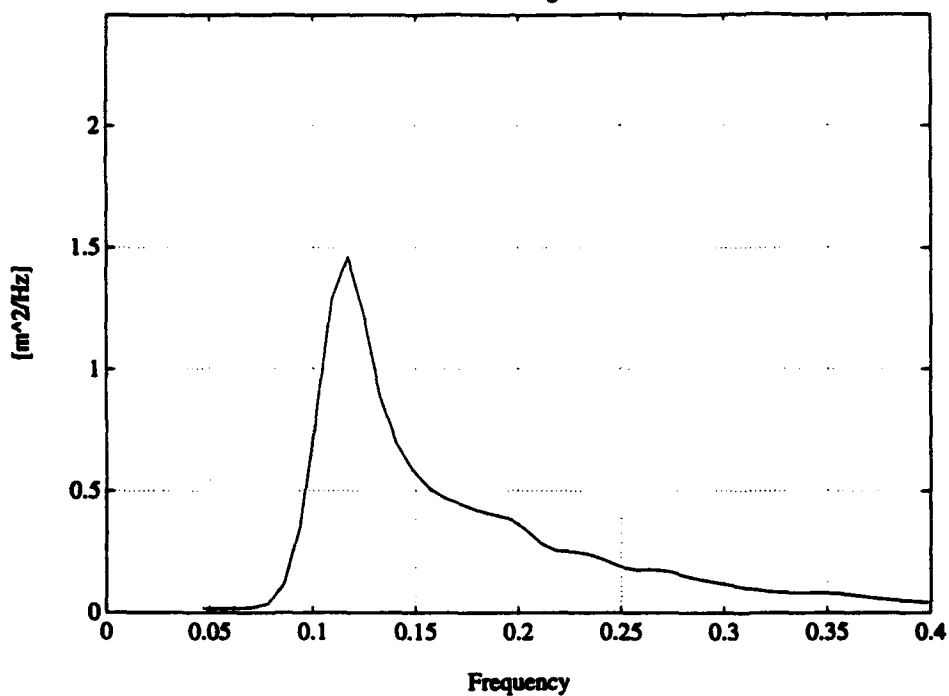


2023 Wave Direction

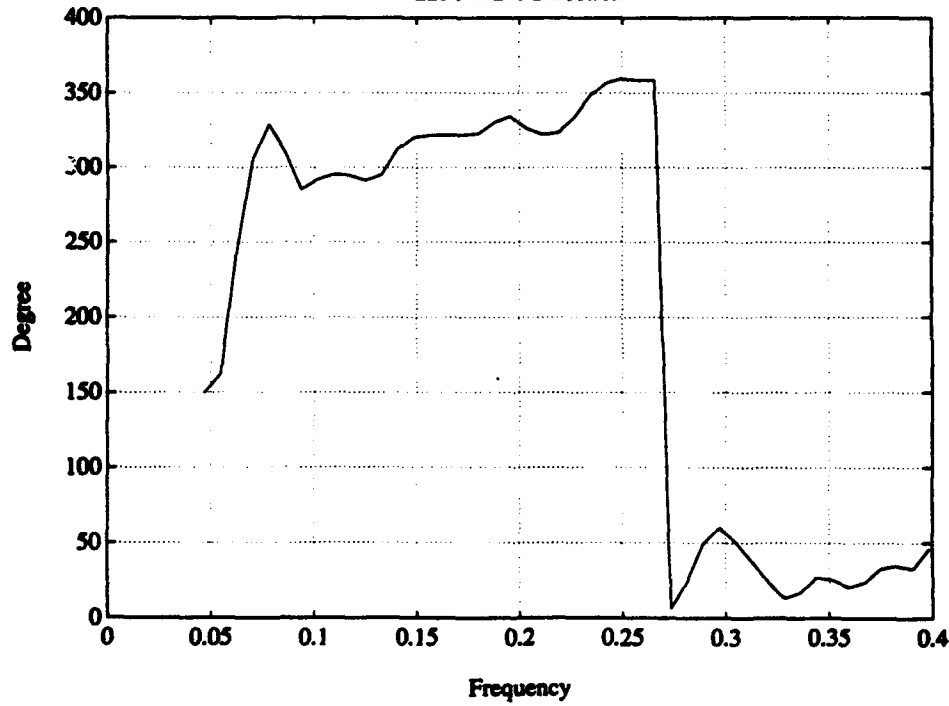


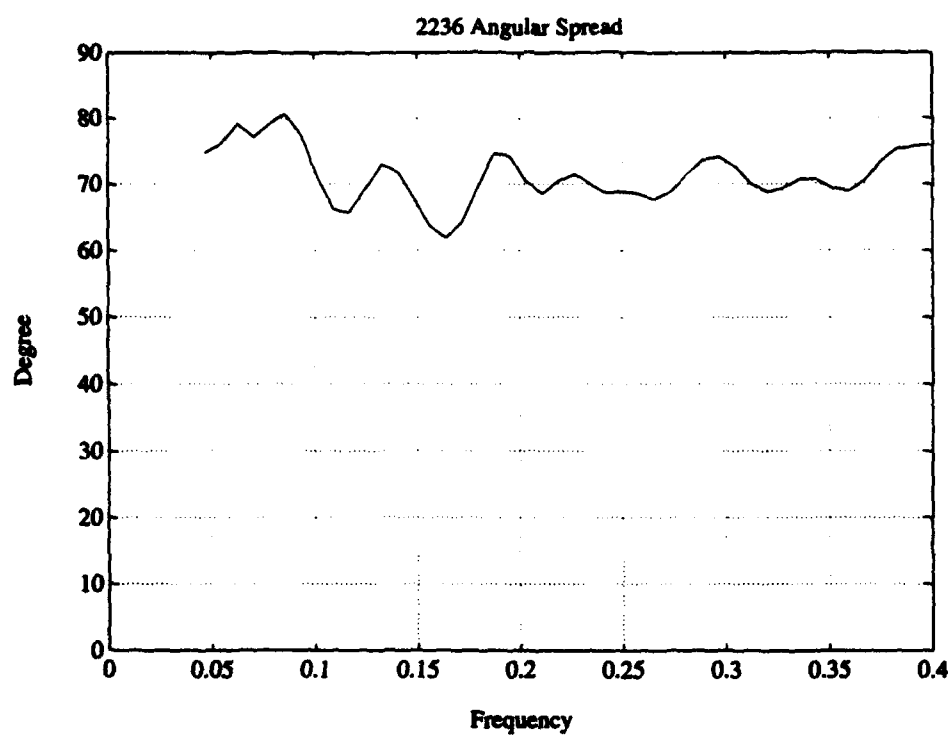


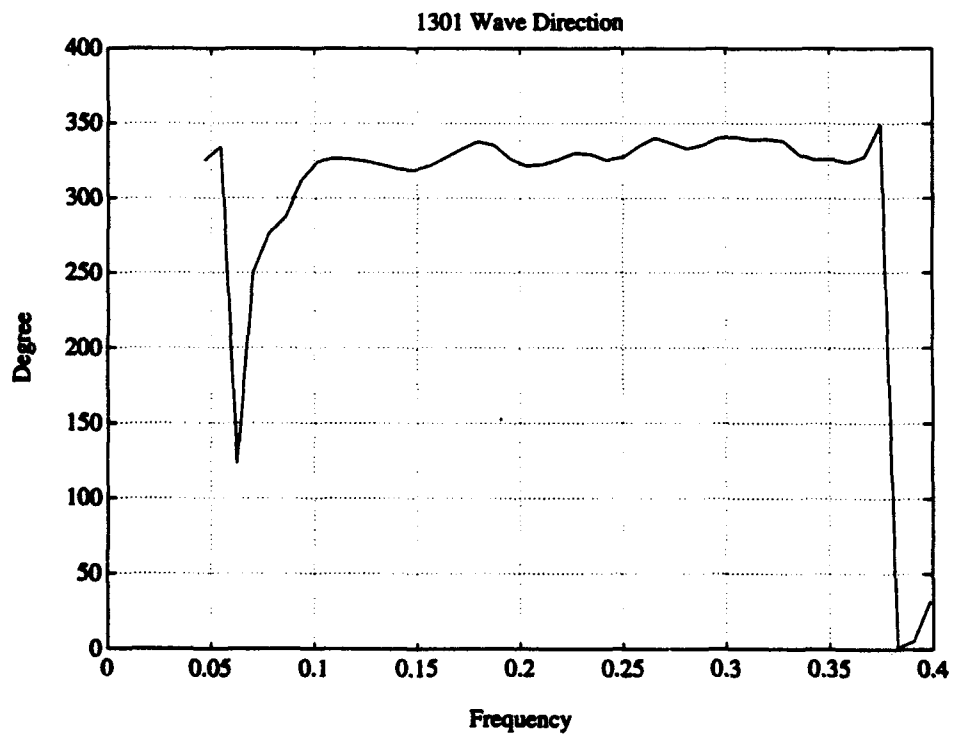
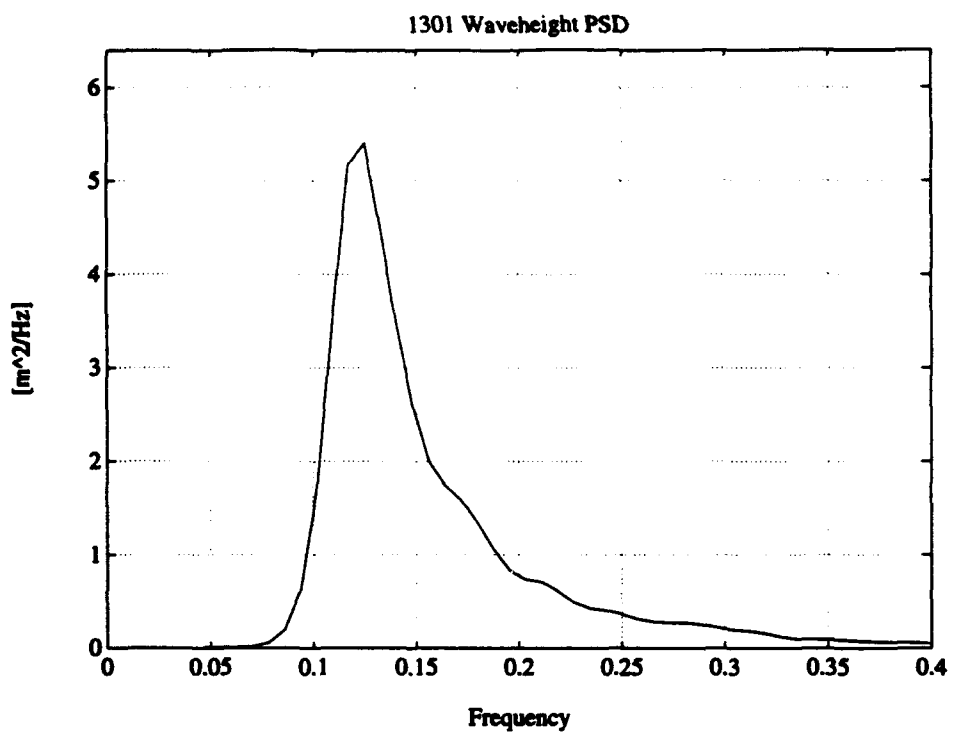
2236 Waveheight PSD

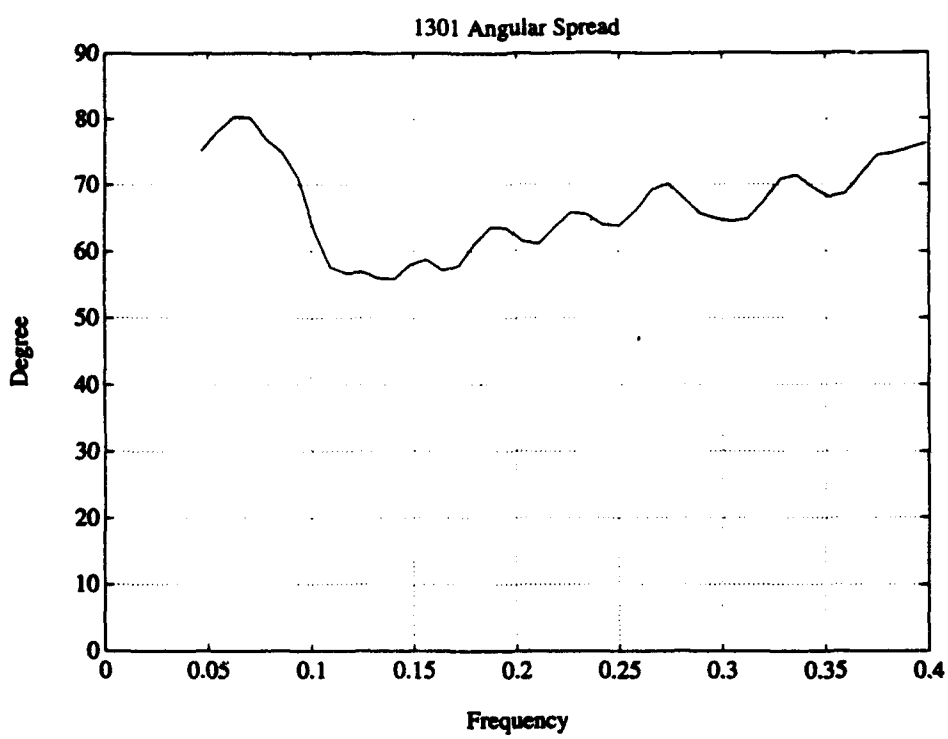


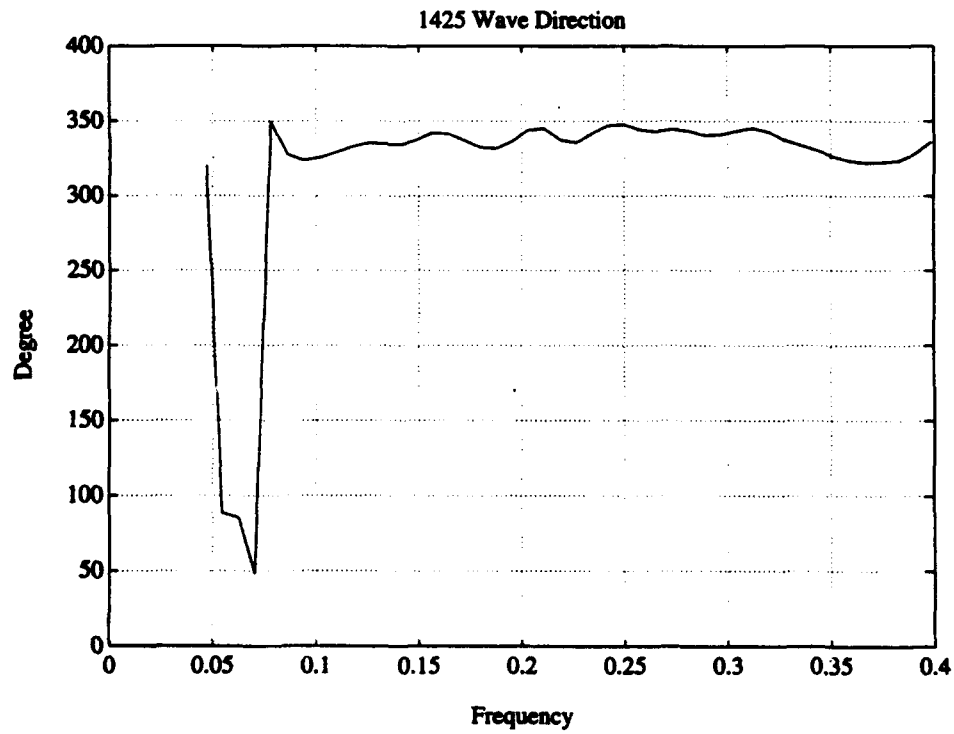
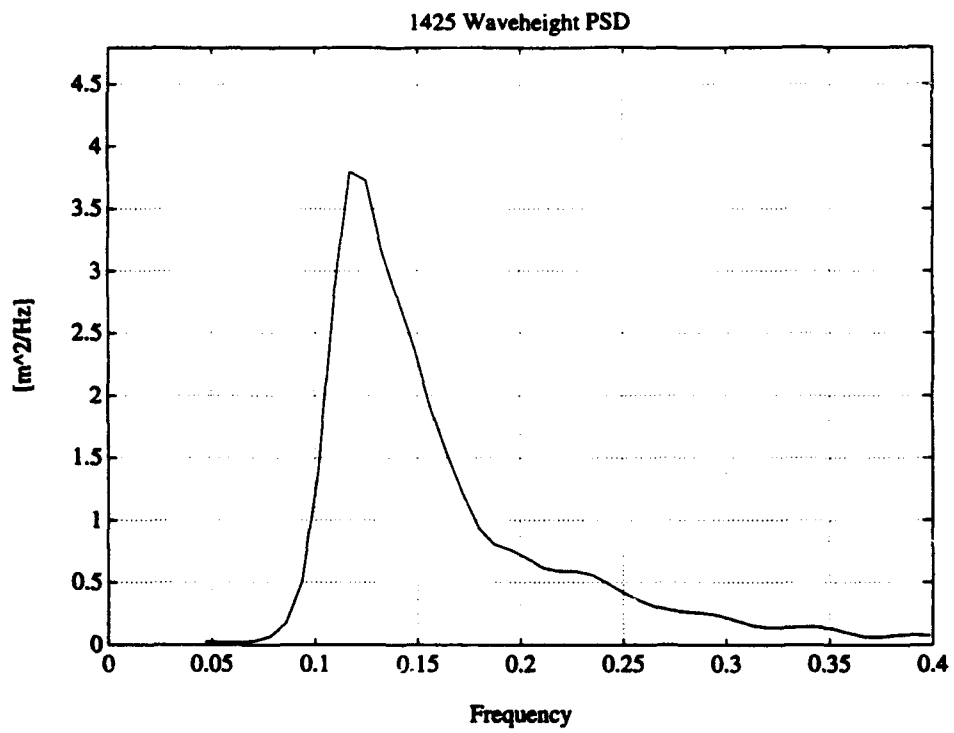
2236 Wave Direction

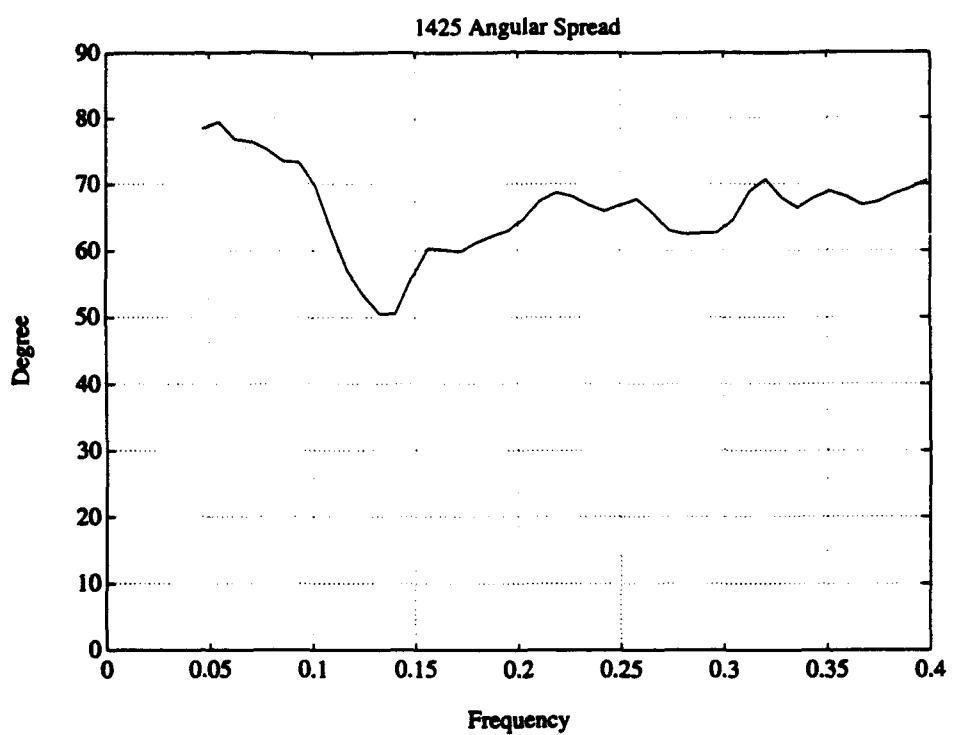




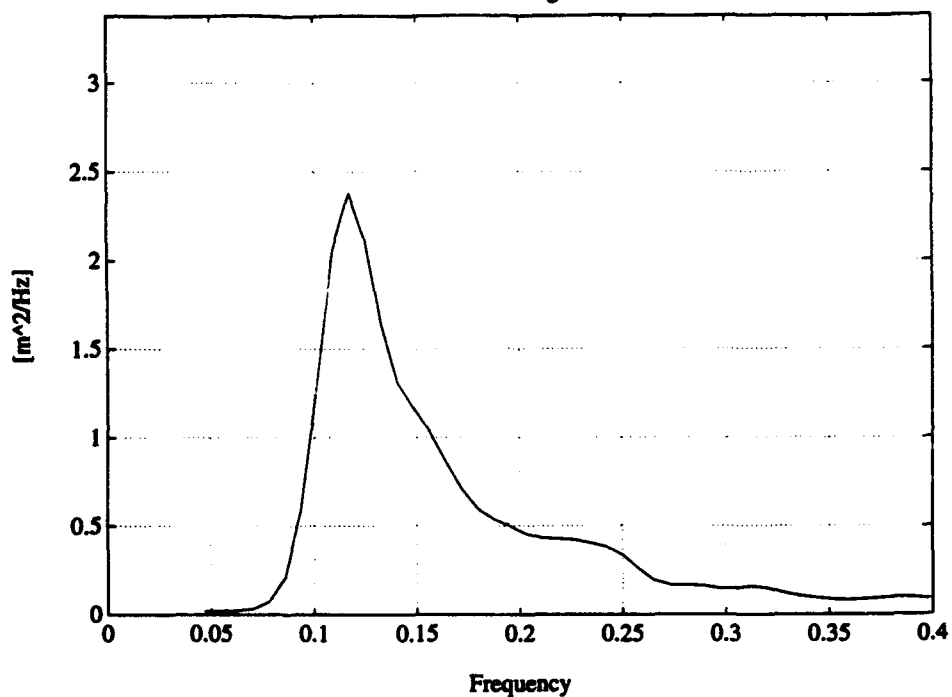




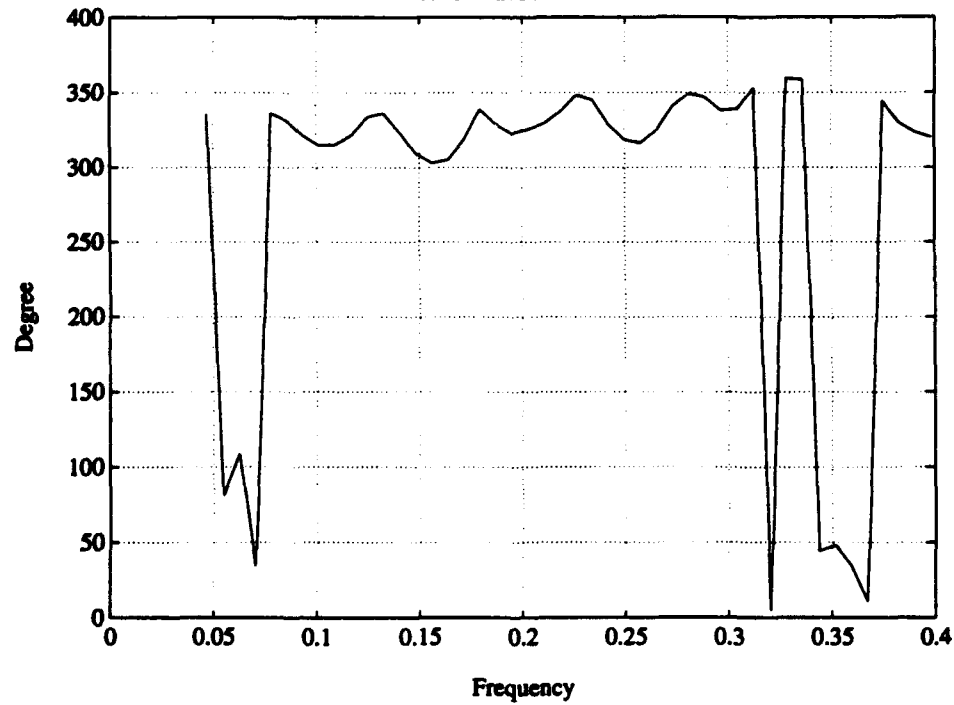


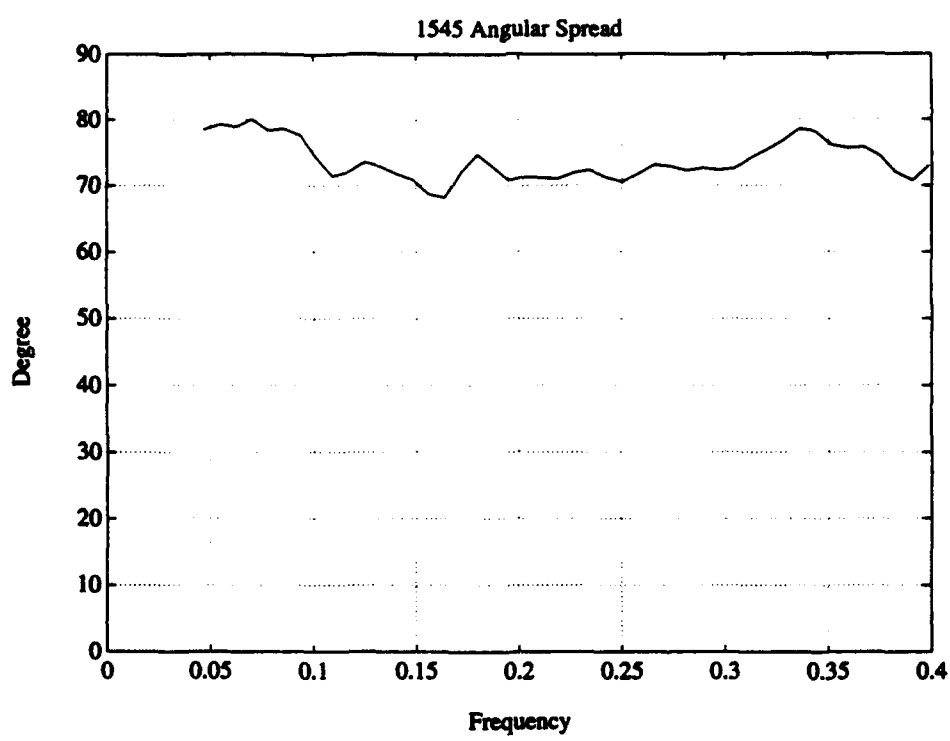


1545 Waveheight PSD

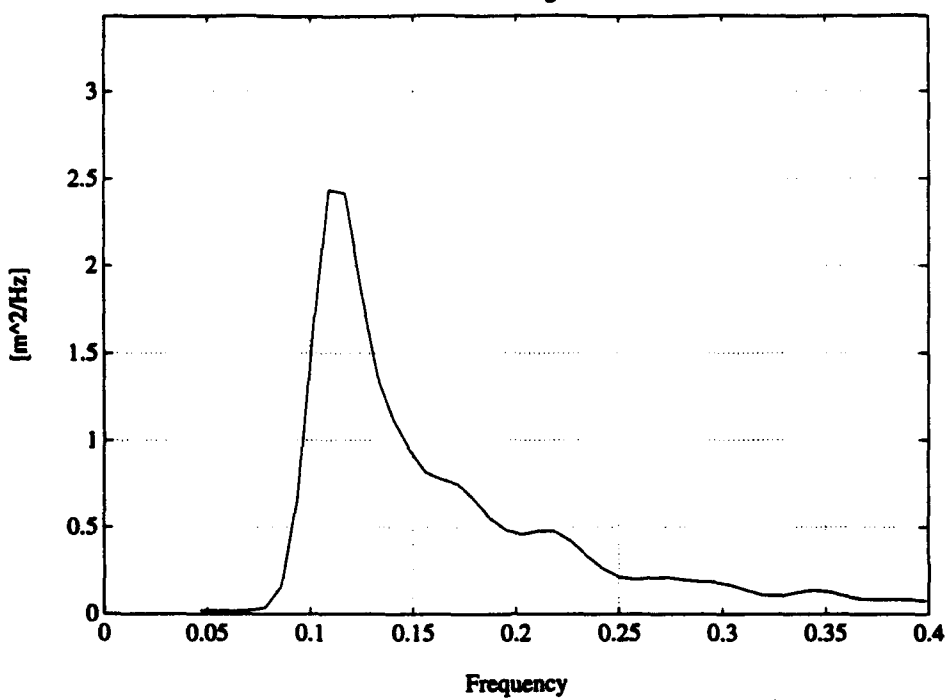


1545 Wave Direction

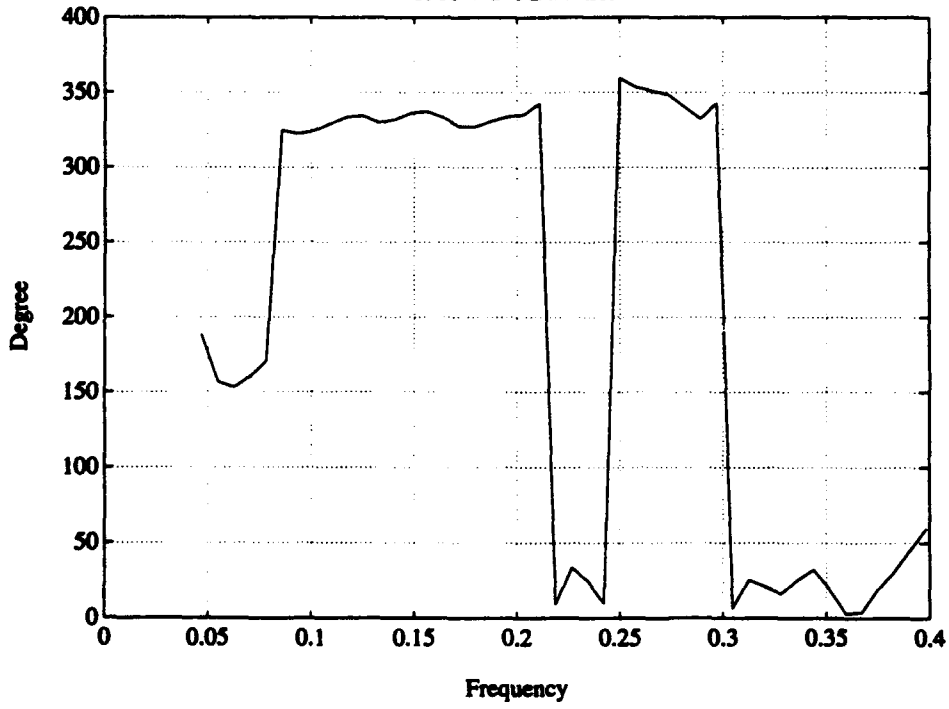


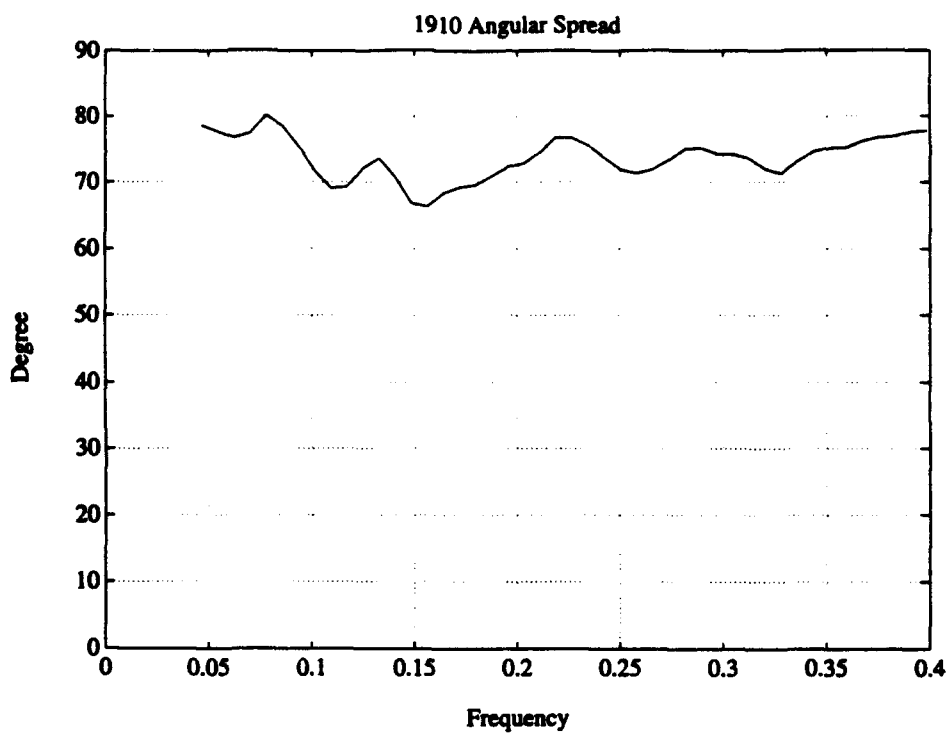


1910 Waveheight PSD

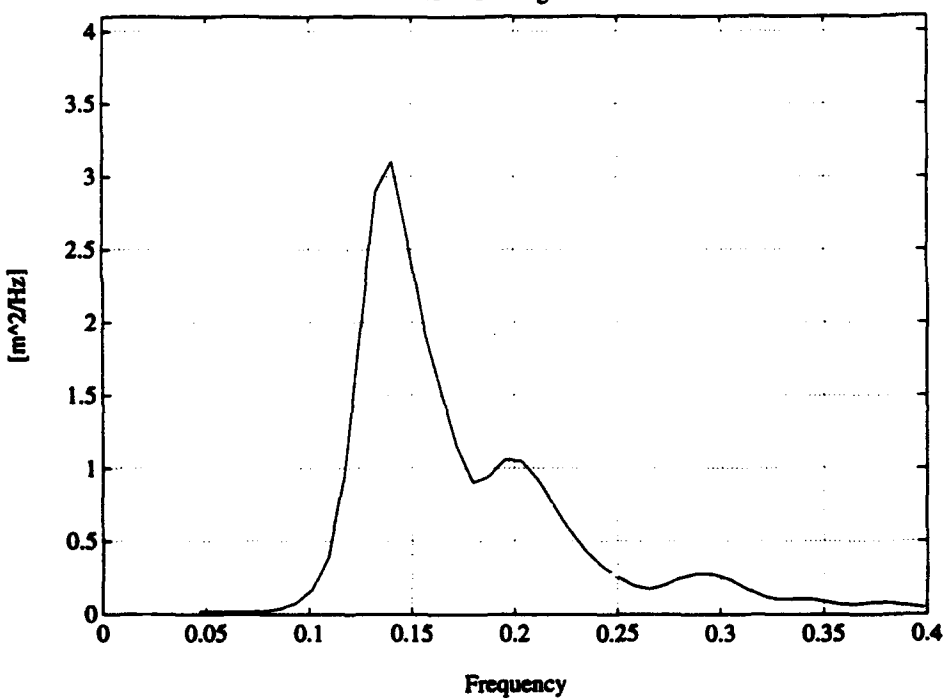


1910 Wave Direction

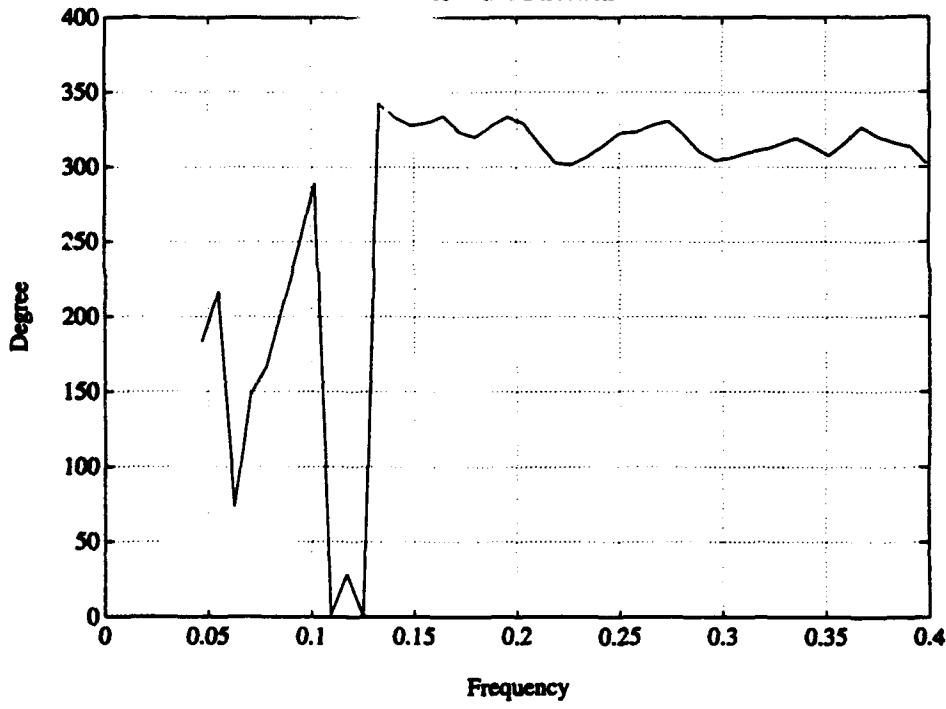


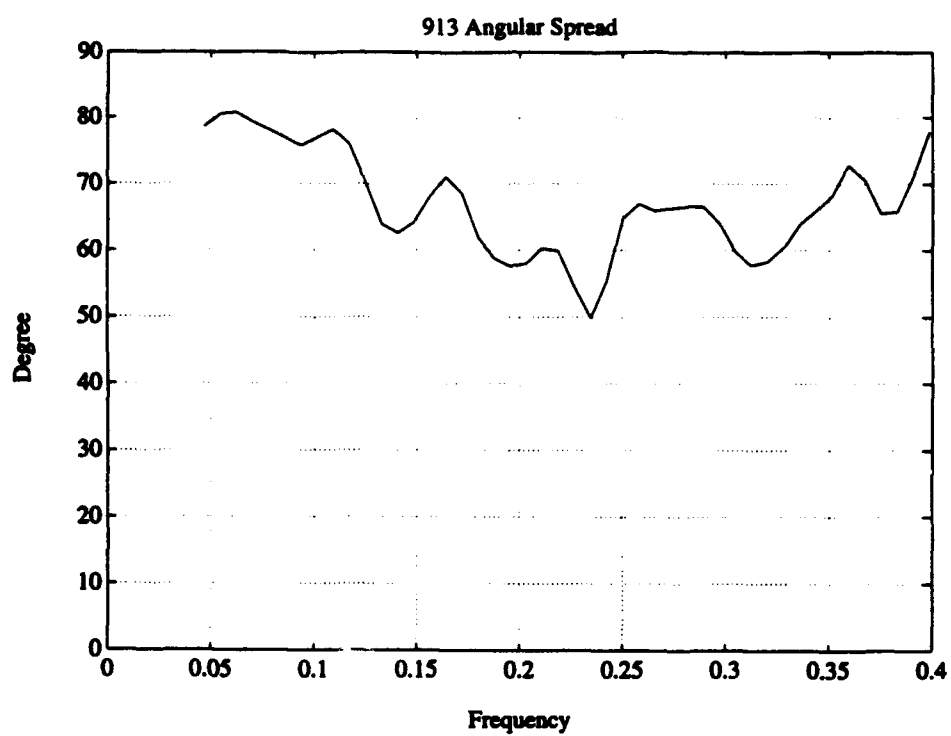


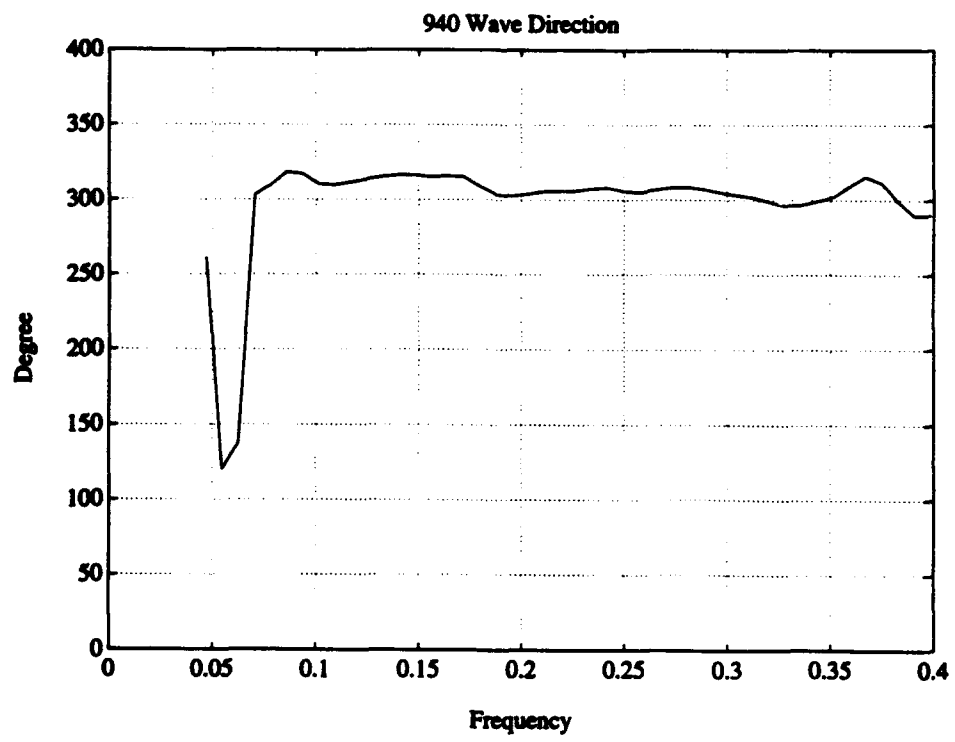
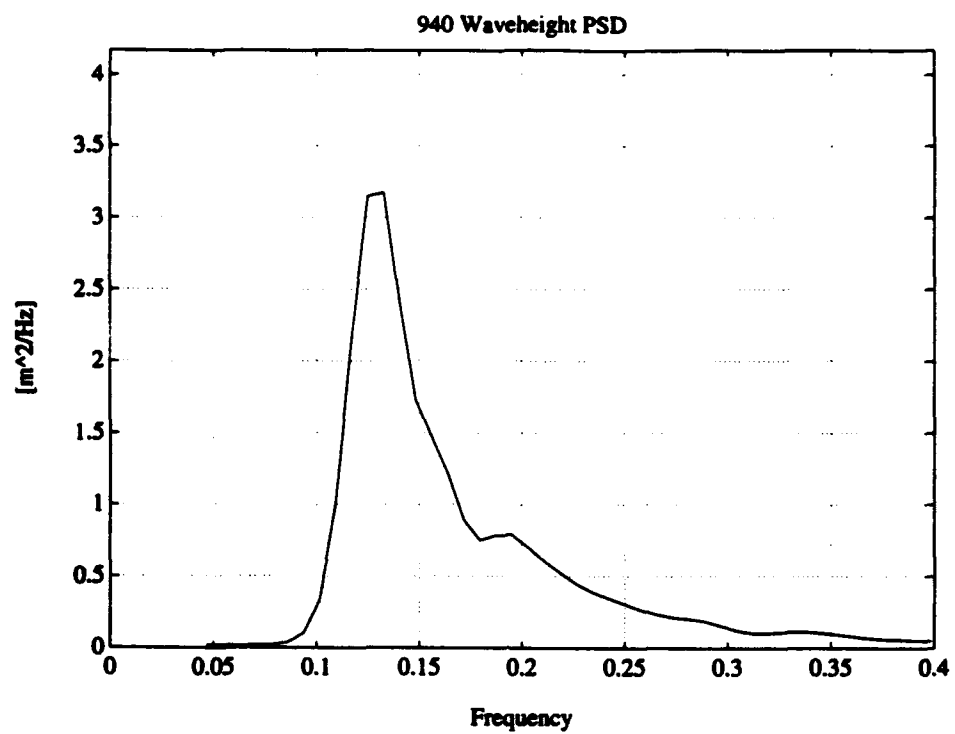
913 Waveheight PSD

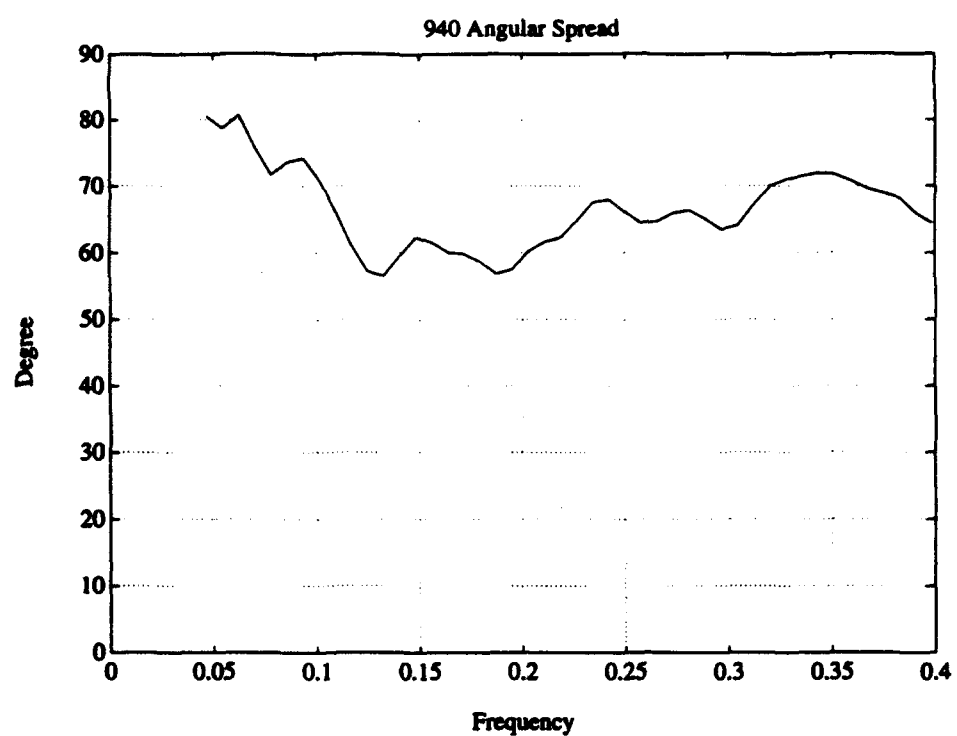


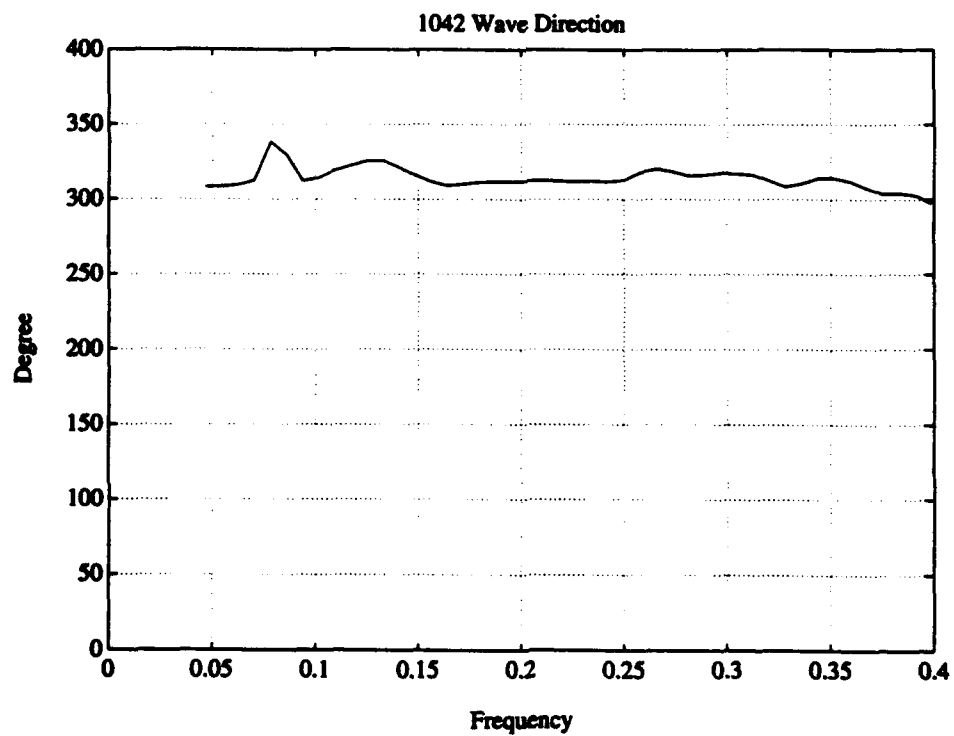
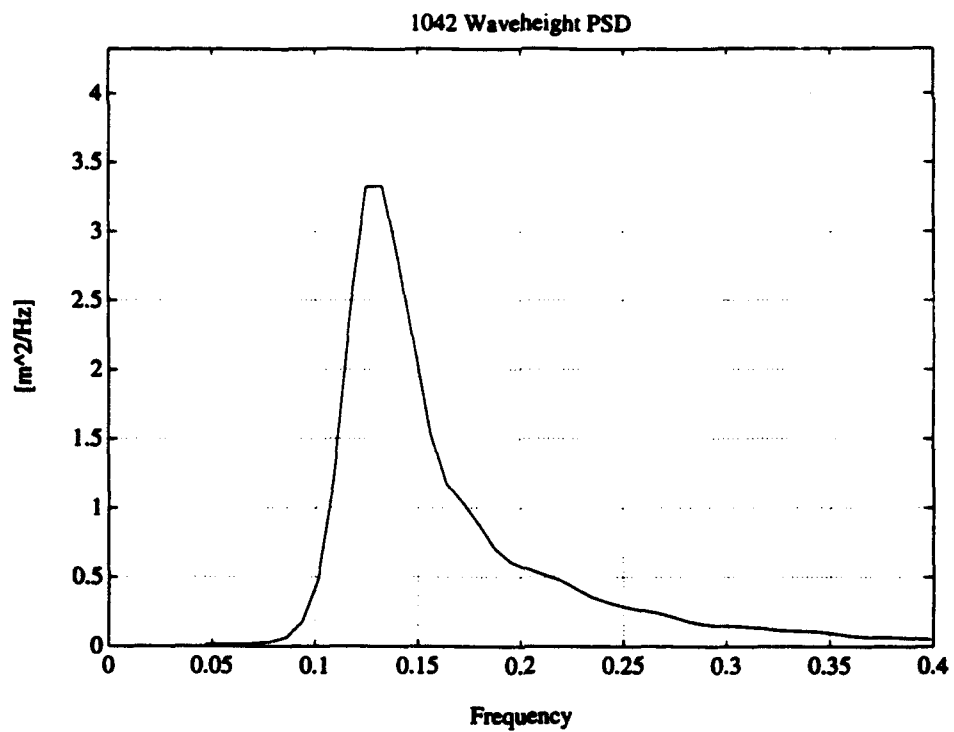
913 Wave Direction

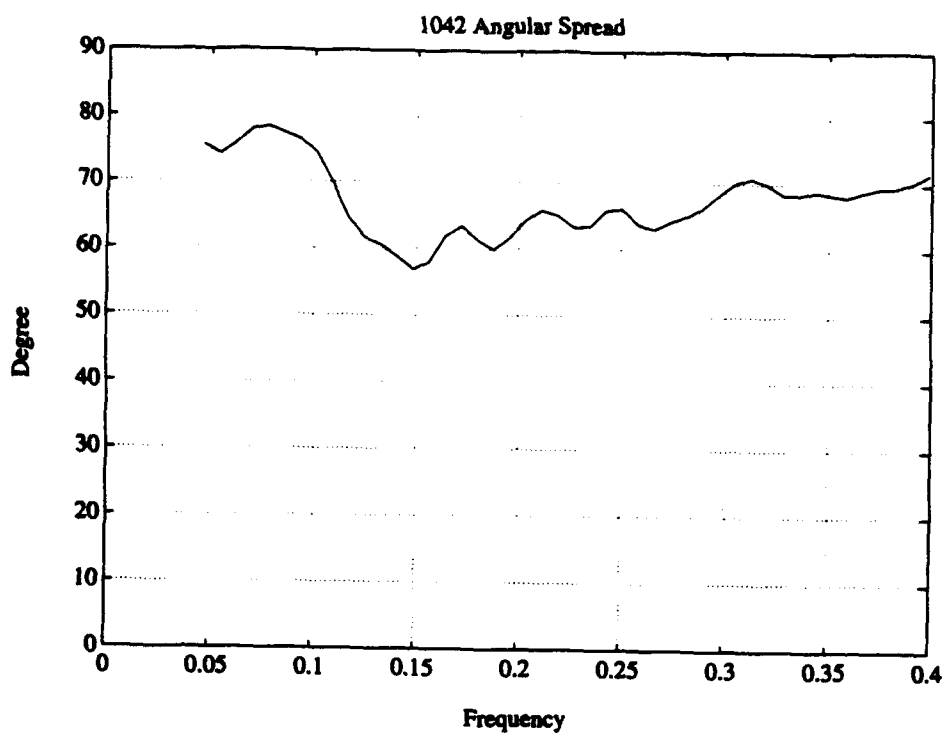


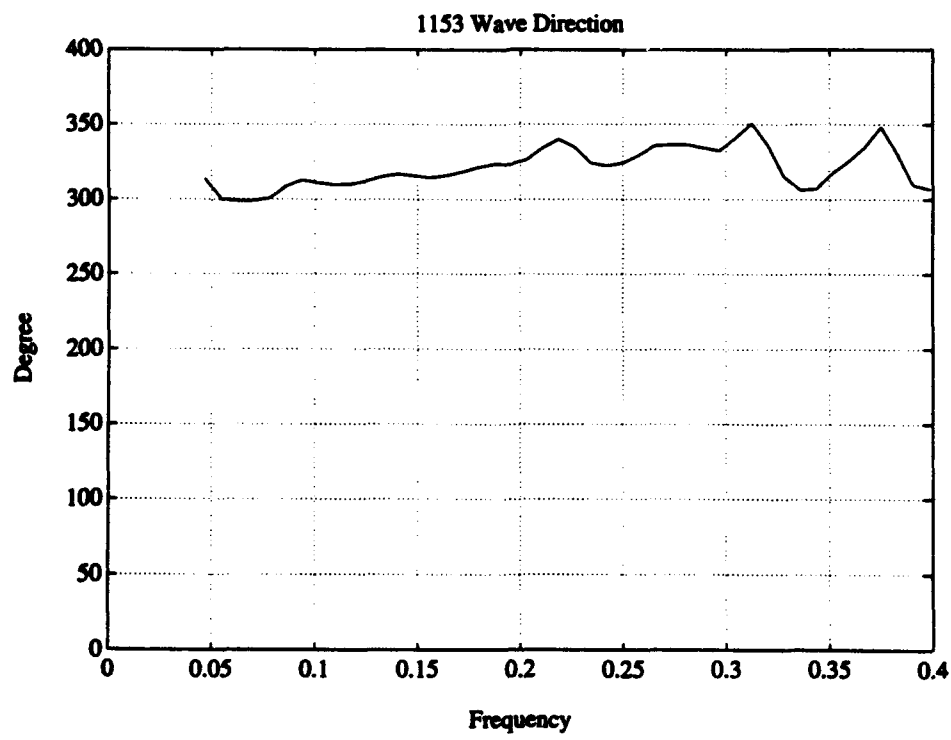
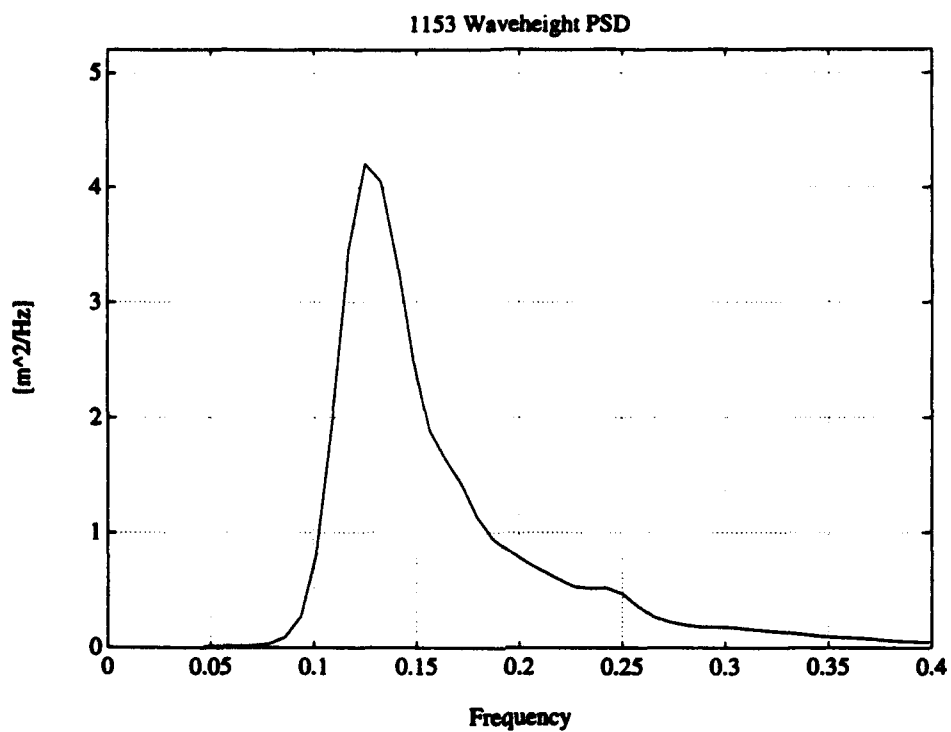


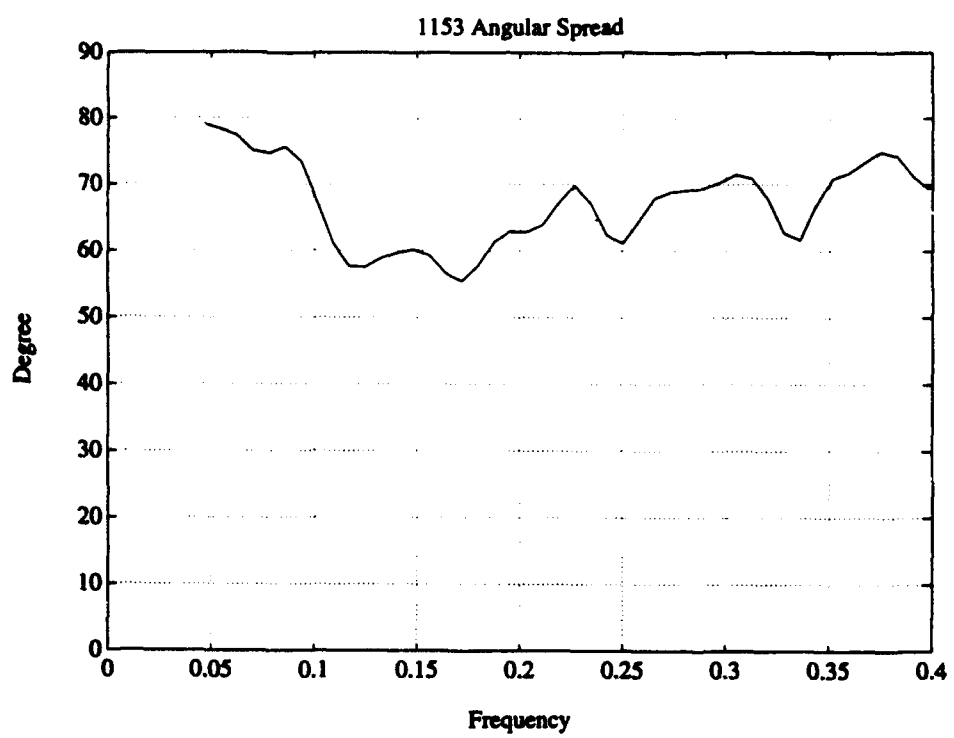




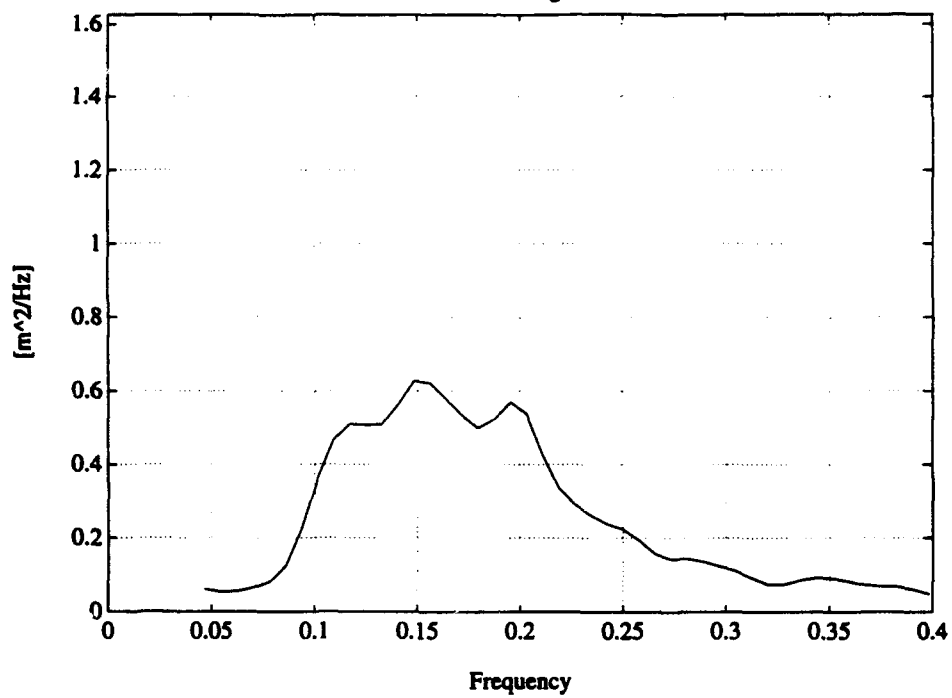




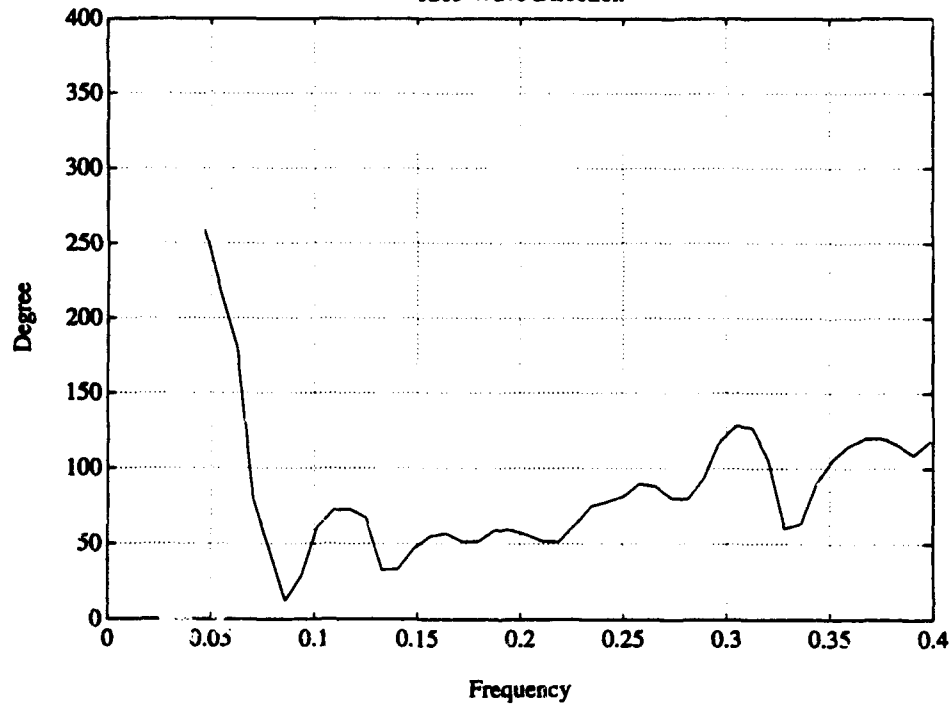


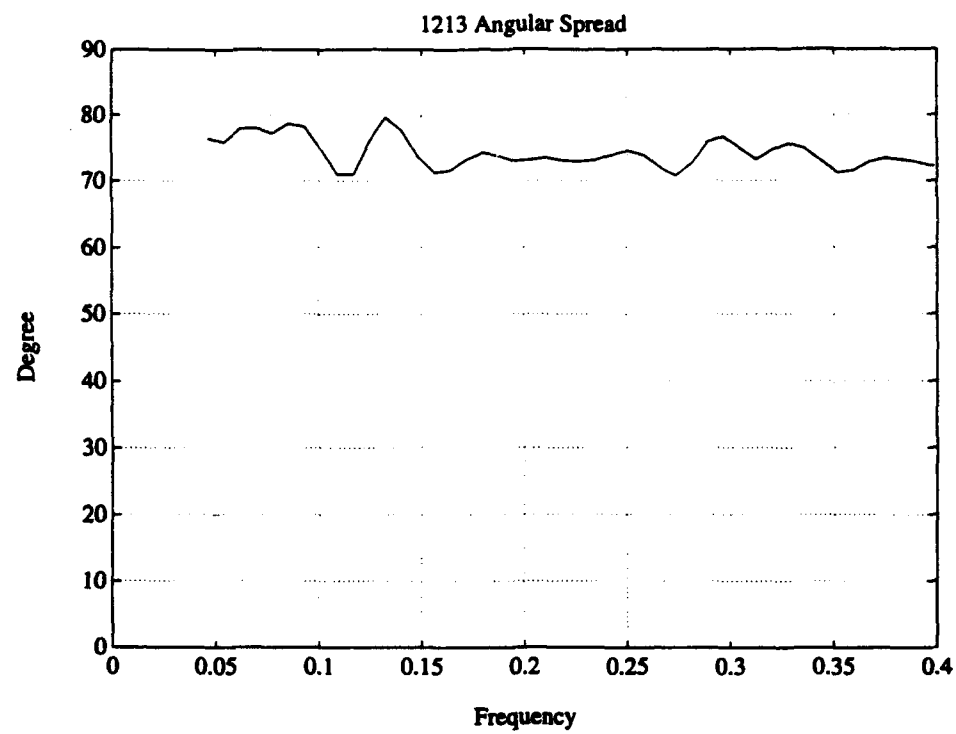


1213 Waveheight PSD

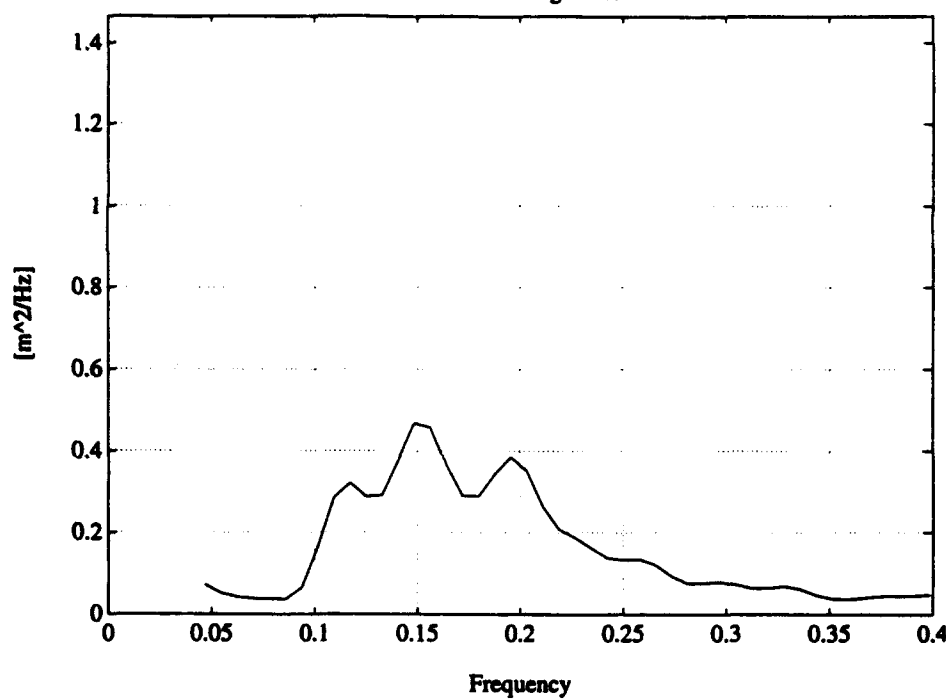


1213 Wave Direction

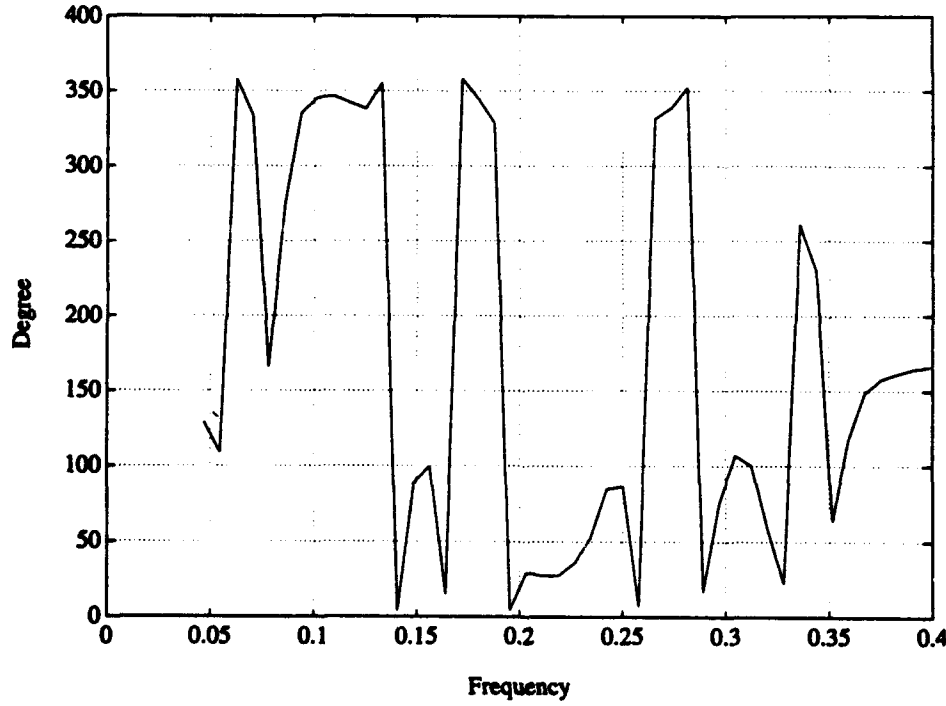


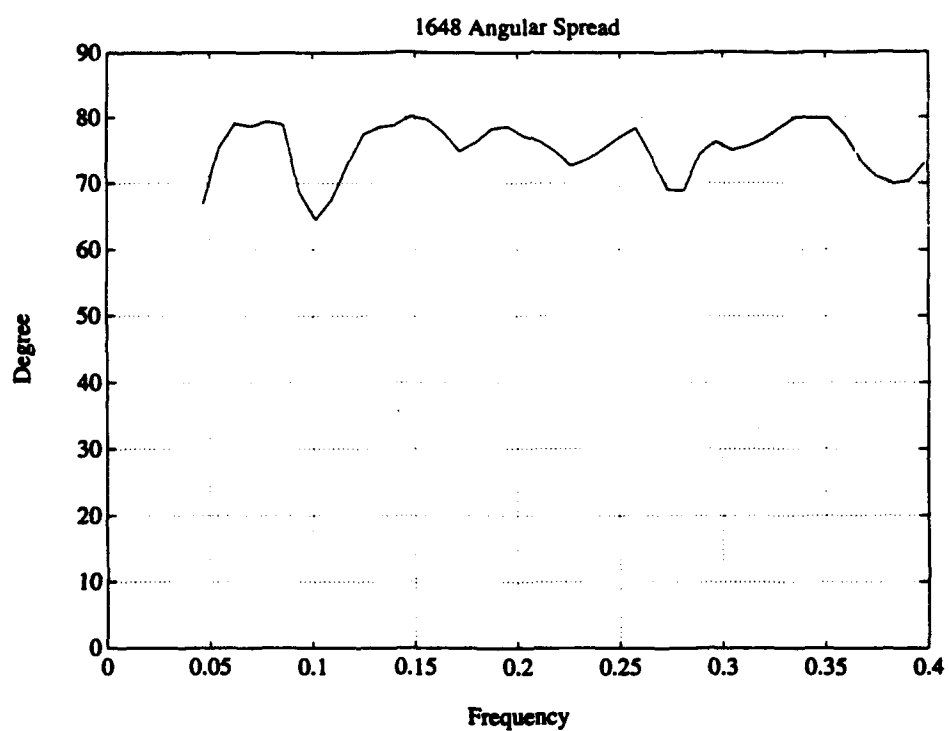


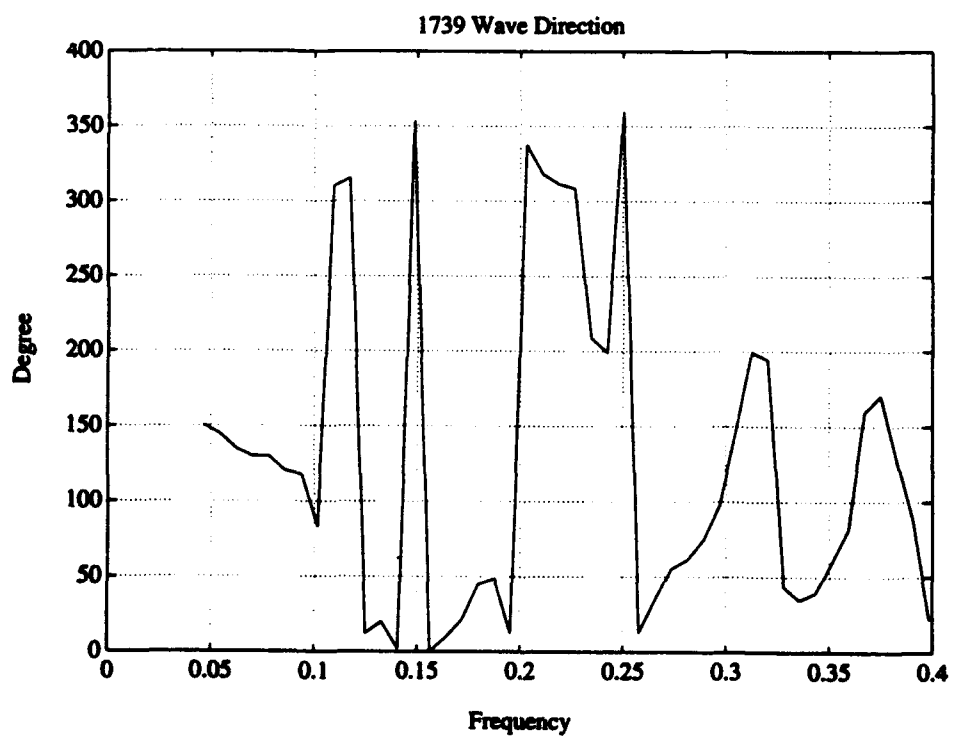
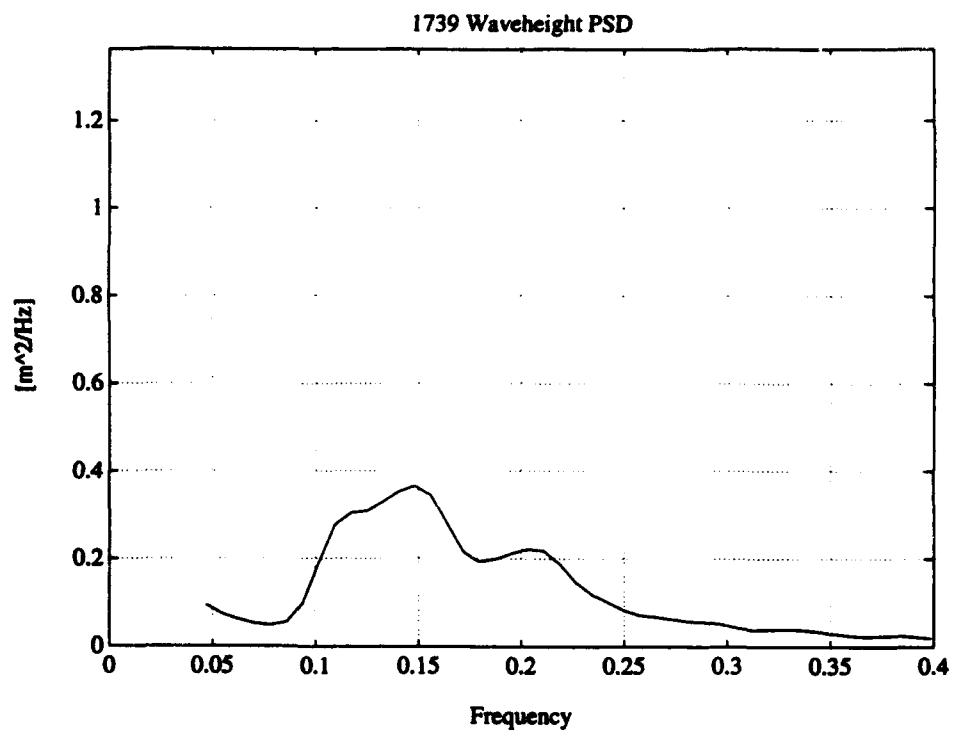
1648 Waveheight PSD

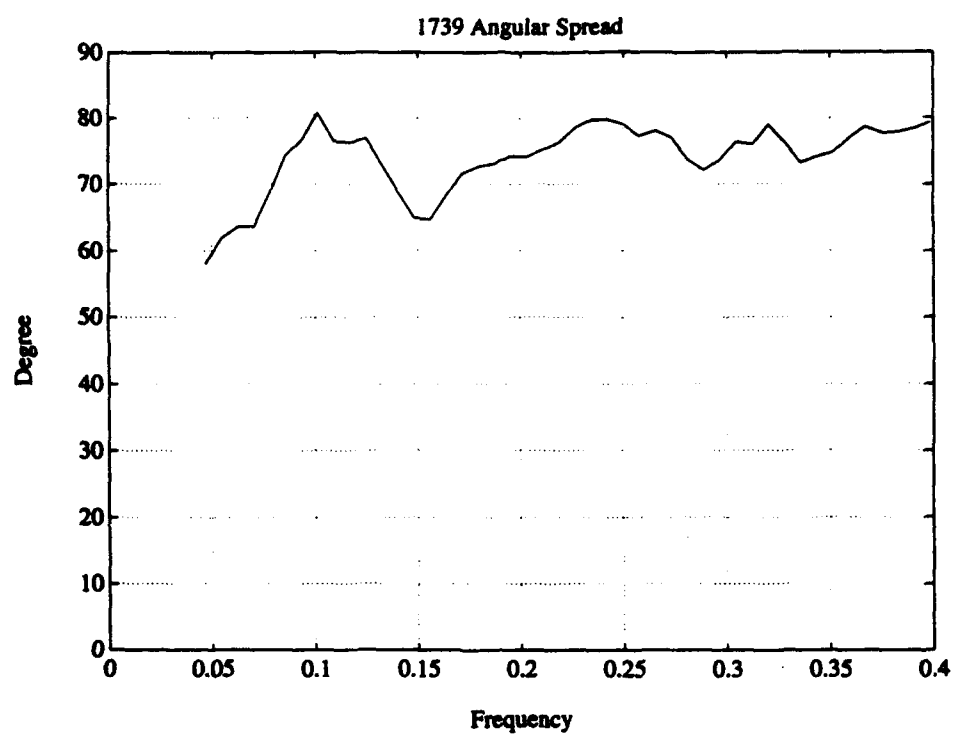


1648 Wave Direction

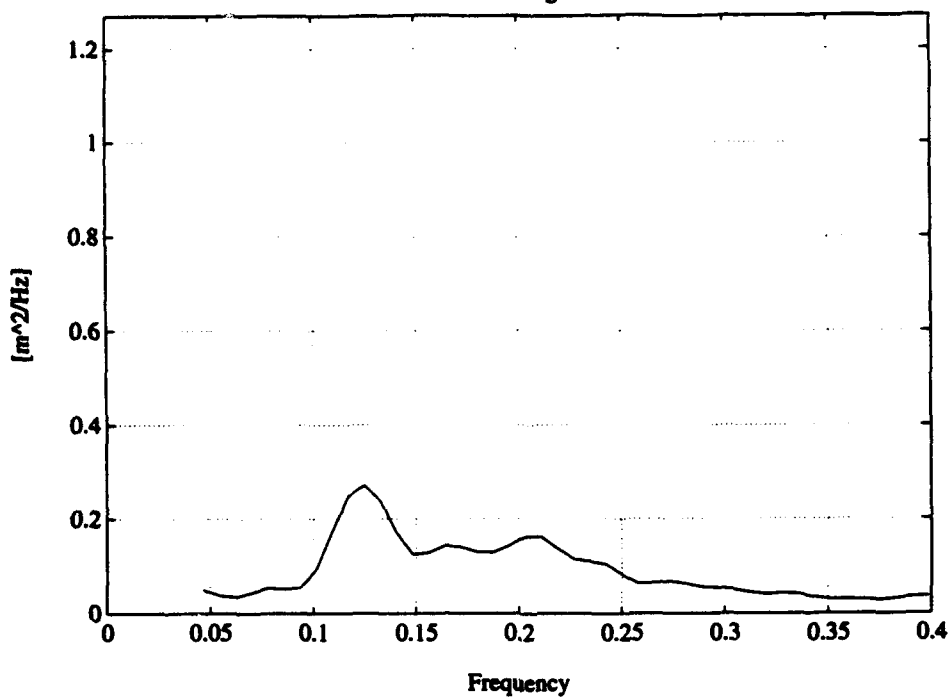




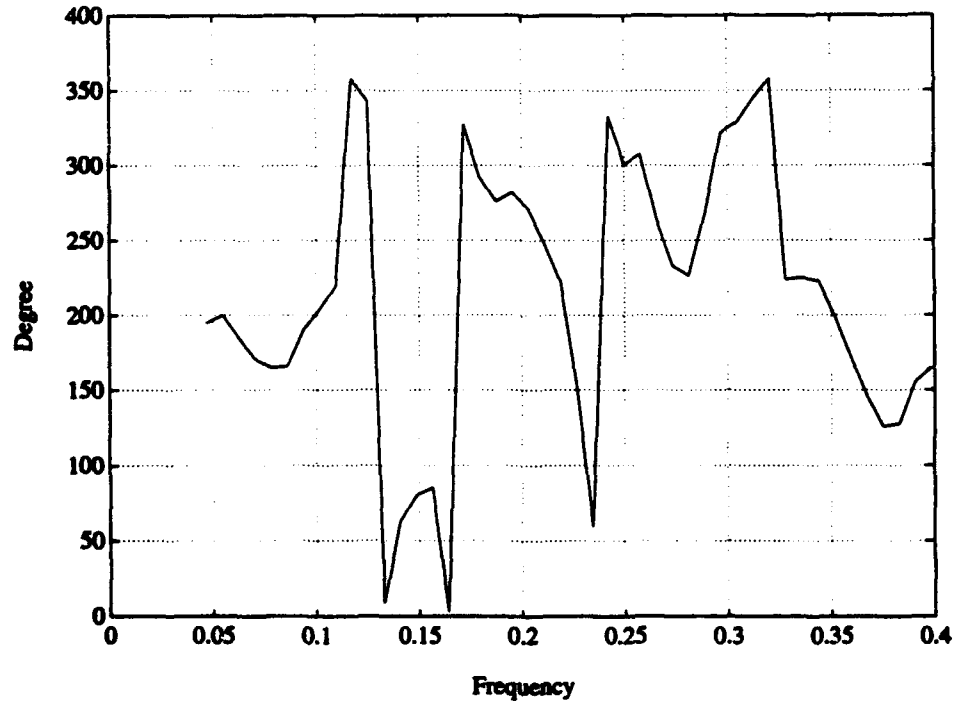


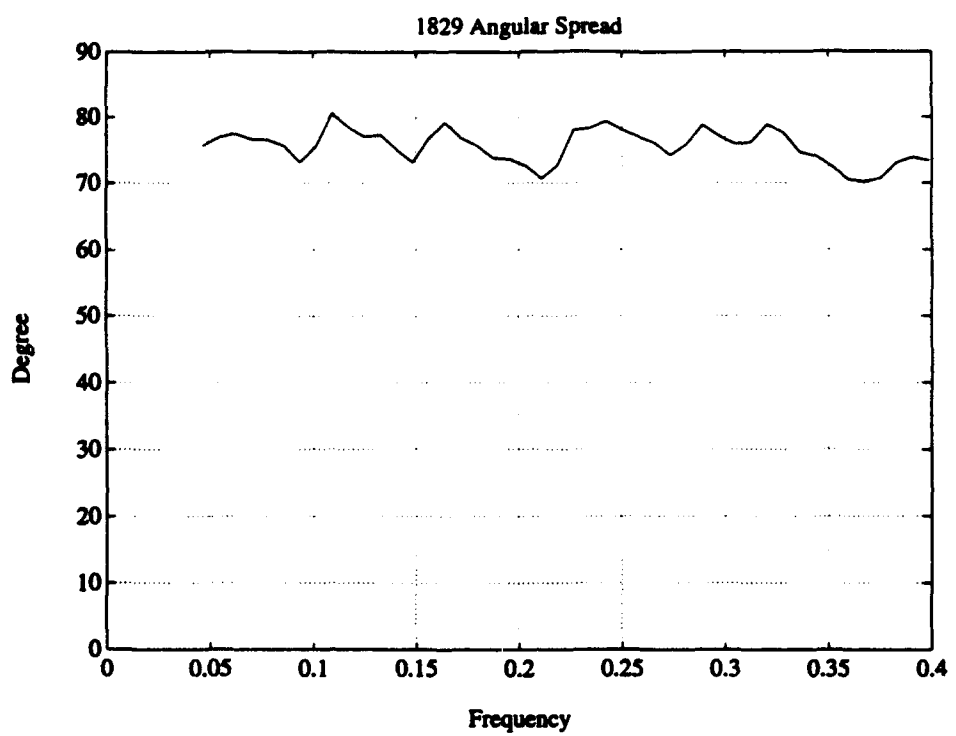


1829 Waveheight PSD

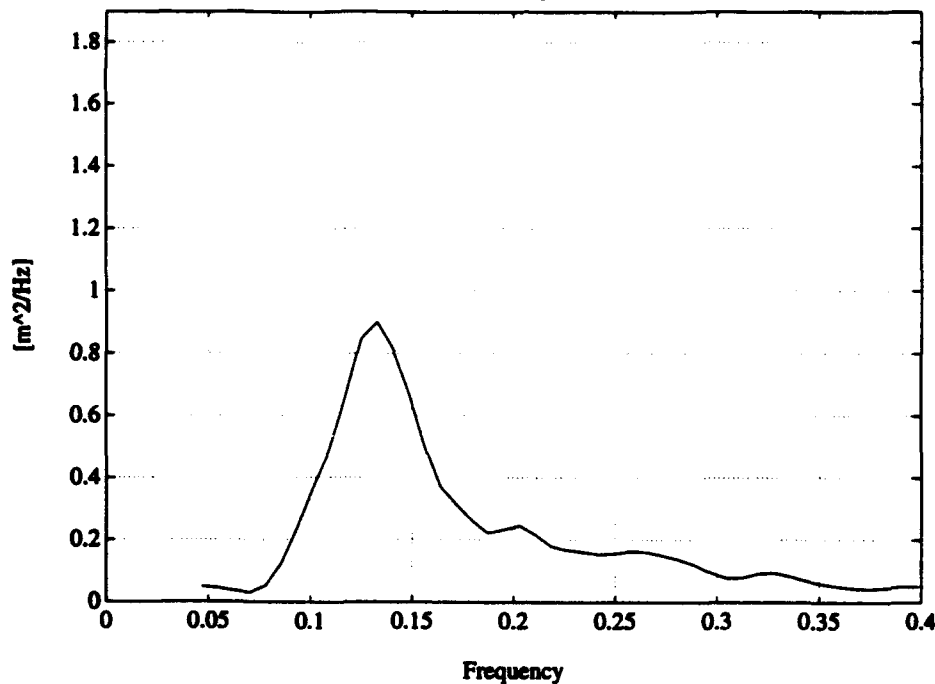


1829 Wave Direction

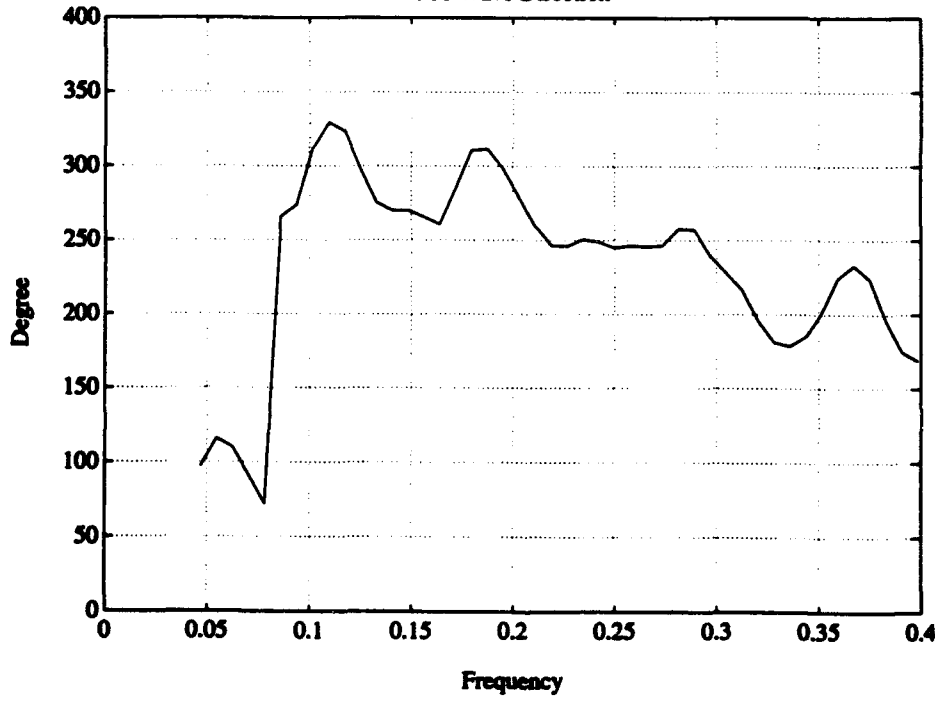


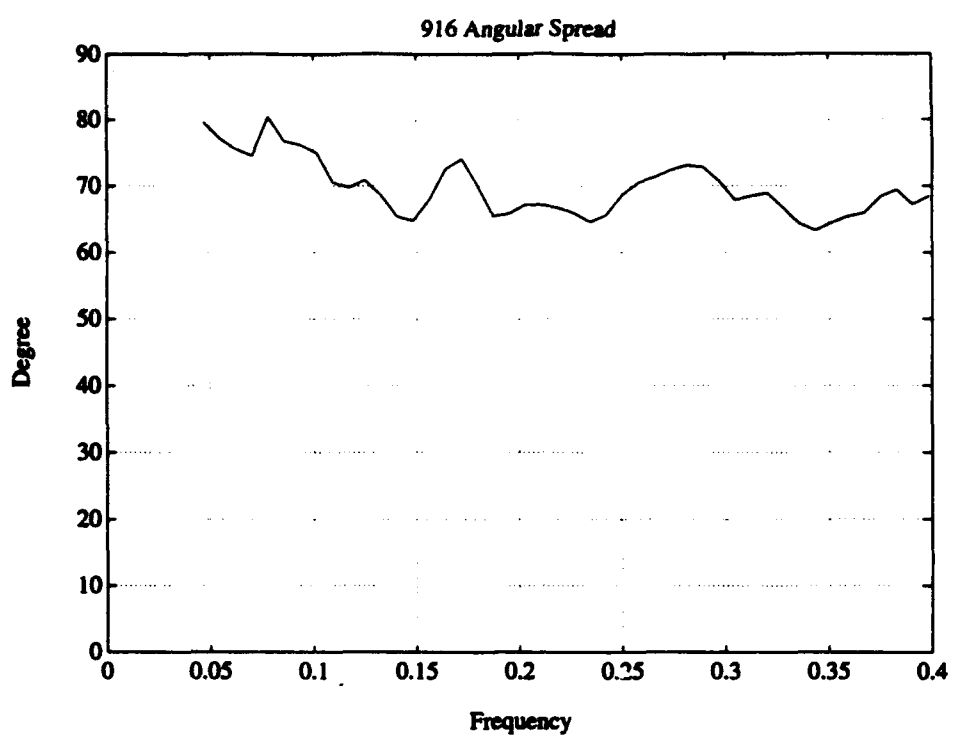


916 Waveheight PSD

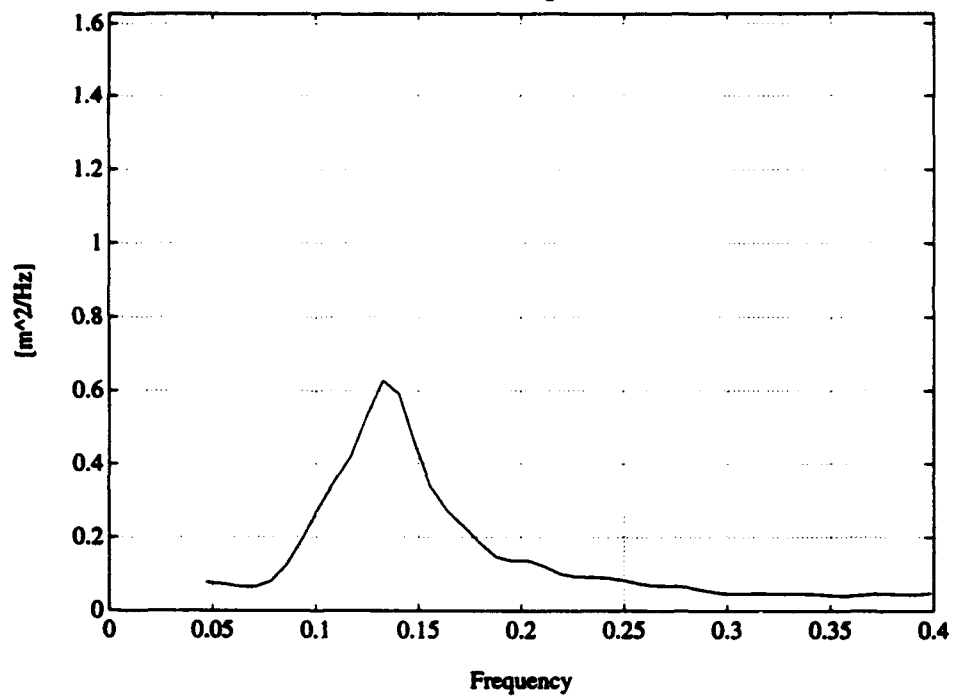


916 Wave Direction

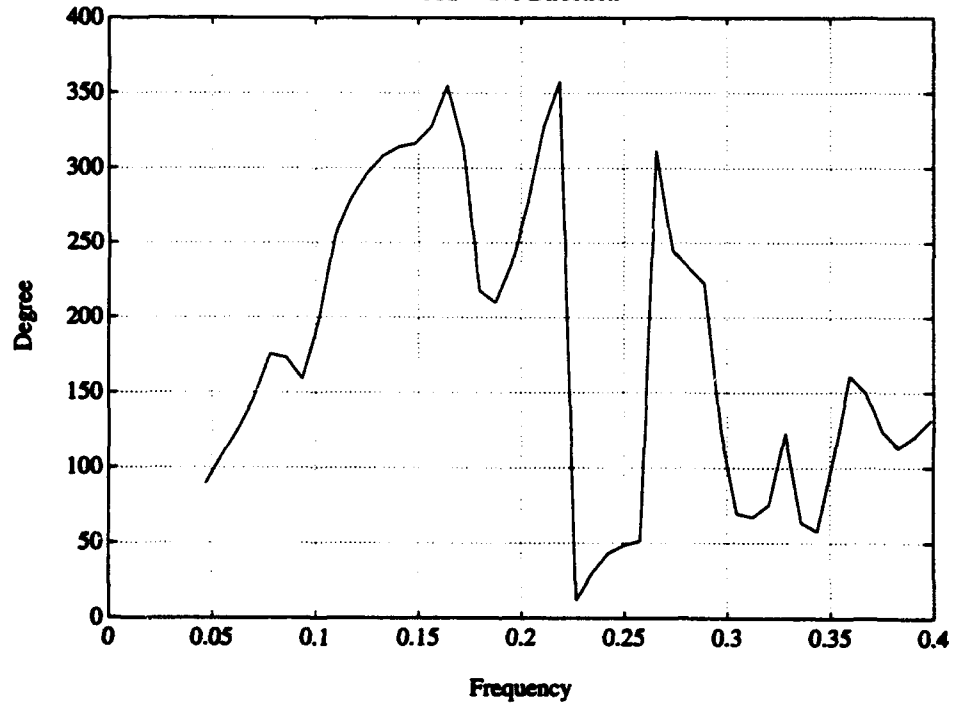


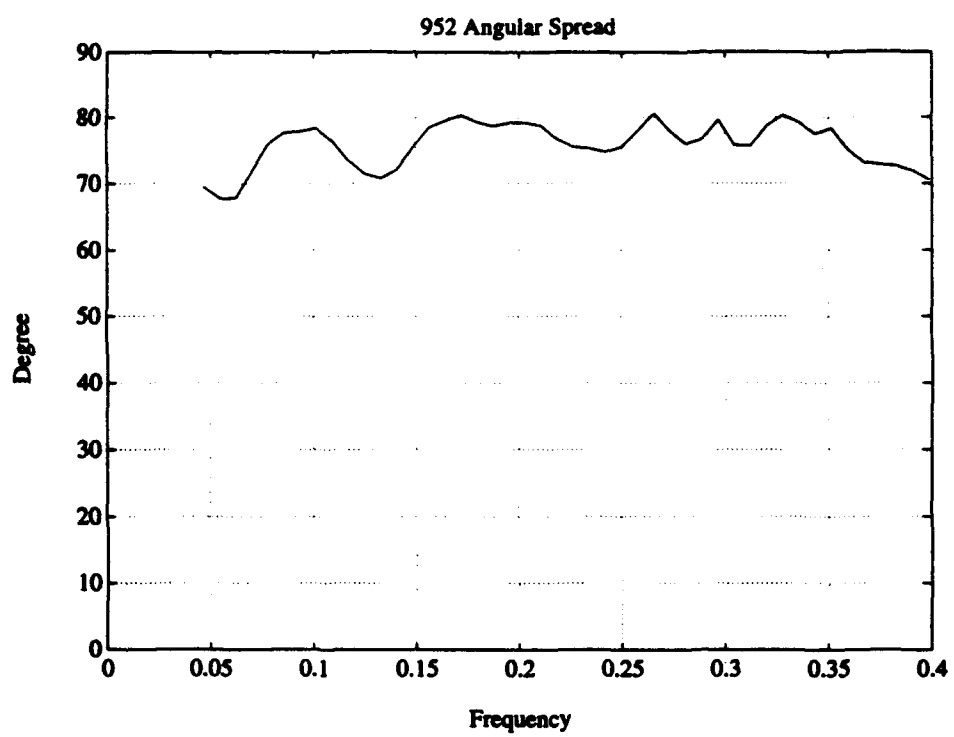


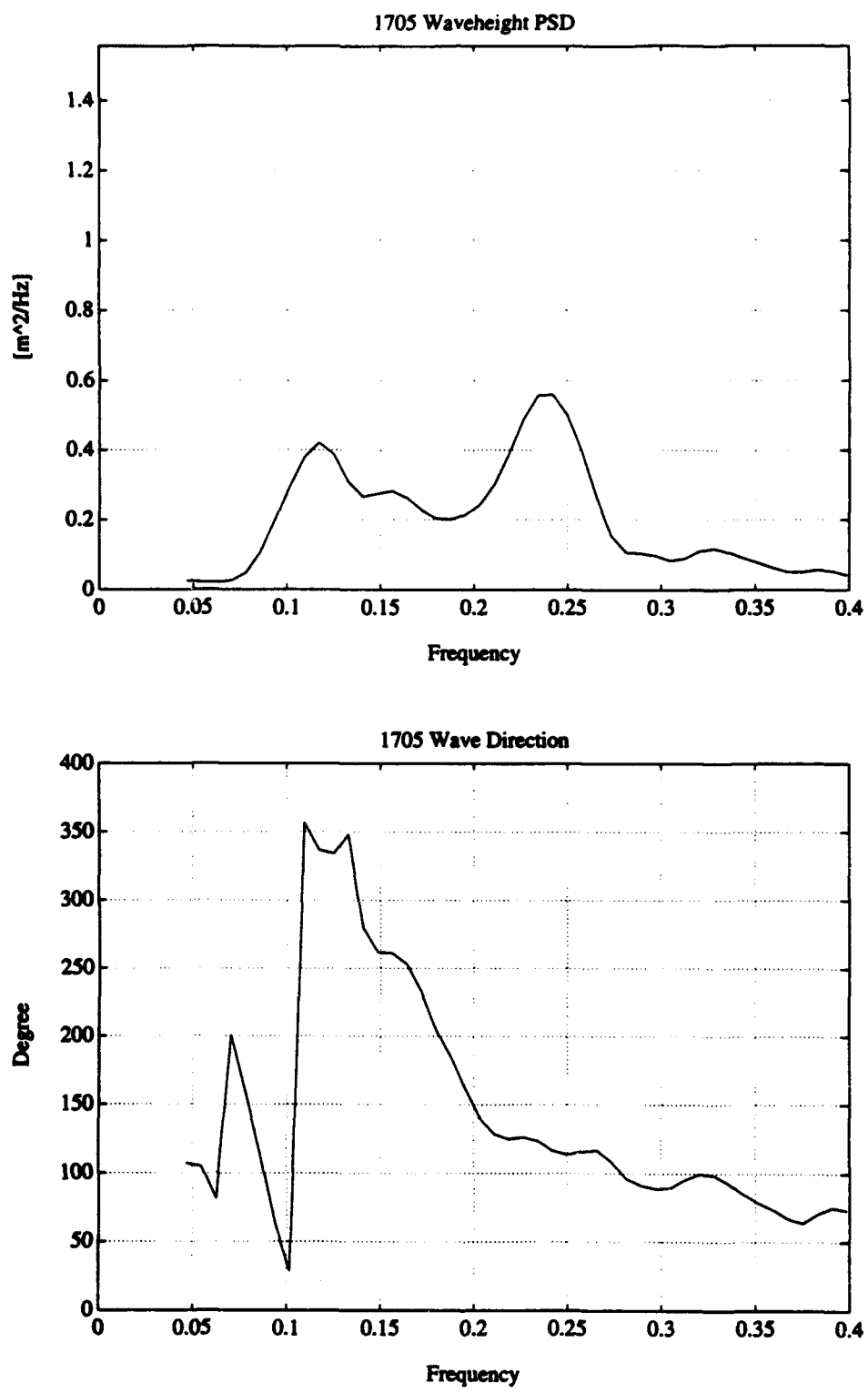
952 Waveheight PSD

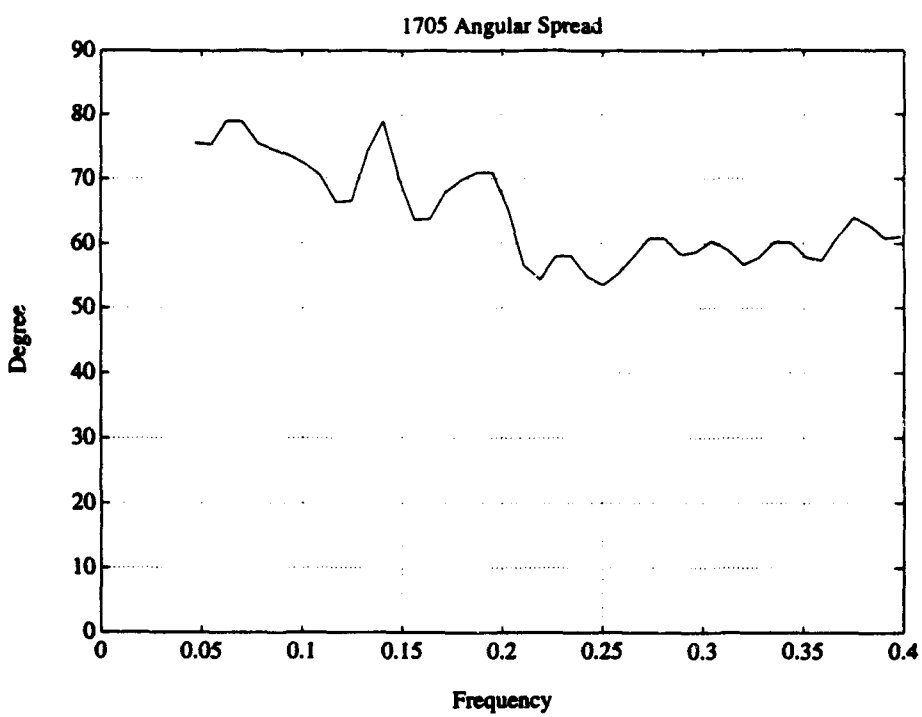


952 Wave Direction

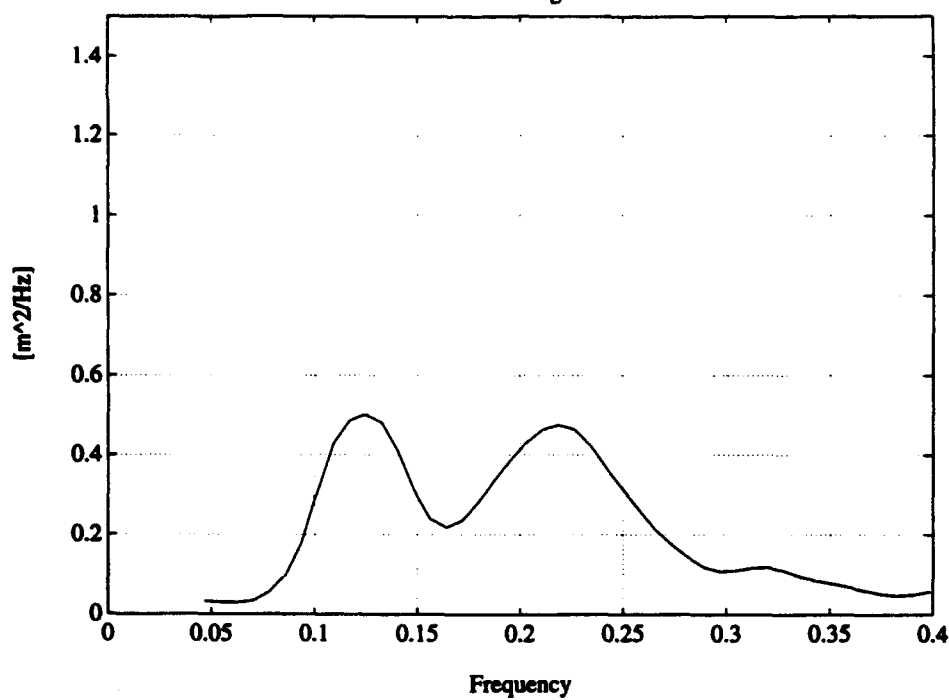




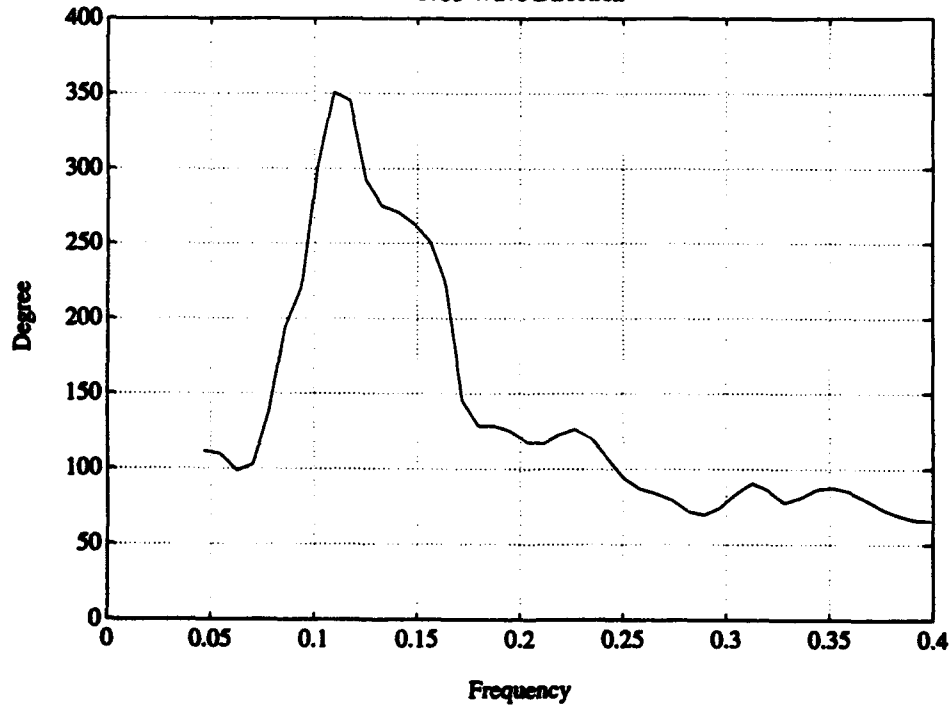


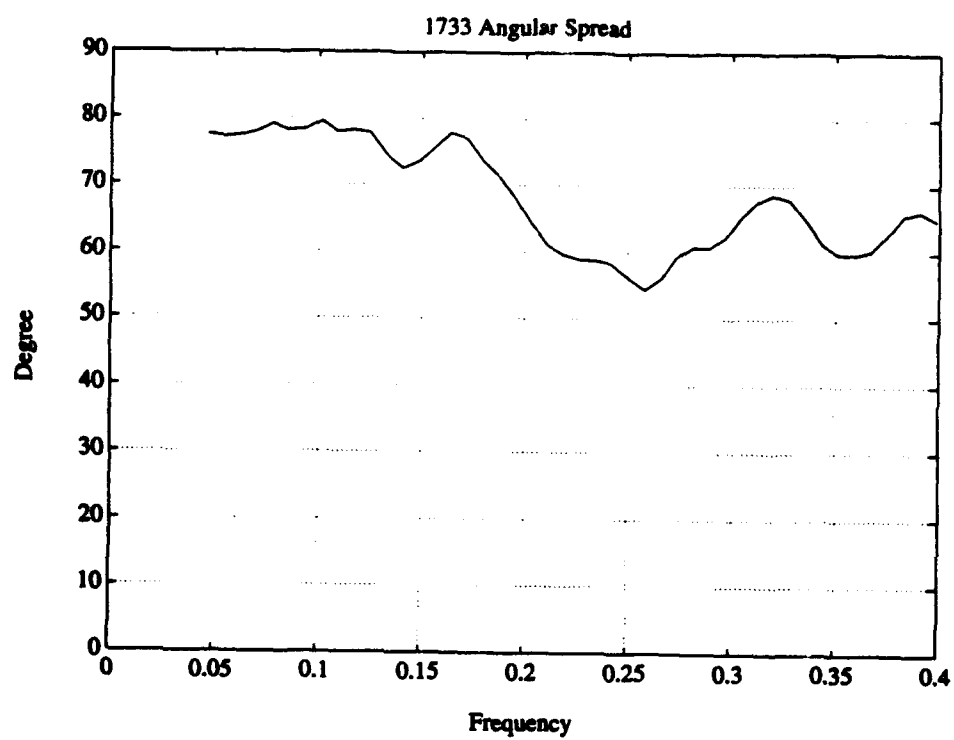


1733 Waveheight PSD

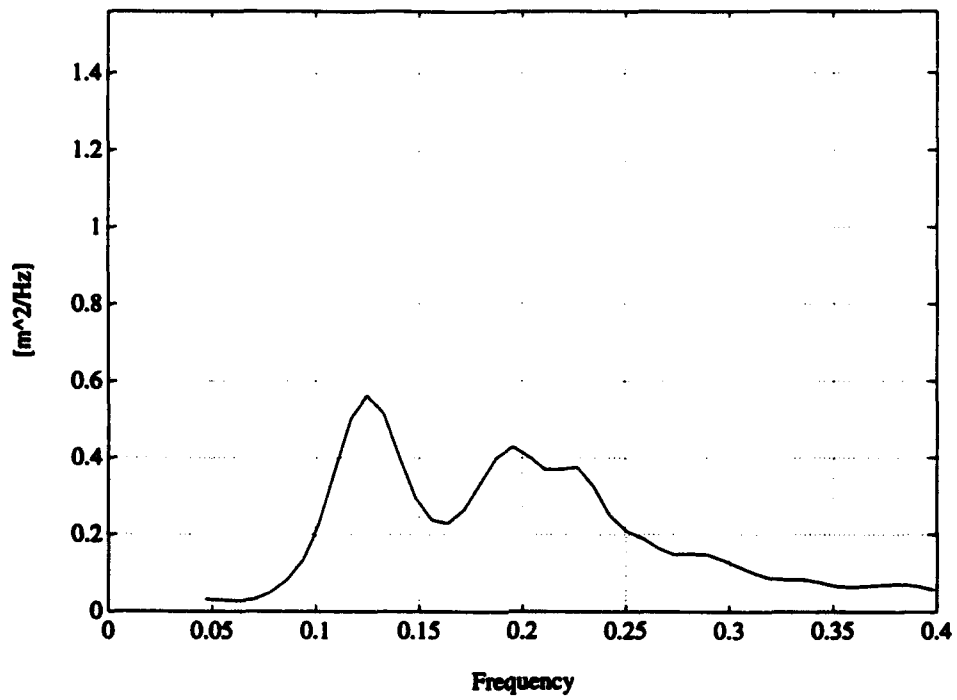


1733 Wave Direction

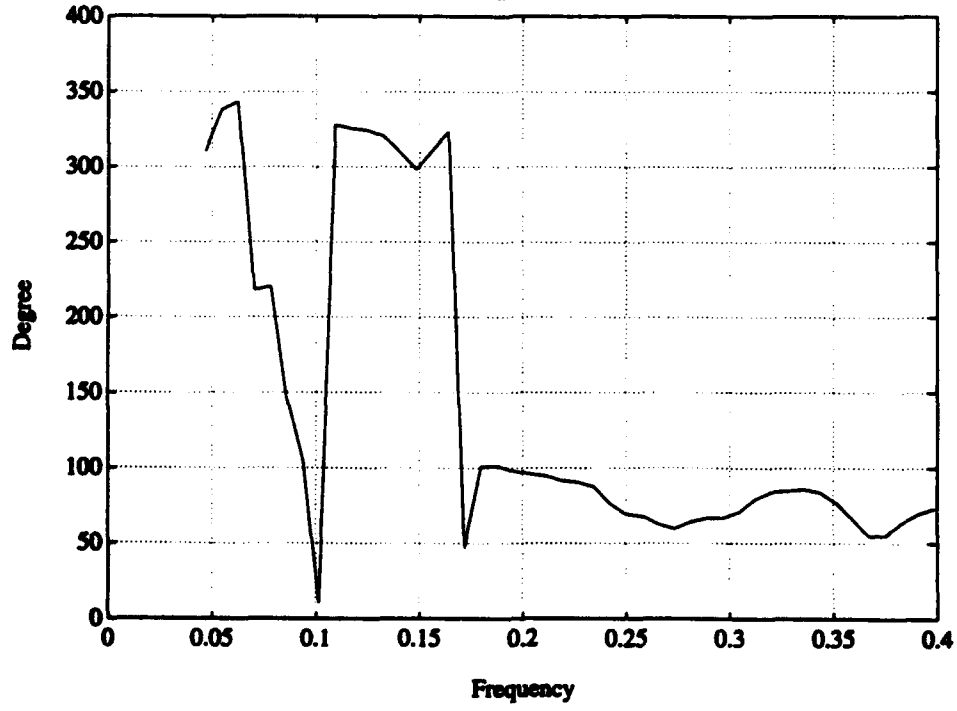


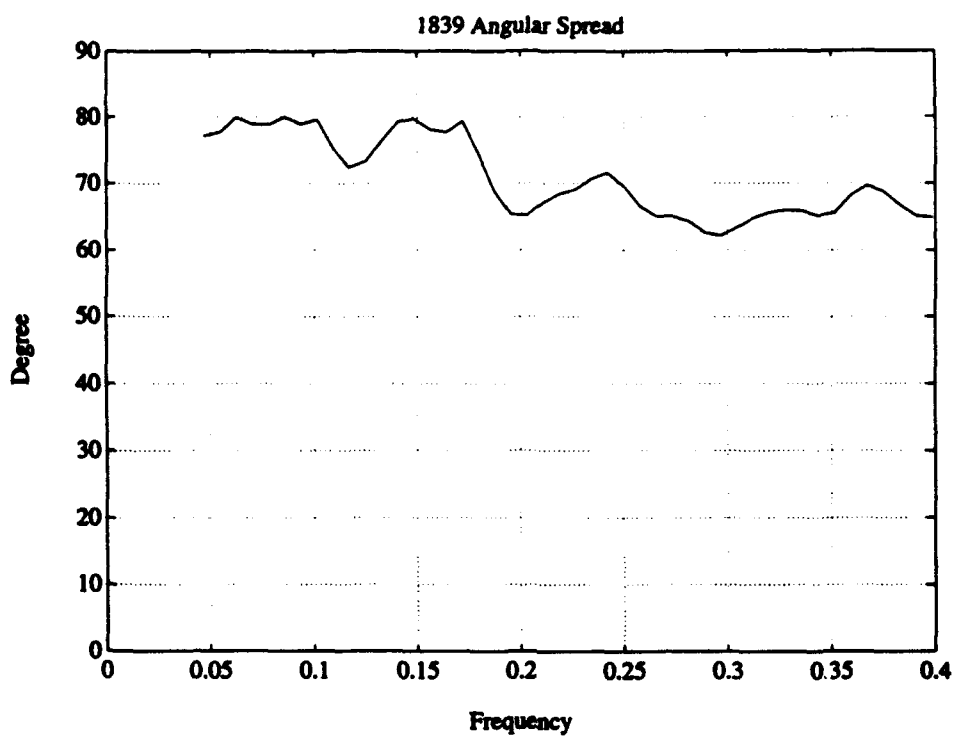


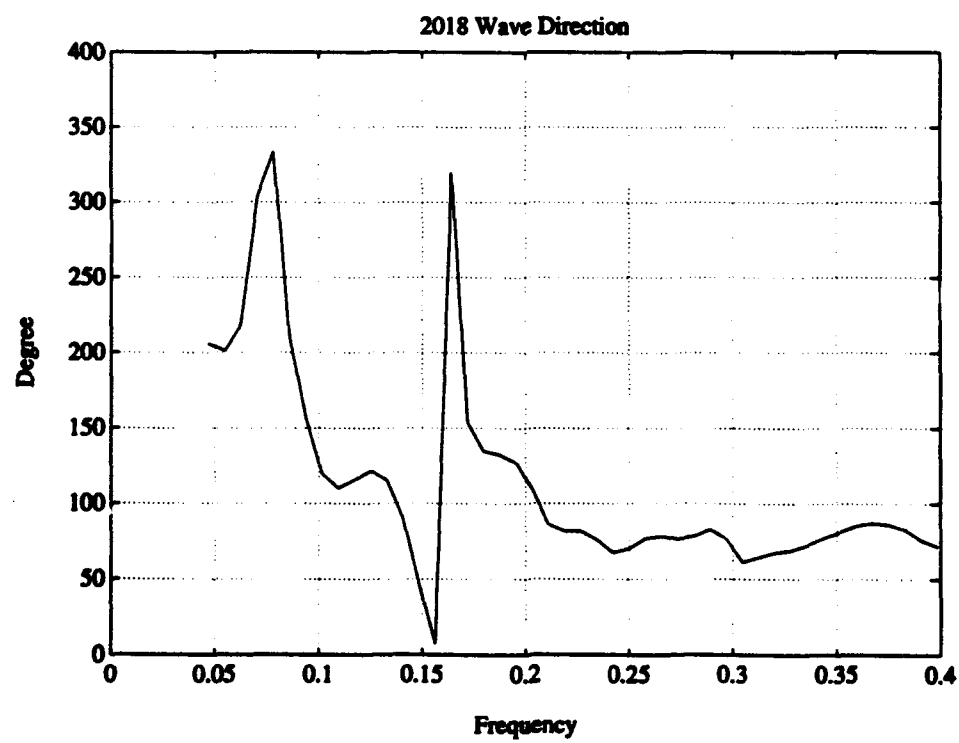
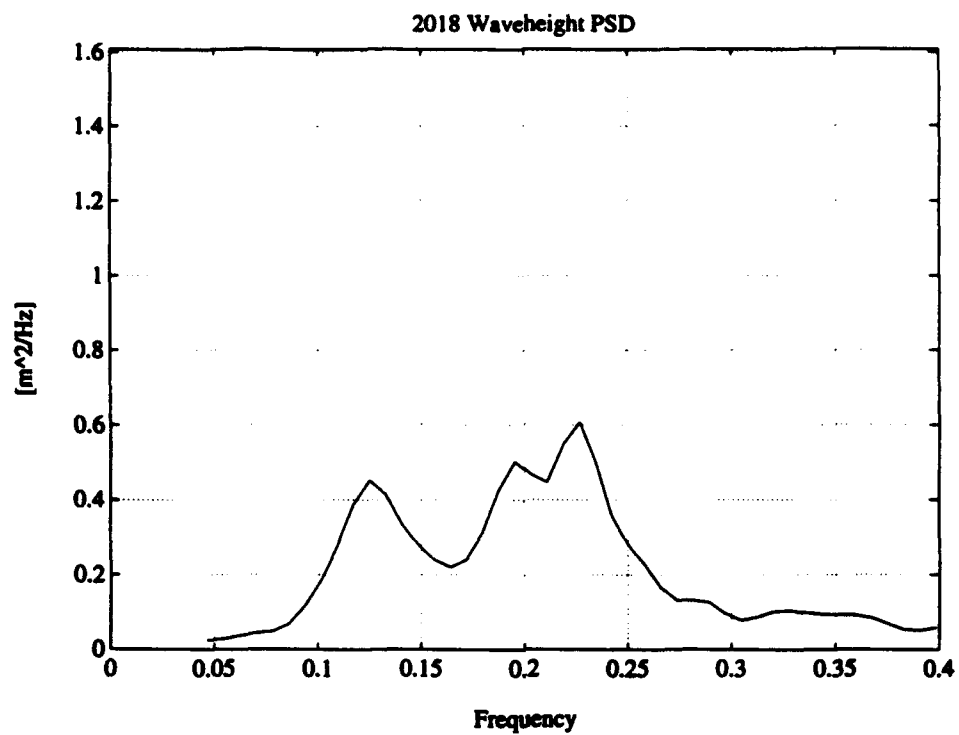
1839 Waveheight PSD

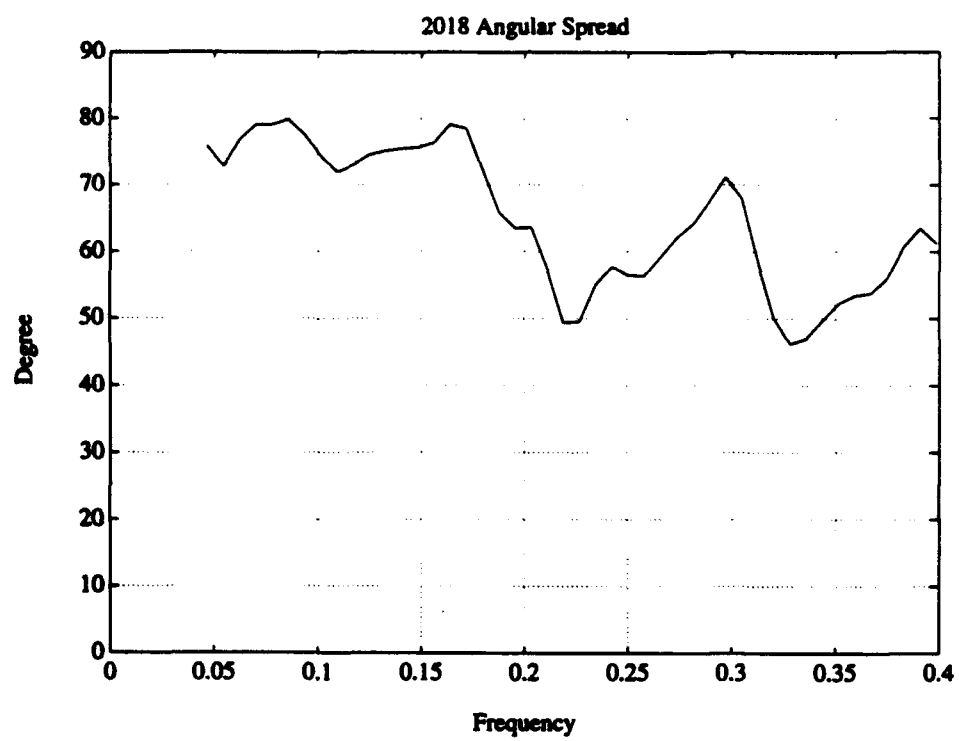


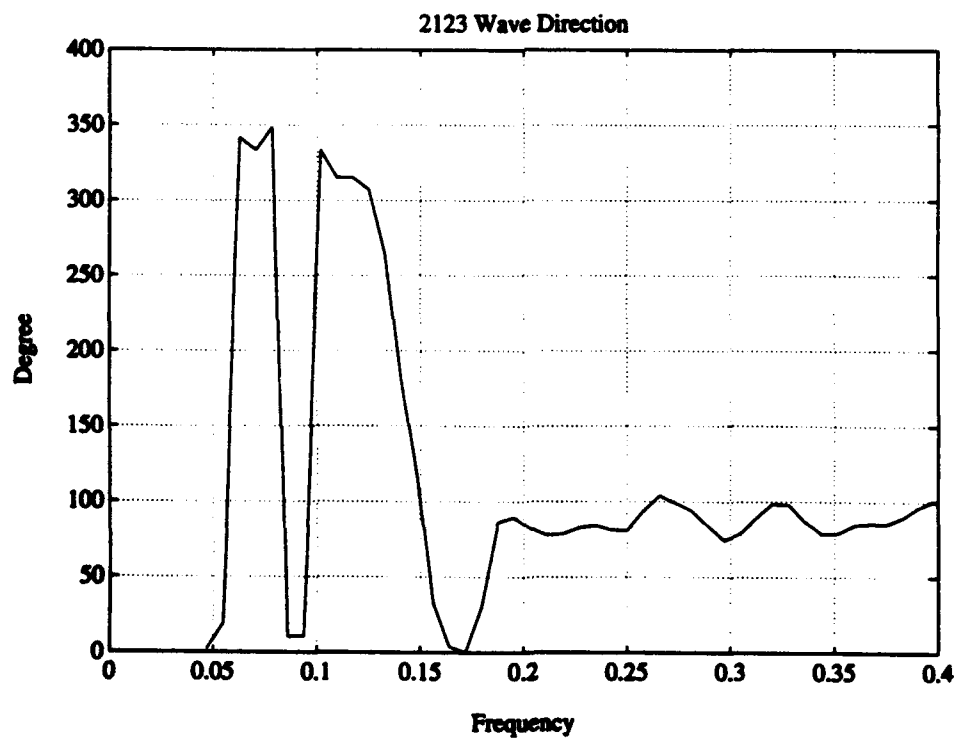
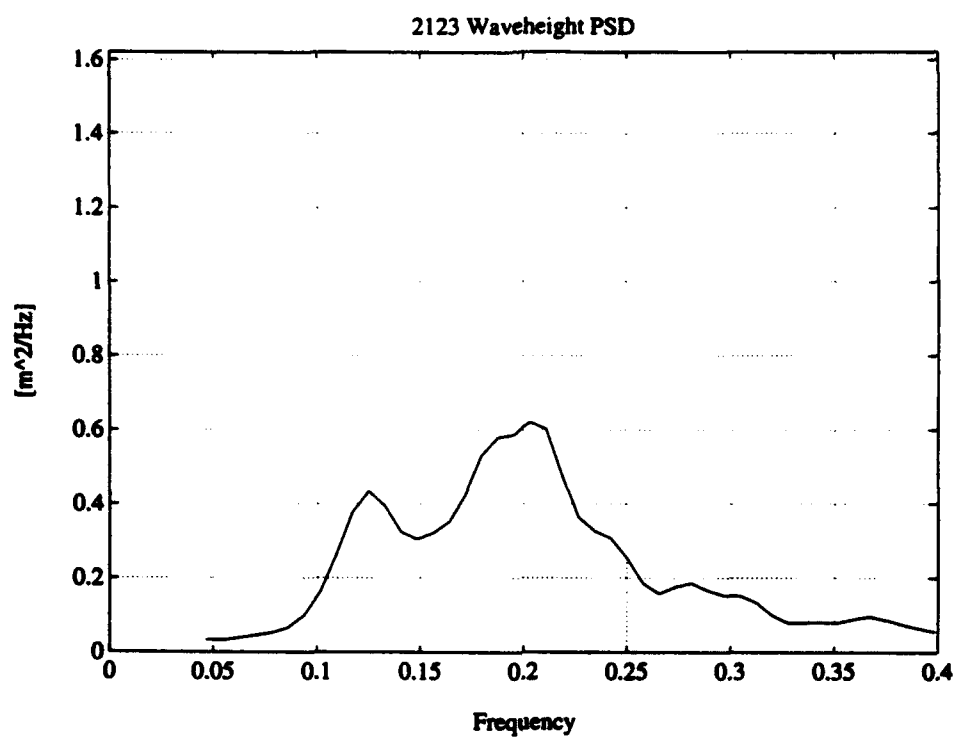
1839 Wave Direction

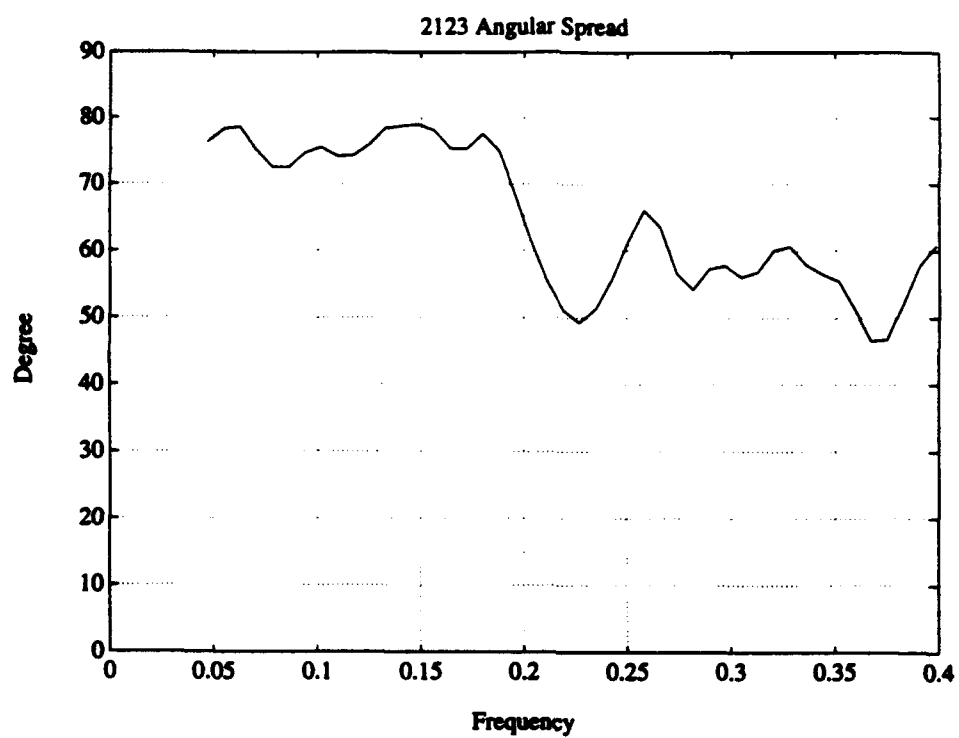




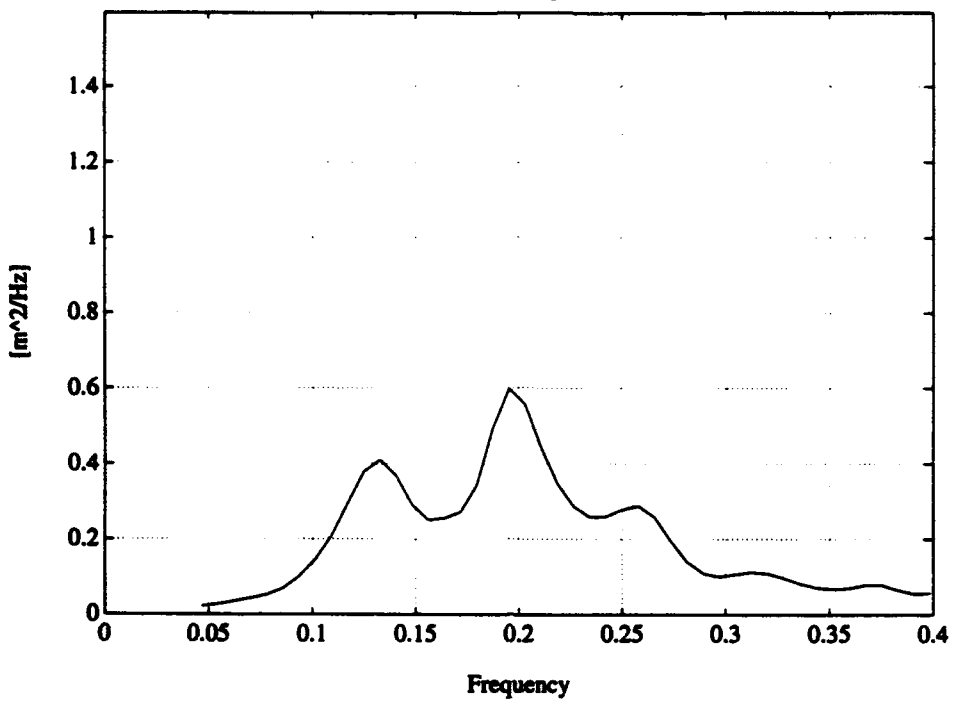








2155 Waveheight PSD



2155 Wave Direction

